UNIVERSITY OF SOUTHAMPTON

DEPARTMENT OF ELECTRONICS AND COMPUTER SCIENCE

POLARISATION EFFECTS IN FIBRE LASERS

BY

Jin-Tong LIN

A Thesis Submitted

for the Degree of Doctor of Philosophy

January 1990

UNIVERSITY OF SOUTHAMPTON

ABSTRACT

FACULTY OF ENGINEERING
ELECTRONICS AND COMPUTER SCIENCE

Doctor of Philosophy

POLARISATION EFFECTS IN FIBRE LASERS

by Jin Tong Lin

Single-mode fibre lasers are a new class of active fibre device, which play a remarkable role in optical fibre communications and sensors. They also exhibit a number of new phenomena, one of the most important being polarisation effects.

In this thesis, new unexpected fundamental polarisation effects in fibre lasers have been discovered. The phenomena are fluorescence depolarisation, the existence of orthogonal polarisation eigenmodes, and the dependence of the output polarisation on the pump polarisation state.

A unified theoretical model, incorporating the electric dipole model for rare-earth ions in a glass matrix, is formulated. The concept of effective pump power is introduced and can be applied to existing laser theory; thus laser performance characteristics such as thresholds, slope efficiencies and the polarisation state of the output can be predicted accurately. The good agreement between theory and experiment enables the derivation of the polarised cross-section ratio. This has been done for Nd^{3+} and Er^{3+} ions in silica fibres.

From the theoretical analysis the optimum condition for single polarisation operation is deduced. An effective technique for making single-polarisation single-mode (SPSM) fibre lasers has been developed using an integral fibre polariser. The advantages of this technique are low insertion loss, high polarisation extinction ratio and compatibility with existing single-mode fibre components. Laser-diode-pumped SPSM fibres of high performance, both in continuous-wave and Q-switched operations, have been achieved.

Contents

Page

Chapter 1
Single-mode fibre lasers:
A new class of active fibre device 1
1.1 Introduction 1
1.2 Single-mode fibre lasers 2
1.3 Polarisation behaviour of fibre lasers 7
1.4 Contents of the thesis 10
References to Chapter 1 12

Chapter 2
Special properties of fibre lasers 15
2.1 Differences between fibre lasers and
conventional glass lasers 15
(1) Linearly-polarised and narrow-band
pump radiation
(2) Birefringent cavity
(3) Longitudinal pumping system
2.2 Differences between passive and active fibres 23
References to Chapter 2 31

Chapter 3
Basic factors governing polarisation effects
in fibre lasers 32
3.1 Three basic factors 32
3.2 Experimental arrangements 32
3.3 Fluorescence depolarisation 33
3.4 Two orthogonal polarisation eigenmodes 39
(1) Existence of orthogonal polarisation eigenmodes
(2) Orientation of orthogonal eigenmodes
(3) Different slope efficiencies
(4) Phase independence of the eigenmodes
(5) DOP of the individual polarisation eigenmodes
3.5 Dependence of polarisation state
on pump and dopant 50
(1) cos(2a) function

(2) DOP as a function of pump power
(3) Dependence of DOP on dopant characteristics
3.6 Discussion 54
References to Chapter 3 55

Chapter 4
Theoretical modelling of polarisation effects in fibre lasers **56**
4.1 The physical basis of polarisation effects 56
(1) Glass structure
(2) Electric dipole model
(3) Electric dipole radiation
(4) The Stark effect
(5) Spontaneous emission and stimulated emission
(6) Laser excited fluorescence spectroscopy in glass
4.2 Understanding of polarisation effects in fibre lasers 68
(1) Fluorescence depolarisation
(2) Existence of two orthogonal eigenmodes
(3) Dependence of laser polarisation on pump
4.3 Effective pump power of polarisation eigenmodes 79
(1) Polarisation-dependent cross-section ratio
(2) Effective absorbed pump power
(3) Polarisation selection ratio
(4) Discussion
References to Chapter 4 90

Chapter 5
Analysis of lasing characteristics **92**
5.1 Threshold 93
5.2 Slope efficiency 99
5.3 Relaxation oscillation frequency 102
5.4 Degree of polarisation (DOP) 107
5.5 45° effects 113
5.6 Measurements of polarised cross-section ratio 119
(1) Method
(2) Complementary angle compensation

(3) Results
References to Chapter 5 129

Chapter 6
Single-polarisation operation **130**
6.1 Basic considerations 130
(1) Superfluorescence
(2) Superfluorescence of the y mode
(3) Small-signal gain and gain saturation
(4) Measurement of saturated gain ratio S
6.2 Conditions for single-polarisation operation 138
6.3 Modelling of single-polarisation operation 140
(1) Solid-angle ratio
(2) Modelling
6.4 Polarisation efficiency
of single-polarisation operation 143
(1) Comparison of two configurations
(2) Polarisation efficiency
as a function of pumping orientation
(3) Polarisation efficiency
as a function of polarised cross-section ratio
6.5 Influence of polarisation misalignment 158
(1) Intracavity polariser
(2) Acoustic-optic Q-switch
(3) Other devices
References to Chapter 6 162

Chapter 7
Single-polarisation single-mode (SPSM) fibre lasers **163**
7.1 Introduction 163
7.2 Integral fibre polariser 165
(1) D-shaped polariser
(2) Twin-hole fibre polariser
(3) Metal-plated fibre polariser
(4) Discussion
7.3 The first SPSM fibre laser 169
7.4 Optimal design of SPSM fibre lasers 170
(1) Analysis of metal-clad fibre

(2) Numerical calculations
(3) Minimum additional loss Ly required for SPSM laser
(4) Proper design steps
(5) Optimizing laser cavity
(6) Measurements of cavity parameters L, K, P(o)
(7) Consideration of normalized separation D
(8) Theoretical prediction
(9) An example of numerical calculation
7.5 Experimental Results 191
7.6 LD-pumped SPSM fibre lasers 191
(1) The original experiment with LD-pumped fibre laser
(2) LD-pumped SPSM fibre lasers
References to Chapter 7 199

Chapter 8
Polarisation Mode Competition in Fibre Lasers 202
8.1 Introduction 202
8.2 Polarisation competition in the time domain 214
(1) Polarisation mode competition
(2) Pull-push relaxation oscilation
(3) Influence on Q-switched operation
8.3 Polarisation competition in the frequency domain 222
(1) Non-polarisation resolved spectrum
(2) Polarisation-resulved spectrum
8.4 Conclusions 222
References to Chapter 8 222

Chapter 9
Conclusions and Discussion **224**
9.1 Concluding remarks 224
9.2 Discussion 226
9.3 Future Work 227
References to Chapter 9 229

Ackowledgements
Publications and Prize

Chapter One

THE SINGLE-MODE FIBRE LASER
—— A NEW CLASS OF ACTIVE FIBRE DEVICE

1.1 Introduction

Since the published description by Schawlow and Townes[1] of an optical maser, or laser, a number of solid materials have been made to undergo stimulated emission. Most of the lasers have utilised rare-earth ions in a variety of crystals or glasses. Of the rare-earth ions trivalent neodymium[2] has been the most important because it can be operated at room temperature with high efficiency. Continuous wave (CW) laser output at room temperature has been obtained from Nd^{3+} in a number of crystalline hosts, most notably in yttrium aluminium garnet (YAG)[3].

An early comparison of glass and crystals hosts suggests that these materials complement each other[4]. Glasses are more suitable for high-energy pulsed operation because of their broad fluorescence linewidths and the flexibility in their physical parameters. On the other hand, crystals have the advantage of higher thermal conductivity and narrower emission linewidths, which makes them more appropriate for CW and high repetition rate applications.

The inherent nature of the glass host produces inhomogeneously broadened lines which are wider than would be found in crystals. This makes it more difficult to attain threshold, because a large inversion is required for the same gain at the centre of the line. However, the broadening of the emission line provides an advantage in Q-switched and amplifier applications. As compared with a narrow line, the broadened line gives less loss due to amplified spontaneous emission for the same inversion.

The major disadvantage of glass is its low thermal conductivity. This imposes limitations on the diameter

that can be used in CW operation and in high repetition rate applications. The optical fibre offers the opportunity of reducing the diameter to the Gaussian limit whilst increasing the length to offset the reduction in stored energy per unit length.

The first laser action in glass fibres dates from 1964[5]. At that time, the laser cavity was a multimode, doped, glass fibre with a core diameter of 10μm. The fibre laser cavity in a self-supporting coil was pumped radially by a flashtube as in bulk glass laser configurations. Since there was no essential improvement of the laser performance over bulk lasers, the fibre laser did not develop much until recently. It is the current widespread use of single-mode optical fibre for telecommunications, and the availability of low-cost semiconductor lasers, which has stimulated interest in single-mode fibre lasers[6,7,8].

1.2 Single-Mode Fibre Lasers

Single-mode fibre lasers possess a number of advantages over both their bulk counterparts, and the early multimode fibre lasers. That is why the original research and development of single-mode fibre laser by the Optical Fibre Group at Southampton University have caused a wave of interest internationally[9,10,11].

Typical single-mode fibre laser configurations are shown in Fig.1.1 and Fig.1.2 for Fabry-Perot, and ring cavities, respectively. The main performance of various fibre lasers achieved to date are listed in Table 1.1.

With the recently developed technique of making single-mode fibre containing rare-earth ions[12,13], the single-mode fibre laser cavity can be made to have a very small diameter, typically 3.0~5.5μm for the core and 90~125μm for the cladding. Such a small diameter minimizes the thermal effects which plague bulk-glass lasers. All the fibre lasers demonstrated to date at

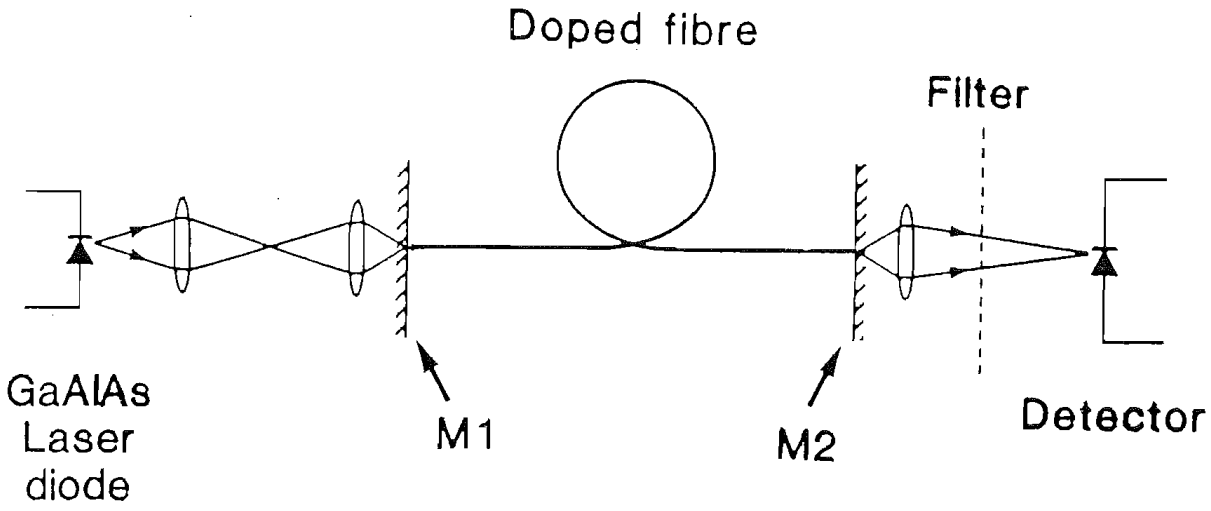

Fig.1.1 Diode laser pumped fibre laser with Fabry-Perot cavity.

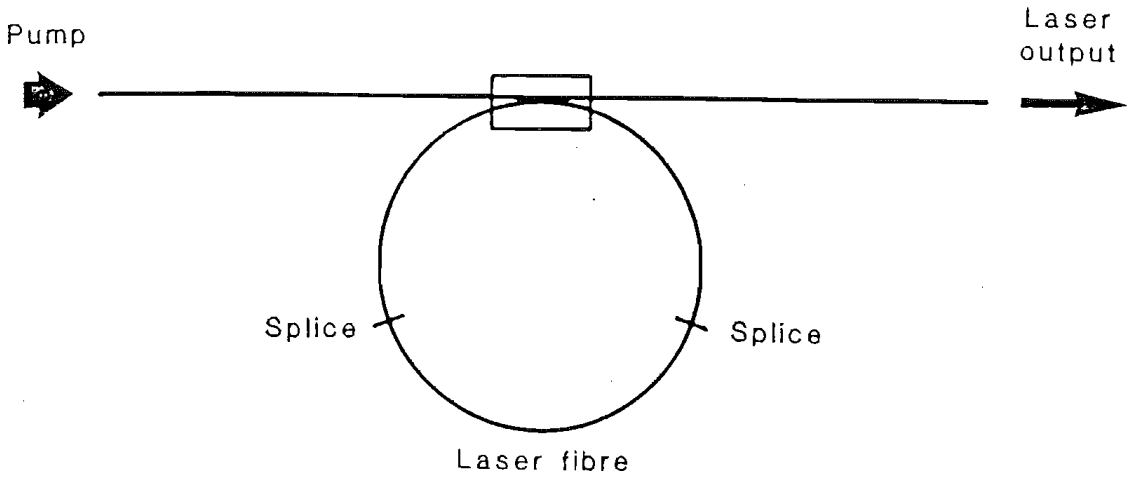

Fig.1.2 Schematic diagram of a fibre laser with a resonant ring cavity.

DOPANT	PUMP SOURCE	OUTPUT WAVELENGTH (μm)	LABORATORY
Nd^{3+}	Diode Diode Argon/Dye	0.94 1.05-1.09 1.3-1.4	SO, PO SO,BT,HOYA, BELL,NTT,PO GTE, BT, PO
Er^{3+}	Diode Argon/Dye Argon/Dye	1.6 1.55 2.4	SO, BT, PO SO,BT,PO,GTE GTE
Pr^{3+}	Argon/Dye	1.06	SO
Yb^{3+}	Dye	0.9, 1.06	SO
Sm^{3+}	Argon	0.651	SO
Codoped Yb^{3+}/Er^{3+}	Diode	1.55	PO, SO
Ho^{3+}	Argon/Dye	2.1	BT

SO: Southampton University

PO: Polaroid

BT: British Telecom.

Table 1.1 A summary of the fibre laser work to date.

Southampton, as listed in Table 1.1, show a total absence of thermal problems.

The radial dependence (with respect to variable r) of the scalar mode, ψ, of a step-profile single-mode fibre can be expressed as[14]

$$\psi = \frac{J_o(ur)}{J_o(ua)} \exp[j(\omega t-\beta z)] \qquad 0\leq r\leq a \qquad (1.1a)$$

$$\psi = \frac{K_o(wr)}{K_o(wa)} \exp[j(\omega t-\beta z)] \qquad a\leq r<\infty \qquad (1.1b)$$

where J_o is the Bessel function of the first kind and K_o is the modified Bessel function of the second kind. The mode parameters u and w are defined as

$$u = a(k^2n_{co}^2-\beta^2)^{1/2} \qquad (1.2a)$$

$$w = a(\beta^2-k^2n_{cl}^2)^{1/2} \qquad (1.2b)$$

and are related to the fibre parameter by

$$V^2 = u^2+w^2 \qquad (1.3)$$

$$V = ka(n_{co}^2-n_{cl}^2)^{1/2} \qquad (1.4)$$

In these equations, $k=2\pi/\lambda$ and λ is the free-space wavelength, ω is the angular frequency of the light, a is the core radius of the fibre, n_{co} and n_{cl} are the refractive indices of the fibre core and cladding, respectively. β is known as the propagation constant of the transmitted mode, whereas the dimensionless parameter V is known as the normalized frequency.

By using a single-mode fibre as the laser cavity, the fibre laser automatically offers a reliable fundamental mode output, as expressed by eqs(1.1). The higher modes are rejected by a cut-off property with the proper choice of core diameter 2a and of refractive index difference between the core and the cladding, namely with a normalized frequency $V\leq 2.405$. This means that the

complicated process of transverse mode selection as in conventional solid-state laser engineering[15] can be avoided. In addition, single longitudinal mode operation of fibre lasers has also proved possible[16] when a reasonably short length of fibre cavity is employed. In practice, single-transverse and single-longitudinal mode operations are both compulsory conditions for spectral purity of a laser source.

The longitudinal pumping system as shown in Fig.1.1 and 1.2 provides a possibility of a higher launching efficiency, especially for a pump source emitting into a narrow solid-angle such as a laser beam. The preliminary design for experiments in the laboratory has shown a launching efficiency as high as 25% for a semiconductor laser diode (LD) pumped Nd^{3+}-doped fibre laser[17], compared with 16% for conventional bulk-glass lasers[15]. Moreover, since the pump light is guided along the single-mode fibre, i.e. the laser cavity, a high proportion of pump power can be absorbed, when an appropriate fibre length is chosen.

As a consequence of the high pump intensity within the small diameter core (typically $2a=3.0\sim5.5\mu m$), single-mode fibre lasers are characterised by ultralow lasing threshold (typically order of mW), as well as high slope efficiency (up to 44%). Some exciting results have been reported. For example, the CW operation of an Er^{3+}-doped glass laser, corresponding to a three-level transition, $^4F_{9/2}$-$^4I_{15/2}$ has been realized at room temperature for the first time with a fibre form[18]. The first visible lasing line has also been seen from the three-level transition, in a Sm^{3+}-doped fibre laser[19]. It is worth pointing out that the lasing wavelength region of Er^{3+}-doped fibre lasers, $1.55\mu m$, is the lowest-loss window for silica and is thus of particular interest for optical fibre communications and related measurements.

Obviously, single-mode fibre lasers retain the good power-handling properties of silica glass, the host medium, and broadened rare-earth transitions, thus

enabling tunable lasers, high peak-power pulsed lasers and broadband amplifiers to be constructed.

Fibre lasers represent a new class of active fibre devices which are fully compatible with existing single-mode fibre components. Their low threshold, wide tunability and high-power pulsed output provides a new all-fibre laser technology. To date, considerable progress on fibre lasers and amplifiers has been made for application both in telecommunications and the traditional laser area. For telecommunications it is anticipated that applications will be as (1) a high-power pulse source for fibre optical time-domain reflectometry (OTDR) measurements and non-linear effects, (2) a narrow linewidth source at a wavelength of 1.55μm and (3) a high-gain in-line and power amplifier in the third window for optical fibre communications.

1.3 Polarisation Behaviour of Fibre Lasers

Polarisation, intensity and the spectrum are the three main characteristics of radiation. In Newton's "Opticks" polarisation is referred to as one of the "original properties of light". The part played by polarisation in the formulation of the transverse nature of light wave is well known. However, before the advent of the electromagnetic theory, classical optics was not concerned with polarisation in the elementary act of radiation, and regarded polarisation as a given property of the light wave. There was no experimental or theoretical basis for studying this problem.

The electromagnetic theory of light was established in the second half of the nineteenth centary, leading to the Hertzian dipole, which remains the simplest and the most important classical model of an elementary radiator.

The electron theory put forward by Lorentz gave a physical interpretation to this elementary dipole radiator and treated it as a quasi-elastically bound electron.

In the quantum theory, the polarisation properties of radiation are even more closely, although not so graphically, linked with the properties of the radiating system.

When it was understood that there is a connection between the polarisation characteristics of radiation and the properties of the microscopic system giving such a radiation, new ways were opened up for studying the system. Two possible methods for further studies became immediately clear: first, polarisation studies could be used to obtain information on the structure of a radiating system in an isolated state, and secondly, during its interaction with the surrounding medium, the study could be a method for investigating the behaviour of the radiating system in the ambient medium. These two aspects can be clearly noted in all branches of spectroscopy.

For a laser source, polarisation behaviour is still one of the most important characteristics. Since the light emitted by a laser is the result of several procedures: excitation of the activators, relaxation to a metastable state, spontaneous emission from upper to lower levels, and amplification of stimulated emission, the relation between the polarisation of the lasing light and the microscopic systems of the activators is more complicated than in a simple radiating system.

In principle, the output of a single-mode CW laser would be expected to be almost completely linearly polarised. In gas lasers, this is found to be the case. However, most measurements are performed with lasers using Brewster-angle windows. This favours oscillation in the plane of incidence, for this polarisation is transmitted without loss through the windows. It is therefore not unexpected that the output of these lasers is found to be nearly completely linearly polarised.

In Zeeman-effect studies with the helium-neon laser, circularly-polarised components in the emitted radiation have been observed.

In the case of solid-state lasers both polarised and unpolarised outputs have been observed. For example, in ruby lasers the output of 0-degree orientation rods (C axis coincident with the rod axis) has been found to be unpolarised, while that of 60 and 90-degree orientation rods has been found to be completely linearly polarised.

The observations of semiconductor lasers showed several features analogous to those derived from observation of ruby lasers, indicating the effects of inhomogeneous laser materials. In the lowest-order mode the semiconductor laser light is expected to be completely linearly polarised. For some diodes, using the Parallel Plane Fabry-Perot (PPFP) geometry, the output was found to be almost completely polarised with the electric vector parallel to the junction, and for others the output was found to be nearly completely polarised with the electric vector perpendicular to the junction. In still others neither polarisation was observed.

During this doctoral study on polarisation effects in fibre lasers a parallel polarisation study of the diode-laser-pumped mini-YAG laser has been carried out at Sandia National Laboratories, USA[20]. The research reports indicate that for certain transitions the emitted light is strongly polarised parallel to the pump radiation, while for other adjacent transitions the emission may be 100% polarised orthogonal to the pump beam. The exact physical basis for the phenomena is still unclear.

All this research, previous and current, indicates the complicated nature of the study of polarisation in laser sources.

Fibre lasers differ from conventional solid-state lasers by having a coherent pump source, a birefringent cavity and a longitudinal pumping system. All of these cause special output polarisation properties of fibre lasers. On the other hand, the fibre laser provides an opportunity, for the first time, to investigate the relation between the polarisation states of the pumping

light and the lasing light, and to study the influence of a curved birefringent laser cavity on the lasing action, so that more information of both the microscopic system of rare-earth ions in a glass matrix, as well as the interaction between such ions and the curved host material can be obtained.

Technically, an understanding of the polarisation properties of fibre lasers is essential for producing single-polarisation lasers, as well as a number of sensor and switching devices. Also, many potential applications of fibre lasers, such as the optical fibre gyroscope and telecommunications, depend strongly on the output polarisation behaviour of fibre lasers. In addition, polarisation-sensitive intracavity components such as fibre gratings[21], acousto-optic modulators[22], and crystals for frequency doubling[23] are frequently employed. Their operation in laser cavities also requires a knowledge of the polarisation properties of fibre lasers.

1.4 Contents of the Thesis

The contents of the thesis are based on the author's own research. They were first discovered and then studied, and many aspects have already been published (see the list of publications). Material adopted from other sources is, as a rule, introduced only in order to make the account more coherent and to consider all the problems in a unified manner.

One of the principal aims of this thesis is to provide an understanding of polarisation effects in fibre lasers, and therefore to provide sufficient information about the microscopic system of rare-earth ions in a glass matrix, the influence of polarisation effects on the operation of fibre lasers, and to give a theoretical model for interpretating the effects. In addition, a technique for fabricating an integral fibre polariser was

contributed by the author to make single-polarisation single-mode fibre lasers.

It is intended to explore the possibility of explaining the polarisation phenomena based on the fundamental principles of both classical and quantum theory. The research work is restricted to the single-mode fibre laser with a Febry-Perot cavity configuration, and confined to non-Zeeman effects. The Nd^{3+}-doped fibre lasers based on the $^4F_{3/2}$-$^4I_{11/2}$ transition, which is a four-level system, are intensively studied both theoretically and experimentally, although Er^{3+}-doped fibre lasers, a three-level system, and other lasers are also considered.

Chapter 2 points out the special properties of fibre lasers. Three main differences between fibre lasers and conventional glass lasers are discussed. Also, the difference between the passive and active fibres are analysed.

To emphasize fundamental phenomena of polarisation effects, most of which are unexpected, the experimental investigations are characterised by "**three basic factors**" in Chapter 3. The existence of orthogonal polarisation eigenmodes in a fibre laser cavity is described. The phase independence of two polarisation eigenmodes and the degree of polarisation of linearly-polarised eigenmodes are experimentally studied.

The concept of "**effective pump power**" for polarisation eigenmodes is introduced in Chapter 4, where the basic consideration of introducing the concept, derivation of the mathematical expression and some discussion are presented.

Polarisation properties of fibre lasers are analysed using the concept of effective pump power in Chapter 5. This includes threshold, slope efficiency, relaxation oscillation frequency and polarisation state of the output from the fibre lasers. The good agreement between experimental results and theoretical calculation is also discussed.

Chapter 6 deals with the theory of single-polarisation operation of fibre lasers. The condition for single-polarisation operation is given. The polarisation efficiency of single-polarisation operation is discussed, and the influence of polarisation alignment on single-polarisation operation described.

Single-polarisation single-mode fibre lasers, Chapter 7, describes the techniques for making various integral single-mode fibre polarisers. The optimum design of a single-polarisation single-mode fibre laser is discussed, and some notable technical achievements in single-polarisation single-mode fibre lasers are presented.

Polarisation competition is another aspect of polarisation effects in fibre lasers. Temporal polarisation comprtition affects Q-switched operation and spectral polarisation competition leads to a polarisation frequency splitting. Both phenomena are treated in Chapter 8.

Finally, in Chapter 9, the future prospects for polarisation study of fibre lasers are considered.

References to Chapter 1

[1] A.L. Schawlow and C.H. Townes: "Infrared and optical masers" Phys. Rev., 112, pp.1940-1949, 1958.

[2] E. Snitzer: "Optical maser action of Nd^{3+} in a barium crown glass", Phys. Rev. Lett., 7, pp.444-446, 1961.

[3] J.E. Geusic, H.M. Marcos, and L.G.Van Uitert: "Laser oscillations in Nd-doped yttrium aluminium, yttrium gallium and gadolinium garnets", Appl. Phys. Lett., 4, pp.182-184, 1964.

[4] A.K. Levine: "Lasers", Volume 2, Marcel Dekker, Inc. New York, 1968.

[5] C.J. Koester and E. Snitzer: "Amplification in a fibre laser", Appl. Opt. 3, p.1182, 1964.

[6] R.J. Mears, L. Reekie, S.B. Poole, and D.N. Payne: "Neodymium-doped silica single-mode fibre lasers", Electron. Lett., 21, pp 738-740, 1985.

[7] R.J. Mears, L. Reekie, S.B. Poole, and D.N. Payne: "A low-threshold tunable CW and Q-switched fibre laser operating at 1.55um", Electron. Lett., 22, pp.159-160, 1986.

[8] D.N. Payne, L. Reekie, R.J. Mears, S.B. Poole, I.M. Jauncey, and J.T. Lin: "Rare-earth doped single-mode fibre lasers, amplifiers and devices", Proceedings of CLEO'86, San Francisco, June 9-13, 1986.

[9] See, for example, Proceedings of CLEO'86, Baltimore, 1986.

[10] See, for example, Proceedings of CLEO'87, Anaheim, 1987.

[11] See, for example, Proceedings of ECOC'87, Helsinki, 1987.

[12] S.B. Poole, D.N. Payne and M.E. Fermann: "Fabrication of low-loss optical fibre containing rare-earth ions", Electron. Lett., 22, pp.159-160, 1986.

[13] J.E. Townsend, S.B. Poole and D.N. Payne: "Solution-doping technique for fabrication of rare-earth-doped optical fibres", Electron. Lett. Vol.23, No.7, pp.329-331, 1987.

[14] A.W. Snyder and J.D. Love: "Optical waveguide theory", Chapman and Hall, London/New York, 1983.

[15] W. Koechner: "Solid-State Laser Engineering", Springer-Verlag, 1976.

[16] I.M. Jauncey, L. Reekie and D.N. Payne: "Single longitudinal mode operation of a fibre laser", Post-deadline Paper, CLEO'87, Paper THT9-1, pp.243, Baltimore, 1987.

[17] I.M. Jauncey: Private communications.

[18] R.J. Mears, L. Reekie, S.B. Poole and D.N. Payne: "Low-threshold tunable CW and Q-switched fibre laser operating at 1.55μm", Electron. Lett., 22, pp.159-160, 1986.

[19] M.C. Farries, P.R. Morkel and J.E. Townsend: "A Samarium doped visible glass laser operating at 651nm", Proc. CLEO'88, Paper PD5, Anaheim, California, 1988.

[20] P. Esherick and A. Owyoung: "Polarisation effects in diode-laser-pumped Nd:YAG lasers", Proc. CLEO'88, Paper THB2, pp.296-297, Anaheim, California, 1988.

[21] I.M. Jauncey, L. Reekie, R.J. Mears, D.N. Payne, C.J. Row, D.C.J. Reid, I. Bennion, I. and C. Edge: "Narrow-linewidth fibre laser with integral fibre grating", Electron. Lett., 22, pp.987-988, 1986.

[22] I.P. Alcock, A.C. Tropper, A.I. Ferguson and D.C. Hanna: "Q-switched operation of a neodymium doped monomode fibre laser", Electron. Lett., 22, pp.84-85, 1986.

[23] W.L. Barnes: Private Communication.

Chapter Two

SPECIAL PROPERTIES OF FIBRE LASERS

It is necessary to analyse the special properties of single-mode fibre lasers before dealing with polarisation effects. Although the first rod-glass laser and the first single-mode fibre for transmission were generated about thirty and ten years ago respectively, the single-mode fibre laser, as a combination of these two techniques, is a new topic of study. There are two aspects to be considered: first, the difference between fibre lasers and conventional glass lasers, and secondly, the difference between passive and active fibres.

2.1 Differences between Fibre Lasers and Conventional Glass Lasers

The geometric configurations employed in conventional glass lasers can be classified into two kinds, rod and fibre. Both of them are pumped by flashtubes, a light source of wide band and random polarisation. Although the usual geometry of a flashtube coiled around a laser rod was reversed in the fibre lasers[1], the pump light is transmitted across the laser material radially in both cases.

Single-mode fibre lasers differ from conventional glass lasers by having a narrow band pump source of linear polarisation, a birefringent cavity and a longitudinal pumping system. These three special properties, together with polarisation anisotropy of stimulated emission cross-section mentioned in Chapter 4, determine the polarisation behaviour of fibre lasers.

(1) Linearly-polarised and narrow-band pump radiation

The pump sources used to date for fibre lasers,

including Ar^+-ion, semiconductor and dye lasers, all produce linearly-polarised, narrow band light. This is, in fact, the first time coherent light has been used as a pump source for glass lasers. The polarisation property of a laser source is characterised by the degree of polarisation (DOP) defined as[2]

$$DOP = (I_{max}-I_{min})/(I_{max}+I_{min}) \qquad (2.1)$$

where I_{max} and I_{min} are related to maximum and minimum polarisation components respectively. For example, Fig.2.1 shows the DOP as a function of driving current for a commercial semiconductor laser diode, Sharp LTD15. It can be seen that a laser diode emits linearly-polarised light with a DOP=0.99 (or extinction ratio of around 20dB) when operated significantly above threshold. As for Ar^+-ion and dye lasers, an even higher extinction ratio (>30dB) of linearly-polarised output can be measured.

Owing to the polarisation anisotropy of the stimulated-emission cross-section, as discussed later in Chapter 4, the polarisation-selective interaction between linearly-polarised pump light and the gain ions in the glass matrix is involved in the lasing action, and thus allows a set of new phenomena to be observed in fibre lasers. This interaction is averaged out in the case of conventional glass lasers because of the polarisation randomness of the pump light.

When a narrowband source is used for excitation, only those ions resonant with the excitation quanta are excited. This site-selective excitation effectively reduces the inhomogeneous broadening and a fluorescence line-narrowing (FLN) spectrum is obtained. The technique of FLN is well known as a tool for fluorescence spectroscopy study[3]. It is now expected that fibre lasers, as the first laserbeam-pumped glass lasers, can provide an opportunity to obtain some new information about the rare-earth ions in a glass matrix.

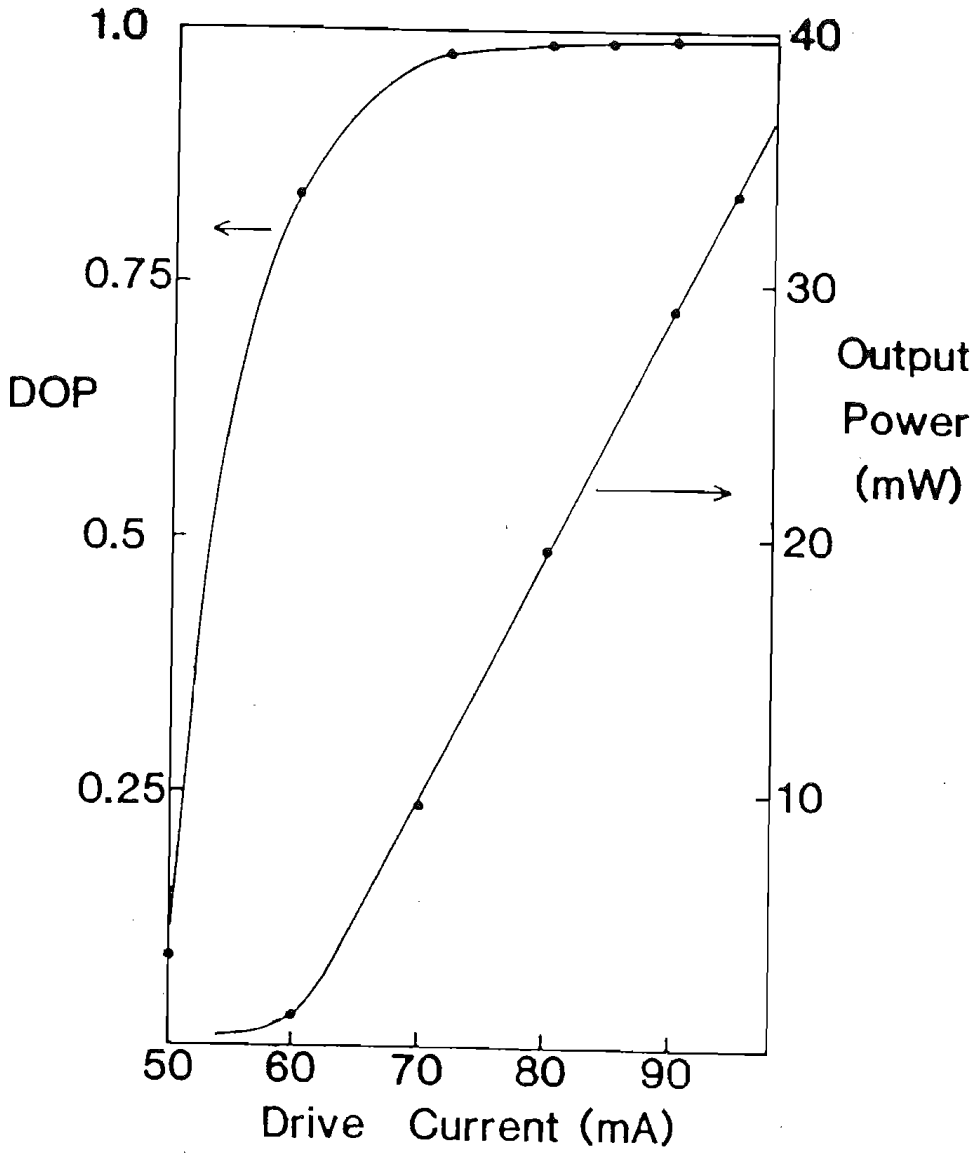

Fig.2.1 Polarisation and lasing characteristics of Sharp LTO15 diode laser.

(2) Birefringent cavity

Single-mode fibres had been exploited for light propagation for more than ten years before the invention of single-mode fibre lasers so that their propagation properties are well known. Theoretically, an ideally-round, straight, strain-free, "single-mode" optical fibre has two degenerate modes of propagation and, therefore, conserves the state of polarisation (SOP) of light guided in the fibre. In a real fibre, various imperfections, such as asymmetric cross section and thermal stress, introduce birefringence. Thus, "single-mode" fibres propagate two orthogonal, linearly-polarised, modes with a difference $\Delta\beta$ in their propagation constants:

$$\Delta\beta = \beta_y - \beta_x \qquad (2.2)$$

The fibre polarisation properties can then be modelled as a linearly-birefringent element whose retardance $\delta(z)$ is proportional to fibre length z[4].

$$\delta(z) = (\Delta\beta)z \qquad (2.3)$$

A useful parameter describing the polarisation properties is the normalized linear birefringence B or the mode effective-index difference Δn.

$$B = \Delta n = \frac{\lambda}{2\pi}\Delta\beta \qquad (2.4)$$

where λ is the free-space wavelength. The mode beat length L_p at which the polarisation state is periodically repeated can be shown to be

$$L_p = \frac{2\pi}{\Delta\beta} = \frac{\lambda}{\Delta n} \qquad (2.5)$$

and varies from <1mm to 140m for high-birefringence and low-birefringence fibres[5]. The corresponding

effective-index difference Δn of the modes is then between 10^{-8} and 10^{-4}.

Although the effective index difference Δn is small, it breaks the space symmetry for light propagation and creates two special orthogonal orientations or birefringence axes in single-mode fibres.

Another aspect of the single-mode fibre birefringence is the circular birefringence, which is caused mainly by fibre twisting. Circular birefringence means that light of different circular polarisation, namely left and right, transmitted by the single-mode fibre have different propagation constants. The difference of propagation constants is given by[6]

$$\Delta\beta_c = g2\pi N \qquad (2.6)$$

where N is the number of twisting turns per metre. The material constant g is expected theoretically to be -0.16 for a silica based, single-mode fibre, and is found to be -0.14 experimentally[7,8].

As a result of circular birefringence, the polarisation orientation of linearly-polarised light transmitted by the fibre is rotated through a certain angle. One explaination of the mechanism is that linearly-polarised light can be resolved into two circularly-polarised components, namely left and right, with different propagation constants due to the circular birefringence. Thus an orientation rotation is exhibited when these two components are composed back into a linearly polarised light after transmission.

In summary, the birefringence of the single-mode fibre can be regarded as a combination of linear and circular birefringence. When linearly-polarised light propagates through the fibre the circular birefringence determines the polarisation rotation, whereas the linear birefringence makes the transmitted light experience the polarisation evolution.

In this thesis, a variety of rare-earth doped fibres with different birefringence are investigated. Their properties of the linear birefringence are listed in Table.2.1. Two typical cross sections of those fibres, which are most frequently used, are illustrated in Fig.2.2. It can be seen that the fibre with an elliptical core has a higher birefringence than those with an ordinary design of round core.

The circular birefringence, which is also inevitably present in a real single-mode fibre, can be ignored if the polarisation study is confined to a non-Zeeman effects in a Fabry-Perot cavity, and is discussed later at the end in this chapter.

(3) Longitudinal pumping system

Since the cavity of a fibre laser is a waveguide itself, a longitudinal pumping arrangement as shown in Fig.1.1 and Fig.1.2 becomes possible. Apart from the high pump efficiency (25%~40% for a laser diode pump, for example), this kind of pump system provides pump light with the same direction of propagation as the lasing light.

As a transmission medium, a single mode fibre laser cavity retains the polarisation orientation information of the pump light which is launched into the fibre longitudinally. When linearly polarised pump light is launched on a birefringence axis of the single-mode fibre, the polarisation state remains constant all the way along the fibre if the polarisation cross talk is negligible[9]. If the light is launched with a angle α relative to a birefringence axis the ratio of two polarisation components remains unchanged during the transmission. Therefore, it is expected that the polarisation-selective interactions between pumping light and gain ions are accumulated along the laser cavity instead of averaged out. This assumption applies in a fibre cavity in which twist, deformation or Faraday rotation is absent.

Sample Lab No.	1 ND199-05	2 ND425	3 YD191-01A	4 ND518
Specifica- tion	Circular core	D-shaped elliptical core	Bow-tie high- birefrin.	Circular core
Clad. dia. (μm)	110	125	110	125
Core dia. (μm)	3.5	4.3(maj.) 3.1(min.)	3.6	4.2
NA	0.21	0.21	0.12	0.16
Cutoff(nm)	850	820	720	890
Dopant concentra. (ppm)	300	300	150	4500
Beat length (mm)	>500	7.5	8.5	>300
Δn	$<10^{-6}$	10^{-4}	10^{-4}	$<2\cdot10^{-6}$

Table 2.1 Properties of fibre samples.

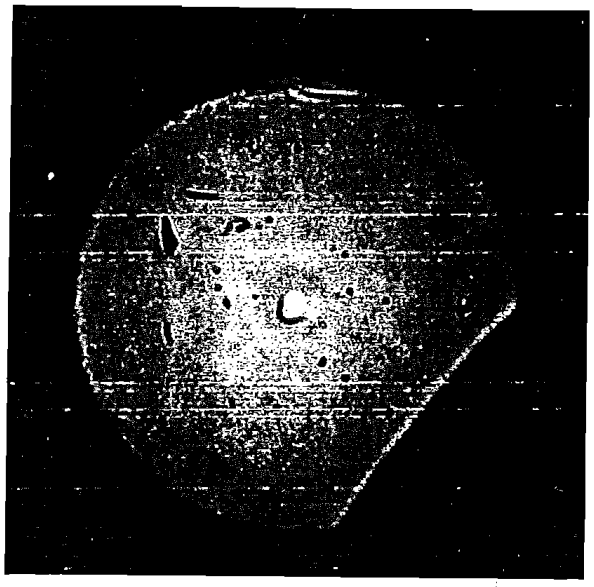

(a)

(b)

Fig.2.2 Typical cross-sections of fibre samples.

(a) Sample ND199

(b) Sample ND425

2.2 Differences between Passive and Active Fibres

When a single-mode fibre is employed as the transmission medium for optical communications or other applications it works as a passive fibre. In contrast, the rare-earth doped single-mode fibre for laser application plays a substantially different role as an active fibre.

The word "passive fibre" means, in general, that there is no interaction between applied electric field of transmitted light and atoms or molecules of the transmitting medium except for attenuation caused by material absorption, scattering and so on.

Assume the electric field of linearly-polarised light **E** described as

$$\mathbf{E}(0) = \mathbf{E}_0 \exp[j(\omega t)] \qquad (2.7)$$

is launched into a single-mode fibre. Let α be the angle between the polarisation orientation of the input linearly-polarised light and the x-axis, where the latter is one of the principal birefringence axes in the fibre. After transmission along a fibre of length z, the field can be written as:

$$\mathbf{E}(z) = \mathbf{E}_0 \exp[j(\omega t - k_z z)] \qquad (2.8)$$

where the complex propagation constant $k_z = ß - j\gamma$. The propagation constant ß must be treated as two different $ß_x$ and $ß_y$ for the x and y components, respectively, due to the linear birefringence. The attenuation coefficient, γ, is assumed to be identical for the x and y components. The frequency ω remains unchanged. As can be seen from eq.(2.8), the polarisation orientation and phase are both affected by the birefringence of the fibre as well as the transmission distance. In general, the electric field at z=l represents elliptically-polarised light. However, the polarisation evolution

follows a certain rule, which can be expressed as follows[10]:

$$\tan 2\phi = \tan 2\alpha \cos\delta \qquad (2.9)$$

where ϕ is the angle between the major axis of the ellipse and the x-axis, and δ is the phase retardation between the x and y modes as defined in eq.(2.3). Actually, the original information about polarisation orientation and phase can be found according to the polarisation state of the output light through the polarisation evolution equation (2.9). This means that single-mode fibre for transmission can record or remember all the information of the transmitted light including amplitude, frequency, phase and polarisation.

In contrast, the rare-earth doped fibre employs the special energy level structure of rare-earth ions in the matrix of silica-based glass to process light actively. A typical energy level structure of Nd^{3+}-doped fibre, which is mainly studied in this thesis, is illustrated in Fig.2.3. The existence of a metastable energy level $^4F_{3/2}$ makes it possible to process the light at the frequencies corresponding to various transitions from this metastable level to a certain terminal level such as $^4I_{11/2}$, or $^4I_{13/2}$. When pump light of an appropriate wavelength is launched into the fibre, the absorption of the dopant ions causes electrons to be excited into the higher energy level. They then decay by a non-radiative transition to the metastable level. Thus population inversion is achieved and possibility of active operation, such as amplification, exists. This kind of fibre is called an active fibre.

Two different frequencies or wavelengths, the pump and the lasing, are involved in the active fibre. For the pump, the polarisation behaviour of the active fibre is expected to be the same as in a passive fibre except for a much stronger absorption. A 3m length of Nd^{3+}-doped fibre laser was used to verify the above points.

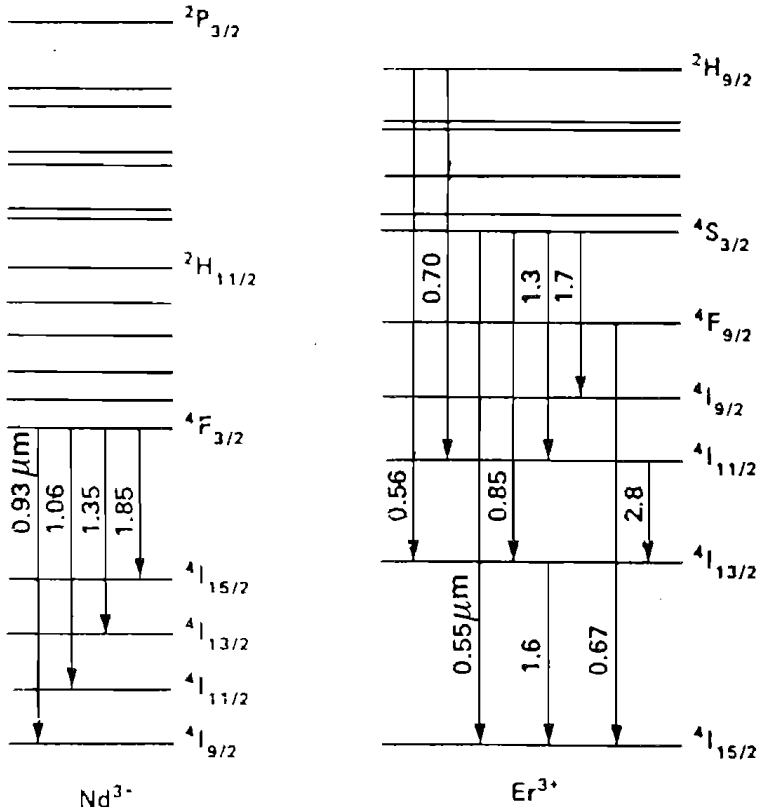

Fig.2.3 Energy levels and laser transitions of Nd^{3+} and Er^{3+} ions in glass.

In order to rotate the polarisation orientation of the pump light, a $\lambda/2$ retardation plate was inserted into the pump beam path, as shown in Fig.2.4. Using a suitable filter, residual pump light at 0.82μm from the output end of the laser cavity was measured and is plotted in Fig.2.5, where the theoretical curve corresponding to eq.(2.9) is also drawn for comparison. The good agreement indicates that the propagation rule of passive single-mode fibre is still valid for the pump light transmitted through an active fibre. It is worth pointing out that this is also true for the case of a Fabry-Perot cavity laser.

However, a knowledge of the state of polarisation of the pump light does not imply an understanding of the polarisation state of the laser light. It is known that the lasing wavelength or wavelengths are determined by the energy level structure as well as the pump wavelength. Usually, there are several terminal levels for electron transition from a metastable level. A typical fluorescence spectrum of the Nd^{3+}-doped fibre pumped by a laser diode operating at 815nm is shown in Fig.2.6 indicating the transitions from $^4F_{3/2}$ to $^4I_{13/2}$, $^4I_{11/2}$ and $^4I_{9/2}$, as shown in Fig.2.3, respectively. This means that the information about the wavelength of the pump cannot be precisely recognised by the behaviour of fluorescence or lasing light.

The amplitude of the electric field of the pump light is affected by the absorption of ions in the active fibre. However the population inversion is related to $|\mathbf{E}_0|^2$, so that the relation between the pump light and the lasing action is much more complicated than in a passive fibre.

What is most important is that the phase information of the pump light, which plays a principal role in the polarisation evolution in a passive fibre, is totally lost during the electron transition. It is impossible to find any phase information of the pump from the lasing light. This is the essential difference

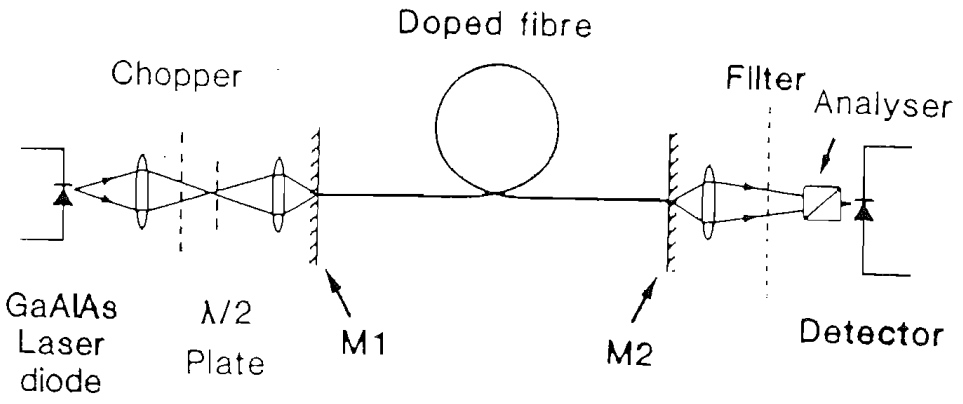

Fig.2.4 Schematic of experimental arrangement for the study of polarisation effects in fibre lasers.

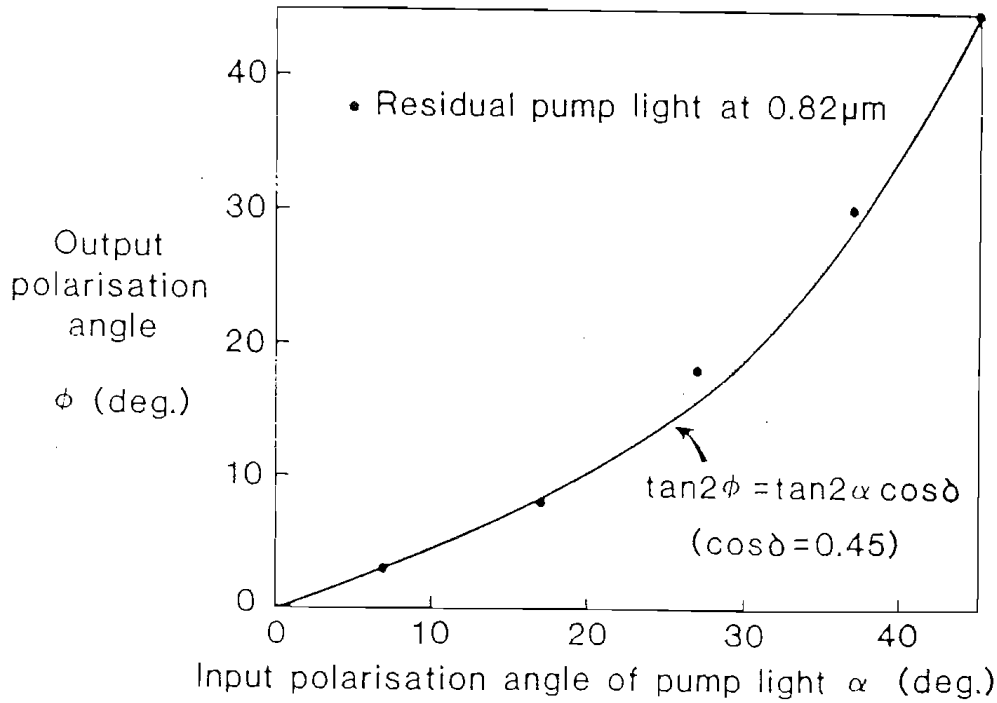

Fig.2.5 Dependence of the output polarisation of the residual pump light on the input polarisation angle.

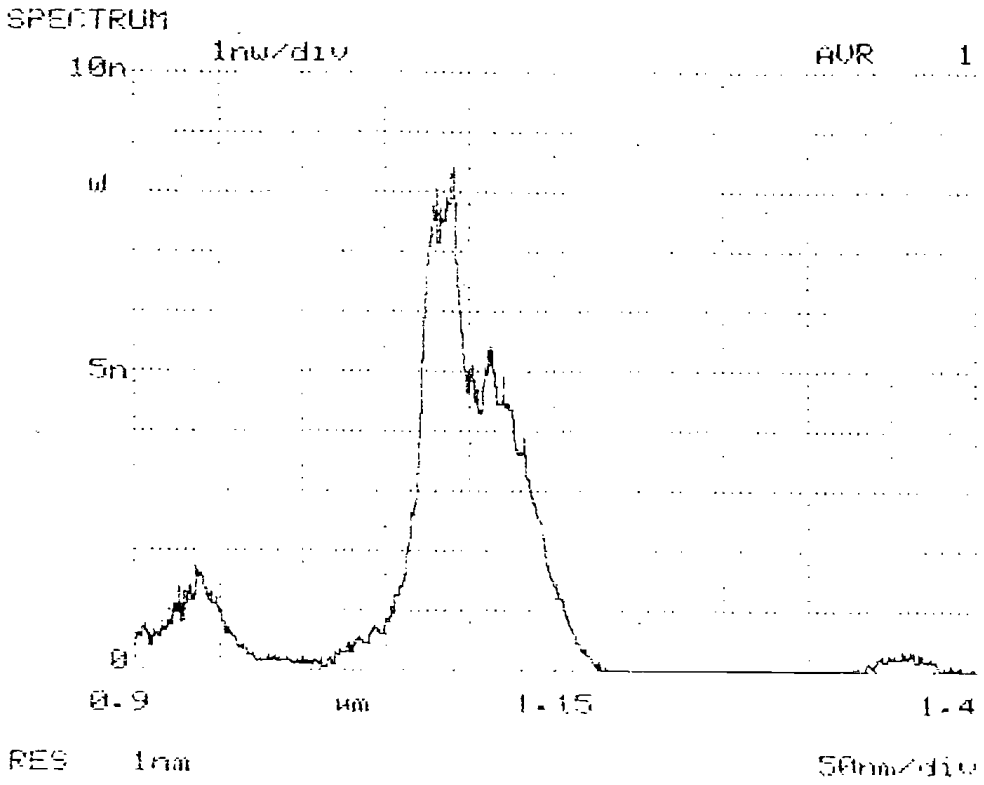

Fig.2.6 Fluorescence spectrum of neodymium in silica-based fibre.
Fibre sample: ND199

between passive and active fibres which makes the latter possess special polarisation properties at the lasing wavelength.

There are two cases to be considered for active fibres. One is the amplifier, and the other is laser oscillator. When an active fibre acts as a traveling-wave amplifier, the population inversion is stimulated by the signal traveling through the pumped fibre. In the fibre laser oscillator, the lasing action is built up from the amplified fluorescence, and the system starts to oscillate if the feedback is sufficiently large to compensate for the internal and external losses of the system.

According to quantum theory, stimulated emission provides a phase-coherent amplification mechanism for an applied signal. The signal extracts from the atoms a response that is directly proportional to, and phase-coherent with, the electric field of the stimulating signal. Thus the amplification process is phase-preserving. The stimulated emission is in fact completely indistinguishable from the stimulating radiation field. In other words, the stimulated emission has the same directional properties, polarisation, phase, and spectral characteristics as the stimulating signal.

It follows that the polarisation state of the amplified signal from a single-mode traveling-wave amplifier is determined by both the fibre birefringence and the polarisation state of the applied signal.

The situation in a fibre laser with a resonant cavity is more complicated. Since the laser oscillation is triggered by the noise of some spontaneous radiation emitted along the active fibre, a fibre laser oscillator will have a substantially different polarisation behaviour from the passive fibre. Equation (2.9) will not be valid for the lasing light due to the absence of the phase correlation with the pump. There is no existing answer to the following questions: how many,

and which, polarisation orientations can the oscillation be built-up from; what is the phase relation between those oscillations with different polarisation orientations if more than one oscillation exist? To search for the answer is one of the aims of this doctoral study.

Last, but not least, in spite of the total memory of the pump polarisation, the influence of the pump polarisation on the polarisation of lasing light must be understood. In the active process, there are two steps dealing with the polarisation interaction between pump and lasing light. The first interaction is between the gain ions in the glass fibre and the electric field of the pump, leading to inversion of the electron population or energy storage in the upper laser level. The second one takes place during stimulated emission, and is between gain ions with electrons in the upper laser level and the stimulating field, either due to a traveling signal or spontaneous emission. Owing to the longitudinal pump system, as described above in the Section 2.1 of this chapter, the fibre laser offers for the first time the opportunity of investigating such an interaction during the process of lasing action in the glass laser family.

If the study is confined to non-Zeeman effects, there is no spontaneous emission with a circular polarisation involved. Furthermore, the lasing action in a Fabry-Perot cavity is always related to a round trip in the cavity, and the circular birefringence caused by the twisting is reciprocal[10], Thus the local orientation of linearly-polarised light propagating backward is identical with the original light propagating forward. Consequently, the effect of the circular birefringence presented by the single-mode fibre on the laser performance, with a Fabry-Perot cavity, can be ignored, provided a local coordinate system fixed in the fibre instead of the laboratory

coordinate system is used to describe the propagation of the light along the fibre.

References to Chapter 2

[1] A.K. Levine: "Lasers", Volume 2, Edward Arnold Ltd., London, 1968.

[2] M. Born and E. Wolf: "Principles of Optics", Pergamon, London, 1970.

[3] M.J. Weber: "Laser excited fluorescence spectroscopy in glass", Chapter 6 of "Laser spectroscopy of solids", Spriger-Verlag, Berlin, 1981.

[4] F.P. Kapron, N.F. Borrelli and D.B. Keck, "Birefringence in dielectric optical waveguides", IEEE J. Quantum Electron., Vol. QE-8, No.2, pp.222-225, 1972.

[5] D.N. Payne, A.J. Barlow and J.J.R. Hansen, "Development of low- and high-Birefringence optical fibres", IEEE J. Quantum Electron., Vol. QE-18 No.4 pp.477-488, 1982.

[6] L.B. Jeunhomme: "Single-Mode Fibre Optics: Principles and Applications", Marcel Dekker Inc., New York/Basel, 1983.

[7] R. Ulrich and A Simon: "Polarazation optics of twisted single-mode fibres", Appl. Opt. 18(13), pp.2241-2251, 1979.

[8] A.M. Smith: "Birefringence induced by bends and twists in single-mode optical fibre", Appl. Opt. 19(15), pp.2606-2611, 1980.

[9] F.P. Payne, D.N. Payne and M.P. Varnham: "Crosstalk in polarisation-maintaining fibres", Proc. 11th ECOC, Barcelona, 1986.

[10] A. Papp, H. Harms "Polarization optics of index-gradient optical waveguide fibres", Appl. Opt. 14(10), p.2406, 1975.

Chapter Three
BASIC FACTORS GOVERNING POLARISATION EFFECTS IN FIBRE LASERS

3.1 Three Basic Factors

The experimental investigations of various fibre lasers containing different rare-earth ions, including Nd^{3+}, Er^{3+} and Sm^{3+} dopants, show that all these rare-earth-doped, silica-based glass fibre lasers demonstrate some general polarisation properties. Such polarisation effects in fibre lasers can be characterised by three basic factors:

(1) The fluorescence from spontaneous emission is depolarised independently of the polarisation of the pump light.

(2) Two orthogonal, phase-independent, linear polarisation eigenmodes exist in "single-mode" fibre laser cavities, with different thresholds, slope efficiencies and relaxation oscillation frequencies.

(3) The state of polarisation of the output from the fibre laser depends on the polarisation of the pump light, the pump level and the dopant characteristics. The degree of polarisation (DOP) of the laser output can be expressed as the following function:

$$DOP = f(P_{ab}, a)\cos(2\alpha) \qquad (3.1)$$

where α is the angle the linearly-polarised pump light makes to the x-axis, P_{ab} is the absorbed pump power and "a" is a parameter introduced to describe the property of dopant ions in a particular fibre relating to the polarisation effects.

3.2 Experimental Arrangements

The experimental arrangement for investigating the polarisation effects in CW fibre lasers is schematically

illustrated in Fig.3.1(a). A compensator with a high optical quality was employed as a $\lambda/2$ or $\lambda/4$ element alternatively for a certain wavelength of the linearly-polarised pump source. The laser cavity was formed by cleaved fibre ends butted against dielectric mirrors. The input mirror M1 had a high transmission at the pump wavelength (T>85%) and a high reflectivity at the lasing wavelength (R>99%). The output mirror M2 had a high reflectivity at the pumping wavelength, while the reflectivity R_2 at the lasing wavelength was chosen according to the experimental requirements. A prism polariser having a extinction ratio of 50dB was located into the output beam path of the fibre laser. Since a longitudinal pumping system is used, a suitable optical filter is sometimes required to block the undesired wavelength(s).

In order to observe relaxation oscillations of the fibre laser, a mechanical chopper needed to be inserted into the pump beam path. For some other experiments, in which a certain intracavity device or component was involved, it was necessary to expand the intracavity beam using a low loss (<0.2dB) lens, as shown in Fig.3.1(b).

3.3 Fluorescence Depolarisation

Previously, the studies on polarised fluorescence line-narrowing measurements of Nd laser glasses[1,2] revealed the fluorescence depolarisation in two compositionally different glasses: LG-650, a small cross-section potassium-barium silicate, and LG-670 (Owen-Illinois ED-2) a larger cross-section lithium aluminium silicate. In their experiments, linearly-polarised light was used to excite the samples. The polarisation-resolved fluorescence intensities were measured in a right-angle excitation-observation geometry. Both resonant and non-resonant excitation-observation wavelengths were observed. In terms of the depolarisation ratio defined as

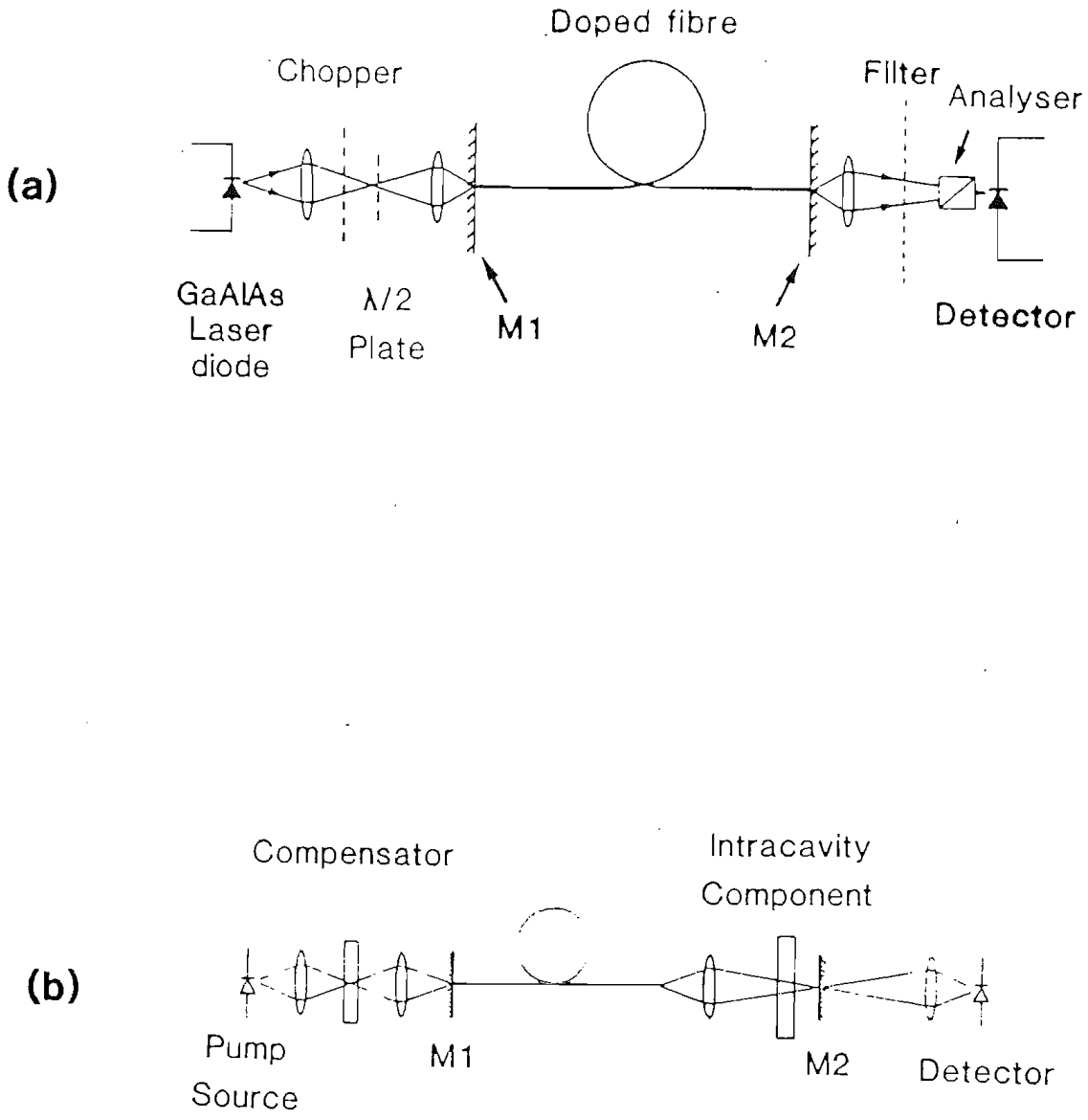

Fig.3.1 Schematic of experimental arrangement for investigating polarisation effects in fibre lasers.

$$\rho = I_s/I_p \qquad (3.2)$$

where I_p and I_s represent the fluorescence intensities polarised parallel with, and perpendicular to, the excitation polarisation, respectively. The measured values of ρ=0.92~0.96 (equivalent to DOP=0.02~0.04) for the non-resonant transition, and ρ=0.88~0.89 for the resonant transition, respectively, were reported.

To investigate the polarisation properties of the fluorescence from spontaneous emission of rare-earth doped fibres, a parallel excitation-observation geometry was employed. The set up of the measurement is similar to that illustrated in Fig.3.1(a) except for the absence of input and output mirrors. Since the measurements deal with the non-resonant transitions, a suitable filter is needed to stop the residual pump light. Also, a short length of fibre and a lower pump level is required to avoid the influence of the superfluorescence, which may be stimulated by those parts of fluorescence intensity guided along the fibre. Under these conditions, a variety of fluorescence, corresponding to certain transitions from Nd^{3+}, Er^{3+}, and Sm^{3+}-doped fibres, have been observed.

The main results of the measurements are summarised in Table 3.1, where the pump wavelengths of the non-resonant excitation are also listed. Due to the different measurement geometry from that for the bulk glasses, the parameter DOP instead of the depolarisation ratio ρ is applied to describe the depolarisations.

It can be seen from Table 3.1 that the fluorescence radiation of the rare-earth doped fibre mentioned above is almost completely depolarised. In addition, the phenomenon of the fluorescence depolarisation seems independent of the polarisation state of the pump light. In the experiments, both circularly, and linearly, polarised light were applied as pump sources, and the orientation of the linearly-polarised light was rotated

Fibre sample	ND518-08		ND425	ND501	ND546-05
Dopant Concentration	Nd 4500ppm		Nd 300ppm	Er 150ppm	Sm 700ppm
Transition	*		*	**	***
Pump source Wavelength(μm)	LD 0.82		LD 0.82	Dye 0.65	Ar^+-ion 0.51
Fibre length (cm)	25	7	1.7	1.5	1.2
Fluorescence Depolarisation	0.98	0.99	0.96	>0.99	>0.99
DOP	0.01	0.005	0.02	<0.005	<0.005

* $^4F_{3/2} - {}^4I_{11/2}$
** $^4I_{13/2} - {}^4I_{15/2}$
*** $^4G_{5/2} - {}^6H_{9/2}$

Table 3.1 Summarised measurements showing the fluorescence depolarisation for various rare-earth ions in glass fibres.

by a $\lambda/2$ plate. No significant difference was observed, within the experimental accuracy, in all the cases.

In order to compare the light of three different wavelengths, involved in fibre lasers, the pump, the fluorescence and the lasing light, under an identical experimental condition, a Nd^{3+} laser pumped by an Ar^{+}-ion laser operating at 514.5nm was set up. The fibre was 2.5m long. An extreme case, namely $\alpha=0$, was chosen for making the residual pumping light reach the maximum DOP. When measuring the fluorescence depolarisation, the fibre was slightly spaced from the output mirror in order to stop the lasing action. The experimental results are shown in Fig.3.2. The maximum DOP of the fluorescence from the spontaneous emission of $^4F_{3/2}$—$^4I_{11/2}$ was measured as only 0.02, compared with 0.98, the DOP of the residual pumping light, which was measured at the lasing stage of the fibre laser. Also shown in Fig.3.2 is the DOP of the lasing light from the fibre laser.

Table 3.1 and Fig.3.2 show significant evidence of the depolarisation of fluorescence from spontaneous emission of rare-earth ions in silica-based fibres. The results are believed to be reasonable as they agree with the measured figures for the bulk glasses containing Nd^{3+} dopant. Such an agreement of the experimental results indicates that the fluorescence depolarisation is one of the general properties of rare-earth ions in glasses. It seems that the pumping light can retain its polarisation property of high DOP although it has been heavily attenuated during the pumping process. The measurements also indicate that there is no obvious effect of the superfluorescence on the fluorescence depolarisation within the pump levels applied in the experiments. The decreasing DOP of the lasing light as a function of pump power shows an unusual polarisation behaviour which is different from the depolarisation phenomenon of the fluorescence, implying a special mechanism which plays a role in the polarisation effects.

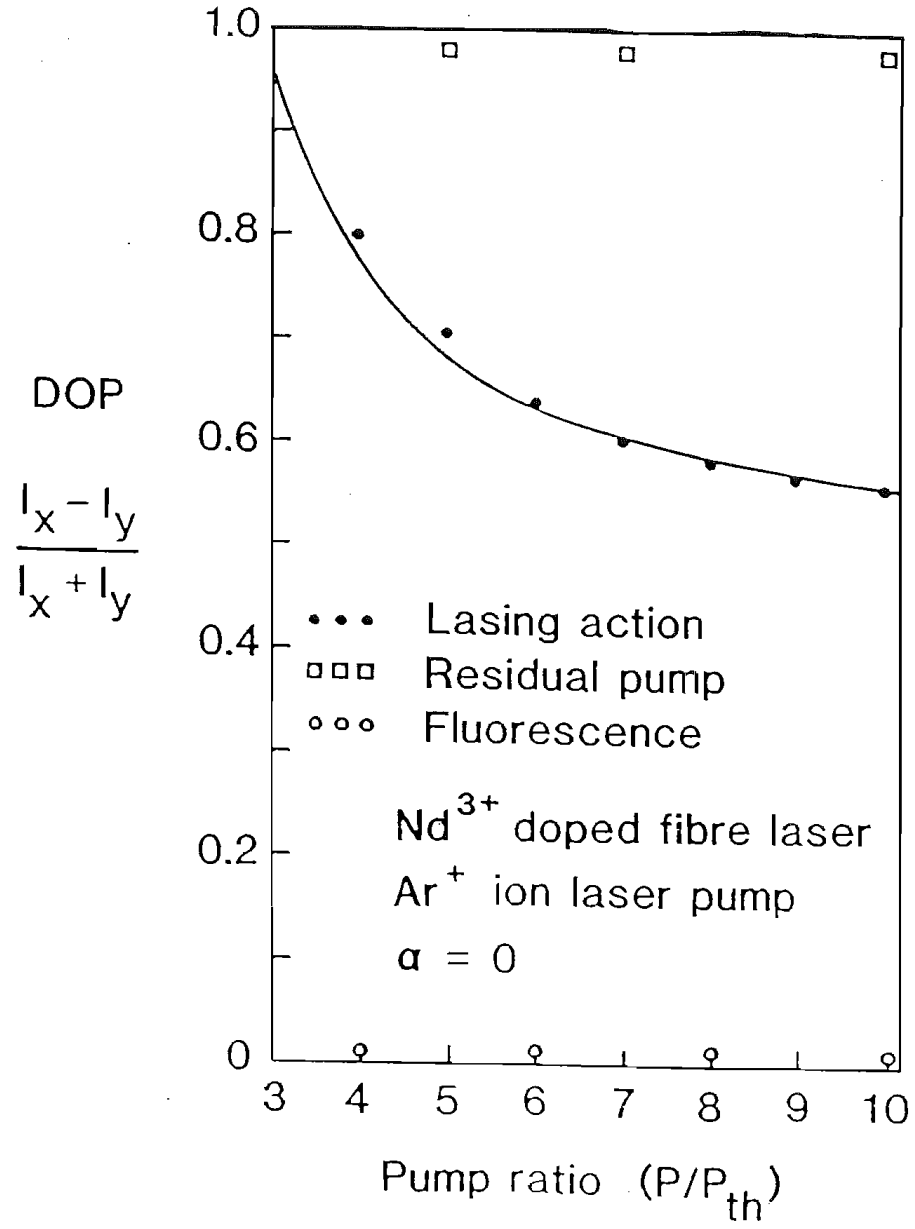

Fig.3.2 Measurements showing fluorescence depolarisation, retained polarisation of the residual pump, and the DOP of the laser output, as a function of the relative pumping power.

3.4 Two Orthogonal Polarisation Eigenmodes

(1) Existence of orthogonal polarisation eigenmodes

The experimental investigations show that two orthogonal, phase-independent, polarisation eigenmodes exist in every fibre laser cavity. The clearest way to prove this is to observe the relaxation oscillation pattern of the output from a fibre laser, since it is believed that only those photons which belong to the same mode make a contribution to a perfect relaxation oscillation pattern.

By using a chopper inserted into the pump beam path and a polarisation analyser in the laser output beam, as shown in Fig.3.1(a), a variety of fibre lasers have been investigated and the results are as follows.

Just above the lasing threshold, a pure damped sinewave-shaped trace of the relaxation oscillation can be observed from the oscilloscope, as shown in Fig.3.3(a), which was taken for a Nd fibre laser pumped by a semiconductor laser diode, indicating a pure single mode operation. As the pump power is increased, the relaxation oscillation pattern becomes more complex. It is found that the complex pattern is composed of two orthogonal, pure relaxation oscillation patterns. If the analyser is adjusted to a suitable position, namely the extinction position of the stronger mode, which appears first, the secondary mode relaxation oscillation can be clearly exhibited as shown in Fig.3.3(b), which was taken with the analyser adjusted close to the extinction position of the stronger mode. The secondary mode was found to have an exactly orthogonal polarisation orientation to the preliminary mode according to the analyser reading.

The same phenomenon can be observed in Er^{3+} and Sm^{3+}-doped fibre lasers. It is thus concluded that two orthogonal polarisation eigenmodes exist in a "single mode" fibre laser cavity, they have different relaxation

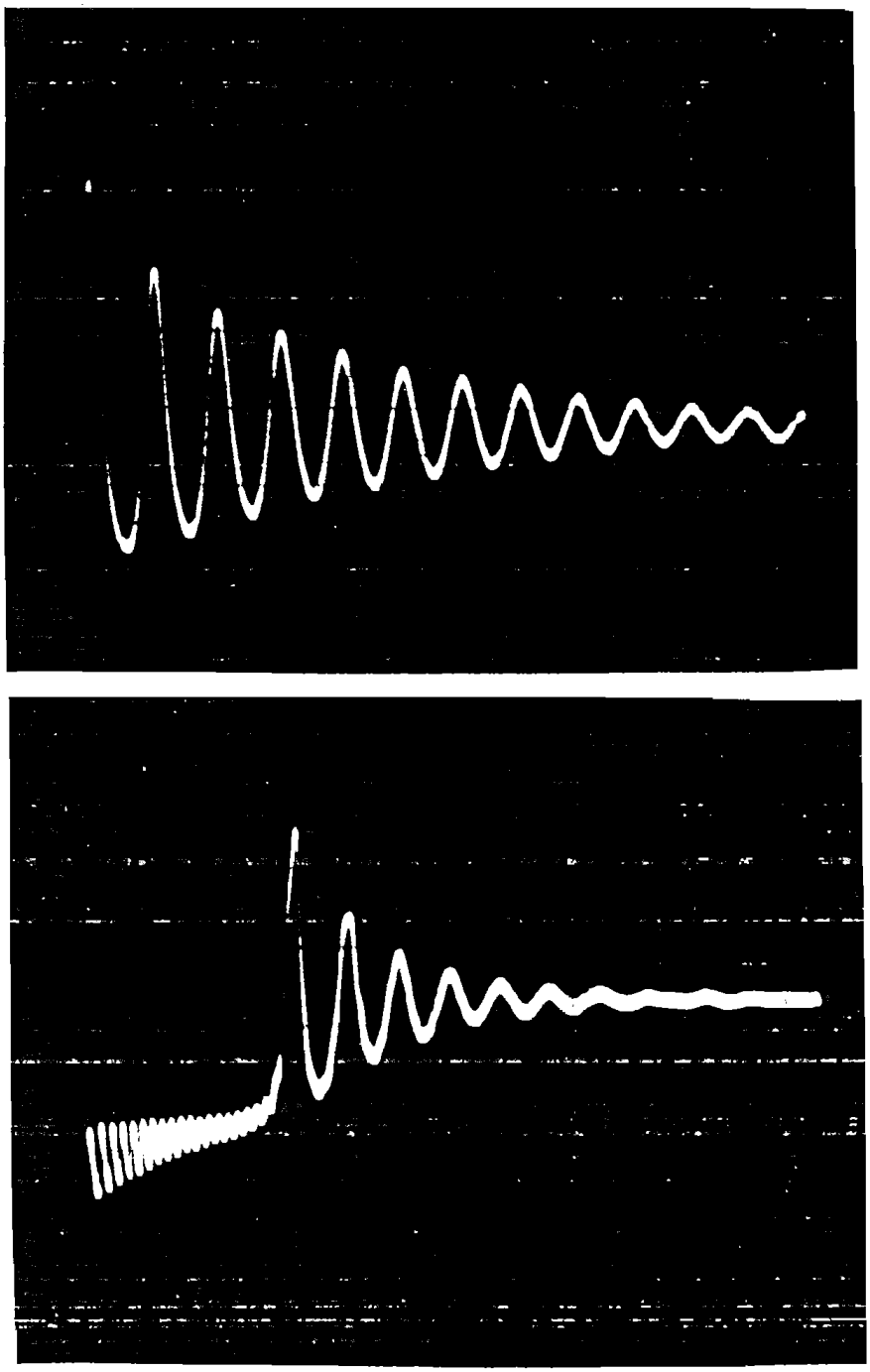

Fig.3.3 Relaxation oscillations showing the existence of two orthogonal polarisation eigenmodes.
(a) Single-mode relaxation oscillation
(b) Double-mode relaxation oscillation

oscillation frequencies, different build-up times and thresholds.

(2) Orientation of orthogonal eigenmodes

In order to determine whether the orientations of these two orthogonal polarisation eigenmodes are fixed in space or depend upon the pump polarisation, experiments were designed with a rotatable linearly-polarised pump source by using a $\lambda/2$ plate, as shown in Fig.3.1(a). Obviously, the best way to find the orientation of the preliminary polarisation eigenmode is to measure the analyser reading for the extinction position according to the relaxation oscillation patterns on the oscilloscope screen. This method was used in all the experimental studies in the thesis.

One of the experiments was carried out with a laser cavity formed by a 3m length of Nd^{3+}-doped (ND199-05) fibre wound on a drum of diameter d=11cm. Using a suitable filter, lasing light at 1.08μm was measured and is plotted in Fig.3.4, where the orientation of the stronger or preliminary mode is shown as a function of the pump orientation. It can be seen from Fig.3.4 that the lasing light at 1.08μm retains the fixed orientation of maximum output when the input polarisation angle of pump light is varied from 0° to 45°. On the other hand, when the input polarisation angle of the pump light was rotated by more than 45°, the maximum axis for lasing light became the minimum axis, which means that the axes of preliminary and second eigenmodes are exchangeable and can be switched by the polarisation orientation of the pump light.

To search for the relation between the orientation of the polarisation eigenmodes and the birefringent axes of the cavity fibre the latter were measured using the residual pumping light, with which the laser fibre works as a passive fibre. The results are also shown in Fig.3.4, where the orientation of the major axis for the ellipse of the residual pump light at 0.82μm is plotted

as a function of the pump orientation. As shown before in Chapter 2, the polarisation of the residual pump light is determined by the polarisation of the input pump radiation. When a correct origin is chosen for the diagram according to eq.(2.9), as done in the Fig.3.4, the birefringent axes of the single-mode fibre can be determined. From Fig.3.4, as well as experiments performed for different dopant lasers, it can be concluded that the orientations of the lasing polarisation eigenmodes are coincident with the birefringent axes of the cavity fibre.

(3) Different slope efficiencies

Fig.3.5 shows the polarisation-resolved power output from a fibre laser as a function of pump power for two different pump polarisation orientations. The Nd^{3+}-doped fibre laser was pumped by an Ar^{+}-ion laser operating at 514nm, and the 40m-long fibre cavity had a conventional design and the fibre contained 30 ppm of Nd^{3+}-ions. Both individual polarisation outputs have a linear relation with the total absorbed pump power. When the pump polarisation is aligned with the fibre principal axis, i.e. $\alpha=0$, it can be seen that a considerable difference exists in the thresholds and slope efficiencies of x and y polarised modes. However, the differential slope efficiency is strongly dependent on the pump polarisation. As shown in Fig.3.5, when $\alpha=45^{o}$ to the fibre principal axes, the characteristics of the two polarisation eigenmodes are almost identical.

(4) Phase independence of the eigenmodes

The dependence of fibre laser output power on orientation angle was also measured in order to verify the phase independence of the two eigenmodes. The measurements are given in Fig.3.6, where two theoretical curves are also shown for comparison. The idea behind this comparison is simple. If two polarisation components have a certain phase relationship, the output

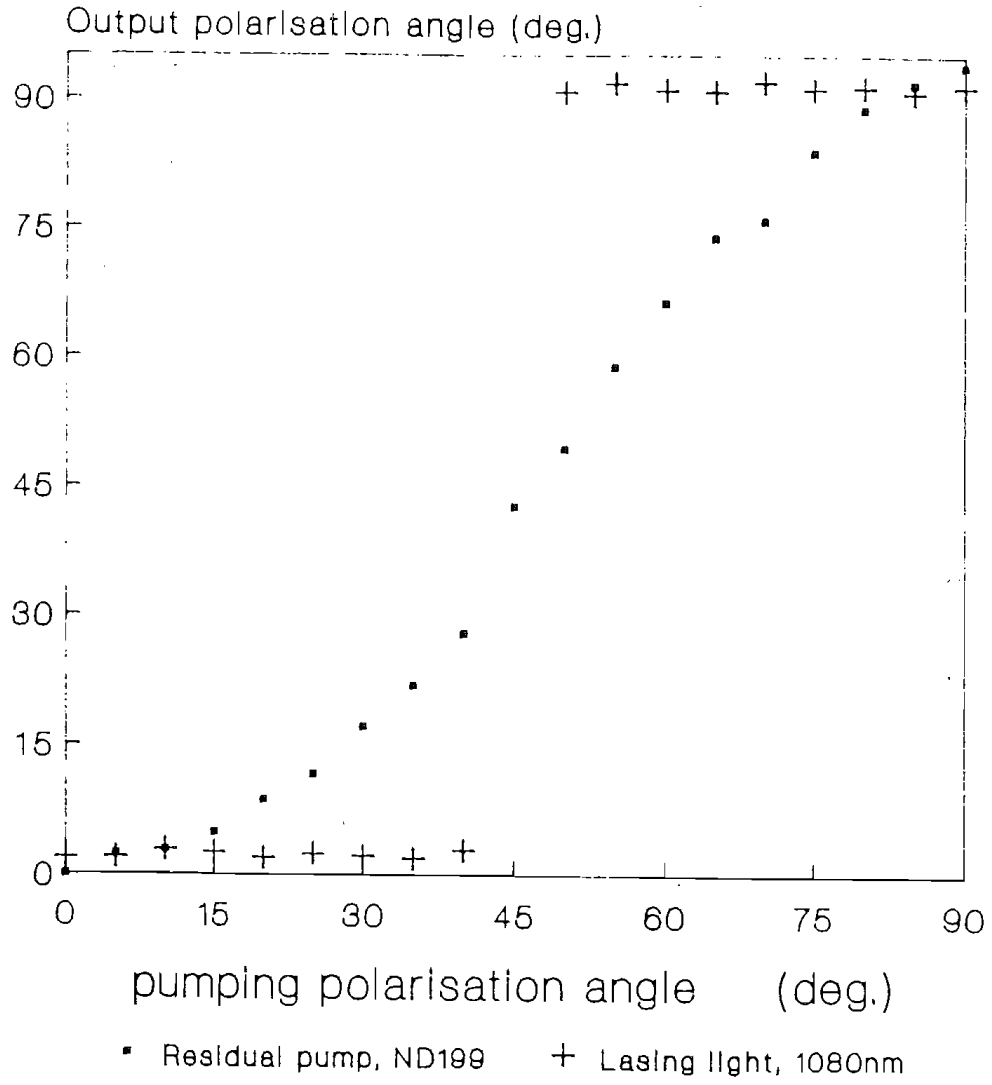

ND199-03: 3m
pump: 814nm

Fig.3.4 Measurements showing the fixed principal axes of two polarisation eigenmodes.

will consist of elliptically-polarised light and the optical intensity will follow the equation

$$R = I_x I_y / (I_y \cos^2\theta + I_x \sin^2\theta) \qquad (3.3)$$

which is derived from the ellipse equation

$$\frac{\rho^2 \cos^2\theta}{a^2} = \frac{\rho^2 \sin^2\theta}{b^2} \qquad (3.4)$$

In (3.3) and (3.4), $R=\rho^2$ is the optical intensity and $I_x=a^2$ and $I_y=b^2$ are the intensities of the major and minor axes of the ellipse, respectively. In contrast, if there is no phase relationship between the two eigenmodes, the intensity as a function of θ will be

$$R = I_x \cos^2\theta + I_y \sin^2\theta \qquad (3.5)$$

The experimental data is in very good agreement with (3.5), as shown in Fig.3.6.

It is worth pointing out that all the experiments were carried out under the condition that the optical path difference between the two eigenmodes in the laser cavity is smaller than the coherence length of the pump source. For example, the single-longitudinal-mode, semiconductor laser diode operating at 825nm with a spectrum width of $\Delta\lambda$=1nm has a coherence length $L_c=2\pi\lambda^2/\Delta\lambda=4\cdot10^{-3}$m, while the fibre used in the experiment has a beat length of 5cm corresponding to $\Delta n=1.7\cdot10^{-5}$ and the optical path difference for the 3m long fibre is about $5\cdot10^{-5}$m.

The above experiment, together with the fixed orientation of the lasing modes and the independence of the slope efficiency for an individual lasing mode, prove the phase independence of the polarisation eigenmodes. It means that the two orthogonal polarisation eigenmodes will have lost their phase correlation with the pump light, as analysed in Chapter 2, and can establish their

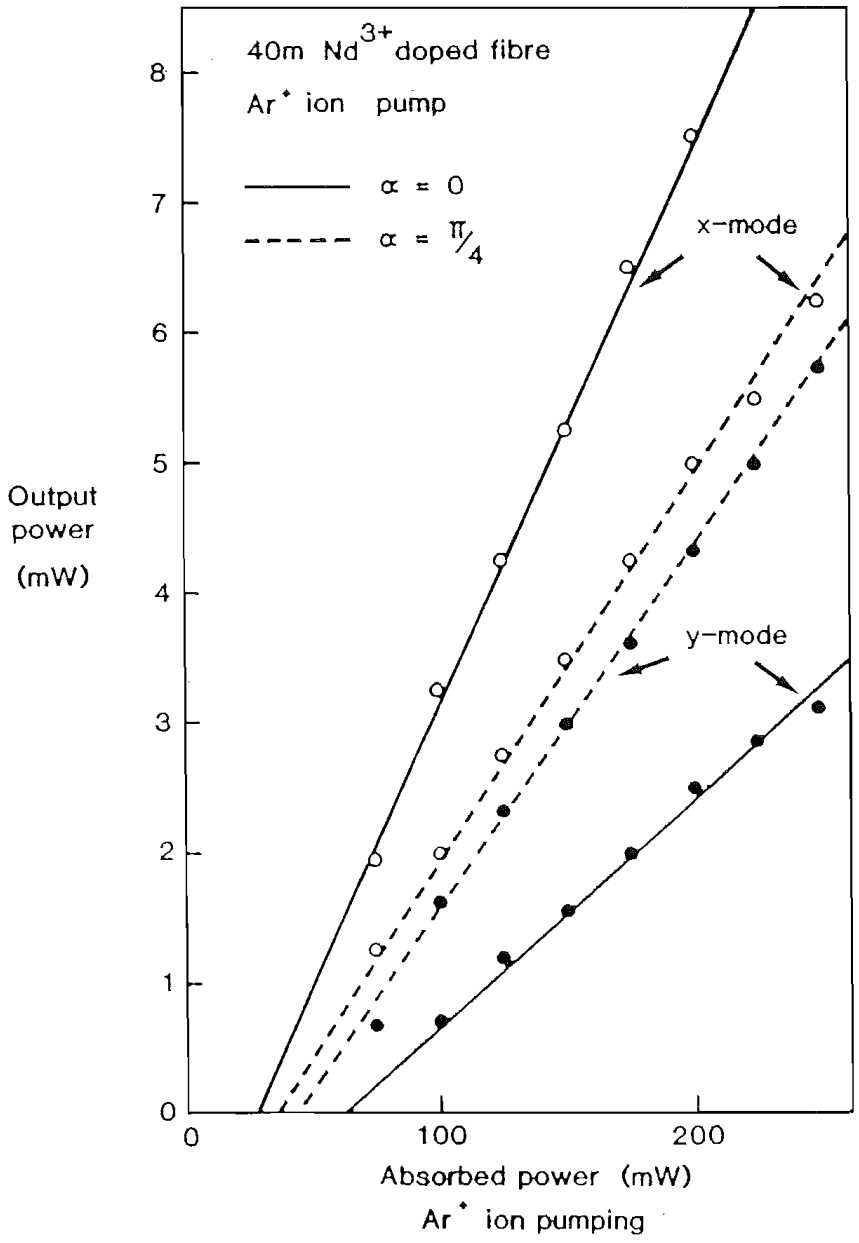

Fig.3.5 Lasing characteristics of two polarisation eigenmodes for two pump polarisation angles.

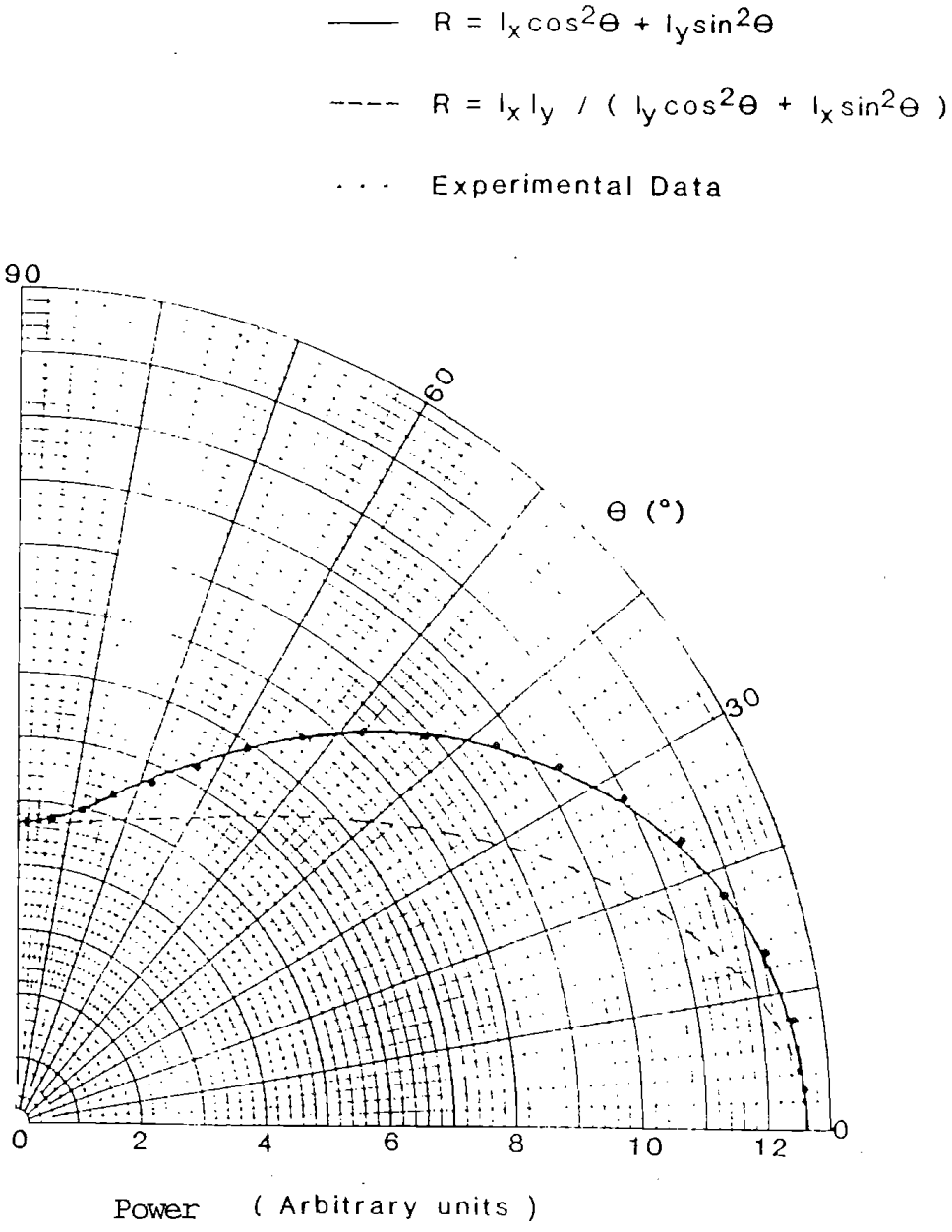

Fig.3.6 Dependence of fibre laser output on orientation angle verifying the phase independence of the two orthogonal polarisation eigenmodes.

own phase-independent lasing actions by the noise of the fluorescence of each mode.

(5) DOP of the individual polarisation eigenmode

There are two facts which affect the degree of polarisation of an individual lasing eigenmode in the fibre laser cavity. The first is the polarisation purity of the stimulated emission, and the second is the cross polarisation.

In a passive single mode fibre, the general form of equations governing the mode coupling between $E_1(z)$ and $E_2(z)$ of the eigonmode fields is[3]

$$\frac{dE_{1o}(z)}{dz} = j\frac{\Delta\beta}{2}E_{1o}(z) + \frac{C}{2}E_{2o}(z) \qquad (3.6a)$$

$$\frac{dE_{2o}(z)}{dz} = -j\frac{\Delta\beta}{2}E_{2o}(z) - \frac{C^*}{2}E_{1o}(z) \qquad (3.6b)$$

where E_{1o} and E_{2o} are the amplitudes of the fields E_1 and E_2 respectively, C is a coupling coefficient, the symbol "*" stands for the complex conjugate, $\Delta\beta$ is the difference of the propagation constants defined as in (2.2), and a common phase factor equal to $(-j\beta z)$ has been omitted in the diagonal term. In the case of linear birefringence and twist, C can be expressed as[3]

$$C = (2+g)2\pi N \qquad (3.7)$$

Assume that at the fibre input only $E_{1o}(0)=1$ is launched, and $E_{2o}(0)=0$. After a length l of fibre, $|E_{2o}(l)|^2$ represents the intensity on the unwanted polarisation or cross-polarisation. From eqs.(3.6), we obtain

$$|E_{2o}(l)|^2 = \frac{C^2}{\Delta\beta^2 + C^2}\sin^2\left[l\left(\frac{\Delta\beta^2 + C^2}{2}\right)^{1/2}\right] \qquad (3.8)$$

In the case of a fibre laser, as listed in Table 2.1, $\Delta\beta$ varies from 10^2/m to 10^3/m, whereas the twisting is carefully avoided, so that a very small $|E_{2o}(l)|^2$ is expected. For example, if the fibre is twisted by one turn/metre, C is then about 10, and the cross polarisation is about -20dB for a ordinarily designed fibre or -40dB for a fibre of high birefringence.

In principle, it is expected, as described in Chapter 2, that a lasing mode should consist of pure linearly-polarised light. To verify this in the case of a fibre laser an experiment was arranged to measure the DOP of a lasing mode. The laser cavity was formed by a 3m long ordinarily designed fibre containing Nd^{3+} dopant. A polarised beam-splitter having an extinction ratio of 25dB was inserted into the laser cavity, which had been expanded by a low loss lens, as shown in Fig.3.1(b). The polarised beam-splitter was orientated with a pass-through position coincident with the axis of the preliminary mode, say the x mode. Since the beam-splitter deflects the y component out of the cavity no lasing action of the y mode can occur, whereas the x mode can still lase with a output mirror of 80% reflectivity. The lasing light of the x mode, and the signal of the y mode, were detected, respectively, and displayed on the same screen of an oscilloscope for comparison.

Fig.3.7 shows the result for a pump ratio $P/P_{th}=1.2$. By using the mathematical relation between the output power and the intra-cavity intensity of the lasing mode[4], the intra-cavity intensity of the x mode was calculated. After calibration the intensity ratio of the x and y modes was found to be 250/1, equivalent to 23dB of extinction ratio.

This result indicates that the linearly-polarised lasing mode in the fibre laser cavity has a high polarisation purity. Even with an ordinarily designed fibre laser, no obvious polarisation mode coupling was measured, and thus the polarisation cross-talk is negligible in most cases.

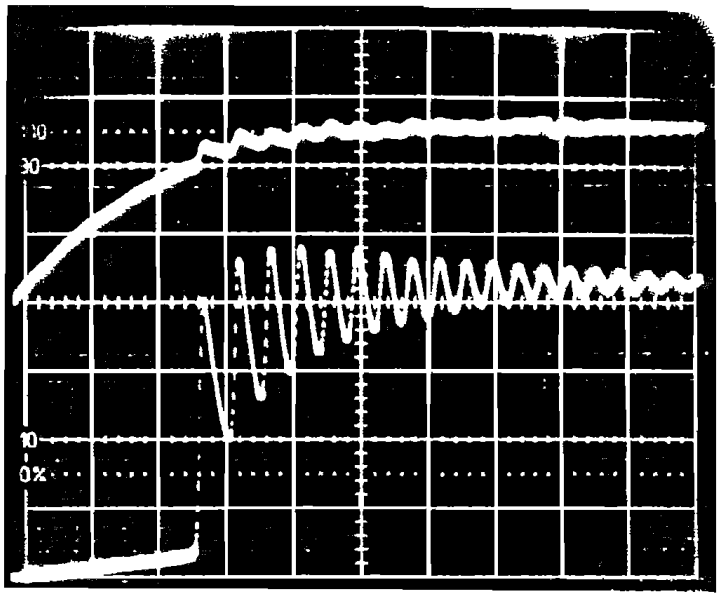

Upper trace: the y-mode at fluorescence stage (2mW/div., 150kΩ load).
Lower trace: the x-mode measured with a 80% reflectivity output mirror (50mV/div., 210kΩ load).
Time domain: 0.2ms/div.

Fig.3.7 Polarisation purity of linearly-polarised mode in a Nd^{3+}-doped fibre laser.

3.5 Dependence of Polarisation State on Pump and Dopant

Apart from the fact, as described above, that the axes of the two polarised modes can be exchanged by rotating the pump orientation, the relation between the polarisation state of the output from the fibre lasers and the pump orientation was also investigated with the experimental set-up shown in Fig.3.1(a).

(1) $\cos(2\alpha)$ function

The DOP of the laser output was found to be a cosine function of twice of the launching angle, $\cos(2\alpha)$, when the laser operates with both polarisation eigenmodes lasing simultaneously. Typical measurements for Nd and Er fibre lasers are shown in Figs.3.8 and 3.9 respectively. Since the polarisation eigenmodes are phase-independent of each other, the $\cos(2\alpha)$ function of the DOP reflects the phenomenon that the distribution of the output power from fibre laser among both eigenmodes is related to the polarisation orientation of the linearly polarised pump.

(2) DOP as a function of pump power

In addition, the DOP of the laser output was found to be a decreasing function of the absorbed pump power. Fig.3.10 shows three cases with different pump conditions for a Nd laser pumped by an Ar^+-ion laser. At a lower pump level, the fibre laser has an output DOP as high as 0.98, when pumped on one of birefringence axes of the fibre. This corresponds to the stage of single polarisation operation. When the pump power is increased, the DOP of the laser output decreases, apparently because the secondary polarisation mode has started lasing and contributing to the laser output. Far above threshold, the DOP of the output from fibre laser is flattened and reaches a certain value. The tendency of DOP to decrease with increase of the pump power can also been seen in Fig.3.2.

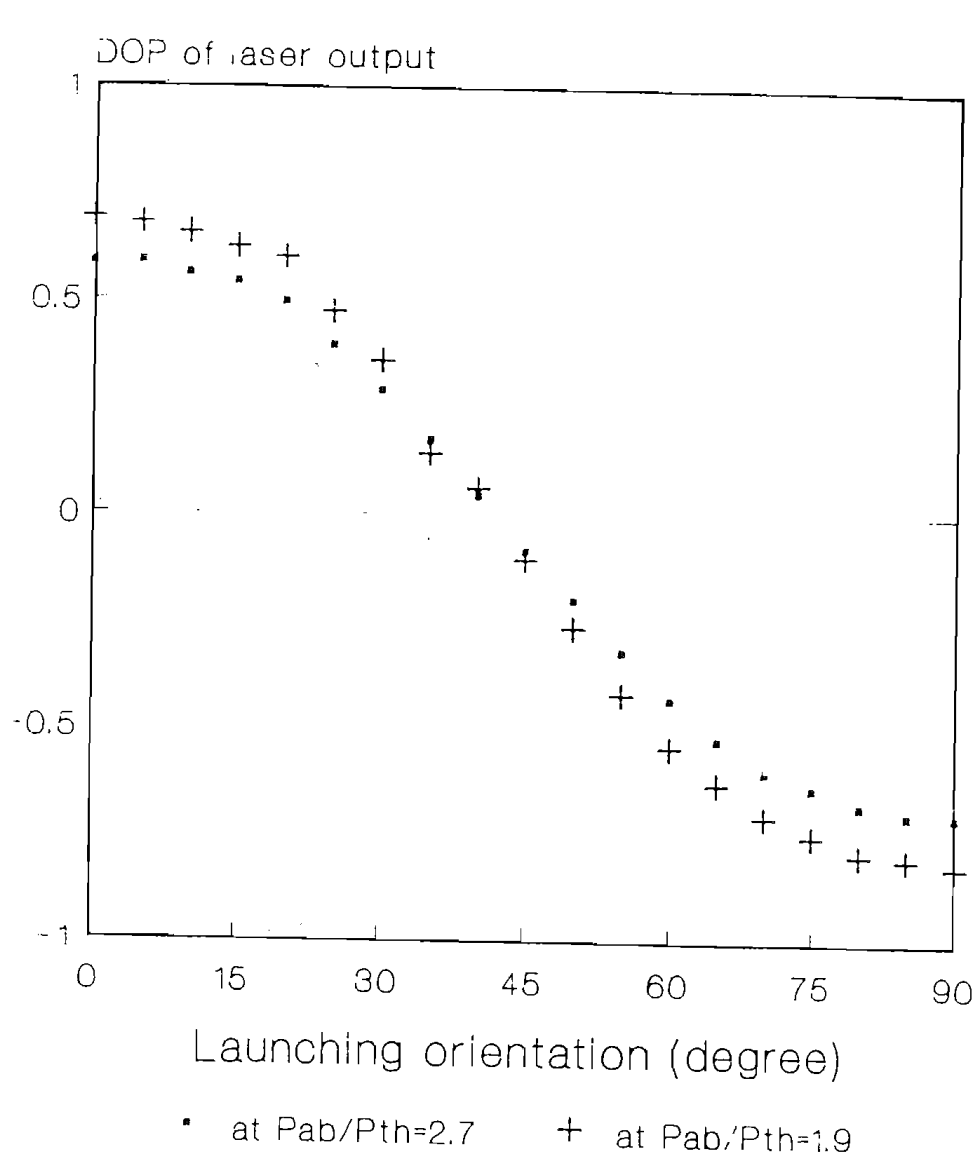

ND425, 2m, pp.37-38

Fig.3.8 Dependence of the degree of polarisation on the polarisation orientation of the launched pump light for Nd^{3+}-doped fibre laser.

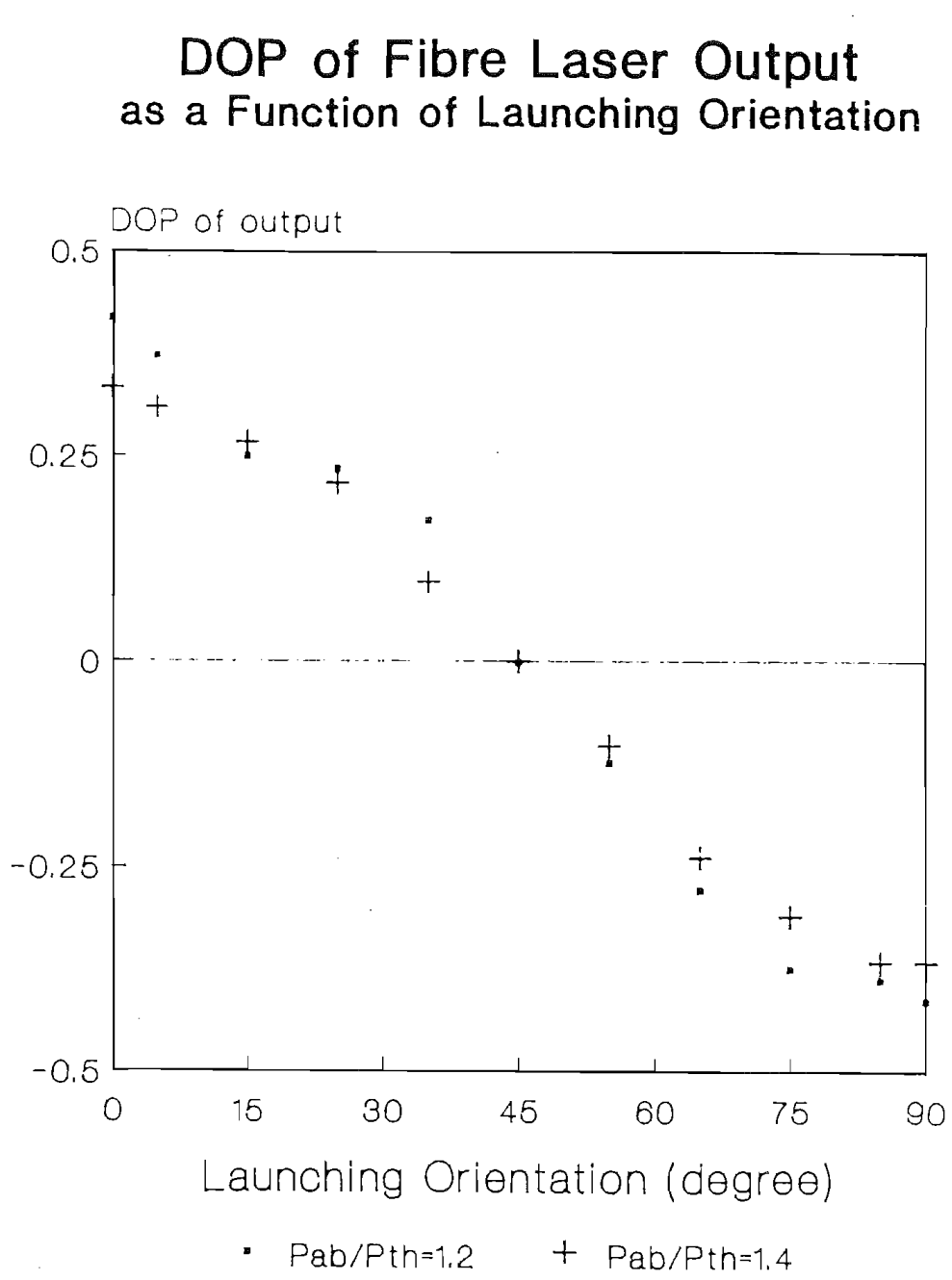

Fig.3.9 Dependence of the DOP on the polarisation orientation of the launched pump light for Er^{3+}-doped fibre laser.

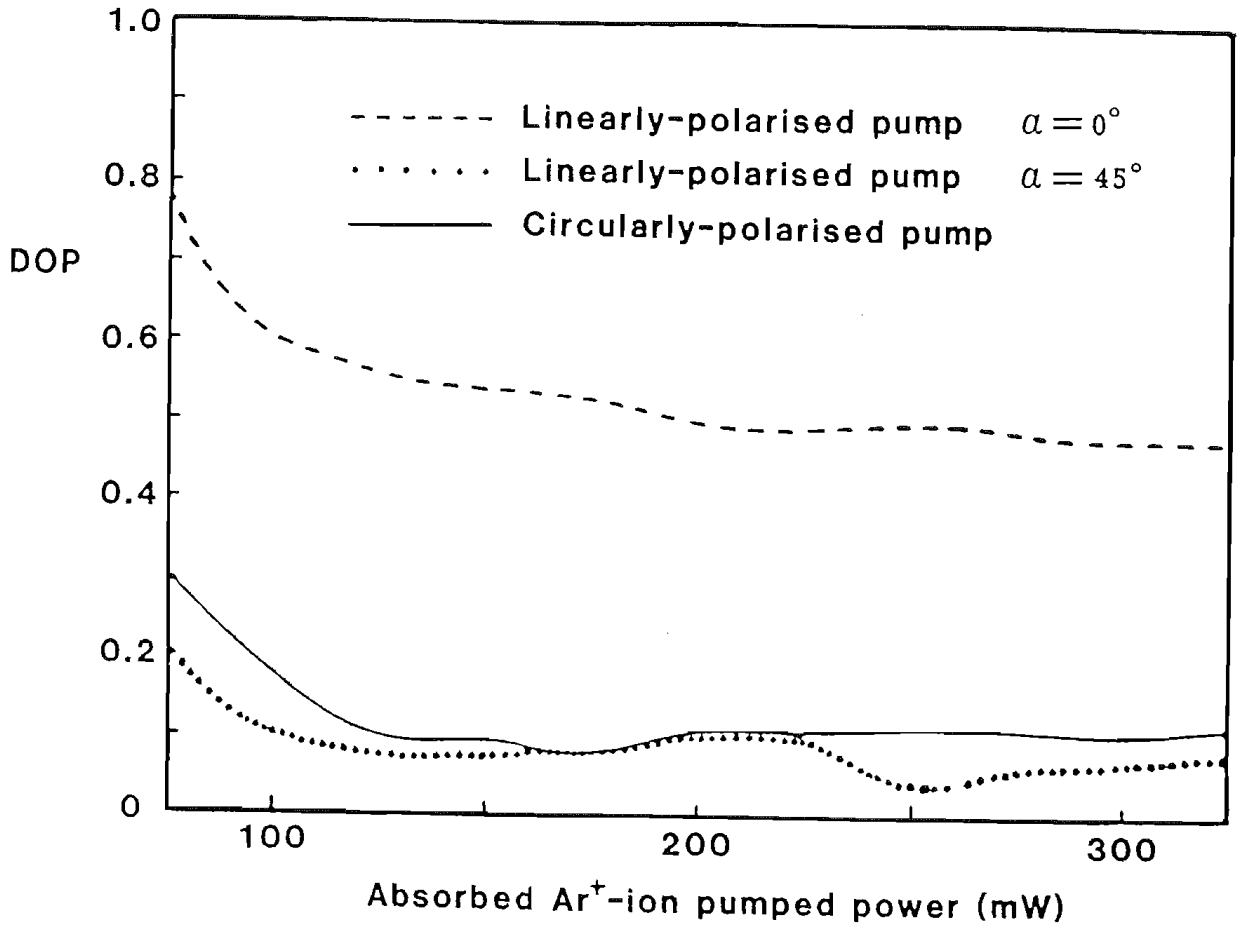

Fig.3.10 Degree of polarisation of fibre laser output versus absorbed pump power for various pump polarisations.

(3) Dependence of DOP on dopant characteristics

Although a $\cos(2\alpha)$ function of the DOP was measured for various fibre lasers with different dopants the magnitude of the DOP was found to be dependent on the dopants. For example, a limitation value of the DOP, 0.5, was measured for a Nd fibre laser far above threshold, whereas a value of 0.3 for a Er laser under the same condition was measured, as shown in Fig.3.9.

By combining these factors, the DOP of fibre laser output can, therefore, be expressed as:

$$DOP = f(P_{ab},a)\ \cos(2\alpha) \qquad (3.1)$$

3.6 Discussions

Although fluorescence depolarisation of fibre lasers is expected as a consequence of the previous work on rare-earth doped bulk glasses, most basic factors of polarisation effects in fibre lasers exhibit, for the first time, special properties different from other laser sources. It can clearly be seen, when comparing Fig.3.10 with Fig.2.1, that a substantial difference exists between semiconductor laser diodes and fibre lasers. The DOP of the output light from the laser diode increases with a increased output power or driving level, while the fibre laser possesses an opposite behaviour. This is caused by the existence of two orthogonal polarisation eigenmodes, as described earlier in this chapter. However, there remains the question why such a phenomenon does not appear in laser diode, in which the cavity is also a light waveguide containing the possibility of two orthogonal polarisation modes.

The dependence of the polarisation state of fibre laser on the pump polarisation orientation indicates that the polarisation-selective interaction between the electric dipole of the gain ions and the applied electrical field of the pump light plays a role in the

lasing action. If the mechanism behind this phenomenon can be revealed the information on the rare-earth gain ions in glass host is then obtained.

An interpretation is needed; a specific function form of $f(P_{ab}, a)$ in eq.(3.1) is asked; and a unified theory is required.

References to Chapter 3

[1] D.W. Hall and M.J. Weber: "Fluorescence line narrowing in neodymium laser glass", J. Appl. Phys. 55(7), pp.2642-2647, April 1984.

[2] D.W. Hall and M.J. Weber: "Polarized fluorescence line narrowing measurements of Nd laser glasses: Evidence of stimulated emission cross section anisotropy", Appl. Phys. Lett. 42(2), pp.157-159, January 1983.

[3] L.B. Jeunhomme: "Single-Mode Fibre Optics: Principles and Applications", Marcel Dekker Inc., New York/Basel, 1983.

[4] W. Koechner: "Solid-State Laser Engineering", Springer-Verlag, 1976.

Chapter Four

THEORETICAL MODELLING OF POLARISATION EFFECTS IN FIBRE LASERS

This chapter is devoted to an extension of the theory. Section 4.1 concentrates on the physical basis of the polarisation effects. The glass structure, electric dipole model, the Stark effect and laser-excited fluorescence spectroscopy in glass are introduced. Based on these understanding and three basic factors governing polarisation effects in fibre lasers, section 4.2 gives a physical model of the rare-earth ions in glass fibres. In Section 4.3 a theoretical model is developed by adapting a physical concept of polarisation -dependent cross-section ratio to treat the polarisation effects in fibre lasers. An engineering parameter, effective absorbed pump power, is then deduced to connect a measurable macroscopic parameter with some microscopic characteristics of the activated ions in fibre lasers.

It is necessary to emphasize that the point-by-point agreement between experimental measurements and theoretical computation is of relatively little importance, especially in the engineering domain. The importance of comparing observations with a theoretical model lie in the fact that once agreement is obtained using a given set of parameters, the theory can be reliably used to predict the performance of the system even if one or several operating parameters are changed. From this point of view, the theoretical models presented in this Chapter are reasonable and useful.

4.1 The Physical Basis of Polarisation Effects

(1) Glass structure

Glass, on a microscopic scale, epitomizes an inhomogeneous system. Structurally, glass is a continuous random network lacking both symmetry and periodicity. The basic structural units which make up the glass network

have a definite geometry but are connected at corners to form a random three-dimensional network[1]. Several components exist singly in an amorphous phase and constitute simple glass formers. Other compounds added to the glass modify the network.

Paramagnetic ions, depending upon their size and valence state, enter a glass as a network-modifier cation or substitutionally as a network-former cation. The networks of single-component glasses such as SiO_2, GeO_2 and B_2O_3 are tightly bonded by bridging oxygens. Trivalent rare-earth ions cannot easily enter this structure substitutionally because of size. Therefore the predominant case is that rare-earth ions in such a glass act as network-modifier cations to which the study in this thesis restricts since our fibre lasers are all made of silica-based fibre.

Being an inherently disordered medium, the environment of each rare-earth ion in a glass is not identical to that in a crystal. In addition, because of differences in the bonding to nearest-neighbor ions, the local fields at individual ion sites vary. This results in site-to-site differences in the energy levels and the radiative and nonradiative transition probabilities of paramagnetic ions in glasses[2]. Broadband-excited optical absorption and emission spectra, and excited-state decays, consist of a superposition of contributions from individual ions distributed among the entire ensemble of local environments. The spectra exhibit inhomogeneous broadening and the decays do not have a single exponential time dependence[1].

(2) Electric dipole model

Any system which includes electric charge and current is capable of absorbing and, in certain circumstances, emitting electromagnetic radiation. The mechanisms may be quite complicated, but for systems which are compact in comparison to the radiation wavelength it is possible to analyse the radiation into a

sequence of contributions of decreasing importance: electric dipole, magnetic dipole, electric quadrupole, ...[3]

For rare-earth doped fibre lasers, the radiation wavelengths dealt with are within the regime of visible and infrared (around 1μm) The radii of the rare-earth ions are estimated to be around 0.1nm (for example, Nd^{3+} has a radius of 0.0995nm, Er^{3+} 0.0881nm and Pr^{3+} 0.1013nm[4]). Although the numerical values of the radii of the ions may vary depending on the kind of the salt used or the method of calculation, the size of the radiation "antenna" of the rare-earth centres in glass is at least four orders of magnitude smaller than the wavelength of the emitted radiation, as far as lasing actions are concerned in fibre lasers. It is therefore believed that the conclusion mentioned in the preceding paragraph is suitable for the rare-earth ions in glasses.

According to quantum mechanics, the energy of a stationary state in a atom or free-ion is represented by the Hamiltonian operator. If a small perturbation is applied, the changes experienced by stationary states can be described by writing the Hamiltonian as two terms[3]:

$$H = H_o + H' \qquad (4.1)$$

where H_o the is unperturbed Hamiltonian, and the perturbation H' is in some sense small. The perturbation method is then to expand whatever entity interests us as a 'power series' in H'; more exactly, to evaluate the entity to first, second,... order of smallness of H', as far as we need to go.

For a paramagnetic ion in a solid, the Hamiltonian operator can be expressed as[1]

$$H = H_{el} + H_{so} + V \qquad (4.2)$$

where H_{el} is the electrostatic interaction of the electrons, H_{so} is the spin-orbit term, and V is the perturbation term, being the potential at the ion site due to its environment. The relation

$$H_{el} >> H_{so} >> V \tag{4.3}$$

is true for the rare-earth ions in glasses. V can thus be treated as a small perturbation on the free-ion energies.

(3) Electric dipole radiation

The moment of an electric dipole is defined as[5]

$$\mathbf{p} = q\mathbf{r} \tag{4.4}$$

where q is the charge and **r** the positional vector with r being the separation of the positive charge from the negative charge, and the direction being defined as pointed from negative to positive charge. The classical theory regards the spontaneous emission from a radiating dipole as a damped oscillation process of the electron. If the simplest coordinate system is chosen for an electron oscillating around a positive charge located at the origin, as shown in Fig.4.1, the moment of the electric dipole can be expressed by

$$\mathbf{p}(t) = e\mathbf{r}_0\cos\omega t = \mathbf{p}_0\cos\omega t \tag{4.5}$$

Such a dipole radiates electromagnetic energy. The propagation direction of the electromagnetic wave **S**, the electric field **E** and the magnetic field **H** are perpendicular to each other. The vector **E** will be along the tangent to a meridian drawn on the sphere shown in Fig.4.1, while the vector **H** will be along the tangent to the corresponding parallel. The light emitted by a linear dipole oscillator in any direction is completely polarised. The magnitude of the radiation field at

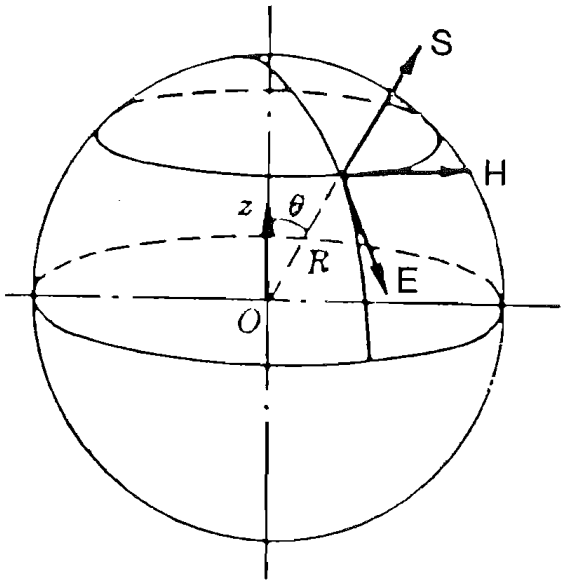

Fig.4.1 The co-ordinate system chosen for an electron oscillating around a positive charge located at the origin.

distance of R can be obtained by solving the Maxwell's eqs.[6] and expressed as

$$E = H = -\omega^2 p_o \cos(\omega t - \omega R/c)\sin\theta/(Rc^2) \qquad (4.6)$$

where θ is the angle between **R** and the z axis, c is the light speed in free-space.

The electric dipole radiation can also be treated by using quantum mechanics. An excited atom described by E_u (the subscript u stands for **upper** level) in complete darkness emits a photon $h\nu$, and in doing so makes a transition to a **lower** level E_l. With dipole model, the interaction or the perturbation term of Hamiltonian is

$$H' = -\mathbf{p}\cdot\mathbf{E}(o) \qquad (4.7)$$

where **p** is the electric dipole moment observable of the atom, and **E**(o) is the electric field intensity at the atom — at the origin, for convenience. The transition probability W from state E_u to E_l expressed by the Golden Rule (as Fermi called it in 1950) is proportional to the square of the matrix element

$$W = C\left|\langle E_l \left| H' \right| E_u \rangle\right|^2 \qquad (4.8)$$

where the Dirac notations "$\langle|$" and "$|\rangle$" are used to represent the quantum state, and the capital C is a constant related to the radiation frequency. The perturbation matrix element of the Hamiltonian operator H' between two eigenstates $|E_l\rangle$ and $\langle E_u|$ is defined as

$$\langle E_l | H' | E_u \rangle = \int \psi_l^* H' \psi_u \, d\tau \qquad (4.9)$$

where ψ_u and ψ_l are wavefunctions of the upper and lower states, respectively, and the symbol "*" stands for the complex conjugate.

Using eq.(4.7) and writing

$$\mathbf{d}=\langle E_1 \left| \mathbf{p} \right| E_u \rangle \tag{4.10}$$

the general prescription for the intensity and the polarisation of the radiation in the direction **u** can be obtained. For the intensity, the transition rate TR for spontaneous emission in the direction **u** is expressed as

$$TR = \frac{\omega^3}{4\pi\varepsilon_o hc^3} [\mathbf{d}\cdot\mathbf{d}^*-(\mathbf{d}\cdot\mathbf{u})(\mathbf{d}^*\cdot\mathbf{u})] \tag{4.11}$$

where ε_o is the permittivity of a vacuum, h is the Planck's constant, and ω the radiation frequency. The unit of transition rate TR is photons per excited atom per second per unit solid angle.

In quantum mechanics, a beam of $\mathbf{P}_\theta$-polarised light is regarded as a beam of photons "in the state $\mathbf{P}_\theta$". The probability that a photon in state $\mathbf{P}_\theta$ survives a polariser with orientation ø (thus being in state $\mathbf{P}_\phi$) is $\cos^2(\theta-\phi)$. Here, as always in quantum mechanics, the word probability really means proportion, where we have a large number of identical situations in mind, for example, a large number of photons striking a polariser. If we rewrite the transition rate as

$$TR = \frac{\omega^3}{4\pi\varepsilon_o hc^3}(|\mathbf{d}\cdot\lambda_1^*|^2+|\mathbf{d}\cdot\lambda_2^*|^2) \tag{4.12}$$

with λ_1 and λ_2 being defined as the two basic polarisation vectors with the directions

λ_1: parallel to $\mathbf{d}-\mathbf{u}(\mathbf{d}\cdot\mathbf{u})$, (4.13a)

λ_2: parallel to $\mathbf{u}\wedge\mathbf{d}^*$, (4.13b)

taken as a legitimate choice since λ_1, λ_2, **u** are orthogonal in pairs. The two terms in eq.(4.12) are interpreted as probabilities. Now imagine a polariser

which certainly transmits a photon in polarisation state λ_2; the probability that the radiation from **d** gets through the polariser is proportional to $|\mathbf{d}\cdot\lambda_2^*|^2$, which is zero since $\mathbf{d}\cdot(\mathbf{u}\wedge\mathbf{d})=0$. The radiation is therefore in the orthogonal polarisation state, represented by λ_1. Thus both the intensity and the polarisation are determined by the component **d** perpendicular to **u**. This result coincides with what is concluded from the classical dipole model described above in this section.

(4) The Stark effect

A free ion or atom in a uniform electric field loses its spherical symmetry. Consequently, certain degeneracies are lifted. A further consequence is that the components of the resultant spectral splitting have intensities and polarisations which depend on the direction of emission. This is the Stark effect. The Stark effect in the simplest example of the hydrogen atom has been treated by using quantum mechanics. The conclusions, which agree well with the experimental investigation, are that when viewed from the direction parallel to the applied electric field, two transitions with a line unseparated yield circular polarisation in two opposite senses. A gas of excited hydrogen atoms will undergo these transitions in equal numbers; consequently, this spectral line is completely unpolarised. If viewed perpendicular to the applied field, apart from the unperturbed line two splitted components are observed. These two components have polarisation perpendicular to the unperturbed line. In addition, the intensity sum of these two perpendicular components is just equal to the intensity of the unperturbed line.

The Stark splitting of rare-earth ions in some crystals has also been confirmed[7]. Fig.4.2 illustrates the splitting of the Nd^{3+}-ion in YAG for both $^4F_{3/2}$ and $^4I_{11/2}$ energy level. However, for rare-earth ions in glasses, the inhomogeneous broadening is so strong that

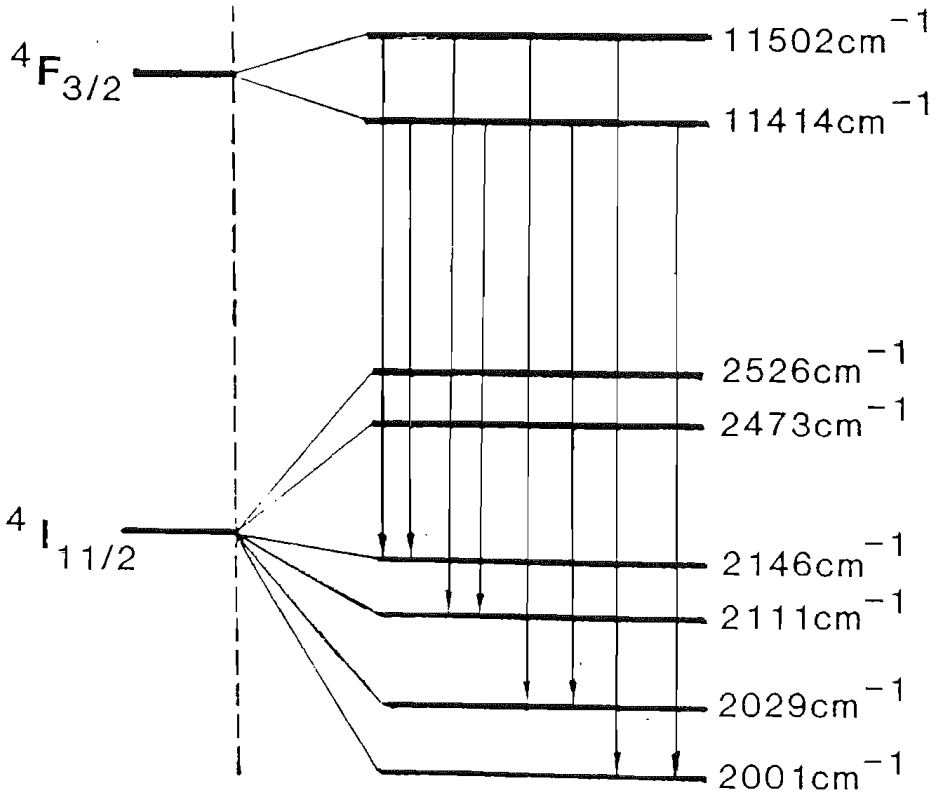

Fig.4.2 Stark splitting of Nd^{3+}-ion in YAG for both $^4F_{3/2}$ and $^4I_{11/2}$ energy levels.

the Stark structure is normally masked and therefore poorly resolved.

(5) Spontaneous emission and stimulated emission

Spontaneous emission deals with the behaviour of an excited system in the complete darkness. Stimulated emission occurs in the presence of an oscillating external electromagnetic field.

Radiation of spontaneous emission from an excited gas is expected to be isotropic and unpolarised even if the emitters themselves are not symmetric, since the orientation of the emitters are random.

For rare-earth ions in glasses, it is also reasonable to consider the ions as a randomly orientated assembly because of the macroscopic equivalence of different directions in glass. Although the Stark effect might be involved due to the local electric field of the glass former, the spontaneous emission from such an assembly of active ions is expected to be still isotropic and unpolarised.

However, an entirely different situation happens with stimulated emission. The study of resonance[3] shows that the external field will have little effect on the system unless its frequency ν matches the gap between two energy levels.

$$E_u - E_l = h\nu \qquad (4.14)$$

The transition from the lower to the upper level requires a supply of energy $h\nu$ from the external field: this is referred to as absorption. The opposite transition is stimulated emission, where the external field gains energy from the system. The fact that the amount of energy transferred is $h\nu$ in each case suggests that it is a single photon that is being absorbed or emitted.

Although eq.(4.7) is still valid for the stimulated emission, a substantial difference arises from the

spontaneous emission, where **E**(o) is considered as the electric intensity between the dark state and a state with one photon present. For the case of stimulated emission, the term **E**(o) in (4.7) is now presented by the electric intensity of the stimulating field, and the matrix element is then expressed as

$$\langle E_1 \left| H' \right| E_u \rangle = -\mathbf{d}\cdot\mathbf{E}(o) \qquad (4.15)$$

where **d** is defined as shown in eq.(4.10). The effect of the external radiation is to make the state of the system swing to and fro between the levels, the time to switch between states being

$$T_{st} = \frac{h}{4\left|\mathbf{d}^{*}\cdot\mathbf{E}\right|} \qquad (4.16)$$

This time is generally very much shorter than the lifetime for spontaneous emission.

The formula (4.15) takes into account not only the magnitudes of the dipole moment **p** (via the matrix element **d**) and the external field **E**, but also any polarisation effects there may be. It is clear that both the stimulated emission probability and the excitation probability are related to the angle the electric dipole makes to the stimulating field, as the scalar product indicates. Furthermore, the relation in (4.15) is true for both the excitation and the stimulated emission.

In the case of lasers, more than a single dipole is involved in the stimulated emission. A dipole sheet is a better model. The theoretical study of a dipole sheet model shows[8] that the in-phase characteristic is one important property of stimulated emission from a sheet of dipoles. Furthermore, the induced field has the same polarisation as the incident field, a second property of this stimulated emission. The third is that the stimulated emission has the same frequency as the incident radiation. These three properties — equality of

phase, direction, and frequency of incident and stimulated field — are completely obtained only for appropriately pumped media whose cross-sectional areas contain many similar dipoles.

(6) Laser-excited fluorescence spectroscopy in glass

The difficulty of constructing a satisfactory model of rare-earth optical centres in glass is due, in particular, to the lack of polarisation characteristics of the spectrum. The anisotropy of the absorption and emission of light by individual centres is not normally observable because of the randomness of the ion orientation in amorphous glass. A promising development for rare-earth activated glasses achieved recently[9,10] is the use of the laser-excited fluorescence spectroscopy.

When a laser source is used for excitation, only those ions resonant with the narrowband excitation quanta within the homogeneous linewidth are excited. This site-selective excitation effectively reduces the inhomogeneous broadening and a line-narrowed fluorescence spectrum is obtained. Moreover, the linearly-polarised excitation provides a further method for site selectivity.

Polarised fluorescence spectra have been used to investigate the Stark structure and the dipole nature of radiative transitions[11,12] for rare earths in glasses. The observation of polarised luminescence from various rare-earth ions in glass have been reported for both resonant and non-resonant transitions. The main results are listed in Table 4.1, and the following conclusion can be drawn:

The form of the luminescence spectrum depends strongly on the excitation range. As the excitation wavelength is varied, the degree of polarisation $DOP=(I_p-I_s)/(I_p+I_s)$ changes not only its magnitude but

also its sign. The value of DOP is considerably greater for resonance excitation than for non-resonance.

The remarkable contribution the polarised luminescence method made is the understanding of the dipole model for resonant transition and the Stark structure of the rare-earth ions in glass, which is usually masked by the strong inhomogeneous broadening. However, the application of this method is limited by strong overlap of the Stark components in some cases[12]. In addition, this method gives no information about the dipole model for the non-resonant transition.

4.2 Understanding of Polarisation Effects in Fibre Lasers

The transitions in fibre lasers are always non-resonant no matter what kind of system, three-level or four-level, is involved. A comparison of fluorescence measurements in the fibre lasers listed in Table 3.1 with the results for bulk rare-earth activated glass in Table 4.1 shows that the DOP of non-resonant transitions has a fairly low value (10^{-2} order). This is true for both the bulk and fibre cases, indicating that the depolarisation of non-resonant fluorescence is a characteristic of the material.

Although some polarisation properties of the Stark structure of rare-earth ions in glass can be detected by using the polarised luminescence method the following question marks still remain[1,11]:

- Why is the DOP so small for non-resonant excitation?
- Is this affected by simultaneous excitation of centres having different orientation but the same excitation frequency?
- Is this due to an angle between the absorbing and emitting oscillators?
  or the fluctuation in this angle because of the variations in the local field?

Ion	Matrix; Concentration mole (%)	Excitation		Recording		DOP
		transition	λ (μm)	transition	λ (μm)	
Nd^{3+}	silicate 0.8*	$^4F_{11/2}$-	1.053	$^4F_{3/2}$-$^4I_{11/2}$	1.064	0.04
Pr^{3+}	phosphate1.25	$^3H_4$-$^3P_2$	0.436	$^3P_0$-$^3H_6$ $^1D_2$-$^3H_4$	0.598	-0.05
Tb^{3+}	phosphate 0.2	$^7F_6$-$^5D_2$	0.366	$^5D_4$-$^7F_6$	0.487	0.03
Er^{3+}	Tellurite 0.8	$^4I_{15/2}$-$^2G_{9/2}$	0.366	$^4S_{3/2}$-$^4I_{15/2}$	0.545	0.04
Tm^{3+}	phosphate1.25	$^3H_6$-$^1D_2$	0.366	$^1D_2$-$^3H_4$	0.450	0.07

* wt %

Table 4.1 Depolarisation of bulk rare-earth activated glass. (after referenc es [4.9] and [4.11])

— Is it possible in principle to get the case where the direction of the emitting oscillator in a rare-earth centre is entirely unrelated to that of the absorbing oscillator as the internal field varies?
— Is this the result of the strong overlap of the Stark components?
— Is this caused by accidental coincidence of excitation levels of ions in different sites?
— Is this influenced by cross relaxation or energy transfer between neighbouring ions?

Laser-pumped fibre lasers provide an opportunity to investigate the validity and properties of the dipole model for the non-resonant transition. Since the lasing action is related to the stimulated emission rather than the spontaneous emission, the fibre laser gives information on the interaction between the applied field and the rare-earth ions in glass, not only during the excitation process but also the lasing transition. In the meantime, the site-selection will have played a role during both processes, absorption and emission. In particular, direct investigation of the existence of correlation between absorbing and emitting oscillators can be made with laser-pumped fibre lasers.

The outer-shell electrons of trivalent rare-earth ions are $4f^n$, three of which, namely $6s^2 5d$ have been removed. If the rare-earth ion has an even number of 4f electrons, the degeneracy of the free-ion level is completely lifted and dipole transitions may be ascribed to a linear oscillator; if the ion has an odd number of 4f electrons, the twofold Kramers degeneracy remains and transitions are modeled by partially anisotropic oscillators[1,11]. The structure of rare-earth ions in glass are listed in Table 4.2, from which it is seen that Nd^{3+}, Er^{3+} have an odd number of 4f electrons. Therefore the partial linear oscillator is used in the following sections to model the rare-earth ions in glasses.

According to the basic factors of polarisation effects in fibre lasers, as described in Chapter 3, the

Trivalent rare-earth ion	Number of $4f^n$	Ground state
La^{3+}	0	$^1S_0$
Ce^{3+}	1	$^2F_{5/2}$
Pr^{3+}	2	$^3H_4$
Nd^{3+}	3	$^4I_{9/2}$
Pm^{3+}	4	$^5I_4$
Sm^{3+}	5	$^6H_{5/2}$
Eu^{3+}	6	$^7F_0$
Gd^{3+}	7	$^8S_{7/2}$
Tb^{3+}	8	$^7F_6$
Dy^{3+}	9	$^6H_{15/2}$
Ho^{3+}	10	$^5I_8$
Er^{3+}	11	$^4I_{15/2}$
Tm^{3+}	12	$^3H_6$
Yb^{3+}	13	$^2F_{7/2}$
Lu^{3+}	14	$^1S_0$

Table 4.2 The structure of rare earth ions in glass.

following points are postulated for modeling the effects:

- **Each rare-earth ion in glass corresponds to a partially anisotropic oscillator;**
- **The orientations of these oscillators, transition dipole moments, are randomly distributed in space.**
- **The absorbing and emitting oscillations of the same rare-earth ion has the same orientation in space related to a system of coordinates which is rigidly fixed to the centre, independently of the non-radiation transition.**

The last point is required by the experimental investigation of the dependence of the polarisation output from the fibre laser on the pump. This assumption is necessary, at least for those non-resonant transitions of rare-earth ions which are measured and discussed in this thesis. The detailed discussion is presented later in this chapter.

With these fundamental points a mathematical model is developed to analyse the polarisation effects in fibre lasers. The good agreement between theoretical calculation and the experimental measurements supports these fundamental points.

(1) Fluorescence depolarisation

The whole lasing process can be described by the following steps: absorption of the pump leading to the excitation of activator ions — non-radiative relaxation towards to the metastable level — build-up of lasing action from the noise of spontaneous emission — stimulated emission caused by lasing light. When laser light is used as a pump source, and a longitudinal configuration as a pumping system, different dipole oscillators have different excitation probabilities according to their orientation, as described in eqs.(4.8) and (4.15). In the case of fluorescence, there is no external field with an energy $h\nu=E_u-E_l$ involved if the influence of superfluorescence can be considered

negligible. Since the time needed for both dipole excitation and non-radiative transition are much shorter than the lifetime of electrons in the metastable state, as seen from eq.(4.16), it seems reasonable to assume that almost all the activators with different orientations are excited before the fluorescence is measured. As a result of randomness of oscillator orientation, the fluorescence from non-resonant spontaneous emission is strongly depolarised.

Cross-relaxation or ion-ion energy transfer may also affect the polarisation behaviour of the fluorescence from the spontaneous emission[1,13], and therefore cause a reduction of the DOP. However, this happens only when the activator ion concentration in glass becomes sufficiently high. It is verified for those fibre lasers with a dopant concentration of around 10^2~10^3ppm, which is the case in this thesis, that the depolarisation caused by cross-relaxation was still small and cannot be the main explanation of the fluorescence depolarisation.

Theoretically, the overlap of the Stark components apparently results in depolarisation of non-resonant fluorescence. However, there is not sufficient information to postulate a model dealing with the Stark components of rare-earth activators in glass. In particular, the relative orientation between the oscillators corresponding to different Stark components still remains unknown. In this thesis, a rare-earth ion is treated as a partially linear oscillator. This means that an excited ion does not necessarily radiate a photon with polarisation parallel to the dipole oscillator. There is a small probability that it will radiate a photon having a polarisation perpendicular to the dipole oscillator. Such a partially linear oscillator model has, in fact, considered the influence of the Stark effect. As a result of the model, the fluorescence is expected to be depolarised to some degree.

In summary, the depolarisation of non-resonant fluorescence is attributed to both the random orientation

of dipole oscillators representing rare-earth ions in glass and the overlap of Stark components. The cross-relaxation or ion-ion energy transition is not the major reason in our case, although it may affect the fluorescence depolarisation in some cases. The idea that there is no correlation between absorbing and emitting oscillators has to be given up according to the experiments described later in this chapter.

(2) Existence of two orthogonal eigenmodes

It is well known that an approximation of the three-level, and four-level, laser systems by a two-level representation is very useful. Also the rate equation, as expressed below, is of prime importance in predicting the grosser features of the laser output. Despite the fact that many details of the nature of the laser emission, such as spectral, temporal and spatial distributions, are inaccessible from the point of view of the simple rate-equation, it will be used in this thesis to analyse the polarisation eigenmodes in fibre lasers since it has been shown that the rate-equation approach is successful in analysing output power, threshold condition, etc.

The rate equation can be expressed as[14]

$$\frac{\partial N}{\partial t} = - Nc\sigma\mu\phi - \frac{N+N_{tot}(\mu-1)}{\tau_{21}} + W_p(N_{tot}-N) \qquad (4.17)$$

where

$$N = N_2 - \frac{g_2 N_1}{g_1} \qquad (4.18)$$

$$\mu = 1 + \frac{g_2}{g_1} \qquad (4.19)$$

$$N_{tot} = N_1 + N_2 \qquad (4.20)$$

$$\sigma = \begin{cases} \dfrac{A_{21}\lambda_0^2}{4\pi^2 n^2 \Delta\nu} & \text{for a Lorentzian lineshape} \\ \dfrac{A_{21}\lambda_0^2}{4\pi\, n^2 \Delta\nu}\left(\dfrac{\ln 2}{\pi}\right) & \text{for a Gaussian lineshape} \end{cases} \qquad (4.21)$$

The parameter σ is the cross section for the radiative transition from the excited upper laser level 2 to the lower level 1, λ_o is the lasing wavelength in vacuum, $\Delta\lambda$ is the width between the half-power points of the atomic line shape, N_1 and N_2 are the population densities of level 1 and 2 respectively, g_1 and g_2 are the level degeneracies, W_p is related to pump parameter W_{13} and pumping efficiency factor η_o by:

$$W_p = \eta_o W_{13} \qquad (4.22)$$

A_{21} is the spontaneous transition probability, ø is the photon density, $\tau_{12}=(A_{21})^{-1}$ is the effective radiative lifetime associated with the laser line, n is the refractive index of the laser medium and c is the light speed in free-space.

Another equation, usually regarded together with (4.17), describes the rate of change of the photon density within the laser resonator,

$$\frac{\partial ø}{\partial t} = Nc\sigma ø - \frac{ø}{\tau_c} + S \qquad (4.23)$$

where τ_c is the decay time for photons in the optical resonator and S is the rate at which spontaneous emission is added to the laser emission.

It is clear from (4.17) and (4.23) that for the onset of laser emission the rate of change of the photon density must be equal to, or greater than, zero. Thus at laser threshold for sustained oscillation the condition

$$\frac{\partial \phi}{\partial t} \geq 0 \qquad (4.24)$$

must be fulfilled, which enables us to obtain from (4.23) the required inversion density at threshold

$$N \geq \frac{1}{c\sigma\tau_c} \qquad (4.25)$$

In deriving this expression the factor S has been ignored as it is very small compared with the other two terms.

It is worth pointing out that these theoretical formulas are valid only for an individual lasing mode. In the case of a fibre laser with the Fabry-Perot cavity configuration shown in Fig.1.1, the question raised is why two orthogonal polarisation eigenmodes exist simultaneously. To answer this question the birefringence of the laser cavity, the single-mode fibre, induced by both fibre imperfections and the surrounding environment must be considered.

In Chapter 2 we saw that the circular birefringence of the single-mode fibre can be neglected in the Fabry-Perot cavity. The generation of the two orthogonal polarisation eigenmodes is attributed to the linear birefringence of the fibre, which creates a modal effective-index difference Δn. Although the Δn is rather small (for example, if λ=1μm, L_p=1cm, Δn is then 10^{-4}), it breaks the space symmetry for light propagation, and creates two orthogonal optical axes, on which two polarisation eigenmodes build up their lasing actions from the noise of the fluorescence.

In fact, we assume that the spontaneous transition behaviour of the dopant ion in a glass matrix is independent of the polarisation orientation of the pump light, which is believed to be reasonable according to the fluorescence depolarisation, i.e. A_{21}, λ_o and $\Delta\lambda$ are the same for different polarisation orientations of the pump light. The only factor which affects the cross-section σ is the normalised linear birefringence or the

mode effective-index difference Δn. From (4.21) it can be seen that the different lasing modes, say x- and y-modes, where the x- and y-axes are the principal axes in the fibre laser cavity, have different cross-sections, say σ_x and σ_y. Since the required inversion density at threshold, and the pump power required to reach threshold, are inversely proportional to the cross section σ, as described in (4.25), these two eigenmodes have different thresholds.

In addition, different effective indices induce different longitudinal mode frequencies in a cavity. The longitudinal mode frequency in a Fabry-Perot cavity can be expressed as

$$\nu = \frac{mc}{2nl} \tag{4.26}$$

where l is the cavity length, c is the light velocity in free space, m is an integer and n is the refractive index of the laser medium. Since there is an effective-index difference Δn between the x and y modes, the frequency difference between the x and y longitudinal modes of the cavity will be

$$|\Delta\nu| = \frac{mc}{2n^2l} |\Delta n| \tag{4.27}$$

For example, if $\Delta n=10^{-5}$, l=1m, and n=1.5, then $\Delta\nu=m\cdot 10^3$Hz.

In summary, the linear birefringence of the single-mode fibre gives rise to two orthogonal axes, on which the polarisation eigenmodes of fibre laser build up from fluorescence noise. These two orthogonal polarisation modes are independent of each other, with different longitudinal mode frequencies, and different cross-sections.

(3) Dependence of laser polarisation on pump polarisation

Beginning from the superfluorescence stage, stimulated emission plays an important role in the building up of laser action. Once lasing has been achieved stimulated emission is the predominant process. Since the orientations of the lasing eigenmodes are determined by the fibre cavity, the strong external electric field stimulating the emission has the polarisation of these principal axes, and thus every dipole transition of every activated centre has a different transition probability for contributing of a photon to either the x-mode or y-mode. Obviously, the site selection provided by the laser pumping takes place only during the excitation process. The lasing action is now the second site-selection process, and thus offers a direct probe whether the correlation between the absorbing and emitting oscillators exists or not. In addition, the possible ion-ion energy transition is extremely limited for a CW fibre laser due to the very short time required by the absorption and emission process. Therefore, if there is no correlation between the absorbing and emitting oscillators, the emitting oscillators of all excited activated centres are expected to be randomly orientated, and consequently the intensities of the x-mode and the y-mode shold be equal to each other independently of the pump. Because complete dependence of output polarisation from fibre lasers on the pump (the third characteristic of the polarisation effects) is observed it follows that a correlation must exist. Furthermore, the exact cosine function of twice the launching angle, $\cos(2\alpha)$, as shown in eq.(3.1), requires the postulation that the absorbing and emitting oscillations have the same orientations for an activated centre. With a mathematical model based on this point of view, as described in the following sections, the $\cos(2\alpha)$ function is well explained.

4.3 Effective Pump Power of Polarisation Eigenmodes

It is now possible to establish a mathematical model to treat the polarisation effects in fibre lasers. As described in Chapter 3, two orthogonal polarisation eigenmodes have their independent thresholds, slope efficiencies and relaxation frequencies. The existing laser theory, on the other hand, points out that all these characteristics of a lasing mode ought to be related to the absorbed pump power[14]. Therefore, there must exist some physical parameter, which connects absorbed pump power for each mode with some microscopic characteristics of the activated ions in fibre lasers. If the relationship between the absorbed pump power, which is a macroscopic parameter, and some microscopic characteristics is found and expressed correctly, the corresponding information about the ions can be extracted from the measurements, and thus the behaviour and performance of the laser can be predicted.

(1) Polarisation-dependent cross-section ratio

As described in the previous sections, rare-earth ions in glass can be represented by a partially anisotropic oscillator. Such ions will interact more strongly with certain directions of the stimulating field. The expression of the interaction is determined by (4.8) and (4.15). To adapt this property to the laser theory, it can be characterized by a polarisation-dependent cross-section.[15]

According to the mathematical model describing such a cross-section anisotropy, all ion sites are identical except for orientation. A local orthogonal co-ordinate system of the surrounding ionic charge distribution, denoted by axes **l**, **m** and **n** as shown in Fig.4.3, is uniquely assigned to the site. A different cross-section, proportional to the probability of absorption or emission of light with the electric-field vector polarised in that direction, is associated with each

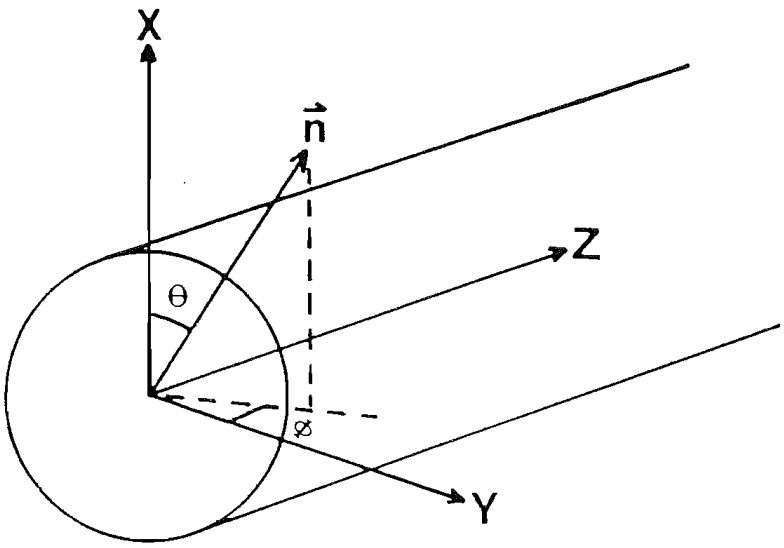

Fig.4.3 The co-ordinate frame referred to the fibre laser for all measurements.

axis. It is assumed that the cross-section in the **n**-direction is larger than the other two and its value is denoted by σ_p. The remaining two cross-sections are taken to be equal and are denoted by σ_s. With this model, the polarised cross-section ratio can be expressed in terms of a single parameter

$$a \equiv \sigma_s/\sigma_p \qquad (4.28)$$

When a=1, the system is represented by an isotropic oscillator; when a=0, the system represented by pure dipole.[16]

Although for a general anisotropic oscillator there is no *a priori* reason to expect that the two cross-sections σ_l and σ_m are equal, this simplifies the mathematical model while still allowing for a cross-section anisotropy. Also the site-to-site variations in the line strength are neglected.

The polarised cross-sections σ_p and σ_s for the absorbing and emitting oscillators need not be the same in magnitude because the transitions correspond to different energy level gaps. Nevertheless, $a \equiv \sigma_s/\sigma_p$ is assumed to be identical for both cases at every ion site.

The justification for the above assumption, and the hypothesis of the identical orientation of both oscillators, ultimately rests on the ability of the model to predict experimental results.

By utilising both the polarisation-dependent cross-section model and the concept of two orthogonal polarisation eigenmodes, a new concept, the effective pump power of the eigenpolarisation mode, is then introduced.

Since there exists two principal polarisation axes (say x and y) and thus two polarisation eigenmodes, in fibre lasers, a linearly-polarised pump beam must be resolved into two components corresponding to the principal axes. On the other hand, every active ion

possesses more or less probability of contributing to the x- or y-mode. The magnitude of the probability is dependent on both the polarised cross-section ratio a and the ionic dipole orientation. As a statistical result, the effective pump power for each eigenmode is defined as the fraction of the pump power which produces the population inversion belonging to the corresponding eigenmode.

The laboratory frame is denoted by x, y and z or spherical angles θ and ø (collectively Eulerian angle Ω) as shown in Fig.4.3, where θ is the angle of $(\mathbf{n},\mathbf{x})$ and ø the angle of $(\mathbf{n},\mathbf{y})$. The principal polarisation axes are always assumed to be coincident with the x and y axes and the transmission direction coincident with the z axis.

The normalized probability density function $f(\Omega)$ of ionic sites is a uniform distribution because of the assumed isotropy of orientation.

$$f(\Omega) = \begin{cases} 1/4\pi & 0<\theta<\pi,\ 0<ø<2\pi \\ 0 & \text{otherwise} \end{cases} \qquad (4.29)$$

The stimulated-emission cross-sections of a given ion site with $(\mathbf{l},\mathbf{m},\mathbf{n})$ local co-ordinate system for x- and y-polarised light are

$$\sigma^{x}(\Omega) = \sigma_p(\mathbf{n}\cdot\mathbf{x})^2 + \sigma_s(\mathbf{l}\cdot\mathbf{x})^2 + \sigma_s(\mathbf{m}\cdot\mathbf{x})^2$$

$$= \sigma_p\cos^2\theta + \sigma_s\sin^2\theta \qquad (4.30a)$$

$$\sigma^{y}(\Omega) = \sigma_p(\mathbf{n}\cdot\mathbf{y})^2 + \sigma_s(\mathbf{l}\cdot\mathbf{y})^2 + \sigma_s(\mathbf{m}\cdot\mathbf{y})^2$$

$$= \sigma_p\sin^2\theta\cos^2ø+\sigma_s(\sin^2ø +\cos^2\theta\cos^2ø) \qquad (4.30b)$$

respectively.

In deriving the above eqs., the Golden rule (4.8) and the matrix element (4.15) are applied, and reflected by the scalar product terms in (4.30).

It is worth noting that in the case of an isotropic cavity, such as a conventional glass rod laser, the effective stimulated emission cross-sections, defined as a mathematical expectation of the random variable $\sigma(\Omega)$ for both x and y polarised light, are the same, that is

$$\sigma^{x}(\Omega) = \int_{\Omega} f(\Omega)\sigma^{x}(\Omega)d\Omega = \int_{\Omega} f(\Omega)\sigma^{y}(\Omega)d\Omega = \sigma^{y}(\Omega)$$

$$= (\sigma_{p} + 2\sigma_{s}) / 3 \qquad (4.31)$$

which means that there is no priority for any direction in such a laser cavity.

(2) Effective absorbed pump power

In the fibre laser, the total population inversion is divided into two parts, which are assigned to the x and y polarisation eigenmodes, respectively. One ionic site can, of course, only transit from the upper level to the lower level to create one photon which contributes to either the x or y polarisation mode. The important concept here is that it is the polarisation-dependent cross-section which determines the transition probability. It is also assumed that the photon density of each mode in the cavity is proportional to the transition probability, since macroscopic lasing action is a statistical result of many microscopic transitions.

We assume that the principal axes of the polarisation eigenmodes coincide with the x and y axes of the laboratory co-ordinate system, and a linearly-polarised pump beam is launched into the end of the fibre cavity with a polarisation angle of α with respect to the x-axis. Thus, the absorbed power density of the pump light is

$$I(z) = I(o)\exp(-\gamma z) \qquad (4.32)$$

and

$$\begin{vmatrix} I_x(z) \\ \\ I_y(z) \end{vmatrix} = I(o)\exp(-\gamma z) \begin{vmatrix} \cos^2\alpha \\ \\ \sin^2\alpha \end{vmatrix} \qquad (4.33)$$

where γ is the absorption of the fibre at the pump wavelength and I(o) is the absorbed pump power density at z=o. In equations (4.32) and (4.33), the intrinsic scattering loss of the fibre at the pump wavelength has been neglected since it is, in practice, very small compared with the absorption.

Considering that the lasing action is associated with not only the absorption cross-section but also the stimulated emission cross-section, we can express the probability per unit time for an ion to contribute a transition to the x and y modes as follows:

$$P_x(\Omega,z) = C[I_x(z)\sigma^x(\Omega)+I_y(z)\sigma^y(\Omega)]\sigma^x(\Omega) \qquad (4.34a)$$

$$P_y(\Omega,z) = C[I_x(z)\sigma^x(\Omega)+I_y(z)\sigma^y(\Omega)]\sigma^y(\Omega) \qquad (4.34b)$$

where C is a normalized constant. The factors $I_x(z)\sigma^x(\Omega)$ and $I_y(z)\sigma^y(\Omega)$ in (4.34) can be regarded as items associated with the absorption transition or population inversion. The product with $\sigma^x(\Omega)$, the last term in (4.34a), or $\sigma^y(\Omega)$ in (4.34b), is related to the stimulated radiative emission. It is readily proved that the difference between the magnitude of absorption and emission cross-sections can be compensated by the normalized constant C due to the assumption of identical polarised cross-section ratios for both transitions. Therefore they are expressed by the same form in eqs.(4.34). $P_x(\Omega,z)$ and $P_y(\Omega,z)$ are related to the final lasing transition of the x and y modes, respectively. By integrating over all possible site orientations, the effective pump power density for the x and y polarised modes can be defined as follows when a suitable normalized constant C is chosen.

$$I^x(z) = \int_\Omega f(\Omega)P_x(\Omega)d\Omega \tag{4.35a}$$

$$I^y(z) = \int_\Omega f(\Omega)P_y(\Omega)d\Omega \tag{4.35b}$$

Using (4.29), (4.30), (4.33), (4.34) and (4.35), Omitting those tedious integration calculations, we obtain

$$I^x(z) = C\cos^2\alpha I(o)e^{-\gamma z}(\frac{1}{5}\sigma_p^2+\frac{4}{15}\sigma_p\sigma_s+\frac{8}{15}\sigma_s^2)$$

$$+C\sin^2\alpha I(o)e^{-\gamma z}(\frac{1}{15}\sigma_p^2+\frac{8}{15}\sigma_p\sigma_s+\frac{6}{15}\sigma_s^2) \tag{4.36a}$$

$$I^y(z) = C\sin^2\alpha I(o)e^{-\gamma z}(\frac{1}{5}\sigma_p^2+\frac{4}{15}\sigma_p\sigma_s+\frac{8}{15}\sigma_s^2)$$

$$+C\cos^2\alpha I(o)e^{-\gamma z}(\frac{1}{15}\sigma_p^2+\frac{8}{15}\sigma_p\sigma_s+\frac{6}{15}\sigma_s^2) \tag{4.36b}$$

The normalized constant C can be obtained by employing the energy conservation, which requires the following eq.:

$$I^x(z)+I^y(z) = I(z) = I(o)e^{-\gamma z} \tag{4.37}$$

Thus

$$C = 15 / (4\sigma_p^2+12\sigma_p\sigma_s+14\sigma_s^2) \tag{4.38}$$

The equation (4.36) can then be simplified to

$$\begin{vmatrix} I^x(z) \\ I^y(z) \end{vmatrix} = I(o)\exp(-\gamma z) \begin{vmatrix} \cos^2\alpha & \sin^2\alpha \\ \sin^2\alpha & \cos^2\alpha \end{vmatrix} \begin{vmatrix} c_1 \\ c_2 \end{vmatrix} \tag{4.39}$$

where

$$c_1=(3+4a+8a^2)/(4+12a+14a^2) \qquad (4.40a)$$

$$c_2=(1+8a+6a^2)/(4+12a+14a^2) \qquad (4.40b)$$

and $a \equiv \sigma_s/\sigma_p$ as defined in (4.28)

Instead of the absorbed pump power density $I(o)\exp(-\gamma z)$ in (4.39), the concept of total absorbed pump power will be more convenient for a practical use without inducing any difference for predicting the laser performance. The total absorbed pump power can be expressed as

$$P_{ab} = \int_o^l AI(o)\exp(-\gamma z)dz = \frac{AI(o)}{\gamma}(1-e^{-\gamma l}) \qquad (4.41)$$

where A is the effective cross-sectional area of the fibre cavity, and l is the length of the fibre.

Thus (4.39) becomes

$$\begin{vmatrix} P^x \\ P^y \end{vmatrix} = P_{ab} \begin{vmatrix} \cos^2\alpha & \sin^2\alpha \\ \sin^2\alpha & \cos^2\alpha \end{vmatrix} \begin{vmatrix} c_1 \\ c_2 \end{vmatrix} \qquad (4.42)$$

in which P_{ab} is the total absorbed pump power, c_1 and c_2 are associated with the polarised cross-section ratio a as shown in (4.40), α is the angle between the polarisation orientation of the pump light and the x-axis, and P^x and P^y are the effective absorbed pump powers for the x and y polarised eigenmodes respectively.

(3) Polarisation selection ratio

We define the fraction of effective absorbed pump power for the polarisation eigenmode from the total absorbed pump power

$$PS^x = P^x / P_{ab} = c_1\cos^2\alpha + c_2\sin^2\alpha \qquad (4.43a)$$

$$PS^y = P^y / P_{ab} = c_1\sin^2\alpha + c_2\cos^2\alpha \qquad (4.43b)$$

as a parameter describing the property of the site-selection for a fibre laser, and call it **polarisation selection ratio.** It follows immediately that

$$\left.\begin{aligned} PS^x &= c_1 \\ PS^y &= c_2 \end{aligned}\right\} \quad \text{when pumped on x-axis} \qquad (4.44)$$

indicating that the physical meaning of the parameter c_1 is the polarisation selection ratio when the laser is pumped on the corresponding axis, while c_2 is that when pumped on the perpendicular axis. The relation

$$c_1 + c_2 = 1 \qquad (4.45)$$

represents the energy conservation. Therefore we call (c_1, c_2) the polarisation selection vector.

Writing

$$|P(\alpha)| = \begin{vmatrix} \cos^2\alpha & \sin^2\alpha \\ \sin^2\alpha & \cos^2\alpha \end{vmatrix} \qquad (4.46)$$

the general relation of polarisation selection ratio is then

$$|PS| = |P(\alpha)||c| \qquad (4.47)$$

where $|PS| = (PS^x, PS^y)^T$, $|c| = (c_1, c_2)^T$, and the superscript symbol T stands for the transpose operation of a matrix.

Although (4.47) or (4.42) is a general expression, it is still necessary to see what happens with the two extreme cases, a=0 and a=1. By substituting a=0 and a=1 into (4.40) and (4.42), we obtain

$$\begin{vmatrix} P^x \\ P^y \end{vmatrix} = P_{ab} \begin{vmatrix} \cos^2\alpha & \sin^2\alpha \\ \sin^2\alpha & \cos^2\alpha \end{vmatrix} \begin{vmatrix} 3/4 \\ 1/4 \end{vmatrix} \quad \text{for a=0} \qquad (4.48)$$

$$\begin{vmatrix} p^x \\ p^y \end{vmatrix} = P_{ab} \begin{vmatrix} \cos^2\alpha & \sin^2\alpha \\ \sin^2\alpha & \cos^2\alpha \end{vmatrix} \begin{vmatrix} 1/2 \\ 1/2 \end{vmatrix} \quad \text{for a=1} \qquad (4.49)$$

From these two expressions, it is clearly seen that even in the case of $\alpha=0$ or $\alpha=\pi/2$ using the pure dipole model (a=0) another polarisation component perpendicular to the pump polarisation direction is created. The mechanism of this phenomenon is the random orientation of the dopant ion dipoles. In fact, the site-selection due to both the polarised pump and the stimulated emission is not perfectly strict. Every dipole oscillator, except those exactly aligned to the y-axis, has a finite probability of making a transition into the x-mode. As a result of the statistics, this leads to energy coupling from pump power on the x-axis to the lasing power on the y-axis.

In addition, it is readily shown that the pure dipole model (a=0) leads to a maximum polarisation selectivity of PS=75%, if $\alpha=0$. That means that the fibre laser will "remember" the polarisation state of the pump to greatest degree. As for the model of the isotropic oscillator system (a=1), the two components of effective absorbed pump power are always equal to each other, independently of the launch polarisation orientation, or PS=50%, which indicates that the laser cavity has no memory of the polarisation state of the pump source.

Fig.4.4 shows the relationship between the polarisation vector (c_1,c_2) and the polarised cross-section ratio a. In general, for a partial anisotropic oscillator, the polarised cross-section $0<a<1$; the maximum polarisation selection ratio $50\%<PS<75\%$; and, as a result, fibre laser will remember the polarisation state of the pump to some degree.

(4) Discussion

Equation (4.42) or (4.47) provides an opportunity to use existing laser theory, valid only for an individual

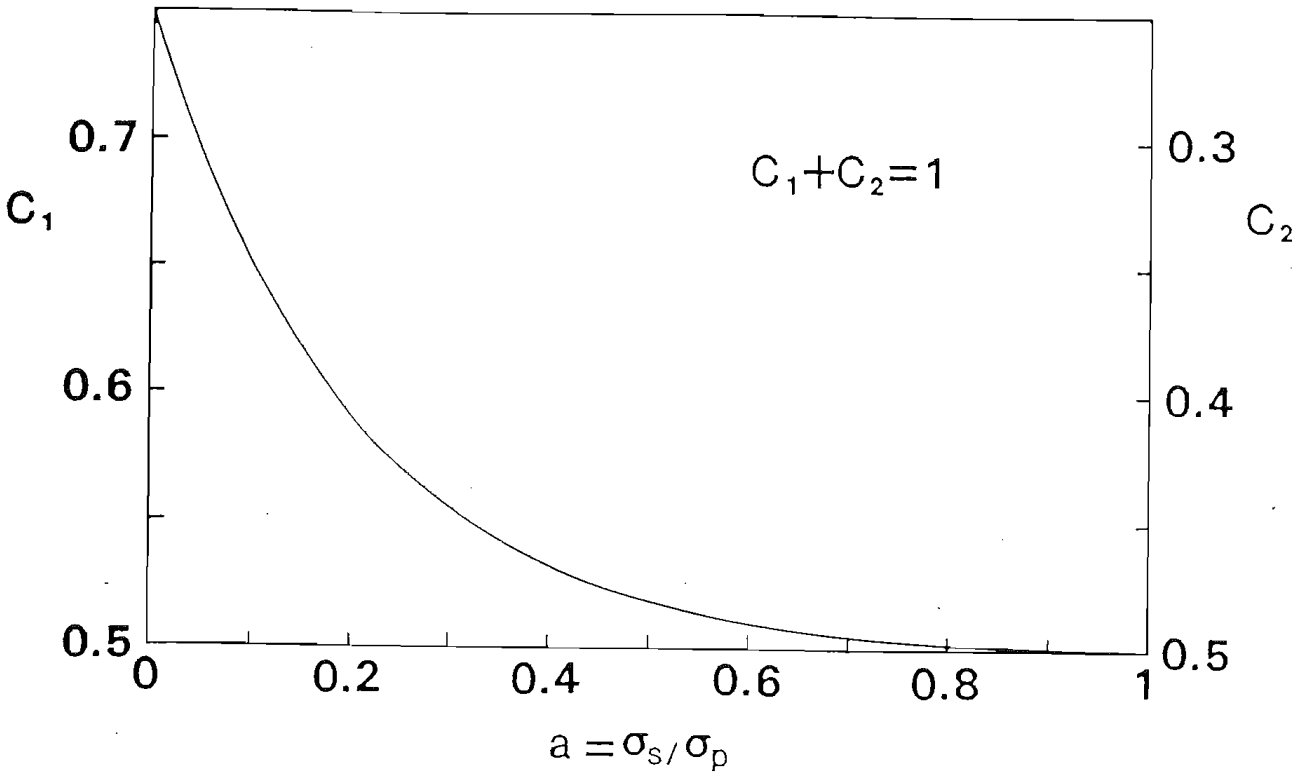

Fig.4.4 Relationship between the polarisation vector (C_1,C_2) and the polarised cross-section a.

lasing mode, to analyse the polarisation properties of the fibre laser, provided we regard P^x as the absorbed power for the x mode and P^y for the y mode.

In (4.42), P_{ab} is a measurable physical parameter and can be theoretically obtained by evaluating the measured total output power from the pump source P_{pu}, the launching efficiency η_{la} and the residual pump power from the end of the laser cavity P_{re} via the equation.

$$P_{ab} = P_{pu}\eta_{la} - P_{re} \qquad (4.50)$$

In most of the experiments dealt with in the thesis, the P_{ab} is measured using the cut-back method, which is described in detail elsewhere[17]. The angle α in (4.42) can be measured directly since the orientation of the birefringence axis can easily be determined, as pointed out in Chapter 3. Thus equation (4.42) eventually gives the relationship between the microscopic parameter $a \equiv \sigma_s/\sigma_p$ and the macroscopic parameter, the effective absorbed pump power, which is reflected in the laser performance. Therefore, not only can justification be made for the mathematical model, but also the parameter, a, pertaining to a specific fibre laser can be determined by experimental investigation.

References to Chapter 4

[1] W.M. Yen and P.M. Selzer: "Laser Spectroscopy of Solids", Springer-Verlag, Berlin, 1981.

[2] M.J. Weber: "Fluorescence and glass lasers", J. Non-Cryst. Solids 47, pp.117-133, 1982.

[3] J.L. Martin: "Basic Quantum Mechanics", Clarendon Press, Oxford, 1981.

[4] M.J. Weber: "Handbook of laser science and technology", Vol.V, CRC Press, 1987.

[5] M. Born and E. Wolf: "Principles of Optics", Pergamon, London, 1970.

[6] P.P. Feofilov: "The physical basis of polarized emission", Consultants Bureau, New York, 1961.

[7] The Editing Group: "Introduction to Solid Laser", Peoples Press, Shanghai, 1974.

[8] Murray Sargent III, M.O. Scully and W.E. Lamb: "Laser Physics", Addison-Wesley Publishing Company, Reading, Massachusetts, 1974.

[9] D.W. Hall and M.J. Weber: "Fluorescence line narrowing in neodymium laser glass", J. Appl. Phys. 55(7), pp.2642-2647, April 1984.

[10] D.W. Hall and M.J. Weber: "Polarized fluorescence line narrowing measurements of Nd laser glasses: Evidence of stimulated emission cross section anisotropy", Appl. Phys. Lett. 42(2), pp.157-159, January 1983.

[11] V.P. Lebedev and A.K. Przhevuskii: "Polarized luminescence of rare earth activated glasses", Sov. Phys. Solid State, 19(8), pp.1389-1391, August 1977.

[12] T. Kushida, E. Takushi and Y. Oka: "Memories of photon energy, polarization and phase in luminesence of rare earth ions under resonant light excitation", J. Luminescence 12/13, pp.723-727, 1976.

[13] A.C.G. Mitchell, and M.W. Zemansky: "Resonance Radiation and Excited Atoms", Cambridge University Press, Reprinted 1971.

[14] W. Koechner: "Solid-state Laser Engineering", Springer-Verlag, 1976

[15] S.B. Brawer and M.J. Weber: "Theoretical study of the structure and optical properties of rare-earth-doped BeF_2 glass", J. non-Cryst. Solids, Vol. 38/39, pp.9-14, 1980.

[16] D.W. Hall, R.A. Haas, W.F. Krupke and M.J. Weber: "Spectral and polarization hole burning in neodymium glass lasers" IEEE J.QE-19, No.11, pp.1704-1717, 1983.

[17] I.M. Jauncey: Private Communication.

Chapter Five

ANALYSIS OF LASING CHARACTERISTICS

The concept of an effective absorbed pump power component presented in the last chapter is now applied to existing laser theory, which is valid only for one individual lasing mode, in order to analyse the polarisation eigenmodes in a fibre laser. Thus the laser performance can be predicted. Furthermore, the agreement between the theoretical predictions and the experimental investigation gives a direct justification of the concept.

In order to employ existing laser theory it is necessary to introduce the small-signal single-pass gain lnG for the fibre laser. Similar to eq.(4.41), lnG can be defined as

$$\ln G_o = \int_0^l g_o e^{-\gamma z} dz = \frac{g_o}{\gamma} (1-e^{-\gamma l}) \qquad (5.1)$$

to replace the formula $\ln G=g_o l$ for the conventional solid-state bulk lasers[1]. Actually, (5.1) includes the case of conventional solid-state lasers, which is a specific example of $\gamma=0$, indicating a uniform gain distribution along the cavity. In (5.1), g_o is now regarded as a small-signal gain at the launching end of the fibre, and γ is the absorption coefficient of the fibre at the pump wavelength, as defined in eq.(4.32).

To simplify the expression as well as the mathematical derivation, the effective length l_e is introduced and defined as

$$l_e = \frac{1}{\gamma} (1 - e^{-\gamma l}) \qquad (5.2)$$

Thus the formula

$$\ln G_o = g_o l_e \qquad (5.3)$$

has the same form as that for conventional bulk lasers. Also a simplified form for the total absorbed pump power

P_{ab} is obtained by substituting (5.2) into (4.41), and expressed as

$$P_{ab} = I(o)Al_e \tag{5.4}$$

where A is the effective cross-sectional area of the fibre cavity and I(o) is the absorbed pump power density at z=0.

5.1 Threshold

The well-known formula for lasing threshold for an individual lasing mode in a four-level system, for example,[1] is

$$P_{th} = (L-\ln R_2) \; / \; (2K) \tag{5.5}$$

with

$$K = \eta_1\eta_2\eta_3\eta_4 \; / \; (I_s A) \tag{5.6}$$

$$I_s = h\nu \; / \; (\sigma_{21}\tau_f) \tag{5.7}$$

where P_{th} is the pump power required to achieve threshold, L is the total cavity loss at the lasing wavelength, and R_2 is the reflectivity of the output mirror (the input mirror is assumed to have R_1=100% at the lasing wavelength). In (5.6) η_2 is the fraction of the electrical input power which results in potentially useful radiation, η_3 is the launch efficiency obtained in transferring the useful radiation the pump source to the fibre and η_4 is the fraction of useful pump light which is absorbed by the laser material. In this thesis, the parameter of absorbed pump power P_{ab} rather than the original pump power is used. In this case (5.6) becomes

$$K = \eta_1 \; / \; (I_s A) \tag{5.8}$$

with

$$\eta_1 = \frac{P_f}{P_{ab}} = \eta_o \frac{\nu_o}{\nu_p} \qquad (5.9)$$

being the pumping efficiency, where the factor ν_o/ν_p is the ratio of fibre laser photon energy $h\nu_o$ and pump photon energy $h\nu_p$, η_o is the pumping efficiency factor defined by eq.(4.22). In these equations, P_{th} is now regarded as the absorbed pump power at threshold, I_s stands for the saturation density and A the fibre cross-sectional area.

If P_{thx} and P_{thy} represent the pure power required for the x and y modes, respectively, to achieve threshold, the threshold condition can be obtained by using the concept of effective pump power, eq.(4.42), and expressed as

$$P_{th}^{x} = P_{thx} \,/\, (c_1\cos^2\alpha + c_2\sin^2\alpha) \qquad (5.10a)$$

$$P_{th}^{y} = P_{thy} \,/\, (c_1\sin^2\alpha + c_2\cos^2\alpha) \qquad (5.10b)$$

where P_{th}^{x} and P_{th}^{y} are real, or total, absorbed pump power for the x and y modes to reach the thresholds, respectively. The P_{thx} and P_{thy} are known as imaginary thresholds since they are unmeasurable. P_{th}^{x} and P_{th}^{y} are always larger than P_{thx} and P_{thy} respectively. For instance, when a=0 or $(c_1,c_2)=(3/4,1/4)$

$$\left.\begin{aligned} P_{thx} &= \frac{3}{4} P_{th}^{x} \\ P_{thy} &= \frac{1}{4} P_{th}^{y} \end{aligned}\right\} \quad \text{for } \alpha=0 \qquad (5.11a)$$

and

$$\left.\begin{aligned} P_{thx} &= \frac{1}{2} P_{th}^{x} \\ P_{thy} &= \frac{1}{2} P_{th}^{y} \end{aligned}\right\} \quad \text{for } \alpha=45^{o} \qquad (5.11b)$$

Fig.5.1 shows the total absorbed pump power at threshold for the x mode as a function of launching angle α for various values of a, the polarised cross-section ratio.

Combining (4.42), (5.5) and (5.8), the absorbed pump power ratio of the x and y modes required to achieve threshold P_{th}^{x}/P_{th}^{y} can be expressed as follows:

$$\frac{P_{th}^{x}}{P_{th}^{y}} = \frac{\sigma^{y}(L^{x}-\ln R_2^{x})}{\sigma^{x}(L^{y}-\ln R_2^{y})} \frac{c_1\sin^2\alpha+c_2\cos^2\alpha}{c_1\cos^2\alpha+c_2\sin^2\alpha} \qquad (5.12)$$

or, substituting σ from (4.21) into (5.12):

$$\frac{P_{th}^{x}}{P_{th}^{y}} = \frac{n_x^2(L^{x}-\ln R_2^{x})}{n_y^2(L^{y}-\ln R_2^{y})} \frac{c_1\sin^2\alpha+c_2\cos^2\alpha}{c_1\cos^2\alpha+c_2\sin^2\alpha} \qquad (5.13)$$

There are two extreme cases to be considered. One is for $\alpha=45^{o}$ and the other is for $\alpha=0^{o}$ or 90^{o}. When $\alpha=45^{o}$, (5.13) becomes

$$\frac{P_{th}^{x}}{P_{th}^{y}} = \frac{n_x^2(L^{x}-\ln R_2^{x})}{n_y^2(L^{y}-\ln R_2^{y})} \qquad (5.14)$$

or alternatively, the relative differential threshold

$$(P_{th}^{x}-P_{th}^{y})/P_{th}^{x} = (P_{thx}-P_{thy})/P_{thx}$$

$$\approx \frac{2(\Delta n)}{n} + \frac{\Delta L}{L-\ln R_2} \qquad (5.15)$$

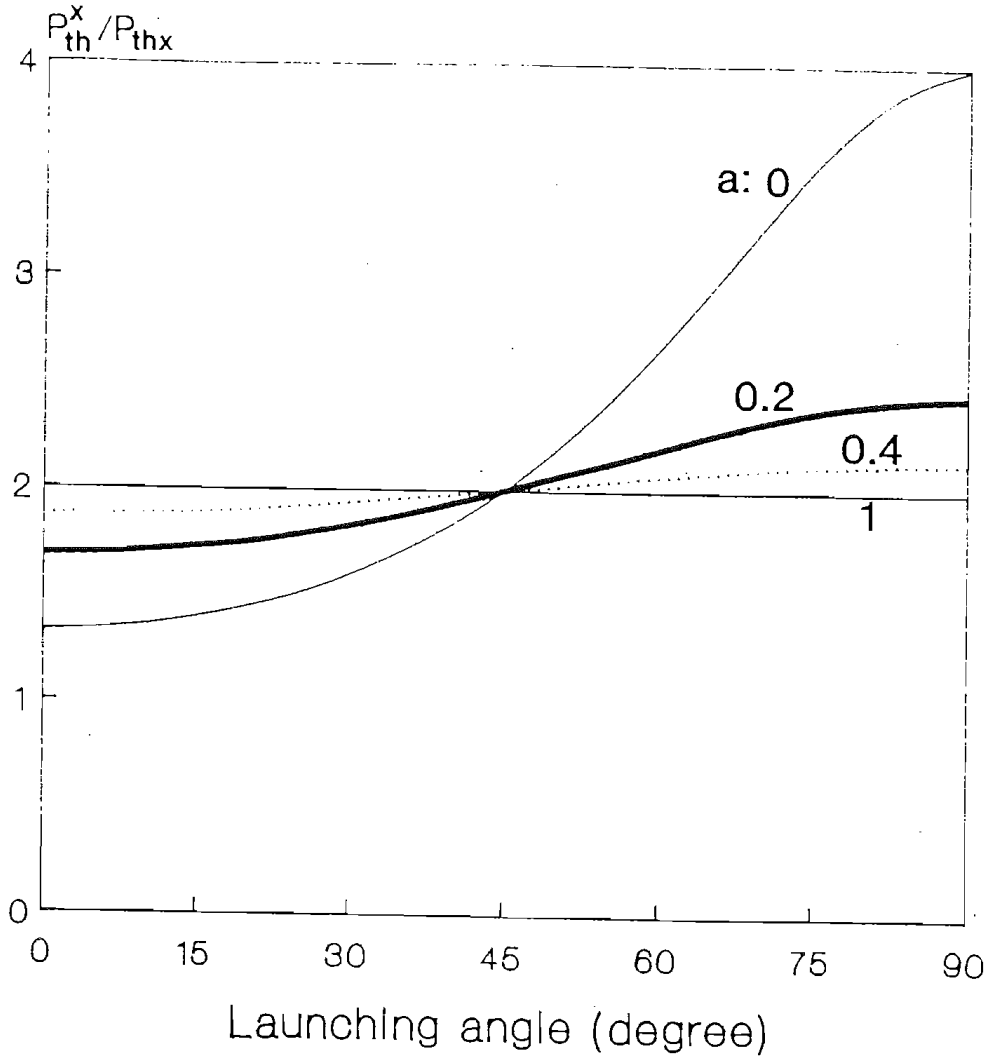

Fig.5.1 Normalized threshold power for the x-mode as a function of launching angle for various polarised cross-section ratios.

This is, obviously, the intrinsic difference between the x and y modes in a fibre laser cavity. Since P_{th}^{x} and P_{th}^{y} are the absorbed pump powers, a measurable parameter, the ratio P_{th}^{x}/P_{th}^{y}, or differential threshold can be obtained by using a circularly-polarised pump beam, or 45° launching of a linearly-polarised pump beam, which is presented in Section 5.5 of this chapter.

When α is not near to 45°, the main source causing the difference of the thresholds between the x and y modes is the difference of the effective absorbed pump power, while the intrinsic difference is negligible and thus the relation $P_{thx} \approx P_{thy}$ applied. In this case, (5.13) can be expressed approximately as

$$\frac{P_{th}^{x}}{P_{th}^{y}} = \frac{c_1 \sin^2\alpha + c_2 \cos^2\alpha}{c_1 \cos^2\alpha + c_2 \sin^2\alpha} \qquad (5.16)$$

The relative differential threshold can be defined and derived as follows

$$\frac{P_{th}^{x} - P_{th}^{y}}{P_{thx}} = \frac{-4(c_1 - c_2)\cos 2\alpha}{4c_1 c_2 \cos^2 2\alpha + \sin^2 2\alpha} \qquad (5.17)$$

The calculated curves are shown in Fig.5.2 for the cases a=0 and a=1. The relative differential threshold shows a decreasing function of the pumping angle α if $0<\alpha<45°$.

It is concluded from the above analysis that with a certain launching angle α, different polarisation eigenmodes have different thresholds. The difference in thresholds between the two modes is dependent on the launching angle. When the laser is pumped on axis, say the x-axis, the differential threshold or threshold ratio reaches a maximum value and when $\alpha=45°$ it is minimised. These conclusions fit the experimental measurements described in Chapter 3 rather well.

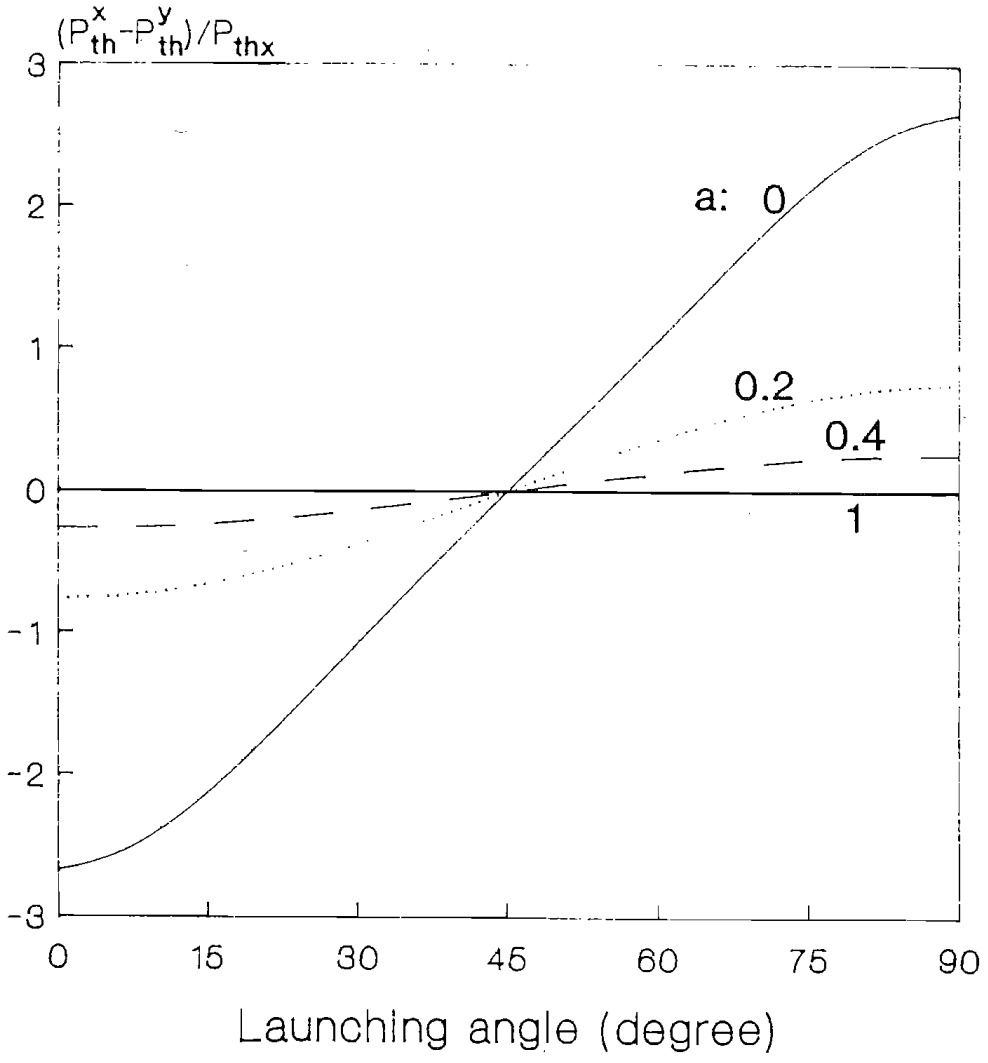

Fig.5.2 Relative differential threshold as a function of launching angle for various polarised cross-section ratios.

It is easy to show that all the formulae presented above are also valid for three-level laser systems.

5.2 Slope Efficiency

It can be shown that the linear relationship between output and the absorbed pump power:

$$P_{out} = \eta\ (P_{ab} - P_{th}) \tag{5.18}$$

is still valid for fibre lasers, provided the particular small-signal single-pass gain expressed in (5.1) is employed. The slope efficiency η in (5.18) is the product of the pumping efficiency η_1 and the output coupling efficiency η_5.

$$\eta = \eta_1\eta_5 \tag{5.19}$$

with

$$\eta_5 = \frac{2(1-R_2)}{(L-\ln R_2)\sqrt{R_2}} \tag{5.20}$$

and η_1 being expressed by eq.(5.9). Here the efficiency η has been treated as identical for both x and y modes.

Substituting (4.42) and (5.10) into (5.18) gives

$$P_{out}^{x} = \eta(c_1\cos^2\alpha+c_2\sin^2\alpha)(P_{ab}-P_{th}^{x}) \tag{5.21a}$$

$$P_{out}^{y} = \eta(c_1\sin^2\alpha+c_2\cos^2\alpha)(P_{ab}-P_{th}^{y}) \tag{5.21b}$$

From equation (5.21) the slope efficiency ratio of the x mode to the y mode is:

$$\frac{SLOPE_x}{SLOPE_y} = \frac{c_1\cos^2\alpha+c_2\sin^2\alpha}{c_1\sin^2\alpha+c_2\cos^2\alpha} \tag{5.22}$$

Fig.5.3 shows the curves of $SLOPE_x/SLOPE_y$ as a function of launch orientation of pump light polarisation with various values of a. Comparing (5.22) with (5.14), it is readily shown that this figure also corresponds to

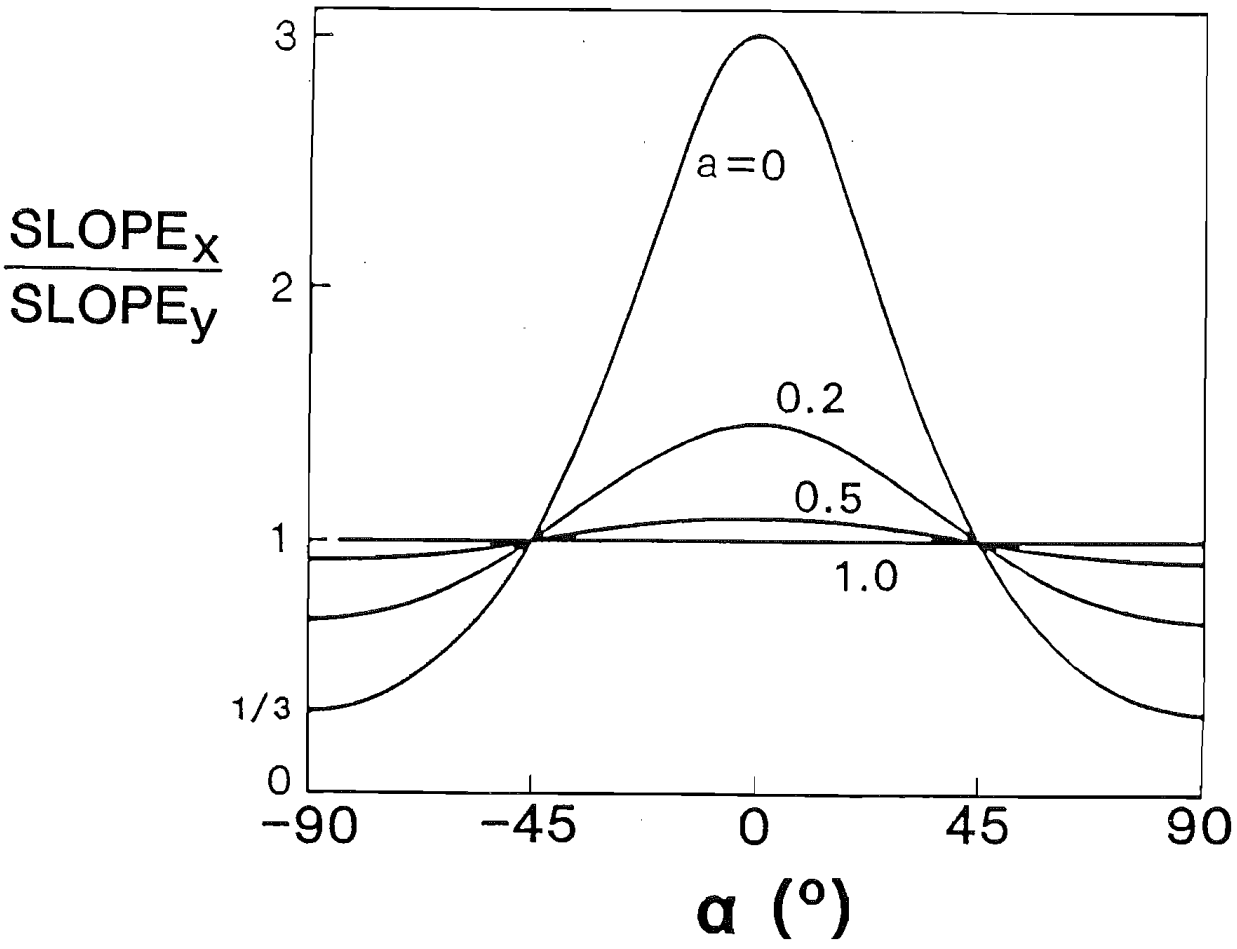

Fig.5.3 Dependence of $SLOPE_x/SLOPE_y$ on α for various values of a.

eq.(5.14), provided the abscissae moves right or left by 90°.

With the pure dipole model, i.e. a=0, the extreme values of $SLOPE_x/SLOPE_y=3$ and 1/3 appear when the pump polarisation orientation $\alpha=0$, and $\alpha=90°$, respectively. As for the case of a=1, the isotropic oscillator model, the slope efficiency is identical for the two eigenmodes. In practice, $1<SLOPE_x/SLOPE_y<3$ for rare-earth doped fibre lasers, if $\alpha=0$.

Eq.(5.22) and Fig.5.3 reveal the relationship between the slope efficiency ratio and the angle α, and gives a good interpretation for the experimental measurements shown in Fig.3.5. Since all the laser parameters such as cavity losses and lasing thresholds, which it is usually difficult to obtain precisely, have been eliminated in (5.22), the ratio $SLOPE_x/SLOPE_y$ can be measured accurately and enables values of the polarised cross-section ratio $a\equiv\sigma_s/\sigma_p$ to be deduced. This is presented in Section 5.6 of this chapter.

Another conclusion drawn from equation (5.21) is that the total output power, or the non-polarisation resolved output, from fibre lasers is still linearly related to the absorbed power P_{ab} with slope efficiency of η. In fact, adding the two equations in (5.21) yields:

$$P_{tot} = P_{out}^{x}+P_{out}^{y} = \eta(P_{ab}-P_{thx}-P_{thy}) \qquad (5.23)$$

where P_{thx} and P_{thy} are defined by the expression (5.10). In addition, eq.(5.23) allows a relation

$$P_{thx} + P_{thy} = P_{th} \qquad (5.24)$$

to be obtained, giving the physical meaning to the imaginary pure threshold for polarisation eigenmodes

$$P_{thx} \approx P_{thy} \approx \frac{P_{th}}{2} \qquad (5.25)$$

where P_{th} is the threshold for the non-polarisation-resolved operation of fibre lasers.

Also, the equation (5.23) indicates that the slope efficiency of the non-polarisation-resolved output from a fibre laser, η, is independent of launching polarisation orientation. This agrees with all the previous work on fibre lasers[2,3,4], which reported the lasing characteristics with non-polarisation-resolved measurements.

A laser-diode pumped Nd^{3+}-doped fibre laser was set up to verify the theory. The experimental arrangement was similar to that described in Chapter 3. The pump orientation was α=0. The results shown in Fig.5.4 demonstrate very good linearity of both polarisation resolved, and non-polarisation resolved, measurements. In addition, the relation $P_{tot}=P_{out}{}^{x}+P_{out}{}^{y}$ is confirmed.

5.3 Relaxation Oscillation Frequency

The basic physical mechanism of relaxation oscillations in a laser consists of an interplay between the field intensity in the resonator and the population inversion. An increase in the field intensity causes a reduction in the inversion due to the increased rate of stimulated transitions. This causes a reduction in the gain which in turn tends to decrease the intensity.

The relaxation oscillation frequency for a lasing mode in an ideal four-level system can be expressed as[7]

$$\omega_m = \sqrt{\frac{1}{t_c \tau}(r-1) - \left(\frac{r}{2\tau}\right)^2} \qquad (5.26)$$

where t_c is the cavity photon lifetime, τ the lifetime due to all causes except stimulated emission, and $r=P/P_{th}$ is the excess threshold power. It has been shown in Chapter 3 that the two polarisation eigenmodes in the fibre laser cavity have independent relaxation

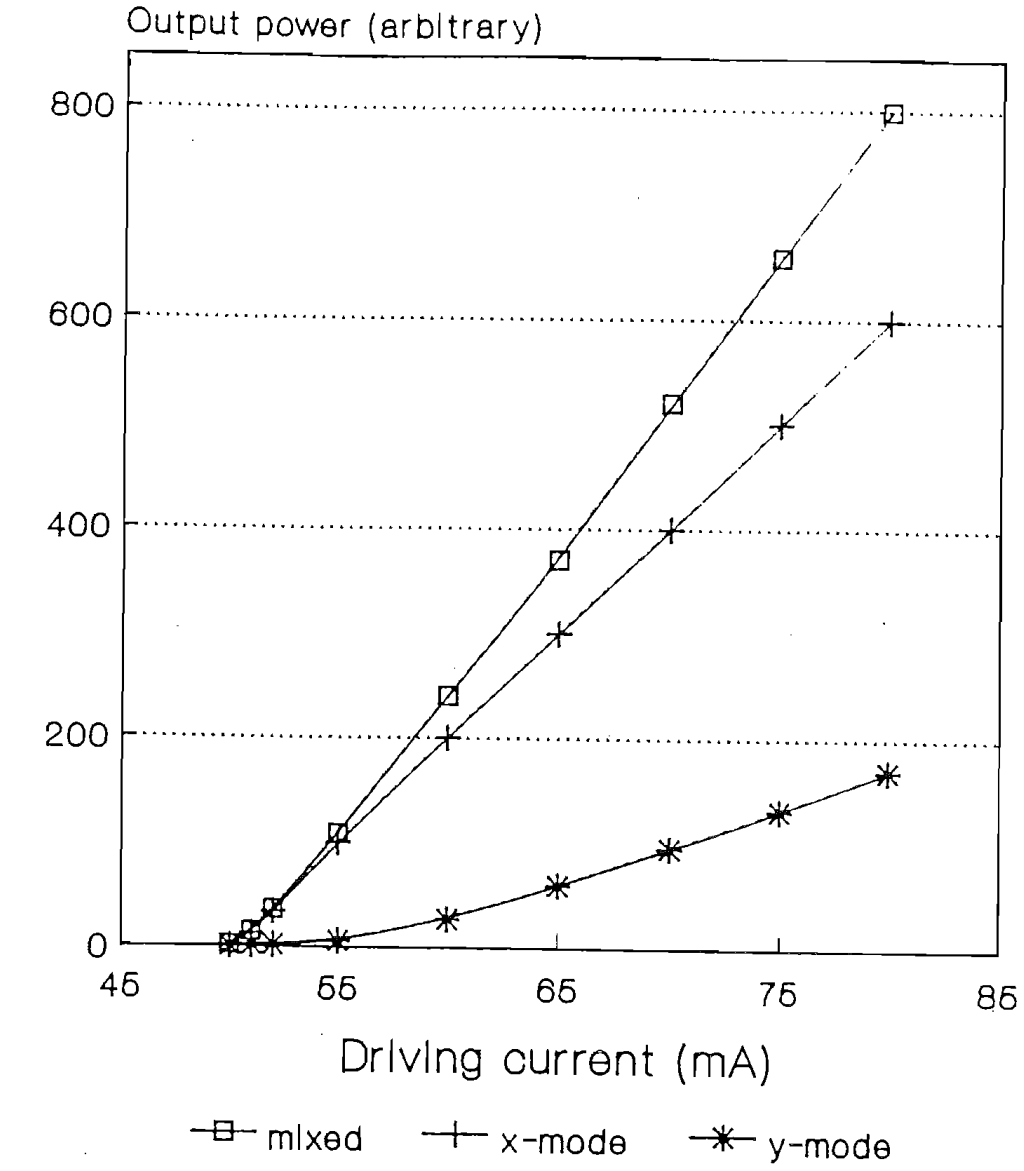

Fig.5.4 Lasing characteristics of a Nd^{3+}-doped fibre laser, showing good linearity of both polarisation-resolved and non-polarisation-resolved measurements.

oscillations. By using P^x/P_{thx} and P^y/P_{thy} instead of P/P_{th} for the x and y mode respectively in the fibre lasers, we obtain

$$\frac{\omega_x}{\omega_y}=\sqrt{\frac{(c_1\cos^2\alpha+c_2\sin^2\alpha)\frac{P_{ab}}{P_{thx}}-\frac{t_c}{4\tau}(c_1\cos^2\alpha+c_2\sin^2\alpha)^2(\frac{P_{ab}}{P_{thx}})^2-1}{(c_1\sin^2\alpha+c_2\cos^2\alpha)\frac{P_{ab}}{P_{thy}}-\frac{t_c}{4\tau}(c_1\sin^2\alpha+c_2\cos^2\alpha)^2(\frac{P_{ab}}{P_{thy}})^2-1}} \qquad (5.27)$$

If $t_c/4\tau\approx 0$, which is the case for a Nd^{3+}-doped fibre laser, $\tau=3\sim5\cdot10^{-4}$s and $t_c=10^{-8}\sim10^{-6}$s, the expression becomes

$$\frac{\omega_x}{\omega_y}=\sqrt{\frac{c_1\cos^2\alpha+c_2\sin^2\alpha-P_{th}/P_{ab}}{c_1\sin^2\alpha+c_2\cos^2\alpha-P_{th}/P_{ab}}} \qquad (5.28)$$

where it has been assumed again that $P_{thx}\approx P_{thy}$

Far above threshold, i.e. $P_{th}/P_{ab}\approx 0$,

$$\frac{\omega_x}{\omega_y}=\sqrt{\frac{c_1\cos^2\alpha+c_2\sin^2\alpha}{c_1\sin^2\alpha+c_2\cos^2\alpha}} \qquad (5.29)$$

Fig.5.5 shows the theoretical calculation of relaxation oscillation frequency ratio ω_x/ω_y as a function of α far above threshold, for various values of a, whereas Fig.5.6 shows the dependence of ω_x/ω_y on α for different pump powers.

As a transient effect, the relaxation oscillations of the intensities of x and y modes are affected by many factors and the patterns seem to be disturbed to some degree, which is discussed in Chapter 8 as a topic of polarisation hole burning in the time domain. It is then difficult, in practice, to measure the relaxation oscillation frequency ratio of the x and y modes with a spectrum analyser due to the disturbed damped shape of

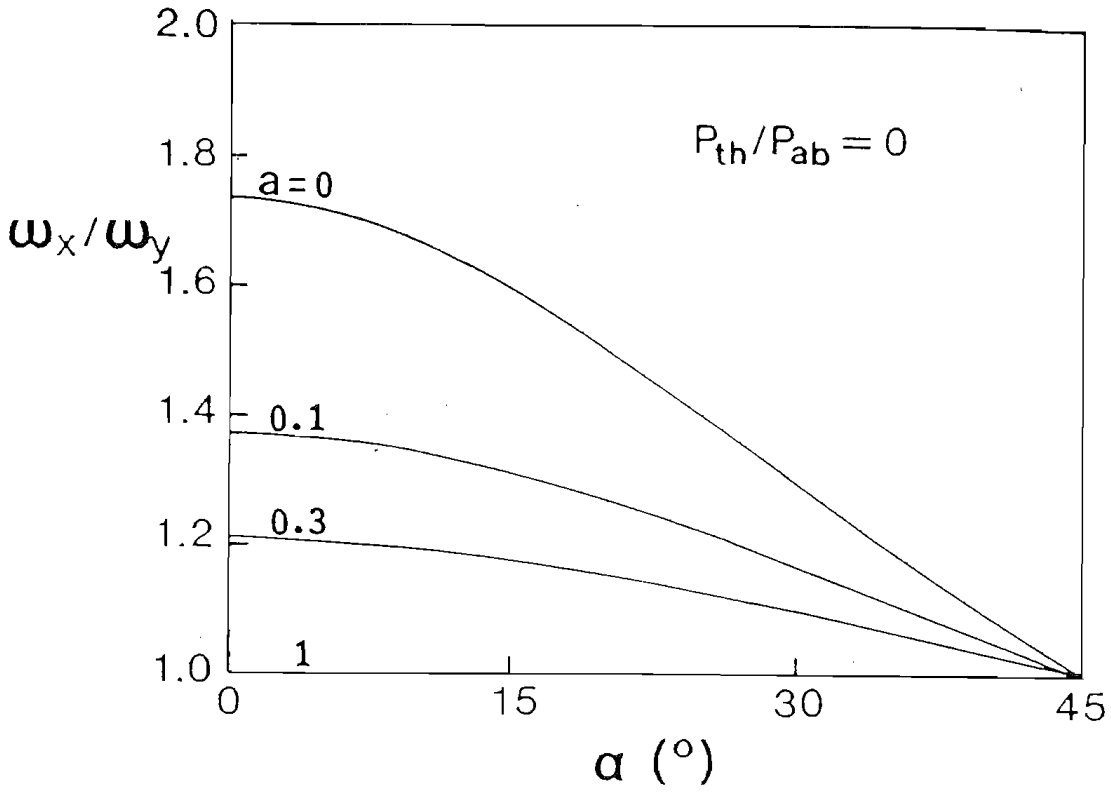

Fig.5.5 Relaxation oscillation frequency ratio ω_x/ω_y as a function of α far above threshold, for various values of a.

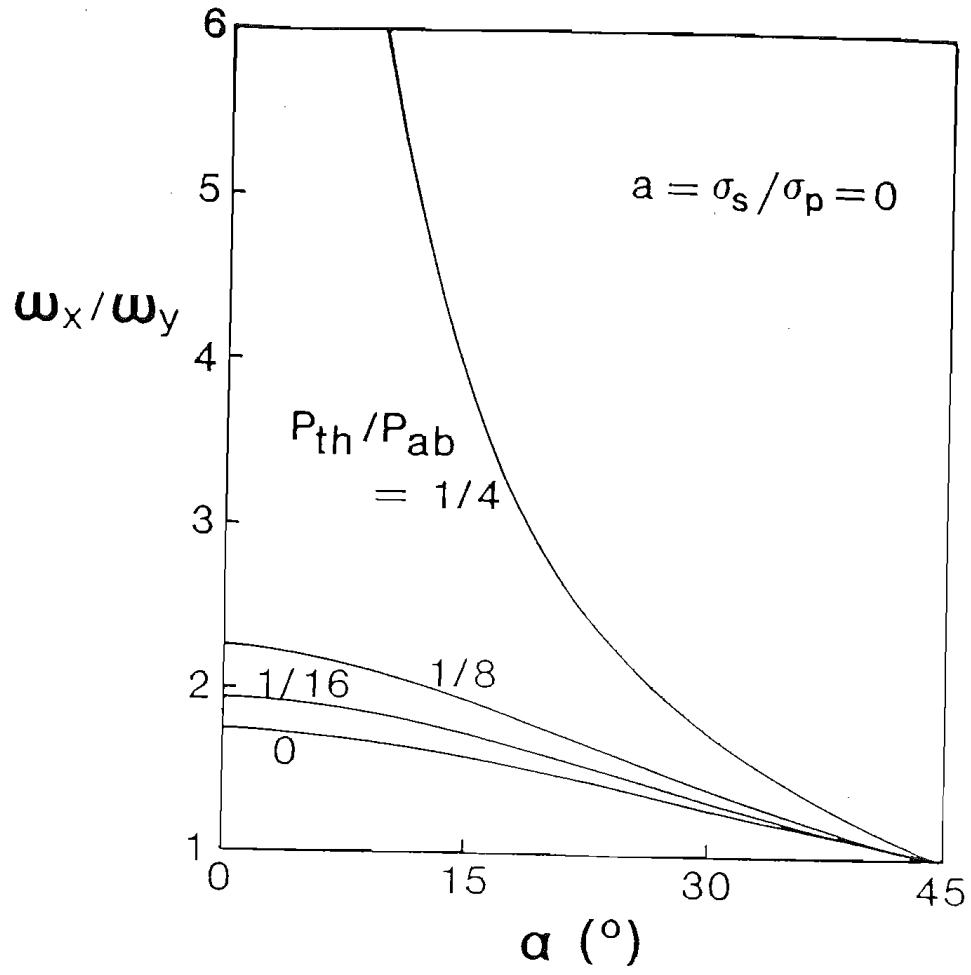

Fig.5.6 Dependence of ω_x/ω_y on α for various absorbed pump powers.

the oscillation, as well as various noise effects. Even so, the relaxation frequencies for the x and y modes can still be distinguished.

To verify the theoretical prediction, namely the tendency of ω_x/ω_y to decrease with increased pump power and/or increased pumping orientation α, the relaxation patterns for a diode-pumped Nd^{3+} fibre laser were investigated. The tendency of ω_x/ω_y to decrease with increased pump power was found to be in agreement with theory.

Fig.5.7 shows typical relaxation oscillation patterns, each showing two orthogonal eigenmodes with different build-up times and oscillation frequencies. The initial part of each trace represents the stronger, which appears first and has been heavily attenuated by a nearly crossed polariser. The upper picture was taken at $P_{ab}/P_{th}=5$, leading to $\omega_x/\omega_y=6$, and the lower at $P_{ab}/P_{th}=7$, leading to $\omega_x/\omega_y=2.9$.

Using a polarised beam splitter with a correct orientation coinciding with the principal axes in a fibre laser, the polarisation-resolved relaxation signals were detected separately and displayed on the same screen, and the ω_x/ω_y as a function of α can then be measured. Fig.5.8 shows four pictures for different pumping angles, $\alpha=0^o$, 10^o, 20^o, 45^o, respectively. The plotted figures for ω_x/ω_y in Fig.5.9 also show good agreement with the theoretical curves in Fig.5.5 and 5.6.

5.4 Degree of Polarisation (DOP)

One of the most important parameters describing the polarisation property of fibre lasers is the degree of polarisation (DOP) as defined in equation (2.1). When the absorbed power exceeds the secondary mode threshold, the lasing characteristics of both polarisation eigenmodes follow equation (5.21), and the DOP can be readily derived as

(a)

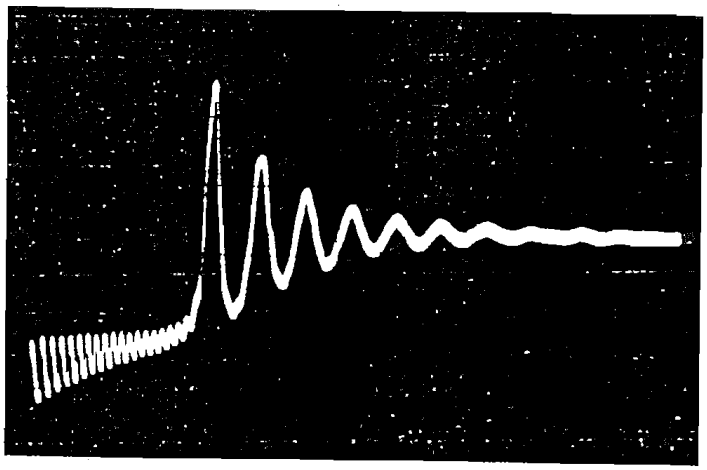

(b)

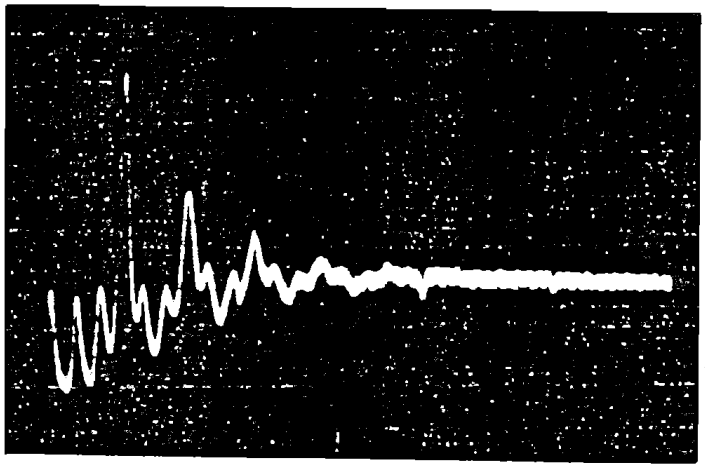

Fig.5.7 Typical relaxation oscillation patterns, showing the tendency of ω_x/ω_y to decrease with increased pump power. The upper picture was taken at $P_{ab}/P_{th}=5$, leading to $\omega_x/\omega_y=6$, whereas the lower $P_{ab}/P_{th}=7$, leading to $\omega_x/\omega_y=2.9$.

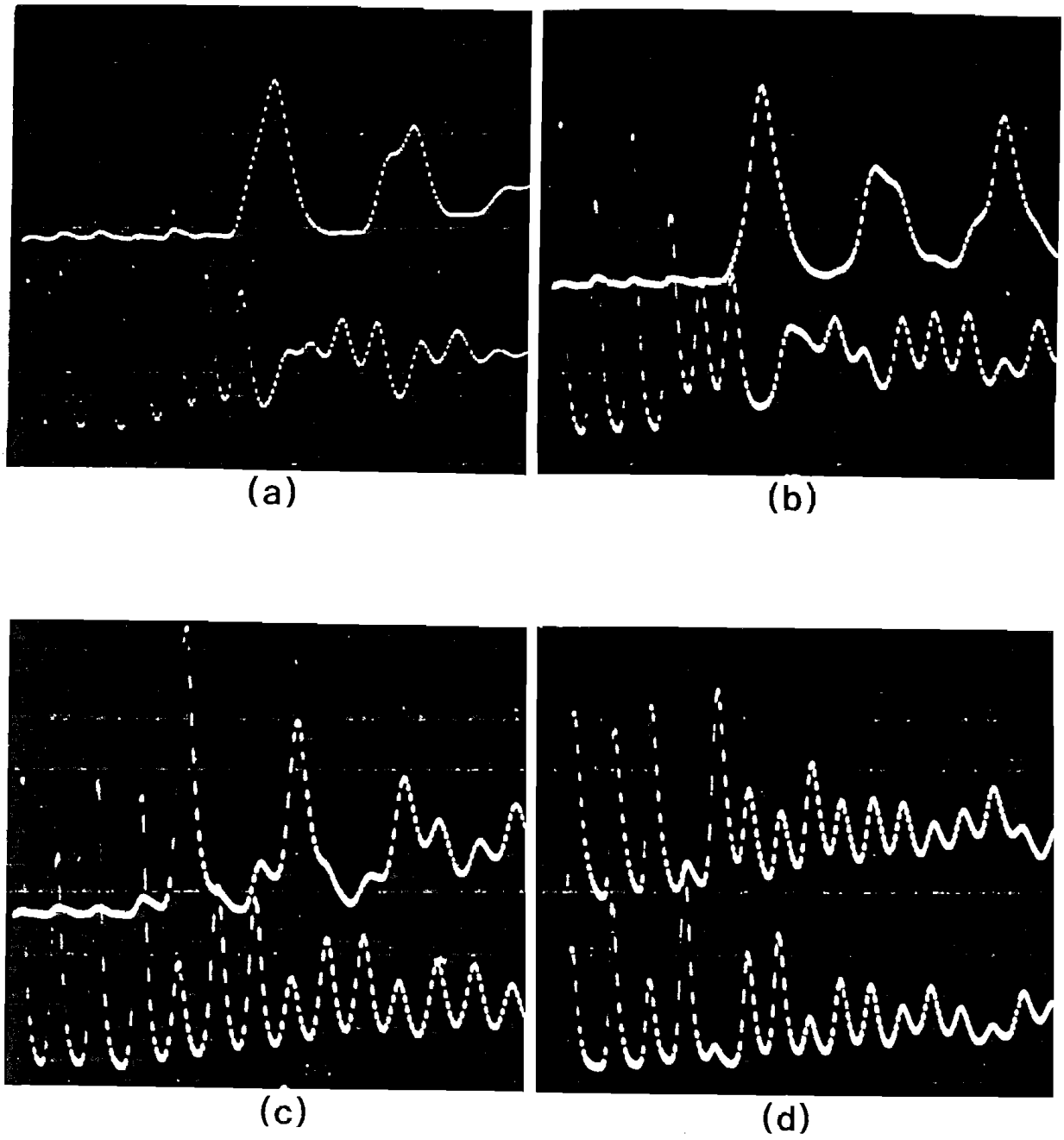

Fig.5.8 Pictures showing polarisation-resolved relaxation oscillation patterns for different pumping orientations.

(a) $\alpha=0^{o}$, (b) $\alpha=10^{o}$, (c) $\alpha=20^{o}$, (d) $\alpha=45^{o}$

Upper traces: y-mode

Lower traces: x-mode

Time scale: 50μs/div.

Pump level: $P_{ab}/P_{th}=4.5$

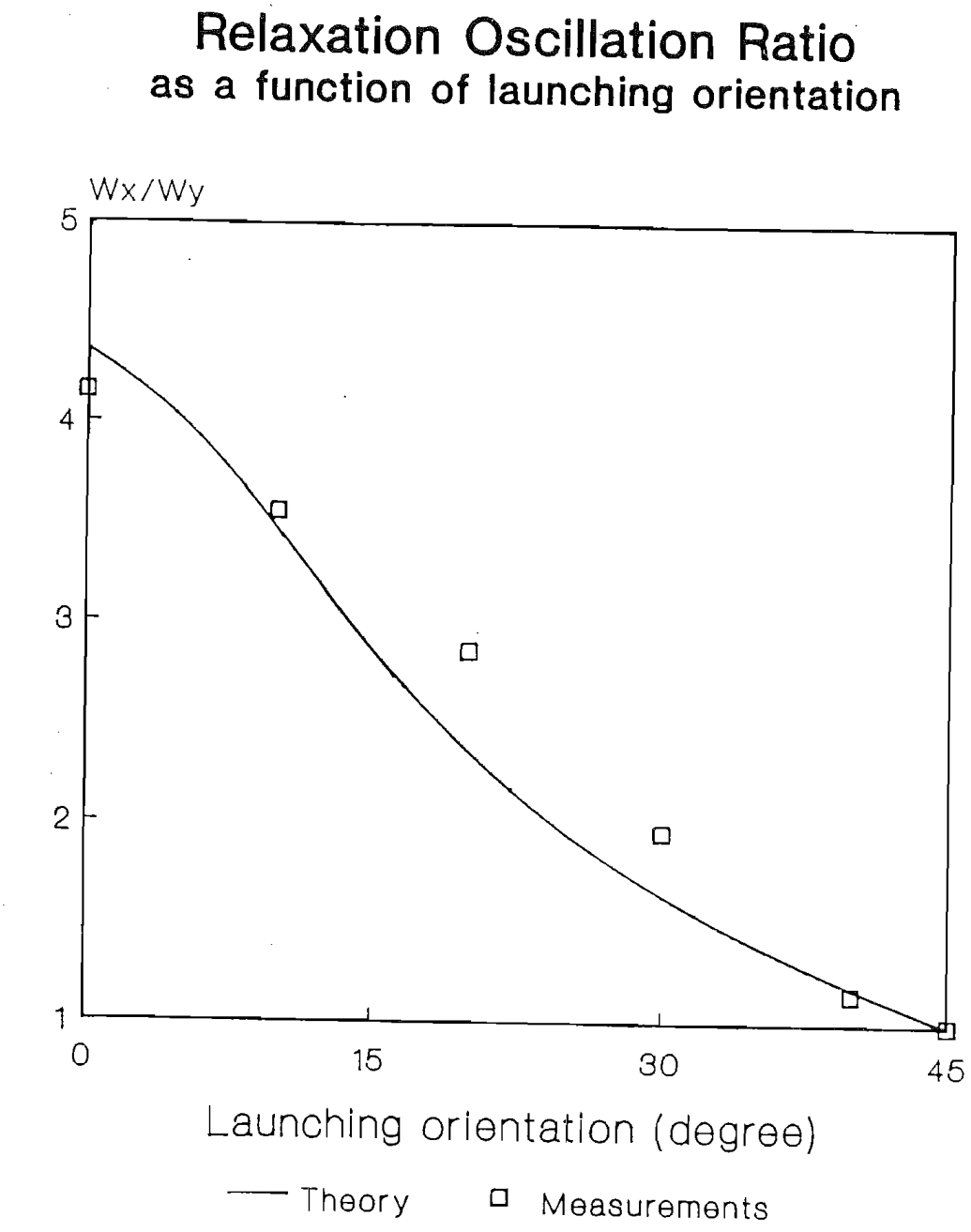

Fig.5.9 Relaxation oscillation frequency ratio as a function of launching orientation, showing agreement with theoretical prediction.

$$DOP = \frac{(c_1-c_2)\cos 2\alpha - (P_{thx}-P_{thy})/P_{ab}}{(c_1+c_2) - (P_{thx}+P_{thy})/P_{ab}} \qquad (5.30)$$

The approximation of $(P_{thx}-P_{thy})/P_{ab}\approx 0$, and $c_1+c_2=1$, gives:

$$DOP = \frac{c_1 - c_2}{1 - (P_{thx}+P_{thy})/P_{ab}} \cos 2\alpha \qquad (5.31)$$

This is an accurate interpretation of the third character of polarisation effects, namely the $\cos(2\alpha)$ function form in eq.(3.1). Furthermore, a certain form of the function $f(P_{ab},a)$ is obtained and expressed as

$$f(P_{ab},a) = \frac{c_1 - c_2}{1 - (P_{thx}+P_{thy})/P_{ab}} \qquad (5.32)$$

This allows us to calculate the dependence of $f(P_{ab},a)$ on the total absorbed pump power P_{ab}. The theoretical curves and the experimental measurements for a Nd^{3+}-doped fibre laser are shown in Fig.5.10 and Fig.3.10, respectively. It is evident that both figures agree with each other very well.

It is worth noting that there is a limiting value of $P_{ab}/(P_{thx}+P_{thy})$. For example, $P_{ab}/(P_{thx}+P_{thy})$ must be larger than 2 for the case of $a\equiv\sigma_s/\sigma_p=0$ since all the calculations are carried out by assuming that the two polarisation eigenmodes are lasing simultaneously. Otherwise, the calculation would exceed the reasonable regime. From the flatness of the right-hand limits of the curves, it may be concluded that $P_{ab}/(P_{thx}+P_{thy})>10$ far above threshold. Thus it is understood that most practical fibre lasers operate far above threshold. Substituting $(P_{thx}+P_{thy})/P_{ab}\approx 0$ into (5.31) results in

$$DOP = (c_1-c_2)\cos 2\alpha \qquad (5.33)$$

For two particular values of the polarised cross-section ratio, a=1 and a=0, DOP can be expressed as

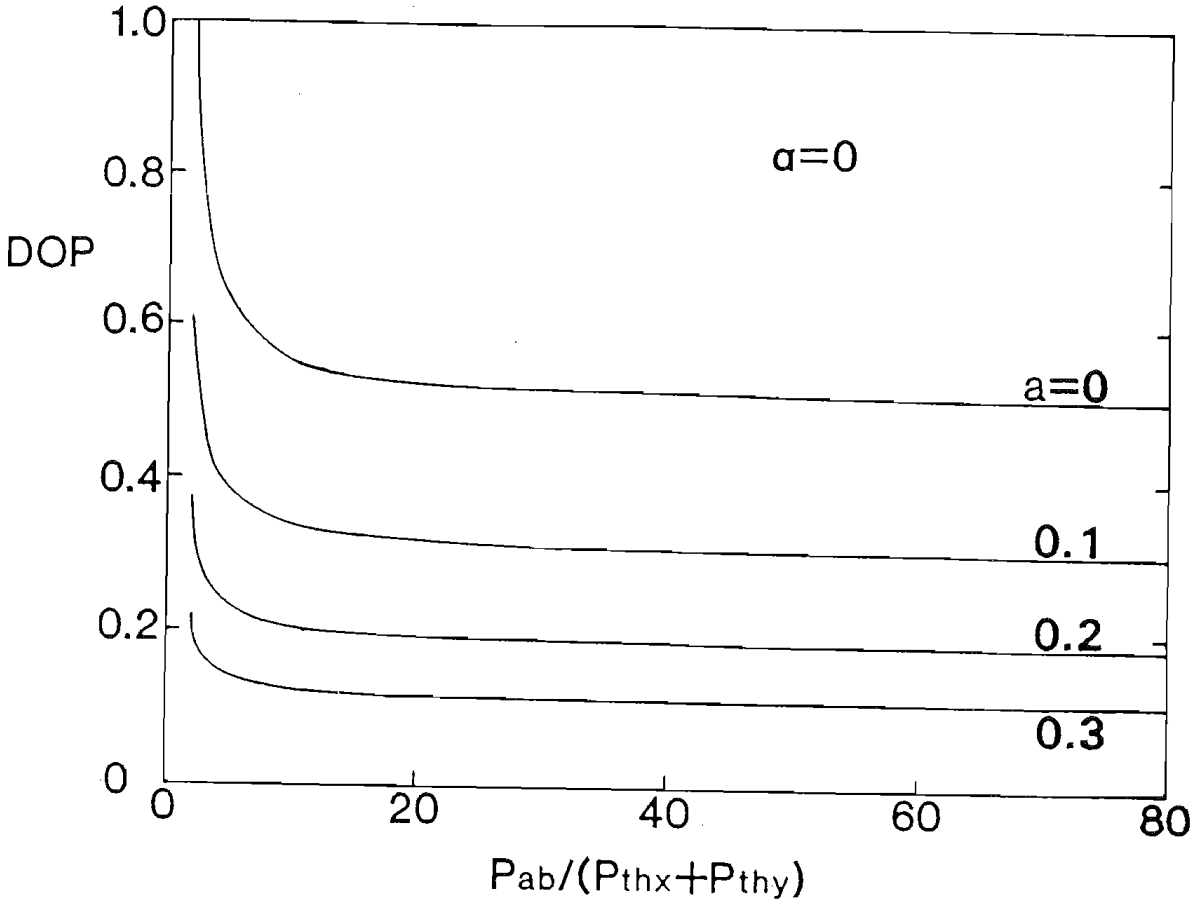

Fig.5.10 Dependence of degree of polarisation of the fibre laser on relative pump power for various values of a.

$$DOP = 0.5\cos 2\alpha \qquad \text{for } a=0 \qquad (5.34a)$$

$$DOP = 0 \qquad \text{for } a=1 \qquad (5.34b)$$

indicating that the maximum value of DOP varies from 0 to 0.5, and depending on the characteristics of the rare-earth dopants.

5.5 45° Effects

It is found from experiment that when a fibre laser is pumped by linearly polarised light at 45° to the fibre axes, a difference in lasing characteristics between the two orthogonal polarisation eigenmodes always exist, sometimes significantly, as can be seen from Fig.3.5.

Two possible reasons for this phenomenon are: firstly, the intrinsic cavity differences between two orthogonal polarisation eigenmodes; and secondly, the different pumping efficiencies for those two modes. The former is reflected theoretically by eqs.(5.14) and (5.15), and affects mainly the threshold conditions. The latter causes a differential slope efficiency between the two polarisation eigenmodes as expressed by eqs.(5.19) and (5.21).

The intrinsic cavity difference includes two terms, as shown in (5.15), the differential index Δn and the differential cavity loss ΔL. The differential index Δn has a value of order 10^{-8}~10^{-4}, as pointed out in Chapter 2. The differential fibre loss between the two polarisation modes due to the material absorption and waveguide scattering is estimated to be even smaller than this[5]. However, a theoretical analysis shows that the imperfection of the cleaved fibre ends as well as the imperfect butting of the fibre end against the mirror may induce a differential cavity loss between the two orthogonal polarisation eigenmodes.

When a lightwave falls on a boundary between two media of different optical properties, glass and air, it is split into two waves: a transmitted wave proceeding

into the second medium and a reflected wave propagating back into the first medium. The direction of the refracted wave is determined by Snell's law[6]:

$$n_i \sin\theta_i = n_t \sin\theta_t \tag{5.35}$$

where the subscript i and t refer to the incident and transmitted lights respectively, n is the refraction index and θ is the angle relative to the normal of the fibre end. The different polarisation components of the refracted light have different transmissions determined by the Fresnel formula[6]. The transmission ratio for components parallel with (p-component) and perpendicular to (s-component) the incident plane are expressed as[6]

$$T_p = \frac{\sin 2\theta_i \sin 2\theta_t}{\sin^2(\theta_i+\theta_t)\cos^2(\theta_i-\theta_t)} \tag{5.36a}$$

and

$$T_s = \frac{\sin 2\theta_i \sin 2\theta_t}{\sin^2(\theta_i+\theta_t)} \tag{5.36b}$$

respectively. The influence of differential reflection at the fibre ends is negligible since the reflection fraction is rather small in comparison with the transmitted fraction in the case of the fibre laser.

Consider an extreme case, with the polarisation aligned to the x axis. The differential loss between the x and y modes caused by a round trip at one end of the fibre can be derived to be

$$\begin{aligned} \Delta L &= \ln T_s - \ln T_p \\ &= -2\ln[\cos(\theta_i-\theta_t)] \end{aligned} \tag{5.37}$$

If we regard the tilt angle θ of the fibre end as the incident angle θ_i the differential loss ΔL as a function of angle θ is calculated as shown in Fig.5.11. It is seen that when θ is smaller than 1^o the induced ΔL only has an order of 10^{-6}. Since the calculation was carried out with

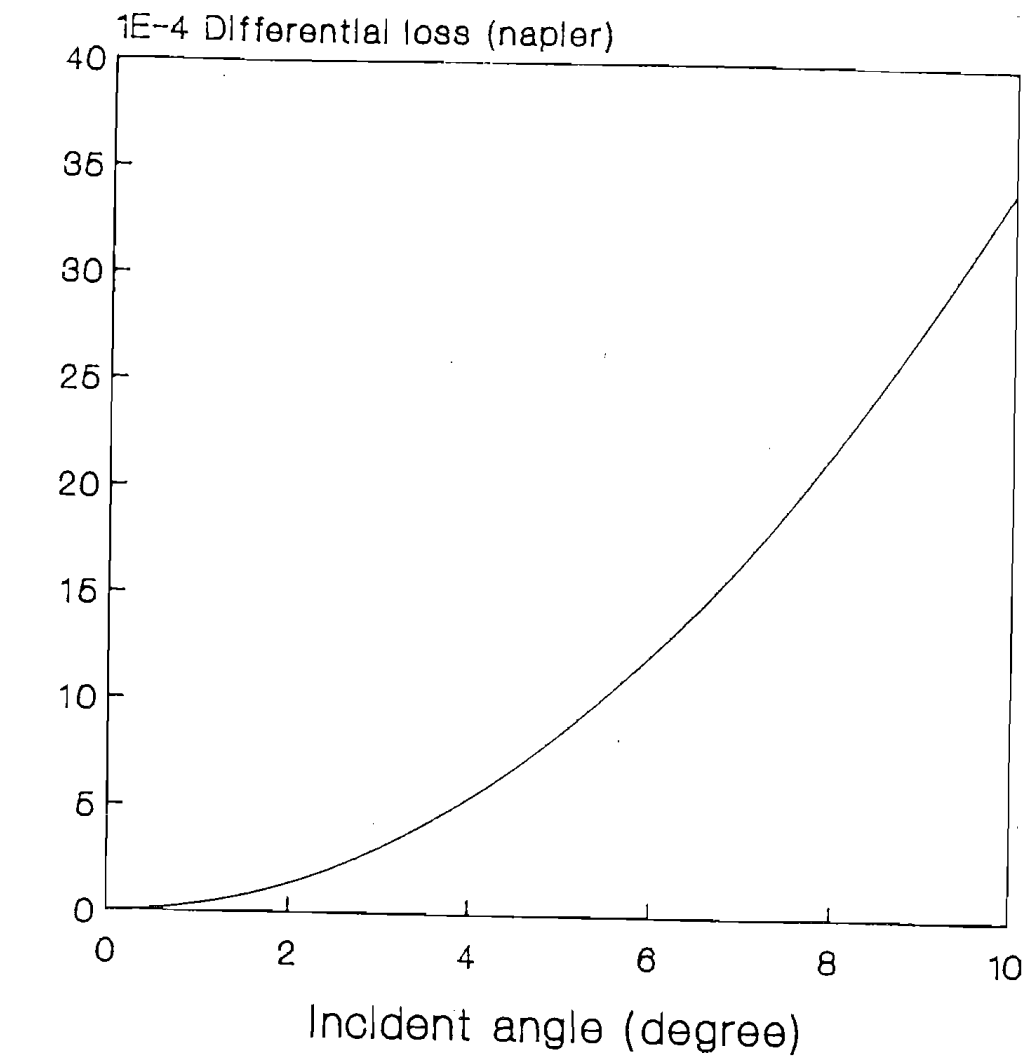

Fig.5.11 Differential loss between s- and p-polarisation components as a function of incident angle of light beam.

the extreme case the practical differential loss may be much smaller than this figure.

When the fibre ends were cleaved with a commercially available machine the cleaving quality offered was within $\theta<1^{o}$[7]. In this case, the differential loss induced by the possible tilt of the fibre ends is not the explanation of the significant difference of lasing characteristics between the x and y modes when pumped with a 45° launching as shown in Fig.3.5.

In order to verify whether this is due to the differential pumping efficiencies between the two orthogonal polarisation eigenmodes an experiment was designed. The fibre prepared for the experiments was Nd^{3+}-doped with a high concentration of 4500ppm, so that a relatively short fibre of 22cm was used to construct the laser cavity. The fibre was kept straight to limit the possible differential bending loss. Linearly-polarised light at 815nm from a semiconductor laser diode was converted by a quarter wavelength plate to circularly-polarised light. This enables the error in the 45° pumping orientation of linearly-polarised light to be avoided. The fibre ends were cleaved by a commercial cleaving machine, which gives a high-quality fibre end with $\theta<1^{o}$. The input end of the laser fibre was butted against the input mirror, whereas the output end of the laser was expanded by a lens and reflected from an output mirror having 80% reflectivity at the lasing wavelength, 1088nm. The tilt of the pumping beam was adjusted by two microscope objectives, which were located between the laser diode and the input mirror to form the pumping system, which is similar to that shown in Fig.1.1.

It is found that adjusting the pumping beam leads to a significant change of the polarisation behaviour of the fibre laser output. The dominant or preliminary lasing mode may be switched to its orthogonal counterpart by adjusting the tilt between the pumping beam and the fibre without any changing in the laser cavity. A changing of

DOP defined as in (2.1), not only in magnitude but also in sign, from 0.13 to -0.069 was measured for a pump ratio P/P_{th}=5.5. The maximum difference measured with such a fibre laser pumped by circularly polarised light is shown in Fig.5.12, where the slope efficiency ratio $SLOPE_x/SLOPE_y$ is measured to be 1.2, and the threshold ratio P_{th}^x/P_{th}^y 1.3. This is significant evidence of the influence of pumping alignment on the polarisation behaviour of fibre lasers. The experimental error caused by this influence can reach 15% and must be considered when the measurement is carried out for the purpose of deducing a microscopic parameter.

With a careful alignment, the minimum difference was obtained and is shown in Fig.5.13, where $P_{th}^x/P_{th}^y \leq 1.05$, while the slope efficiencies for both modes are almost identical. This indicates that the threshold difference may be regarded as a result of the intrinsic difference described by eq.(5.14).

Although the preliminary mode may switch to the orthogonal mode, it is almost impossible to operate the laser with completely identical threshold of two orthogonal polarisation eigenmodes. This is also found to be true when a linearly-polarised light is launched with $\alpha=45^o$. This phenomenon can especially be seen from the relaxation patterns, from which it is realized that the preliminary damped sinusoid oscillation is always completely polarised and attached to a certain polarisation eigenmode. The reason for this phenomenon is believed to be the mode competition during the transient process of building up lasing action. Once a polarisation component has built up its lasing action the lasing light, with much higher intensity than the other polarisation component in the fluorescence stage, makes the preliminary mode more competitive until the secondary mode reaches the lasing stage. More detailed discussion about the mode competition and its influence on the single-polarisation operation of fibre laser is presented later in Chapter 6.

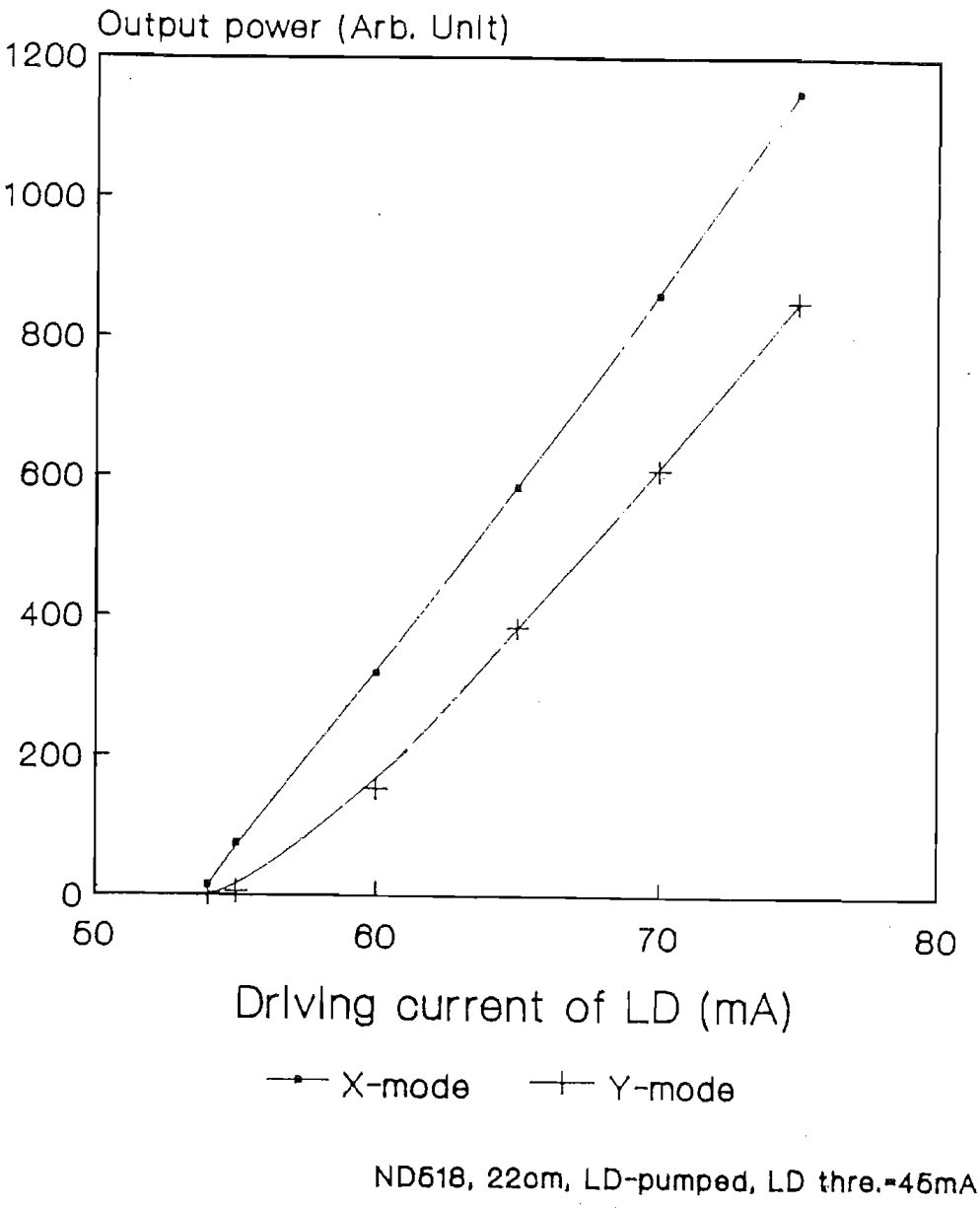

Fig.5.12 Polarisation-resolved lasing characteristics using a circularly-polarised pump, showing the clear influence of the pumping misalignment on the polarisation behaviour of fibre laser.

Owing to mode competition, the measured relative threshold ratio $(P_{th}^{x}-P_{th}^{y})/P_{th}^{x}$ is not correctly related to the differential imaginary threshold ratio $(P_{thx}-P_{thy})/P_{thx}$ or the real differential intrinsic loss ΔL. In addition, the small intrinsic difference between the two polarisation eigenmodes is easily masked by the differential launching efficiency for different polarisation modes, as shown in Fig.5.12. Therefore it is not possible to determine the intrinsic difference by measuring the differential threshold. The relative differential threshold $(P_{th}^{x}-P_{th}^{y})/P_{th}^{x}$ measured under a careful alignment of the pump is only of the order of 10^{-2}, as shown in Fig.5.13, indicating that the intrinsic cavity difference for orthogonal polarisation eigenmodes is rather small, in agreement with the theoretical analysis, and is negligible for most cases.

In summary, the relative magnitude of the intrinsic cavity difference is estimated to be only 10^{-4} or less. However, as a mechanism for creating orthogonal polarisation eigenmodes the intrinsic cavity difference between the two modes is essential, and important. Although this intrinsic cavity difference may be reflected by the 45^{o} effects, it is usually masked by the differential pumping efficiency for the two polarisation eigenmodes. In addition, the mode competition involved in 45^{o} effects makes it difficult to obtain an accurate intrinsic cavity difference by measuring thresholds of two orthogonal polarisation modes.

5.6 Measurement of Polarised Cross-Section Ratio

The good agreement between the experimental measurements in various fibre lasers, and the theoretical analysis based on the concept of effective absorbed pump power, demonstrate the reasonableness and feasibility of the following models:

— **Rare-earth ions in silica-based optical fibre are represented by partial dipole oscillators.**

Intrinsic Difference Measurement
Using a Circularly-Polarised Pump

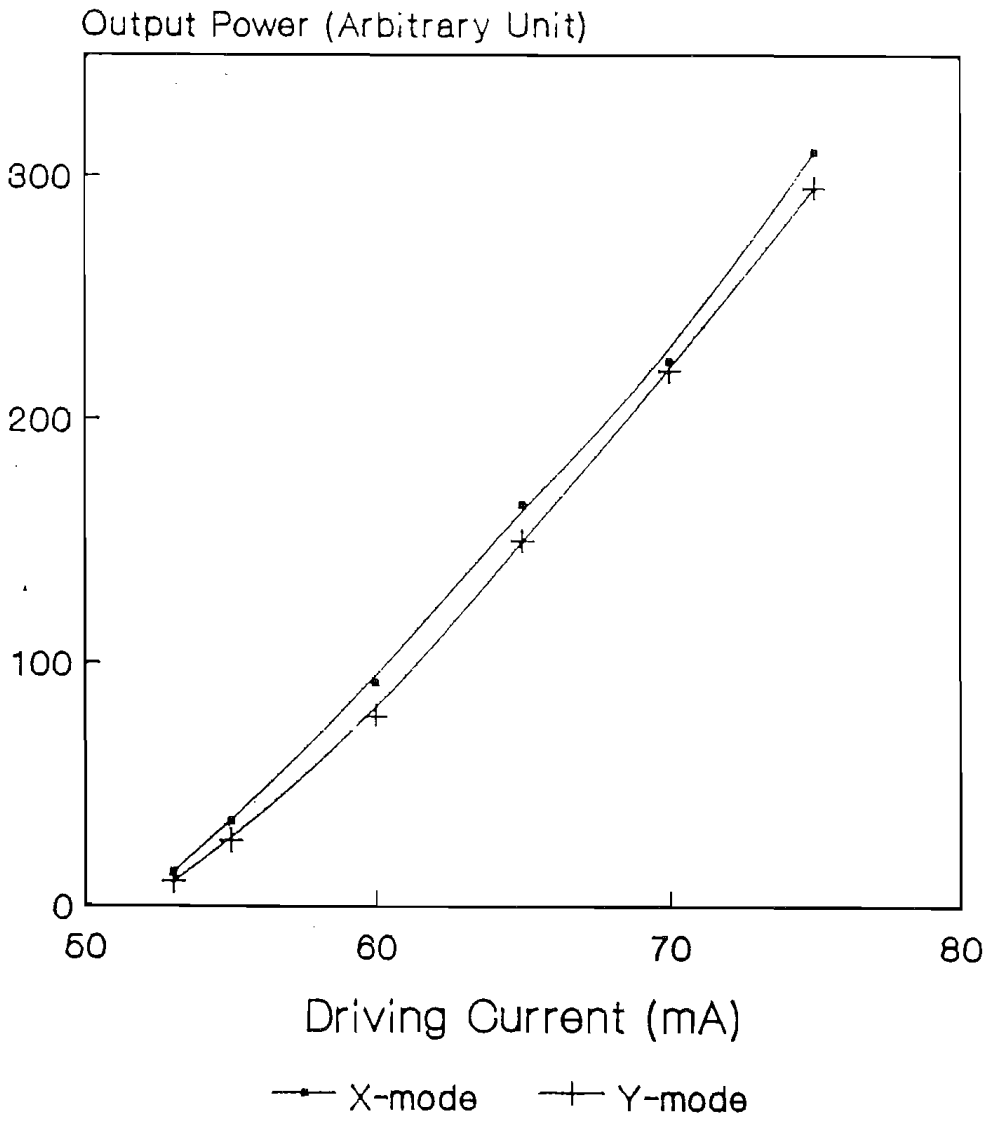

ND618-08, 22cm, LD-pumped, LD thre.=45mA

Fig.5.13 The minimum difference in lasing threshold and slope efficiency measured between the x and y modes, showing the intrinsic difference.

— **These partial dipole oscillators have random orientation in space in the host material.**

— **The oscillators retain their individual orientation during the non-resonant transition process.**

The behaviour of such a partial dipole oscillator is characterised by the parameter $a \equiv \sigma_s / \sigma_p$, the polarised cross-section ratio. The fibre laser technique now contributes to laser spectroscopy an opportunity of obtaining such a microscopic parameter for some materials, namely rare-earth ions in silica-based glasses. With the polarised cross-section ratio being known, a more accurate prediction of fibre laser properties, as well as fibre amplifier performance, can be made.

(1) Method

Based on the concept of the effective absorbed pump power, several formulas have been derived. All of them link the microscopic parameter a with measurable physical parameters: the thresholds, the slope efficiencies, the relaxation oscillation frequencies and the degree of polarisation, as shown in (5.16), (5.22), (5.28) and (5.31), respectively.

All the formulas mentioned above are derived under the condition of simultaneous operation of both orthogonal polarisation eigenmodes, since the assumption is applied that the radiation transition at lasing wavelength is the stimulated emission process, as shown in (4.34). Those measurements related to transient process or single-polarisation operation, are not suitable for deducing the parameter a. It is, therefore, suggested to apply neither eq.(5.16), related to threshold, nor eq.(5.28), connected with the relaxation oscillation frequency, for this purpose. In comparison of DOP with $SLOPE_x/SLOPE_y$, the latter is highly recommended. When the $SLOPE_x/SLOPE_y$ as a function of the pump orientation α is being measured, both polarisation eigenmodes are in steady lasing stage. The very good

linearity of lasing characteristics for both modes, as seen in many diagrams presented in the previous text of this thesis, offers a relatively low measurement error.

(2) Complementary angle compensation

Because of the possible experimental error induced by the differential pumping efficiency between orthogonal polarisation eigenmodes, described in the last section, a method of "**complementary angle compensation**", is introduced. Rewriting eq.(5.21) as

$$SLOPE_x = \eta_1^x \eta_5 (c_1 \cos^2\alpha + c_2 \sin^2\alpha)(P_{ab} - P_{th}^x) \qquad (5.38a)$$

$$SLOPE_y = \eta_1^y \eta_5 (c_1 \sin^2\alpha + c_2 \cos^2\alpha)(P_{ab} - P_{th}^y) \qquad (5.38b)$$

leads to

$$SR \equiv \frac{SLOPE_x}{SLOPE_y} = \frac{\eta_1^x (c_1 \cos^2\alpha + c_2 \sin^2\alpha)}{\eta_1^y (c_1 \sin^2\alpha + c_2 \cos^2\alpha)} \qquad (5.39)$$

where the differential launching efficiency of the pumping light for two orthogonal polarisation eigenmodes is separately expressed by $\eta_1{}^x$ and $\eta_1{}^y$. The method of "complementary angle compensation" means that measuring twice, at the angle α and its complementary angle $\pi/2-\alpha$, can compensate for the influence of the differential launching efficiency. In fact, it is readily obtained from (5.39) that

$$\frac{SR_{(\alpha)}}{SR_{(\pi/2-\alpha)}} = \frac{(c_1 \cos^2\alpha + c_2 \sin^2\alpha)^2}{(c_1 \sin^2\alpha + c_2 \cos^2\alpha)^2} \qquad (5.40)$$

where $SR_{(\alpha)}$ and $SR_{(\pi/2-\alpha)}$ are slope efficiency ratios for a certain angle α and its complementary angle $\pi/2-\alpha$, respectively. Apparently, the experimental error caused by the differential launching efficiency has been compensated in (5.40). The formula for deducing the parameter a is then

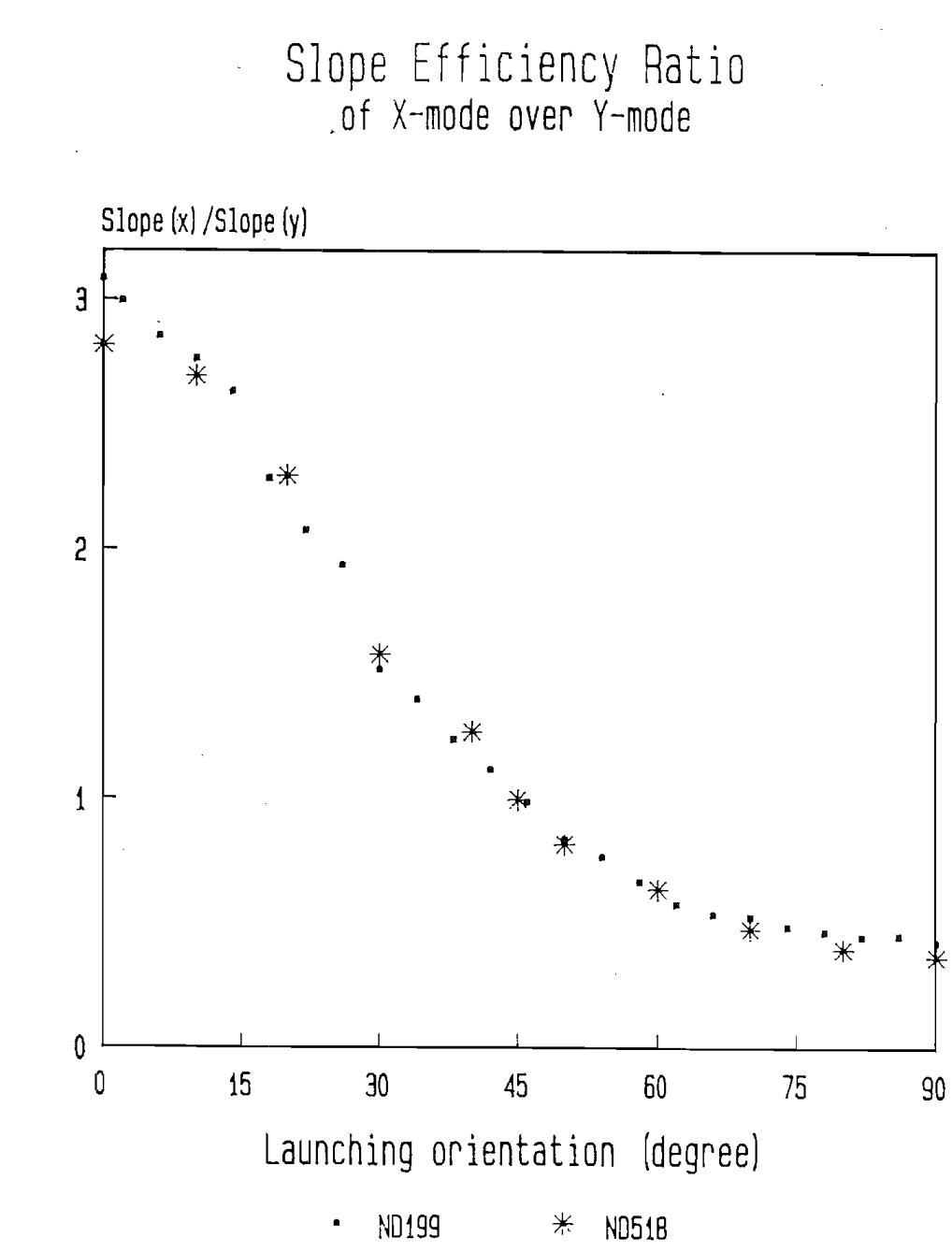

ND199, 280cm; ND518, 22cm.

Fig.5.14 Experimental measurements of slope efficiency ratio as a function of launching orientation for two Nd^{3+}-doped fibre lasers.

$$\sqrt{\frac{SR_{(\alpha)}}{SR_{(\pi/2-\alpha)}}} = \frac{c_1\cos^2\alpha + c_2\sin^2\alpha}{c_1\sin^2\alpha + c_2\cos^2\alpha} \qquad (5.41)$$

By using eq.(5.41) and the definition of the polarisation selection vector (c_1,c_2) in (4.40), the parameter a can be deduced from experimental measurements.

(3) Results

Theoretically, a single measurement for a given α can determine the microscopic parameter a. However, multiple-point measurements as a function of α helps to obtain more accurate measurements.

Fig.5.14 shows measurements for two different samples of Nd^{3+}-doped fibre lasers. The fibres contain different concentration of Nd^{3+} dopants, 300ppm and 4500ppm respectively. The lasers were pumped by a laser diode operating at 815nm. It is found that there is an obvious difference between SR(0°) and SR(90°) in both cases. The "complementary angle compensated" points calculated with (5.41) for the fibre sample ND199 are plotted in Fig.5.15.

A measurement for an Er^{3+}-doped fibre laser is shown in Fig.5.16. The pump source was an Ar^{+}-ion laser pumped dye (DCM) laser operating at 650nm. Although the laser noise for Er^{3+} laser is much stronger than the LD-pumped Nd^{3+} laser, the slope efficiency ratio can still be recognised within a finite error range.

Additional information about the experiments are shown in Fig.5.17, and the results are listed in Table.5.1. It is concluded that the most commonly used rare-earth dopant in glasses to date have the following features:

For the Nd^{3+}-ion in silica based glass, the dipole oscillator corresponding the $^4F_{3/2}$-$^4I_{11/2}$ transition with a non-resonant pump at 820nm absorption band has rather strong polarisation anisotropy with the polarised cross-section ratio being 0.015±0.004.

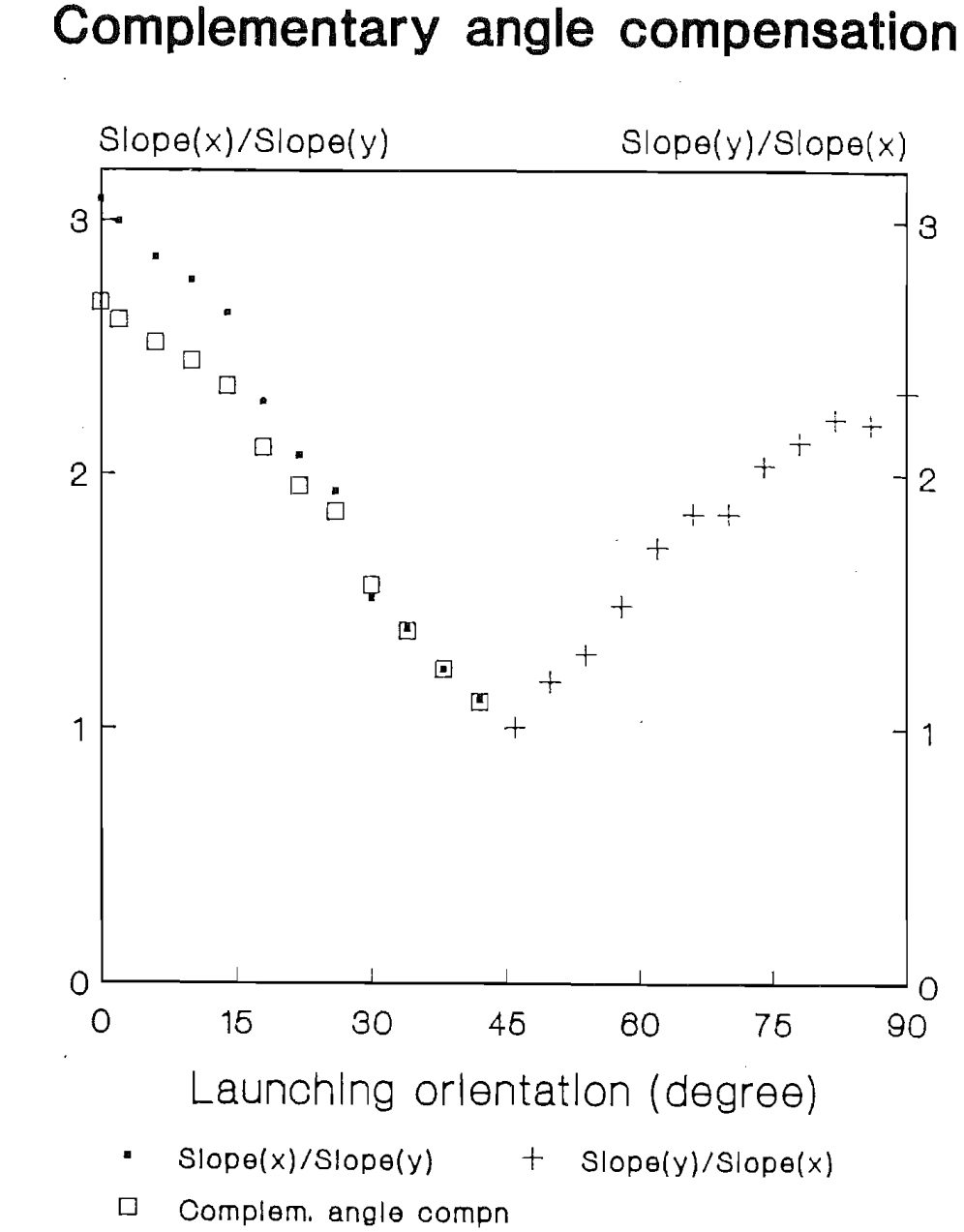

Fig.5.15 Complementary angle compensation of measurements for a Nd^{3+}-doped fibre laser.

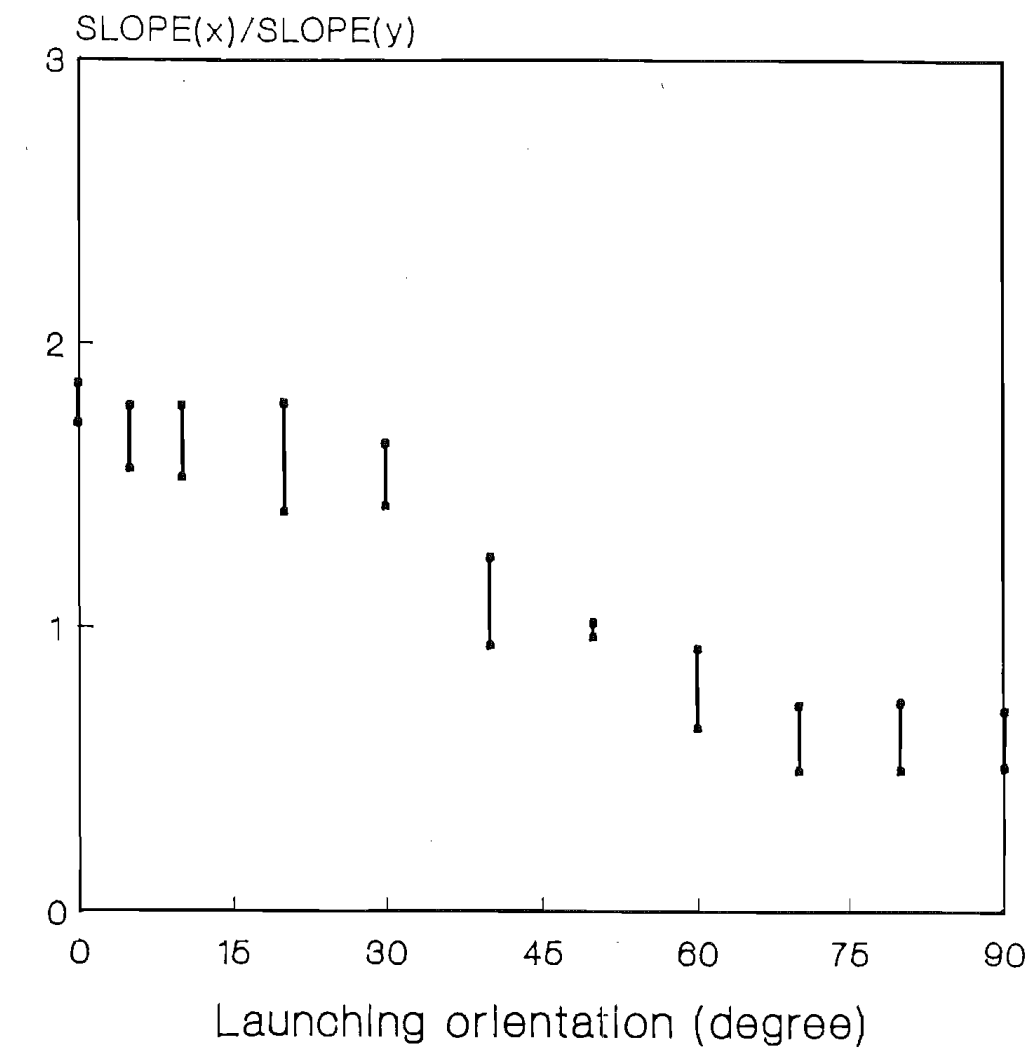

ND601, Er-doped

Fig.5.16 The slope efficiency ratio as a function of launching polarisation orientation for an Er^{3+}-doped fibre laser.

Determination of the parameter a

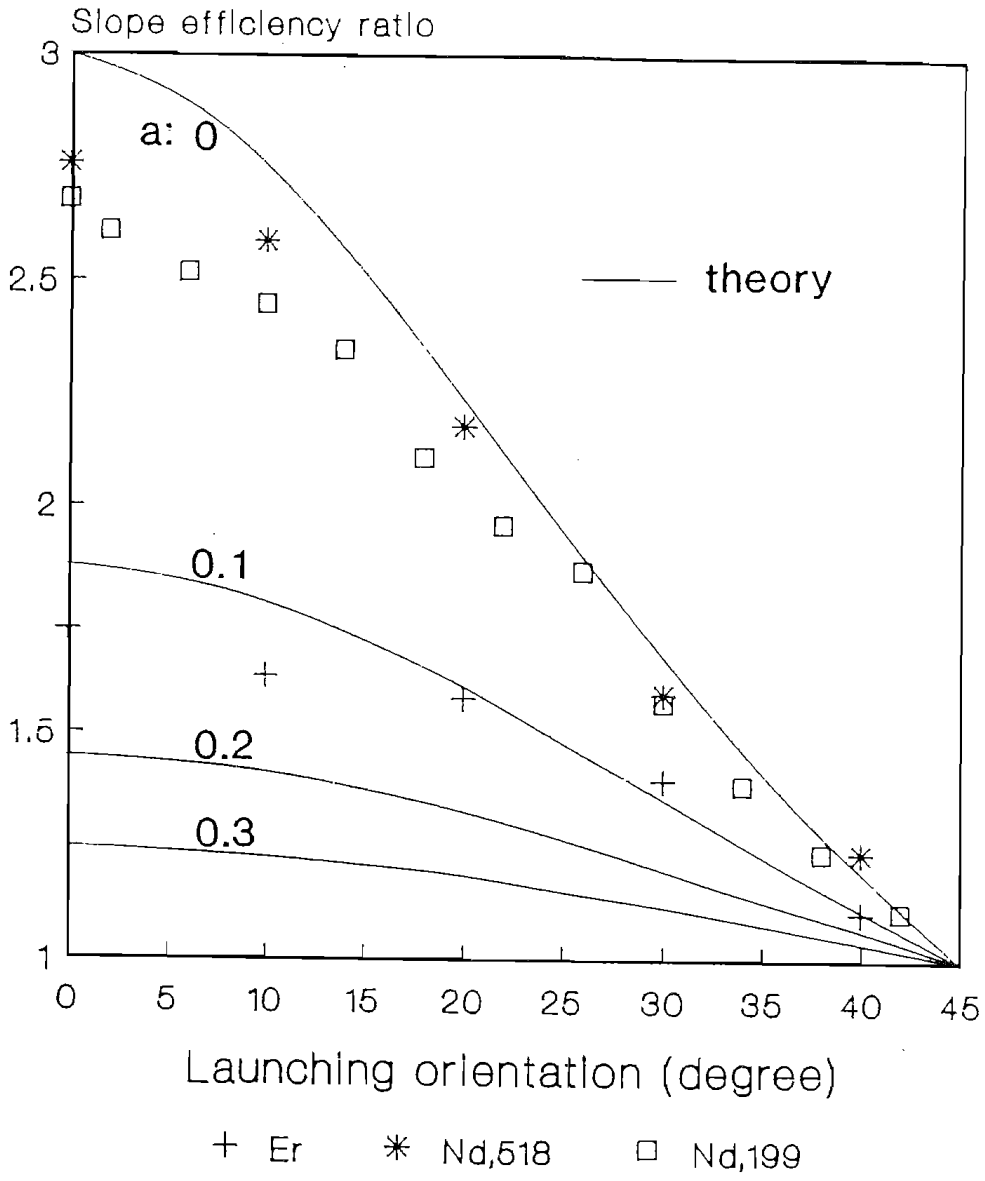

Fig.5.17 Determination of the polarised cross-section ratio a for Nd^{3+} and Er^{3+} ions in silica-based glass fibres.

Dopant	Nd	Er
Transition Wavelength	$^4F_{3/2}$-$^4I_{11/2}$ 1080nm	$^4I_{13/2}$-$^4I_{15/2}$ 1550nm
Pumping Wavelength	LD 820nm	Dye 650nm
Polarised cross-section ratio a	0.015±0.004	0.11±0.02

Table 5.1 Polarisation cross-section ratios for Nd^{3+} and Er^{3+} ions in glass fibres.

The dipole oscillator of Er^{3+}-ion in silica glass has a=0.11±0.02 for the transition of $^4F_{9/2}$-$^4I_{15/2}$ with a non-resonant absorption band at 650nm.

References to Chapter 5

[1] W. Koechner: "Solid-State Laser Engineering", Springer-Verlag, 1976.

[2] R.J. Mears, L. Reekie, S.B. Poole, and D.N. Payne: "Neodymium-doped silica single-mode fibre lasers", Electron. Lett., 21, pp.738-740, 1985.

[3] R.J. Mears, L. Reekie, S.B. Poole, and D.N. Payne:"A low-threshold tunable CW and Q-switched fibre laser operating at 1.55μm", Electron. Lett., 22, pp.159-160, 1986.

[4] D.N. Payne, L. Reekie, R.J. Mears, S.B. Poole, I.M. Jauncey, and J.T. Lin: "Rare-earth doped single-mode fibre lasers, amplifiers and devices", Proceedings of CLEO'86, San Francisco, June 9-13, 1986.

[5] S.B. Poole, Private communication.

[6] M. Born and E. Wolf: "Principles of Optics", Pergamon, London, 1970.

[7] A. Yariv: "Optical Electronics", Holt Rinehart and Winston, New York, 1976

Chapter Six

SINGLE-POLARISATION OPERATION

Single-polarisation operation is one of most important aspects of laser performance. The general aim for the study of single-polarisation operation in fibre lasers is to find the conditions of single-polarisation operation, to understand the mechanism of superfluorescnce and its influence on single-polarisation operation, to establish a model describing the single-polarisation operation, and thus to calculate the polarisation efficiency for single-polarisation operation. Based on these studies, a clear physical picture is given, leading to a theoretical foundation for designing single-polarisation fibre lasers, which are considerable interest for many potential applications.

6.1 Basic Considerations

(1) Superfluorescence

The amplification of spontaneous emission fluorescence as a travelling wave in a pumped active laser material is known as superfluorescence. Two conditions for establishing a considerable superfluorescence are a strong pump and a long active medium. A large pump power offers sufficient excited activators to be involved in the amplification process of the traveling wave formed by the spontaneous emission, whilst a long laser medium provides a long interaction length between excited activators and the spontaneously-emitted photons.

Superfluorescence is an effect which differs from both spontaneous emission and lasing action. The fluorescence of the spontaneous emission is characterised by two factors: firstly, the lifetime of the excited electron, τ_{21}, at the upper level is uniquely determined by the spontaneous transition probability A_{21}, namely $\tau_{21}=(A_{21})^{-1}$, secondly, the radiation of the spontaneous

emission has a uniform distribution in space. As for the lasing state, the stimulated emission dominates the transition process. The photons are no longer distributed uniformly in all the possible radiation modes but are condensed into a few or even one (single-mode) mode. The lifetime of the excited electrons in the upper level is then much shorter than the spontaneous emission, as described in Chapter 4. Superfluorescence is the intermediate state between the fluorescence and lasing states. Such a state possesses some of the characteristics of fluorescence from spontaneous emission, as well as some of the stimulating emission due to the traveling wave amplification of the fluorescence. On average, the lifetime of the excited electron becomes shorter than in normal fluorescence. A significant difference is presented in the radiation distribution in space. Furthermore, the spectrum of the superfluorescence is narrower than that of normal fluorescence.

An optical fibre provides an ideal medium for superfluorescence. As a single-mode waveguide, a fibre propagates all the spontaneous emission within the solid angle corresponding to the numerical aperture, as illustrated in Fig.6.1. A long length of laser medium, usually one or two orders larger than in conventional glass lasers, is easily formed to allow a much stronger superfluorescence to be accumulated. Such a property allows the superfluorescence in active fibres to find some special applications as a wide band source[1].

The evidence of superfluorescence can be exhibited by the different spectral properties of three different states: fluorescence, superfluorescence and lasing. With a normally designed Nd^{3+}-doped fibre laser, these three different spectra were measured and the typical results are shown in Fig.6.2. The first spectral scan in Fig.6.2 is for the normal fluorescence, indicating a 57nm width for the $^4F_{3/2}$-$^4I_{11/2}$ transition around 1.08μm. There was no effect of superfluorescence on the measurement at this stage as the pump power was kept rather low, namely

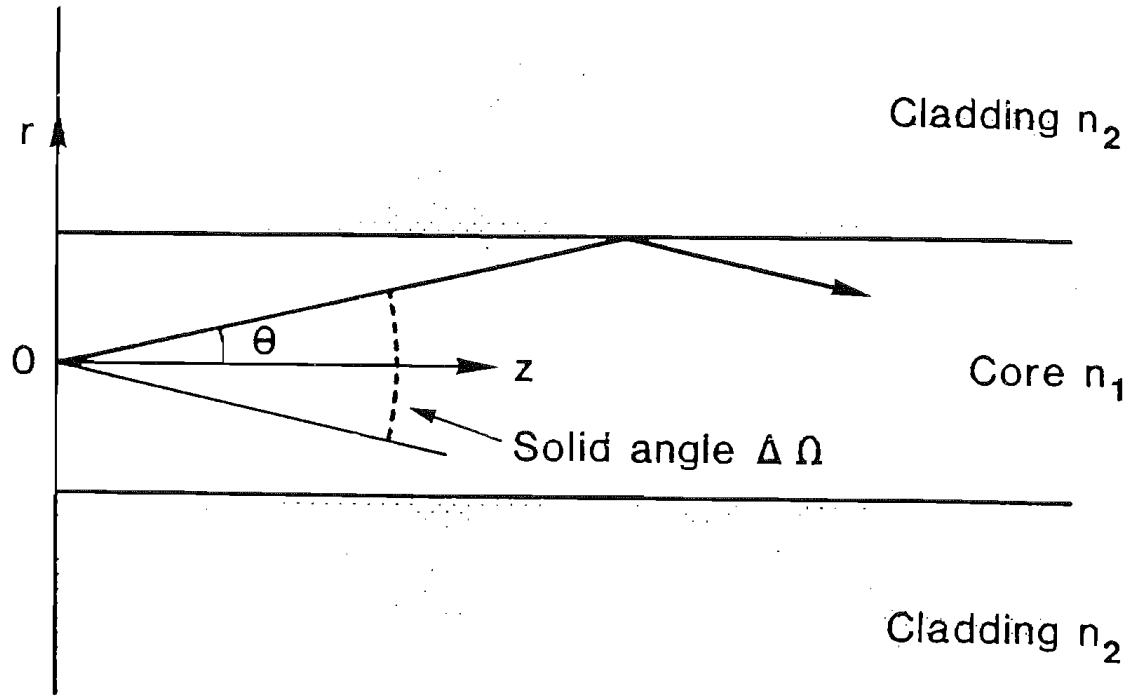

Fig.6.1 Schematic of a single-mode fibre waveguide.

$P=0.2P_{th}$ where the P_{th} is the power required for the threshold for the laser. With all conditions unchanged except for an increased pump level of $P=0.9P_{th}$, a significant spectrum narrowing was observed, and the spectrum width has been narrowed to 16nm as shown in the second scan. For a comparison, the lasing spectrum at pump ratio $P/P_{th}=1.1$ is also shown in the third picture, demonstrating a very narrow spectrum as a result of stimulated emission condensed within a single mode.

(2) Superfluorescence of the y mode

It is now understood that superfluorescence is manifested as a transient state during the establishment process of the lasing action of the preliminary polarisation eigenmode, the x mode. It is also expected that such a mechanism plays a role for the secondary polarisation eigenmode, the y mode, after the x mode has built up its lasing action, since the pump level at this stage is rather high, at least exceeding the threshold. A knowledge of the influence of the superfluorescnce on the laser performance is required for the analysis of the single-polarisation operation of fibre lasers.

An experiment was arranged for investigating the superfluorescence phenomenon of the y mode when the x mode is in the lasing state. The fibre laser used for the measurement was LD-pumped Nd^{3+}-doped fibre laser with an ordinary design. A polarised beam splitter was located in the optical path of the output from the fibre laser, so that the lasing light of the x mode and the fluorescence of the y mode were detected separately. A filter with high attenuation at the pump wavelength was chosen to stop the residual pump light. The measurements are plotted in Fig.6.3, in which the figures have been calibrated for two different detectors. It can be seen that below the threshold of the x mode (at 58mA of driving current for the LD), both x and y modes stay at the superfluorescence stage, according to the tendency of the output power being an exponentially increased curve

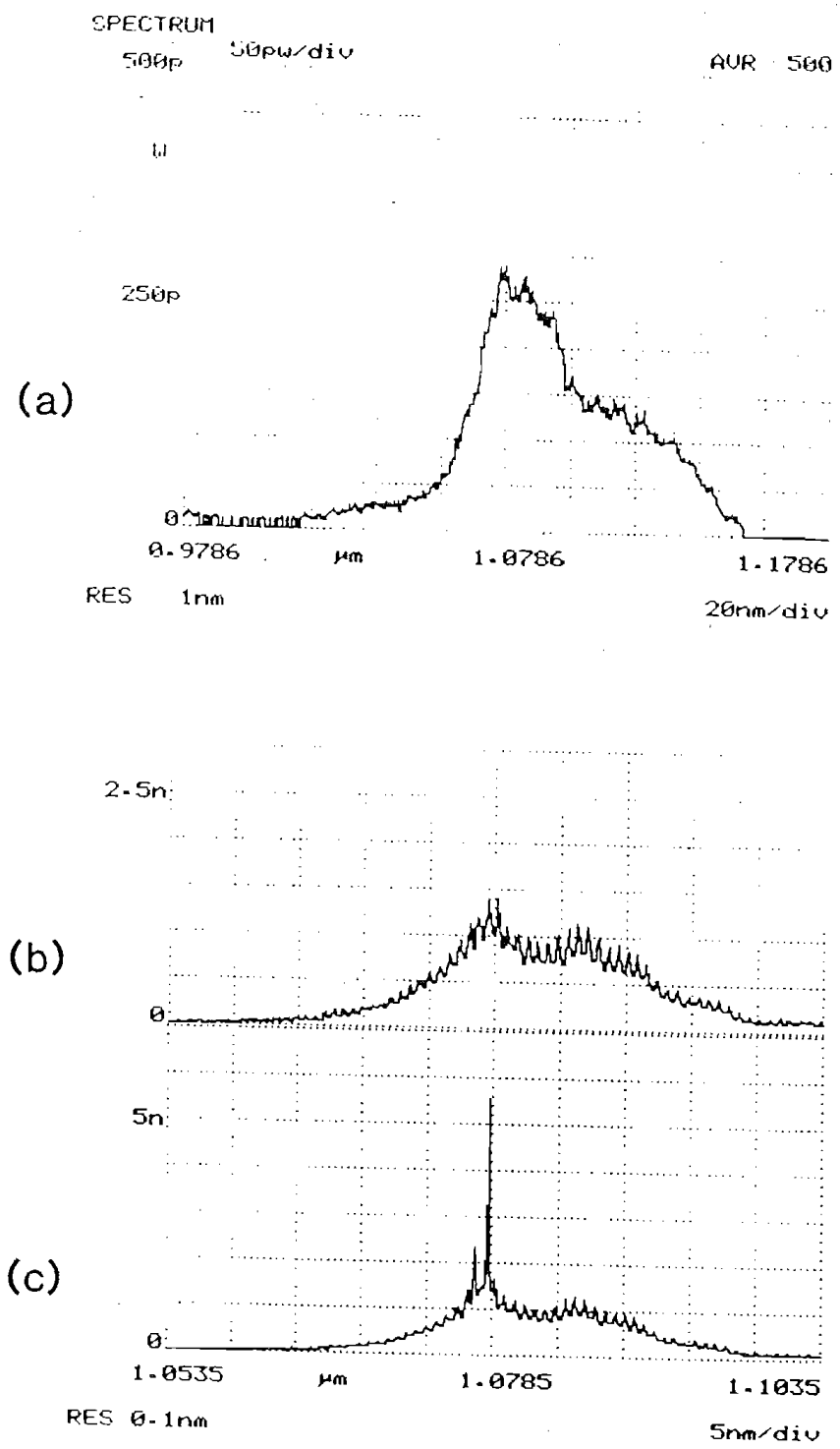

Fig.6.2 Different spectral properties of three different states.

(a) Fluorescence with $\Delta\lambda$=57nm.

(b) Superfluorescence with $\Delta\lambda$=16nm.

(c) Lasing with $\Delta\lambda$<0.2nm.

as a function of pump power. When the pump power increased, the output-input curve above the threshold for the lasing x-mode reaches the linear range, while the superfluorescence output of the y mode shows a faint dip in its exponential curve. Beyond the threshold point of the x mode, the output of the y mode is still increasing exponentially, indicating evidence of superfluorescence. This exponential output/input relation remains until the threshold for the y mode is reached (at 61mA of driving current for LD).

This fundamental experiment tells us that single polarisation operation of fibre lasers is such a state, at which the lasing polarisation mode has an ordinary linear lasing characteristic, and the other undesired polarisation component stays in the superfluorescence process with an exponential input/output relation. Any modeling for the single-polarisation operation in fibre lasers must be based on this experimental phenomenon.

(3) Small-signal gain and gain saturation

In Chapter 5, the conditions for laser threshold are considered. Threshold is characterized by a steady-state population inversion, i.e. $\partial N/\partial t=0$ in the rate equations (4.17). In doing this the effect of stimulated emission is neglected by setting $\phi=0$. This is a perfectly legitimate assumption at threshold, where the induced transitions are few compared with the number of spontaneous processes.

As the threshold is exceeded, however, stimulated emission and photon density in the resonator build up. Far above threshold a large photon density in the resonator has to be considered. If the gain coefficient which the system would have at a certain pump level in the absence of stimulated emission is g_0, as soon as the photon density becomes appreciable, the actual single-pass gain of the system is no longer the small-signal gain $\ln G_0$, defined as in (5.3), but reduced to $\ln G$[2,3]:

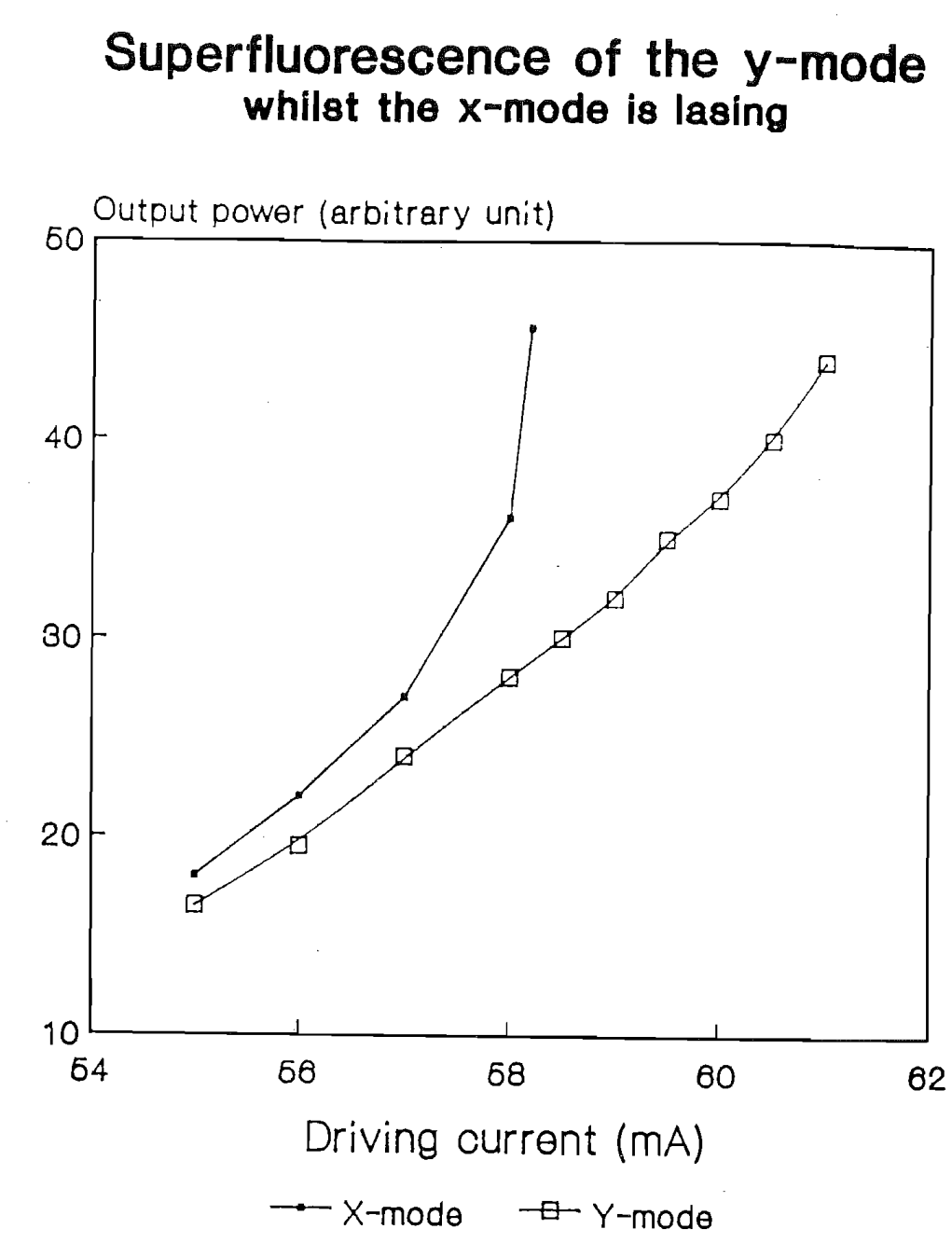

Fig.6.3 Experimental measurements showing the superfluorescence of the y mode whilst the x mode is lasing.

$$\ln G = \frac{g_o l_e}{1 + I/I_s} \tag{6.1a}$$

for a homogeneous laser medium, and

$$\ln G = \frac{g_o l_e}{\sqrt{(1+I/I_s)}} \tag{6.1b}$$

for a inhomogeneous laser medium, where I_s is the saturation density defined as in eq.(5.7), I is the photon density of the lasing mode, and the l_e the effective length as defined in eq.(5.2).

In the range of gain saturation, the laser output varies linearly with pump power instead of exponentially, as described in Chapter 5. Therefore, when the fibre laser is in the single-polarisation state, the lasing x-mode and the superfluorescent y-mode experience differential gain due to the gain saturation. This can be described by introducing an saturation gain ratio, defined as

$$S = \frac{G_y}{G_x} \tag{6.2}$$

where G_x and G_y represent the single-pass gains for the x mode and y mode, respectively.

It is known that the small-signal single-pass gain coefficient g_o for a four-level system, for example, is proportional to the absorbed pump power[4] and can readily be derived to be

$$g_o = \frac{K\, P_{ab}\, (PS)}{l_e} \tag{6.3}$$

for the case of fibre laser, where PS is the polarisation selection as defined in eq.(4.43); l_e is the effective length; K is the pumping coefficient defined in eq.(5.6); and P_{ab} the total absorbed pump power. A certain expression of saturation gain ratio S is then obtained

for the single-polarisation operation of a four-level fibre laser:

$$S = \exp\{KP_{ab}[PS^{Y} - \frac{PS^{X}}{\sqrt{(1+I_x/I_s)}}]\} \qquad (6.4)$$

from which it is seen that the saturated gain ratio increases nearly exponentially with a increased absorbed pump power. That means the gain for the superfluorescent y-mode increases rather quickly in comparison with the gain for the lasing x-mode when the pump power is increased. This is believed to be the explanation of why the y-mode can continue to build up its own lasing action after the x-mode has reached the lasing state.

Measurement of saturated gain ratio S

In order to determine the saturated gain ratio S, the photon densities of both the x and y modes need to be measured. The experimental arrangement for this purpose may be similar to that described in Fig.3.1b. An intracavity polarised beam splitter is required to suppress the y-mode for realizing single-polarisation operation. In the meantime, this beam splitter works as a deflector allowing the superfluorescence of the y mode to be measured. By using eq.(5.20) describing the relation between the intracavity photon density and the output power from the laser, the density of the lasing x mode can be easily determined. With the measured value of K, as described later in Chapter 7, S is then calculated according to eq.(6.4). For example, $K \approx 0.1$ for a LD-pumped Nd fibre laser, and thus the saturated gain ratio $S \approx 1.25$ at $P_{ab}=10mW$.

6.2 Conditions for Single-Polarisation Operation

From the experimental measurements, as well as the analysis, a general idea of the condition for single-polarisation operation can be obtained, i.e. operating a

fibre laser above the threshold of the preliminary polarisation eigenmode, say the x mode, and below the threshold of the secondary polarisation eigenmode, the y mode.

If the output power and the extinction ratio are regarded as main specifications of single-polarisation operation, the optimum operating condition can be concluded to be:

(i) Pumping with polarisation aligned to the principal axis of the fibre.

(ii) Operating the laser at just below the threshold of the secondary polarisation eigenmode.

It is found from the experiments that the regime of the pump power for the single-polarisation operation is quite limited, even for the case of on-axis pumping. The theoretical result from equation eq.(5.9) shows that the maximum pump ratio, in any case, for single-polarisation operation of an ordinary fibre laser is $r_{max}=P_{max}/P_{th}=3$. If the pump ratio r exceeds the maximum r_{max}, the undesired mode will have built up to lase. In practice, r_{max} is even smaller than 3 for rare-earth doped fibre lasers, since $a<1$. The smaller the polarised cross-section ratio a, the lower r_{max} becomes.

The limitation of pump ratio r_{max} leads to a limited output power from a fibre laser in single-polarisation operation. In addition, the extinction ratio of a single-polarisation operated fibre laser is reduced by the superfluorescence of the undesired polarisation component. Experimental measurements of various fibre lasers in the single-polarisation operation state show that the DOP is around 0.95. The maximum DOP was measured to be 0.98 with a Nd^{3+}-doped fibre laser pumped by a semiconductor laser under the optimum operating conditions mentioned above. It is noted that this figure is smaller than that of a pure linearly-polarised mode, 23dB, as described in Chapter 3.

In order to construct a practical single-polarisation fibre laser having more output power as well

as a higher extinction ratio, a method of increasing the difference between the thresholds of the two polarisation eigenmodes is required. This is dealt with in the Chapter 7.

6.3 Modeling of Single-Polarisation Operation

It is now possible to postulate a model describing the behaviour of single-polarisation operation.

(1) Solid angle ratio ξ

The substantial difference between stimulated emission of the lasing mode and the superfluorescent mode is that the spontaneous emission still plays role in the superfluorescence, but affects only slightly the lasing mode. Only those photons, which are spontaneously emitted within the solid angle $\Delta\Omega$ corresponding to the NA of the fibre, can stimulate the superfluorescence. This can be described by introducing a parameter, the solid angle ratio, as we call, ξ_o:

$$\xi_o = \frac{2\Delta\Omega}{4\pi} \tag{6.5}$$

where the factor 2 refers to both directions, forwards and backwards, in the fibre. The physical meaning of the solid angle ratio is the fraction of the fluorescence from spontaneous emission, which is guided by the fibre. Using the geometrical relation illustrated in Fig.6.1, the parameter ξ_o is readily derived to be

$$\xi_o = 1 - \sqrt{(1 - \frac{NA^2}{n_{co}^2})} \tag{6.6}$$

where

$$NA = \sqrt{(n_{co}^2 - n_{cl}^2)} \tag{6.7}$$

n_{co} and n_{cl} are the index of the fibre core and cladding respectively. Fig.6.4 shows the waveguide solid angle

ratio ξ as a function of NA. For example, when NA=0.21, n=1.5, which is the case of the fibre sample ND425 in the Table 2.1, ξ_o=0.0089.

(2) Modelling

The solid angle ratio actually reflects the fraction of the pump power which is inverted to the measurable fluorescence power emitted from the fibre end. From this point of view, it is reasonable to regard the solid angle ratio to be unity for the lasing state since the stimulated emission dominates in this case and almost all the emitted photons are guided by the fibre. Therefore, equation (4.34), describing the probability per unit time for an ion to contribute a transition to the x mode and y mode, needs to be modified for the case of single polarisation operation to

$$P_x(\Omega) = C[I_x\sigma^x(\Omega) + I_y\sigma^y(\Omega)]\ \sigma^x(\Omega) \qquad (6.8a)$$

$$P_y(\Omega) = \xi_o C[I_x\sigma^x(\Omega) + I_y\sigma^y(\Omega)]\ \sigma^x(\Omega) \qquad (6.8b)$$

where it has been assumed that the x mode is the lasing mode and the y is the fluorescent mode.

Strictly speaking, the waveguide solid angle ratio ξ_o is related to the normal fluorescence rather than superfluorescence. If the effective solid angle ratio ξ is introduced to describe the influence of the guided spontaneous emission on the measurable inverted energy, $\xi=\xi_o$ for the fluorescence, $\xi\approx1$ for the lasing state, as for the superfluorescence the effective solid angle ratio must be $\xi_o<\xi<1$.

Furthermore, the fluorescence or superfluorescence experiences a small-signal gain, whereas the lasing signal arises a saturated process, as described earlier in this chapter. Taking this into account, equation (6.8) becomes

$$P_x(\Omega) = C[I_x\sigma^x(\Omega) + I_y\sigma^y(\Omega)]\ \sigma^x(\Omega) \qquad (6.9a)$$

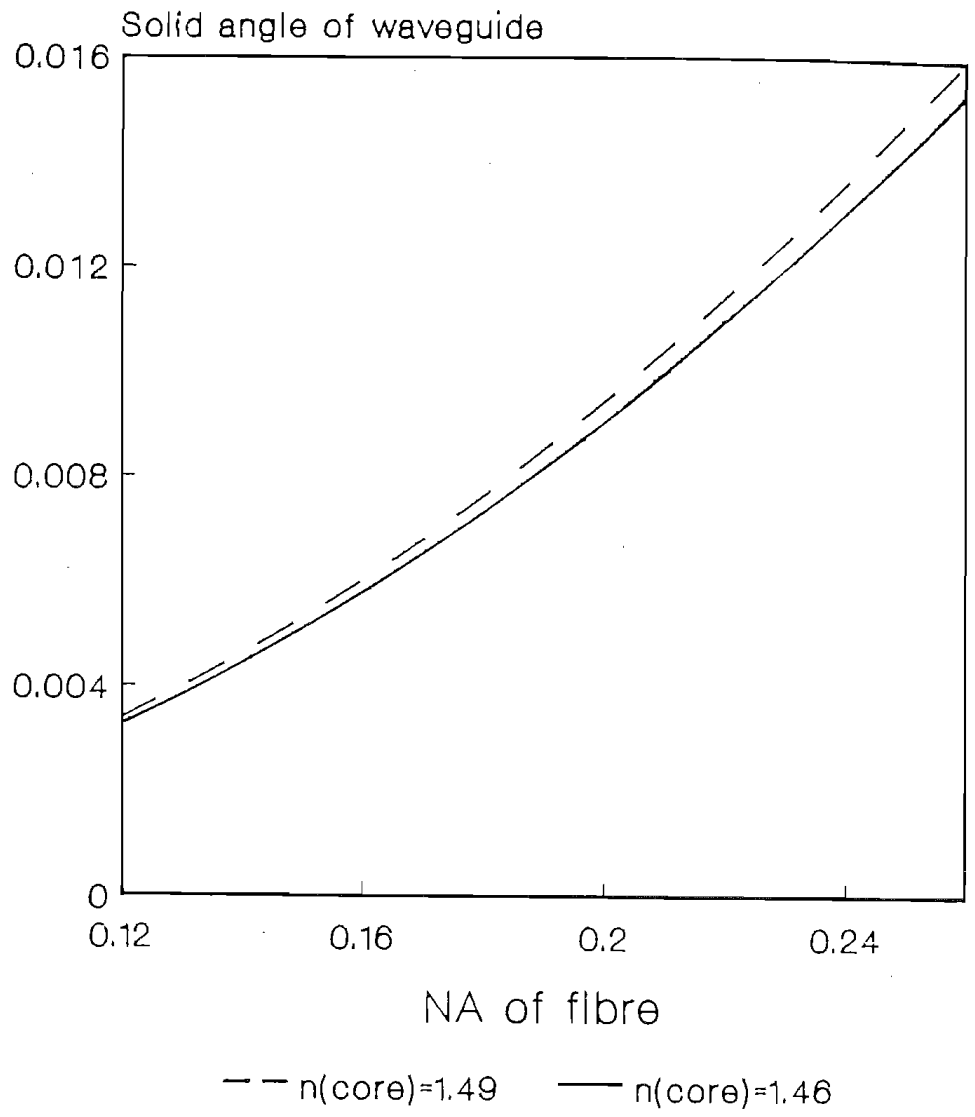

Fig.6.4 Solid angle ratio of fibre waveguide as a function of numerical aperture.

$$P_y(\Omega) = \xi SC[I_x\sigma^x(\Omega) + I_y\sigma^y(\Omega)]\ \sigma^x(\Omega) \qquad (6.9b)$$

where S is the saturated gain ratio, as expressed in (6.4).

Equation (6.9) allows the expressions for effective absorbed pump power to be derived for the case of single-polarisation operation via the same procedure as the derivation from eq.(4.34) to (4.42). The result is expressed as follows

$$\begin{vmatrix} P^x \\ P^y \end{vmatrix} = \frac{P_{ab}}{c_1(\cos^2\alpha+S\xi\sin^2\alpha)+c_2(\sin^2\alpha+S\xi\cos^2\alpha)} \begin{vmatrix} \cos^2\alpha & \sin^2\alpha \\ S\xi\sin^2\alpha & S\xi\cos^2\alpha \end{vmatrix} \begin{vmatrix} c_1 \\ c_2 \end{vmatrix} \qquad (6.10)$$

where all the symbols, expect for ξ and S, have the same meaning as in (4.42). Equation (6.10) is the main formula for analysing the single-polarisation operation of fibre lasers. In comparison with eq.(4.42), it is found that (6.10) is the more general expression, which includes the case of (4.42), letting $S\xi=1$.

6.4 Polarisation Efficiency of Single-Polarisation Operation

The polarisation efficiency of single-polarisation operation η_{sp} is now defined as

$$\eta_{sp} = \frac{P^x}{P_{ab}} \qquad (6.11)$$

where the x-mode has been assumed to be the lasing mode. From (6.10) and (6.11) it may be shown that

$$\eta_{sp} = \frac{1}{1 + S\xi(c_1\sin^2\alpha+c_2\cos^2\alpha)/(c_1\cos^2\alpha+c_2\sin^2\alpha)} \qquad (6.12)$$

The physical meaning of the polarisation efficiency is the fraction of the absorbed pump power, which contributes to the wanted polarisation component, while the residual fraction $(1-\eta_{sp})P_{ab}$ is related to the superfluorescence of the undesired polarisation component. It is worth pointing out that for the extreme case, $S\xi=1$, which means that two polarisation eigenmodes are both in lasing states, equation (6.12) becomes, as expected, the same expression as the polarisation selection PS introduced in chapter 4.

Equation (6.12) indicates that the polarisation efficiency of single-polarisation operation depends on the launching orientation of the pump light. Also it is a function of the saturated gain ratio S as well as the effective waveguide solid angle ratio ξ. On the other hand, the assumption for derivation of eq.(6.12) requires that the lasing mode is always the x-mode, and remains unchanged even when pumping on the y-axis. This can be realised technically in the single-polarisation fibre lasers, where an intracavity polarisation control element is used to suppress the undesired polarisation component, as discussed in detail in the next chapter. In the following sections, presented is the theoretical analysis.

(1) Comparison of two configurations

For any light source, single-polarisation operation can be obtained by using a external polariser, which attenuates strongly the undesired polarisation component, as illustrated in the upper part of Fig.6.5. Another way to achieve a single polarisation emission from a laser source is to use an intracavity polariser to favour the wanted polarisation components, as shown in the lower part of Fig.6.5. With the theoretical formula, eq.(6.12), a comparison can be made for these two different configurations.

By assuming the polarisers used are ideal with an infinite extinction ratio and zero attenuation to the

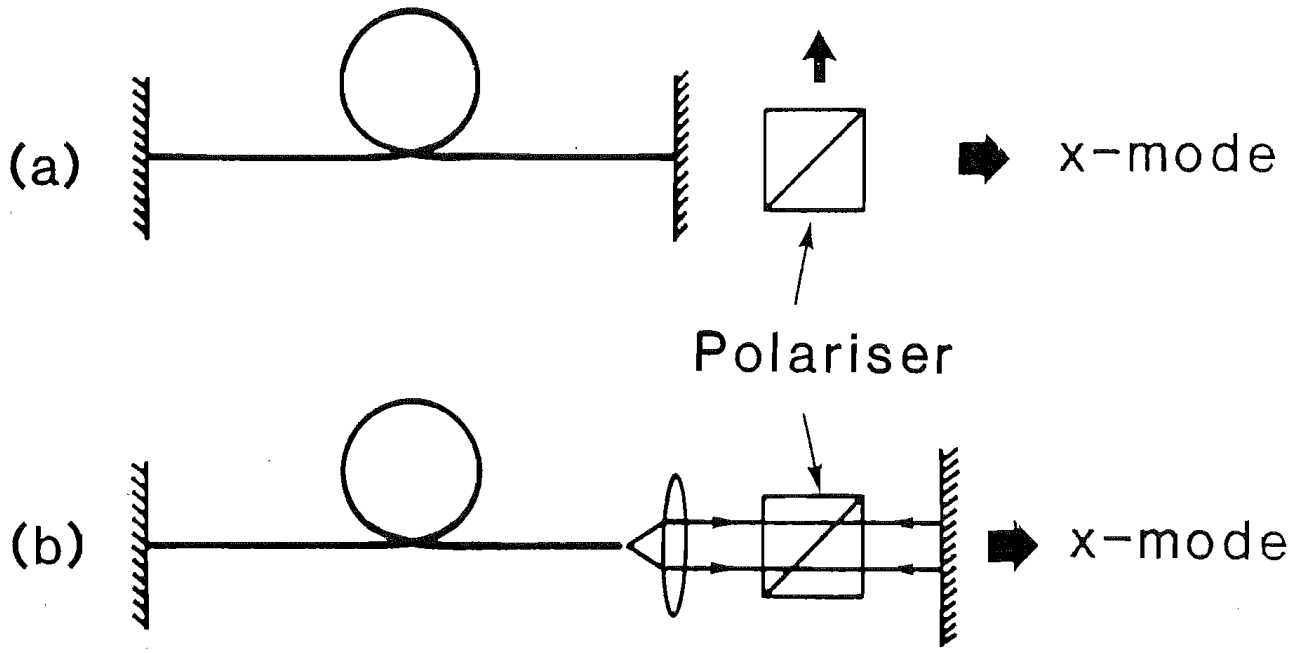

Fig.6.5 Two possible configurations for single-polarisation fibre lasers.

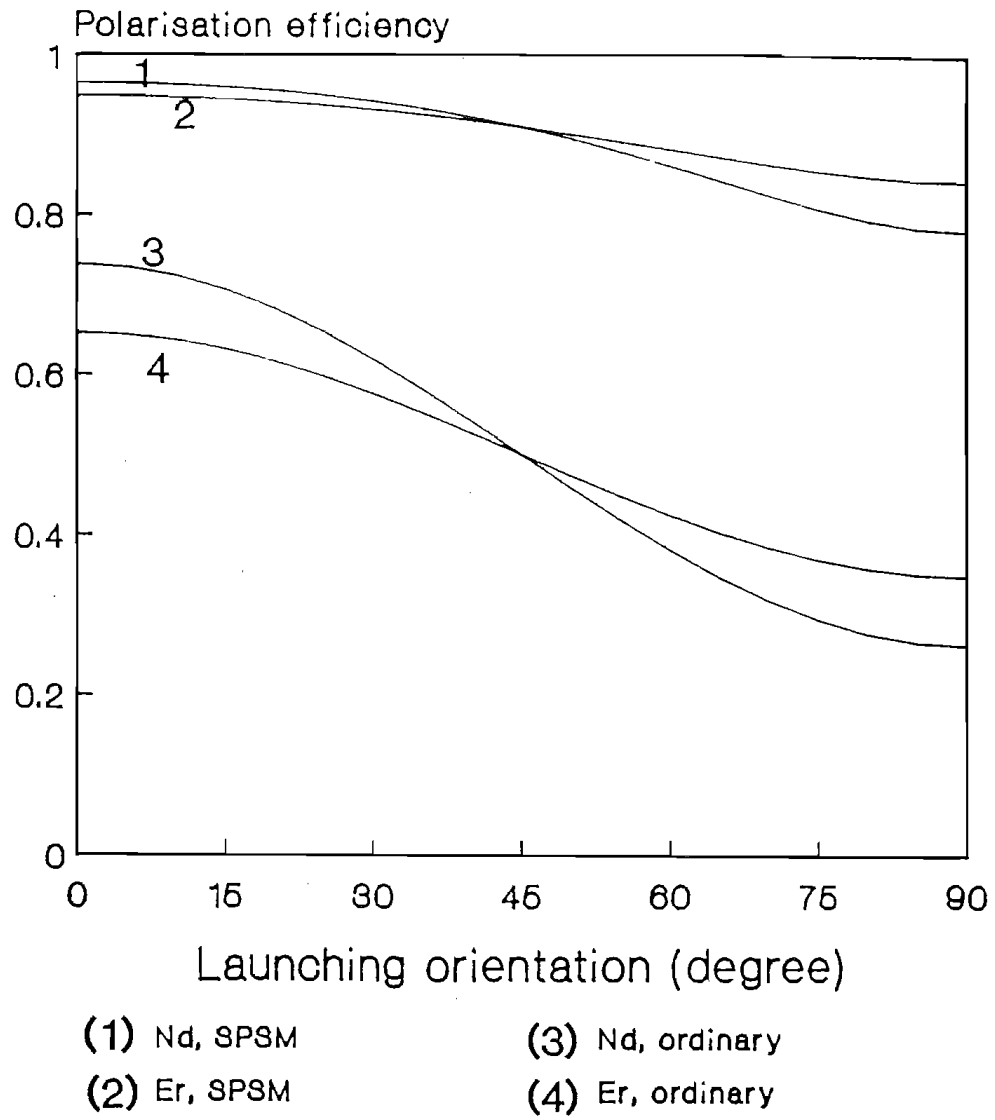

Fig.6.6 Polarisation efficiency as a function of launching orientation for two different configurations.

wanted polarisation component, the calculated curves for both configurations are shown in Fig.6.6, where the polarisation efficiency or polarisation selection ratio, is calculated as a function of launching orientation. The corresponding formulas for the calculations are eqs.(6.12) and (4.43) respectively. The calculation were carried out with the parameter a=0.015 and a=0.11, which are the values for Nd^{3+} and Er^{3+}-doped fibre lasers, respectively. The product of the parameters $S\xi$ was chosen to be 0.1, which was found to be reasonable for the LD-pumped fibre laser, as described later in this chapter.

It is seen from Fig.6.6 that the configuration with an intracavity polariser offers a much higher polarisation efficiency and less dependence on the pump light than its counterpart with an external polariser. The former has a value of polarisation efficiencies varying from 80% to 98% for Nd fibre laser and 85~95% for Er fibre laser respectively, while the later only 26~73% and 36~66%, respectively.

Comparing eq.(6.12) with (4.43), the ratio of polarisation efficiency over the polarisation selection is obtained for the particular cases $\alpha=0$ and $\alpha=\pi/2$.

$$\left.\frac{\eta_{sp}}{PS}\right|_{\alpha=0} = \frac{1}{c_1 + S\xi c_2} \qquad (6.13a)$$

$$\left.\frac{\eta_{sp}}{PS}\right|_{\alpha=\pi/2} = \frac{1}{c_2 + S\xi c_1} \qquad (6.13b)$$

With the measured parameters of a=0.015 for the Nd^{3+} laser and a=0.11 for the Er^{3+} laser, the ratio of η_{sp}/PS is around 1.3 for the case of $\alpha=0$, and 3.1 for $\alpha=\pi/2$. These estimates are also based on the assumption of $S\xi=0.1$.

To verify the above prediction an experiment was arranged with a LD-pumped fibre laser. The laser cavity was formed by 1.75m long Nd^{3+}-doped fibre, the sample ND199, and the output mirror had 80% reflectivity at the

lasing wavelength. The prism polariser had an extinction ratio of 50dB. The cavity was expanded by an intracavity lens of low loss to allow the polariser to be inserted into the cavity.

With a careful determination of the principal axes in the laser cavity, both the launching light and the polariser were aligned to the on-axis position. Two lasing characteristics were then measured, one for the case of intracavity polariser and another for the external polariser. The measured figures are shown in dotes and crosses, respectively, in Fig.6.7. Another comparison was also measured for both cases and plotted in stars and squares respectively in the same diagram.

According to the different slope ratios of these lasing characteristics, it is concluded that the experimental results are in a good agreement with the theoretical prediction, not only qualitatively but also quantitively. The mechanism behind this phenomenon is that a higher proportion of the total population inversion of excited ions has contributed to the polarisation if the undesired polarisation component has been suppressed within the resonator. This suggests that the suitable configuration for making single-polarisation fibre laser is that with an intracavity polariser. In the following, all the discussions are concentrated on this kind of configuration.

(2) Polarisation efficiency versus pumping orientation

When the intracavity polariser is aligned to the x-axis of the fibre, its property of differential attenuation for different modes forces the laser to oscillate in the x-mode only no matter what orientation angle the pumping light is launched with. However, the polarisation efficiency of single-polarisation operation depends upon the pumping orientation. Also it is a function of the polarised cross-section ratio a, as well

Single polarisation operation
in comparison with ordinary FL

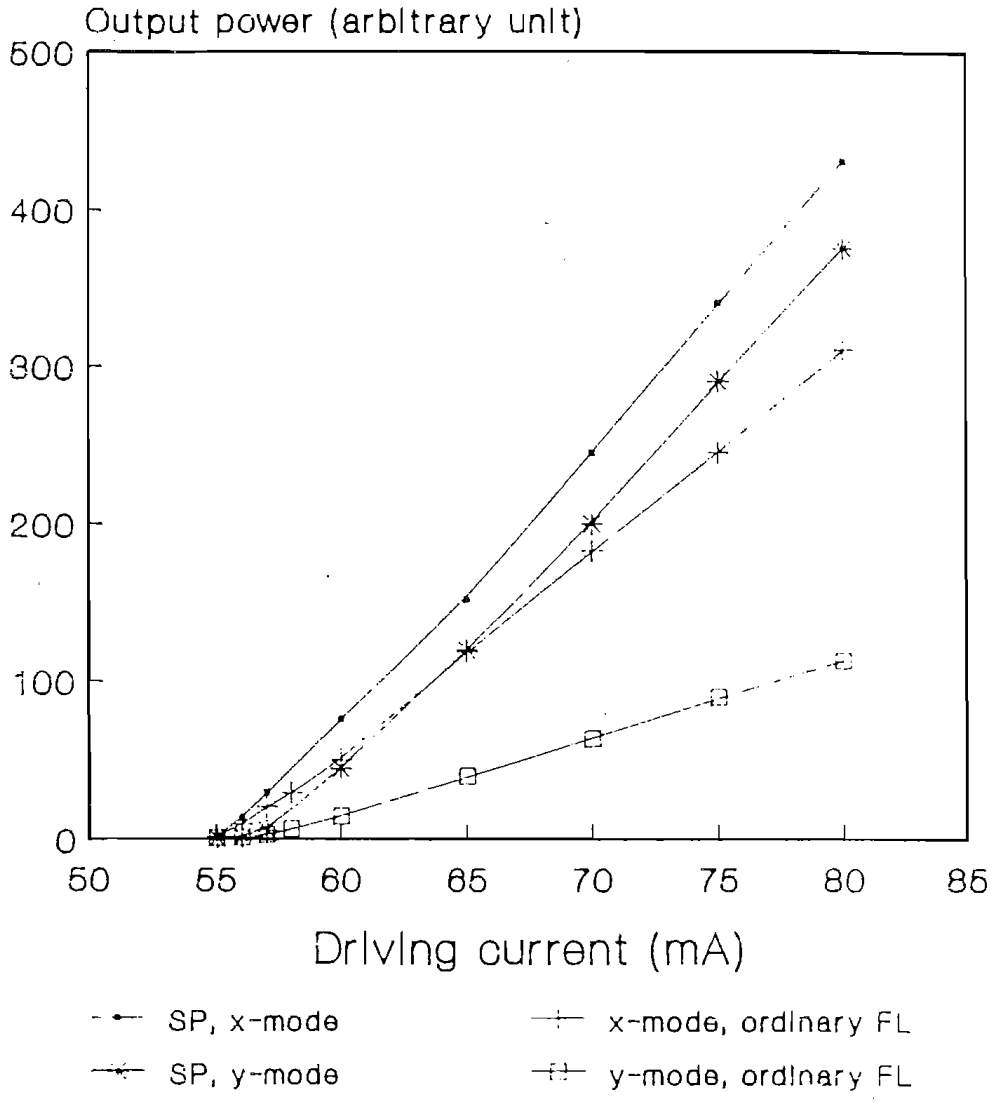

Fibre sample: ND199

Fig.6.7 Lasing characteristics of single-polarisation operation of Nd^{3+}-doped fibre laser showing a higher slope efficiency compared with an ordinary fibre laser.

as the product of the parameters $S\xi$, as seen from eq.(6.11).

Fig.6.8 shows the polarisation efficiency as a function of launching orientation α for a various of $S\xi$ in the case of a=0. It can be seen that the polarisation efficiency decreases with an increased off-axis angle α, or/and with an increased $S\xi$.

Fig.6.9 shows the normalized polarisation efficiency as a function of the launching angle. The normalization is realised to the case of α=0. It is seen that the normalized polarisation efficiency decreases with an increased off-axis angle α more rapidly for a larger $S\xi$.

Obviously, the maximum and minimum polarisation efficiencies are obtained if α=0 and $\alpha=\pi/2$, respectively. They are expressed as follows:

$$\eta_{max} = \eta_{sp}\Big|_{\alpha=0} = \frac{1}{1+S\xi c_2/c_1} \tag{6.14}$$

$$\eta_{min} = \eta_{sp}\Big|_{\alpha=\pi/2} = \frac{1}{1+S\xi c_1/c_2} \tag{6.15}$$

It is understood from eqs.(6.14) and (6.15) that for those rare earth ions having strong polarisation anisotropy (small a) it is necessary to launch the pump light on-axis. As for an isotropic oscillator model (a=0) the polarisation efficiency is independent of the pumping angle α since $c_1=c_2$ and thus $\eta_{max}=\eta_{min}$.

Apart from the experimental measurements shown in Fig.6.7 for the sample ND199, another sample of Nd^{3+}-doped fibre laser was set up for investigating the differential efficiencies between 0° and 90° launching. The fibre sample was YD191-03 which has a high birefringence with a beat length of 8.5mm compared with >50cm of sample ND199. The measured results in Fig.6.10 also show evidence of differential thresholds and slope efficiencies between the two different launching angles.

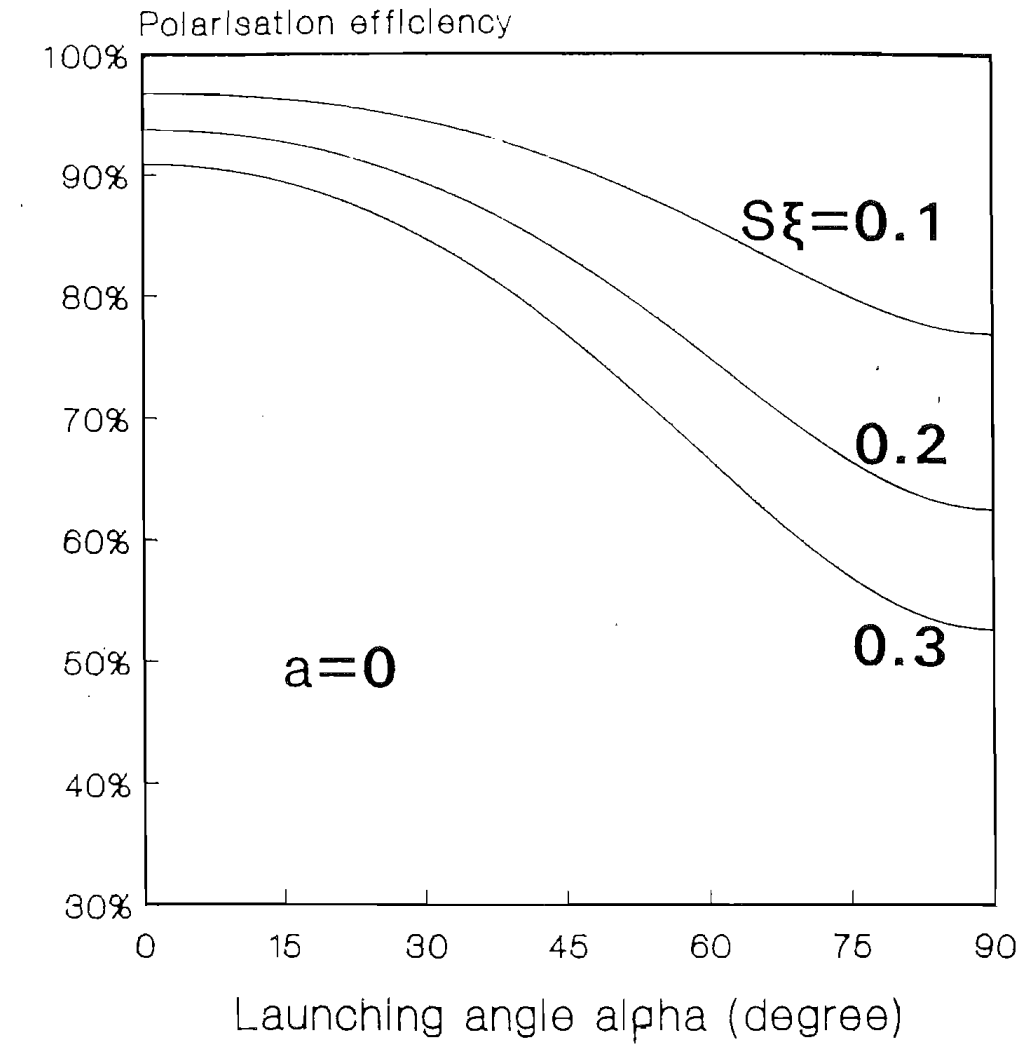

a=0

Fig.6.8 Polarisation efficiency as a function of launching orientation for a various values of S_ζ.

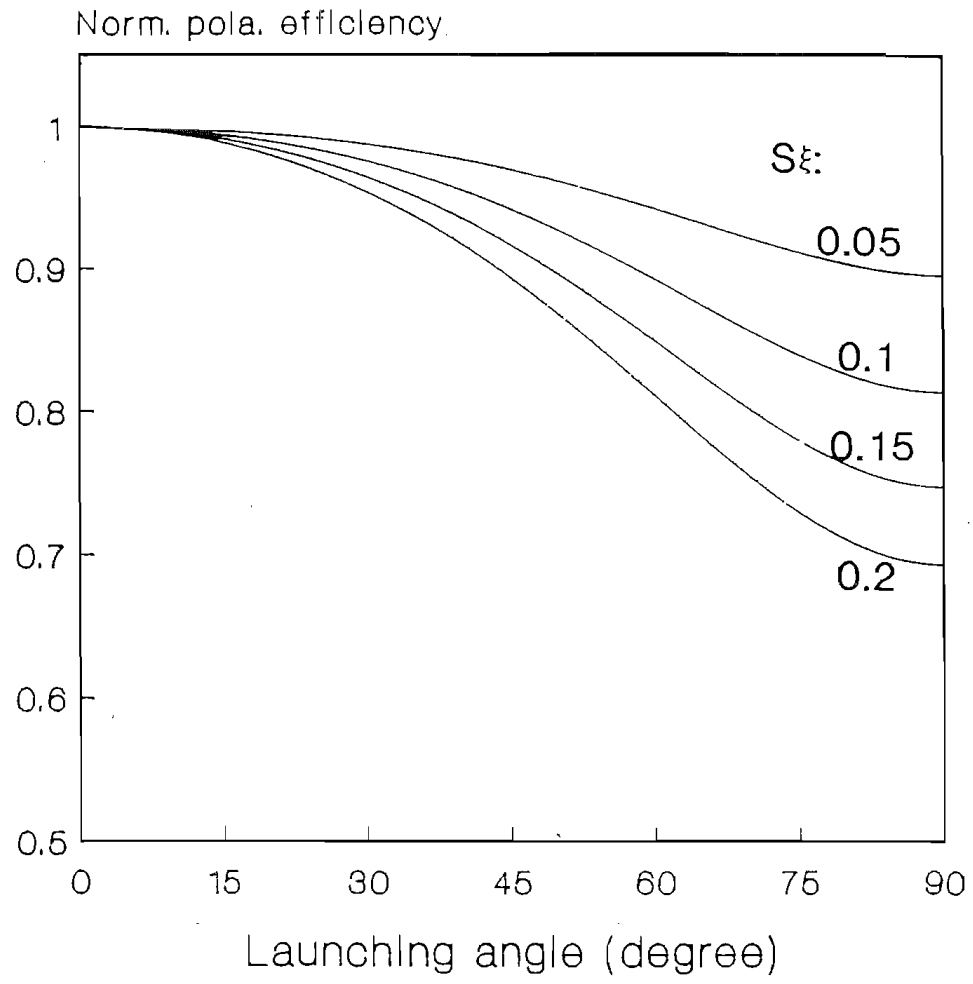

Fig.6.9 Normalized polarisation efficiency of single-polarisation operation as a function of launching orientation for Nd^{3+}-doped fibre laser of a=0.015.

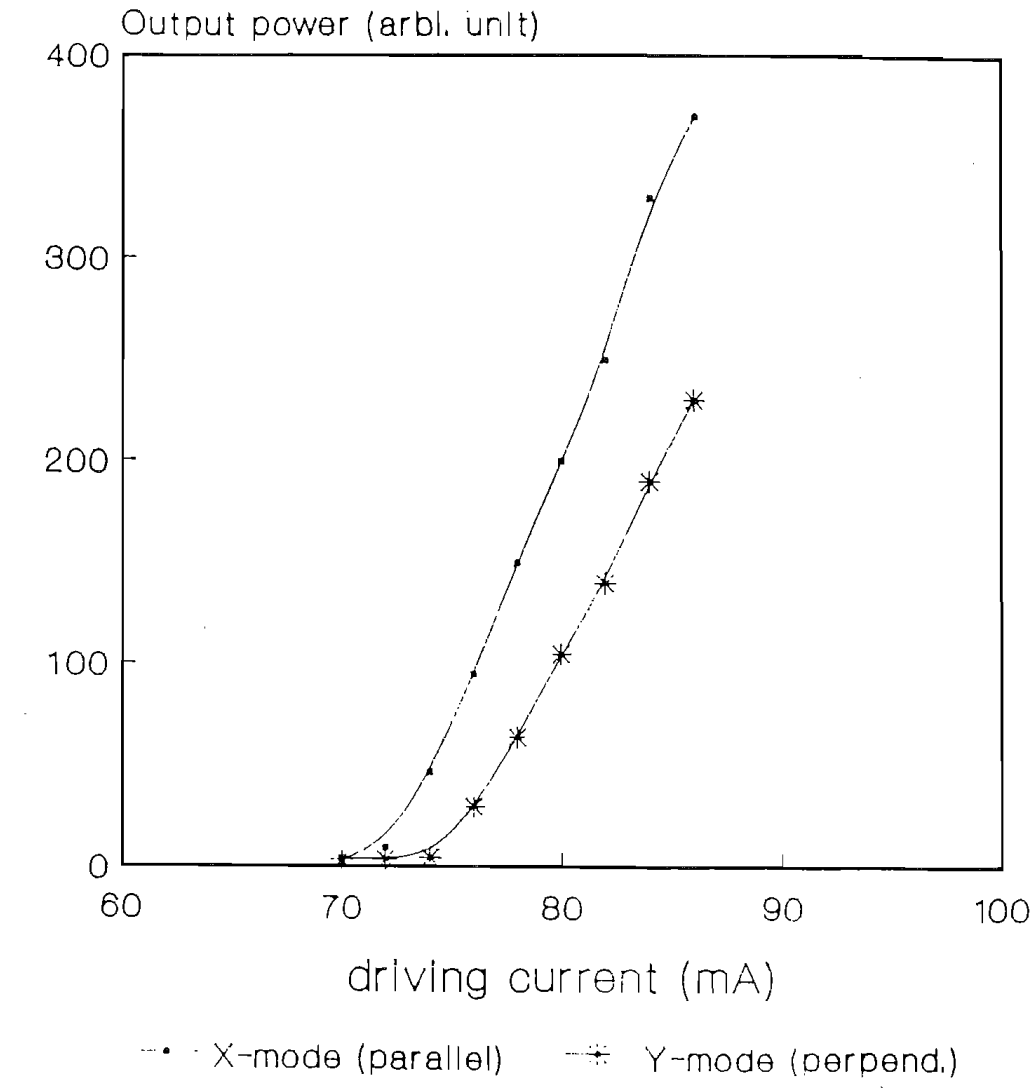

Fig.6.10 Comparison between polarisation efficiencies of single-polarisation operation for parallel and perpendicular launching in a Nd^{3+}-doped fibre laser .

(3) Polarisation efficiency versus polarised cross-section ratio

By utilizing eqs.(6.12) and (4.40), the dependence of polarisation efficiency on the polarised cross-section ratio a is obtained. The corresponding calculation is shown in Fig.6.11, Both the maximum polarisation efficiency as well as the differential polarisation efficiency between the maximum and minimum decrease with an increased polarised cross-section ratio a. The parameter of normalized polarisation efficiency at α=90°, defined as η_{min}/η_{max}, is shown in Fig.6.12 as a function of the parameter a. The conclusion can be drawn that the reduction in polarisation efficiency is caused by the polarisation anisotropy of the cross-section. As for an isotropic oscillator the polarisation efficiency is a constant independent of the pumping orientation.

The LD-pumped Nd^{3+}-doped fibre laser mentioned above was used again for investigating the dependence of the polarisation efficiency on the pumping orientation. The results are plotted in Fig.6.13, where the theoretical curves for a=0.015 are also drawn for comparison. The data in stars is for CW operation, whereas the square symbols refer to the Q-switched operation, which is realised by a mechanical chopper with a mark:space ratio of 1:300 and a repetition rate of 300Hz. The trend of the experimental data is in agreement with the theory. The reduction of the normalised polarisation efficiency for the Q-switched operation is significantly larger than the CW operation. This is expected by the theory as the saturated gain ratio S in the case of Q-switched operation is much higher than CW operation. As shown in Fig.6.13, the difference between the on-axis pumping and the perpendicular pumping ($\alpha=\pi/2$) is evident, indicating again that the Nd^{3+} ions in silica fibre have a strong polarisation anisotropy.

Using the determined parameter, a, and saturated gain ratio S, the experimental data for the CW operation allow the effective waveguide solid angle ξ to be

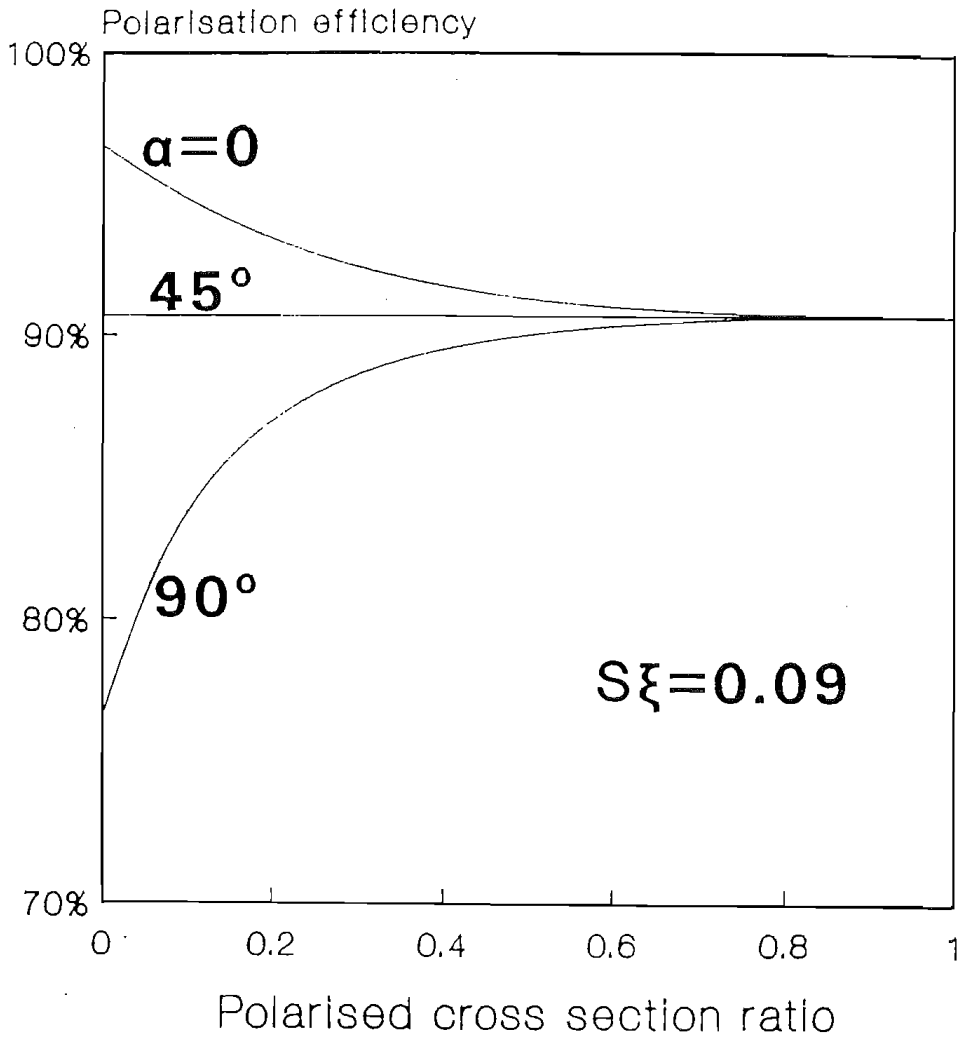

Fig.6.11 Polarisation efficiency as a function of polarised cross-section for three different launching orientations.

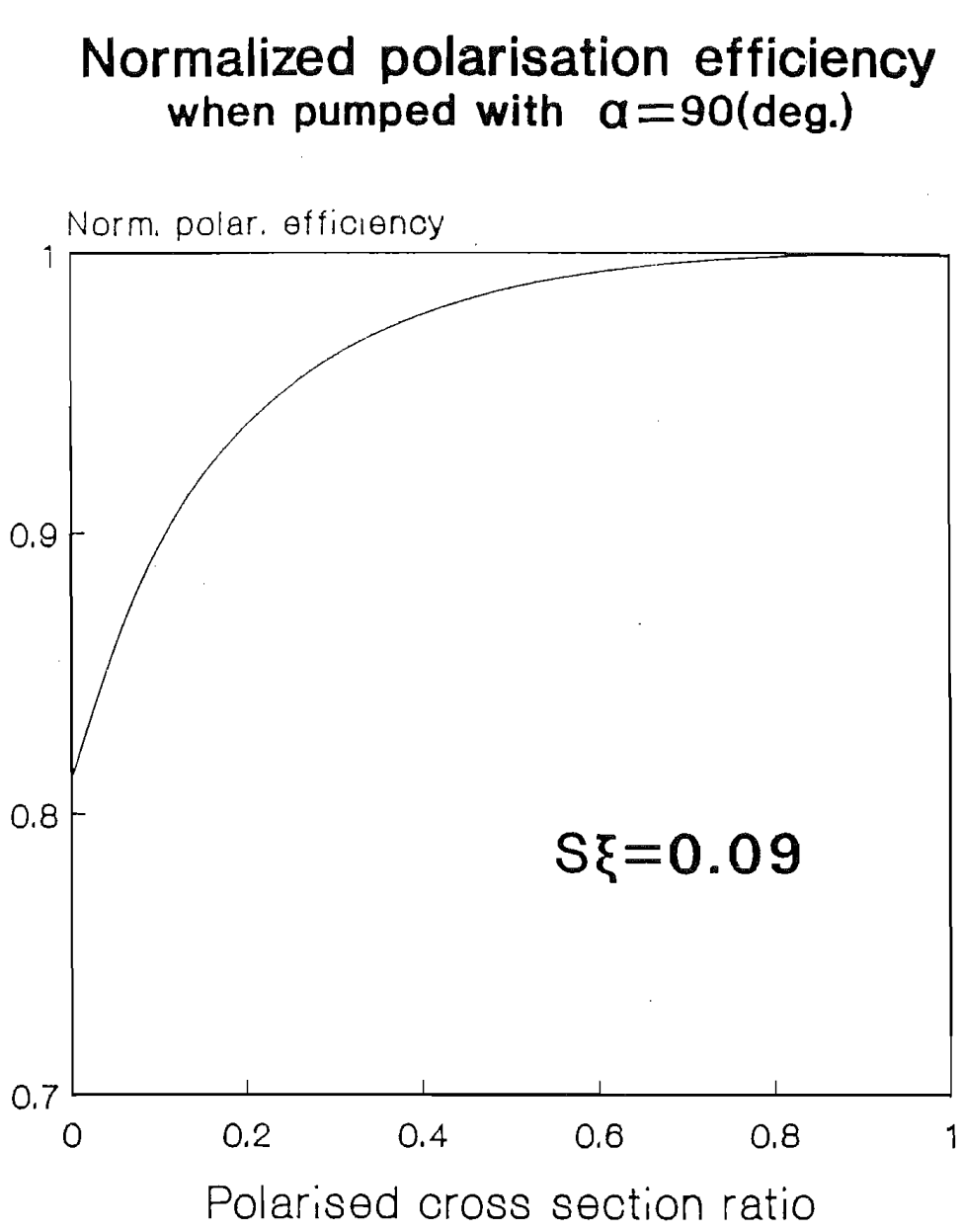

Fig.6.12 Normalized polarisation efficiency as a function of polarised cross-section ratio for $\alpha=90^{o}$ pumping.

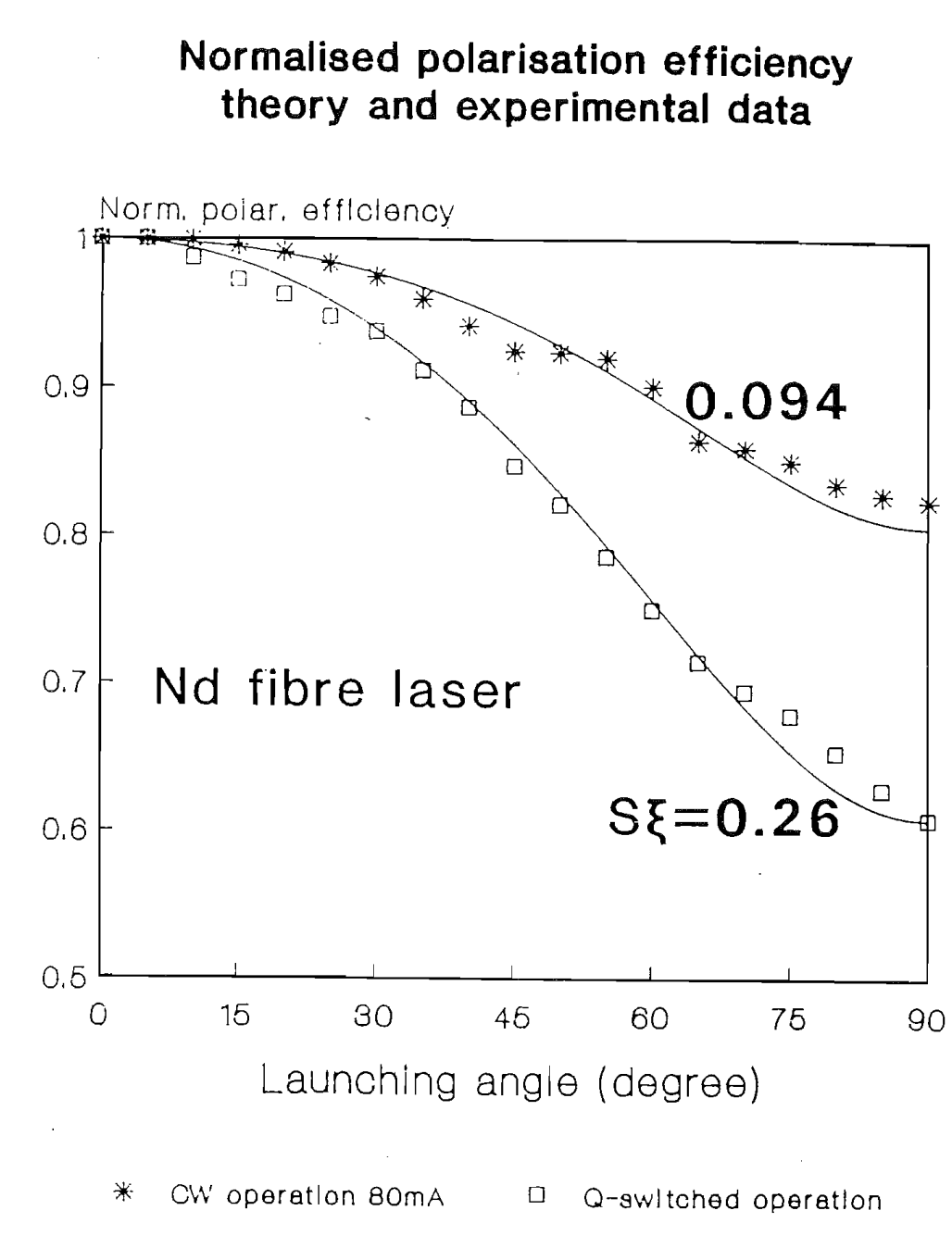

Fig.6.13 Comparison between theoretical and experimental data of normalized polarisation efficiency for a Nd^{3+}-doped fibre laser.

deduced. In our case, a=0.015 for the Nd^{3+} ions in the silica based glass. S=1.25 was measured for the CW operation of the LD-pumped Nd^{3+} fibre laser described in Section 6.1, ξ is thus deduced to be 0.075. This value is reasonable as it falls within the the regime of $\xi_0=0.0089<\xi<1$.

6.5 Influence of Polarisation Misalignment

The birefringence axes of the laser fibre are determined by the fibre itself rather than other intracavity components. When a polarisation-sensitive intracavity component is employed, a misalignment between the optimum operation and the birefringent axes of the fibre will influence the laser performance.

(1) Intracavity polariser

When a polariser is inserted into the cavity with an off-axis angle θ to the x-axis of the fibre, it introduces an additional loss to both polarisation eigenmodes. Assuming $0^o<\theta<45^o$ the induced loss to the x-mode L_x is

$$L_x = \ln\left(\frac{1}{\cos^2\theta}\right) \qquad (6.16)$$

This additional loss makes the threshold increase and the efficiency decrease. In comparison with an aligned system, i.e. $\theta=0$, the normalized threshold ratio can be expressed as

$$\frac{P_{th}(\theta)}{P_{th}(0)} = \frac{L - \ln R_2 - 2\ln\cos\theta}{L - \ln R_2} \qquad (6.17)$$

This is proved to be true by two experiments with LD-pumped Nd^{3+}-doped fibre lasers. The cavity arrangement is similar to that shown in the lower picture of Fig.6.5. The intracavity polariser was orientated with the x-axis at first, and the corresponding threshold was measured.

Then, by rotating the polariser, the threshold power was measured for various θ. The same experiments were carried out with two fibre samples. The normalized threshold ratios $P_{th}(\theta)/P_{th}(o)$ for both cases are plotted in Fig.6.14, in which the calculated curve corresponding to eq.(6.17) is also shown for comparison. The calculation was carried out according to the experimental parameters: R_2=80%, L=0.1 including the insertion loss (L=0.07) to the lasing light due to the polariser. The increase in the normalized threshold power with increased misalignment angle θ fits well the theoretical prediction. For the sample ND199 it was not possible to reach the threshold with the maximum pump power available when the misalignment angle is greater than 30°, indicating the importance of polarisation alignment.

(2) Acoustic-optic Q-switch

An efficient Q-switched operation can be achieved by using an acoustic-optic (A-O) deflector in the laser cavity[5]. The fundamental investigations show that, however, the polarisation state of the Q-switched pulse is strongly dependent on both the polarisation property of the A-O deflector and the relative orientation between the polarisation of the lasing mode and the A-O device. When linearly-polarised light is launched through the A-O deflector, the modulated output light is usually found to be elliptically polarised. This is due to the birefringence of the device. Fig.6.15 shows the extinction ratio of the modulated pulses as a function of the angle the input light makes to the A-O deflector. The deflectors used were both typical commercial products: AO1 was ISOMET 1205 C-2, and AO2 INTROACTION AOM-40R. It can be seen that a variation from 2.3 to 7.8dB for AO1 and 11.8 to 29.3dB for AO2 were measured, respectively. It is evident that acoustic-optic deflectors are usually polarisation-sensitive, and therefore the polarisation alignment is critical in order to achieve a single-

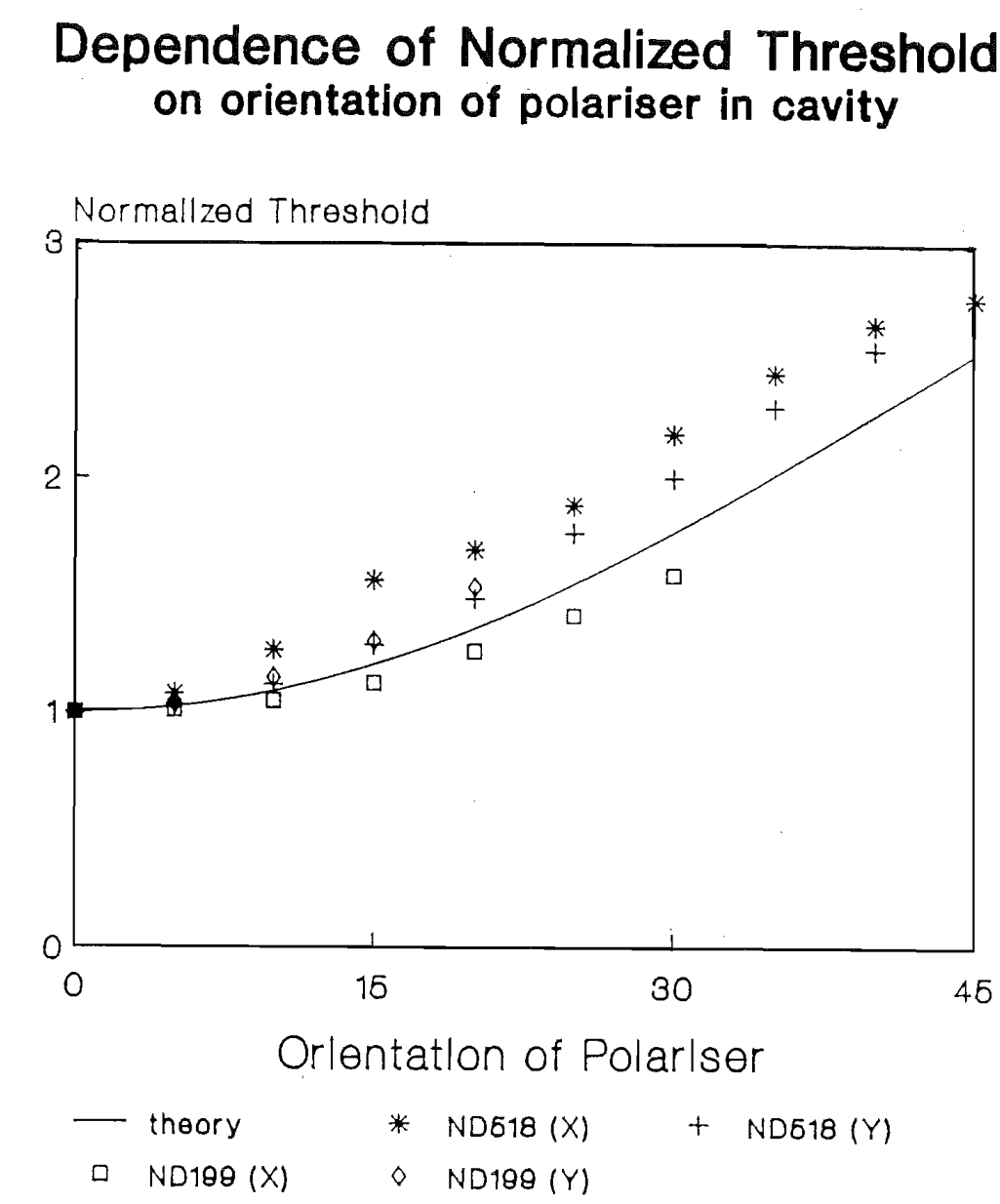

Fig.6.14 Theoretical curve and experimental data showing the influence of polarisation misalignment on normalized threshold.

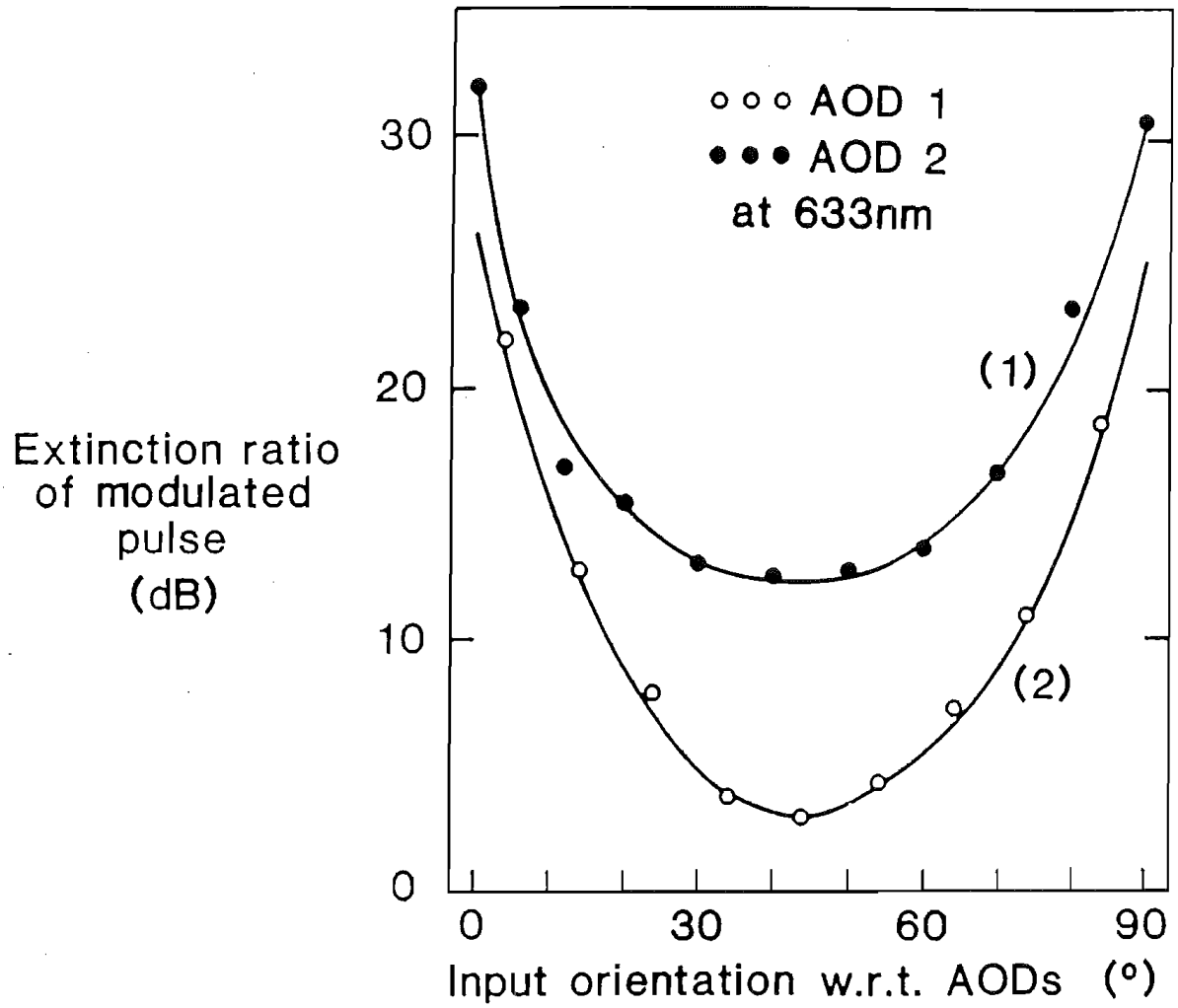

Fig.6.15 Extinction ratio of modulated pulse as a function of input orientation for two different acoustic-optic deflectors.

polarisation Q-switched operation with a high extinction ratio.

(3) Other devices

Additional enhanced operations using various intracavity components in the fibre laser are currently being carried out. The crystal mode-locker is one of those polarisation-sensitive intracavity devices. Some other crystals applied in the frequency doubling experiments such as KTP[6] and $KNbO_3$[7] are also birefringent and thus polarisation-sensitive. Care must be taken to realize the polarisation alignment when these intracavity components are involved in fibre lasers.

References to Chapter 6

[1] K. Liu, M. Digonnet, H.J. Shaw, B.J. Ainslie and S.P. Craig: "10mW superfluorescent single-mode fibre source at 1060nm", Electron. Lett., Vol.23, No.24, pp.1320-1321, 1987.

[2] W. Koechner: "Solid-State Laser Engineering", Springer-Verlag, 1976.

[3] A. Yariv: "Optical Electronics", Third Edition, Holt Rinehart and Winston, New Yoyk, 1976.

[4] I.P. Alcock, A.C. Tropper, A.I. Ferguson and D.C. Hanna: "Q-switched operation of a neodymium doped monomode fibre laser", Electron. Lett., 22, pp.84-85, 1986.

[5] W.L. Barnes: Private Communication.

[6] D.Z. Shen: Private Communication.

Chapter Seven

SINGLE-POLARISATION SINGLE-MODE FIBRE LASERS

7.1 Introduction

It is shown in the last chapter that the configuration with an intracavity polariser is the best choice for making a single-polarisation single-mode (SPSM) fibre laser. However, a bulk polariser is not a very practical candidate due to its large size and incompatibility with the fibre cavity. Furthermore, an additional intracavity lens must be introduced for focusing the laser beam as shown in Fig.6.5(b), which induces an additional cavity loss and therefore reduces the laser performance.

Most conventional gas or solid-state, lasers employ Brewster windows to achieve a linearly-polarised output. The function of the Brewster window in a laser cavity is to offer a differential attenuation between p-and s-polarisation components with directions parallel with, and normal, to the incident plane, respectively. Its mechanism can be described by equations (5.32a) and (5.32b), from which two different expressions for the p- and s-components are clearly seen. When the incident angle θ_i is equal to the Brewster angle, namely[1]

$$\theta_i = \tan^{-1}\left(\frac{n_t}{n_i}\right) , \qquad (7.1a)$$

or $$\theta_i + \theta_t = \pi/2 \qquad (7.1b)$$

where all the parameters have the same meaning as mentioned in Chapter 5, the transmission for the p- and s-components through the Brewster window can then be expressed as follows

$$T_p = 1 \qquad (7.2a)$$

$$T_s = 1 - \sin^2(\theta_i - \theta_t) \qquad (7.2b)$$

The additional attenuation of the s-component due to the Brewster window is then $L_s=-\ln[1-\sin^2(\theta_i-\theta_t)]$. For example, if $n_i=1.5$, $n_t=1$, then $L_s\approx 0.18$. It is this additional attenuation of the s-component which forces the conventional laser to oscillate in p-component.

In the case of a fibre laser, however, there are several points plaguing the application of the Brewster window. First, it is difficult to align the Brewster angle surface to the birefringent axes of the cavity fibre. As presented in the last chapter, such a polarisation misalignment adversely influences the laser performance. Secondly, the additional attenuation to the s-component the Brewster window can offer is limited (to 0.18 for the example mentioned above), and sometimes is not sufficient to suppress the undesired polarisation mode in a fibre laser. This is mainly because of superfluorescence of the undesired polarisation mode, as described in Chapter 6. For example, a typical laser-diode-pumped Nd fibre laser requires an additional attenuation of 0.25, as pointed out later in this chapter, for suppressing the undesired mode, which exceeds the limitation of the Brewster window. Besides, a fibre end at a Brewster angle cannot be applied in those CW fibre lasers having a butted-mirror configuration, which is believed to be the most efficient cavity.

Therefore, a new technique possessing both compatibility with the fibre cavity and the differential attenuation between p- and s-components is required.

A suitable solution is to employ the fibre polariser technique invented in early 1980's. The principles for making a fibre polariser are based on either the use of a polarising fibre[2,3] or the interaction between the evanescent field of the core and an external medium[4,5,6]. In the latter case the evanescent field of the guided mode in the fibre core is exposed by polishing or etching the fibre cladding, and a birefringent crystal or a metal film is employed to induce a differential

radiation loss or absorption between the two orthogonal polarisation modes. However, the fabrication technique is time-consuming and requires considerable skill.

In 1985, a high-performance composite metal/glass fibre polariser was developed by the Optical Fibre Group at the University of Southampton[7]. The fibre fabrication technique allows continuous access to the core, as well as offering an extremely smooth polished surface close to the core. The fibre design permits the integral incorporation of a metal section to yield continuous metal/glass composite polarisers.

Recently, a novel fibre polishing approach has been invented[8], based on which a fibre polariser with a metal plated on the polished region of the fibre can be constructed.

7.2 Integral Fibre Polariser

The integral fibre polariser technique for making SPSM fibre laser is transplanted from the above techniques. Instead of splicing an ordinary fibre polariser to the active fibre in a laser cavity, the integral fibre polariser is fabricated from the rare-earth doped fibres themselves. Three types of the integral single-mode fibre polariser are described in this thesis.

(1) D-shaped polariser

The exposed-field D-shaped fibre is fabricated by a preform shaping method. A standard rare-earth doped fibre preform is firstly made by gas phase deposition or the solution technique[9,10]. A flat is then ground onto the preform to create an optical interaction surface. The resultant D-shaped preform is then enclosed and fused into a sleeving glass tube to construct a composite preform. After drawing, the fibre contains a longitudinal hollow sector.

The size of the hollow sector can be controlled by controlling the appropriate dimensions of the initial preform and the sleeving tubes. Since both the processes of fusing and drawing are carried out simultaneously, special care must be taken to control the proper drawing temperature. In the studies with a silica glass tube a temperature of around 2000°c is normally used.

A cross-section of a typical D-shaped fibre is shown in Figure 7.1. When part of the hollow sector is filled by metal it acts as a polariser. The interaction strength is controlled by two factors, the separation between the flat surface and the core and the metal length. The former is determined at the preform shaping stage, whereas the latter can be controlled by injecting liquid metal into the hollow sector or cutting away the metal-filled part.

(2) Twin-hole fibre polariser

An alternative candidate for integral fibre polariser in fibre lasers is the twin-hole fibre. It is fabricated by drilling a rare-earth doped fibre preform, and then pulling into single-mode fibre. Fig.7.2 shows the cross-section of a twin-hole Er^{3+}-doped fibre.

(3) Metal-plated fibre polariser

The metal-plated fibre polariser is constructed by metal evaporation onto a polished fibre. Instead of the traditional polishing method, which polishes both the fibre fixed in a groove of a quartz block and the block itself, a novel fibre polishing method is employed. The fibre (locally stripped) is suspended under slight tension over a lubricated polishing wheel. The polished length can be altered by changing the contact angle of the fibre on the wheel, or by using a polishing wheel of different diameter. Paraffin is often used as the lubricating liquid. This novel polishing method dramatically reduces the polishing time and can provide a uniform polished region of arbitrary length[8]. The

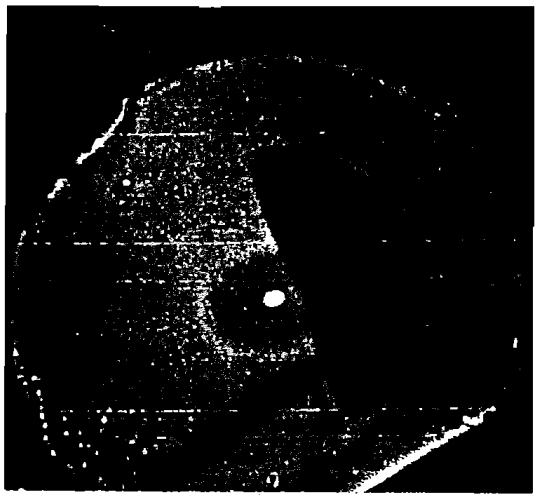

Fig.7.1
Photograph of cross-section of D-shaped integral fibre polariser.

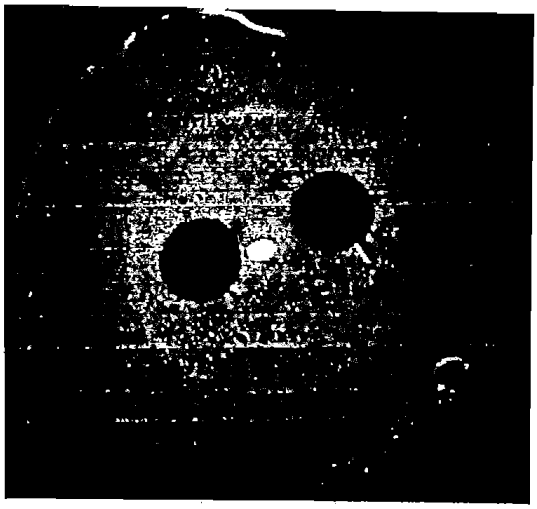

Fig.7.2
Photograph of cross-section of twin-hole integral fibre polariser.

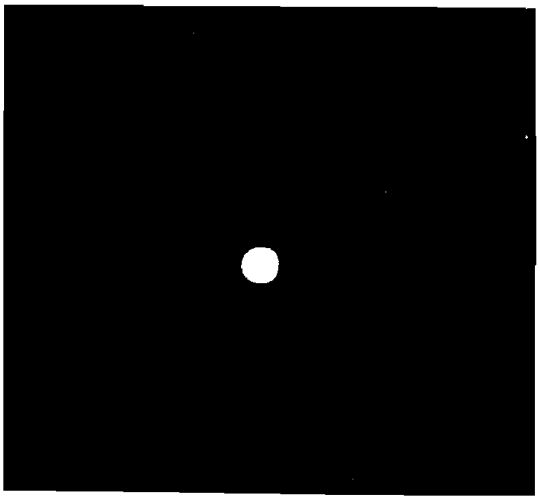

Fig.7.3
Photograph of cross-section of metal-plated integral fibre polariser.

interaction strength is detected by measuring the scattering loss of the polished surface during the polishing process. A typical cross-section of the polished flat close to the core is shown in Fig.7.3.

The integral polariser is then completed by evaporating a metal film such as aluminium and silver on the polished surface of the fibre. A substrate protecting the polished section of the fibre is necessary for the metal evaporation. A thickness of Al evaporation varying from 200nm to 500nm is used in the study and found to be suitable for constructing a polariser if the separation between the polished surface and the fibre core are within a reasonable distance.

(4) Discussion

The general features of D-shaped and twin-hole integral fibre polarisers are described as follows

Due to the asymmetric internal stresses an elliptical core is always obtained. Therefore the minor axis of the ellipse will always coincide with the interaction surface. This is an important advantage as the best performance can only be achieved with the case of polarisation alignment.

Since the ground or drilled hole surface is fire polished in the fibre drawing stage high quality interaction surface is obtained and therefore the scattering losses due to the surface roughness are minimized.

As the distance between the core and the polished surface is determined at the preform stage, it can be controlled more accurately than the fibre polishing approach.

The interaction length can be chosen as desired and controlled by the injecting metal procedure since the hole runs the whole length of the fibre.

As an integral polariser in the laser cavity, it does not suffer from splicing loss.

With two holes located symmetrically by the sides of the core, the twin-hole-type polarisers, after drawing, usually have a core with a higher ellipticity than D-shaped fibre as shown in Fig.7.2. Since no sleeving is needed the fabrication procedure for making the twin-hole fibre is simpler than that of D-shaped fibre.

Both D-shaped and twin-hole integral polariser fibre cause a difficulty in making perfect cleaves at the fibre ends, which is especially important for a high laser performance with a butted-mirror cavity. It is believed, however, that this problem can be solved by the end-polishing technique.

With the metal-plated polariser, it is possible to leave the fibre ends unaffected as the polished part can be in any position, and thus allows the laser to operate in the usual way. However, a possible polarisation misalignment between the interaction surface and the birefringent axes of the cavity fibre may become a disadvantage. Since this can be easily overcome in the case of short, straight cavity, the metal-plated polariser is highly recommended to those active fibres of rather high rare-earth dopant concentrations.

7.3 The First SPSM Fibre Laser

The first demonstration of a SPSM was with a D-shaped low-dopant-concentration Nd^{3+}-doped fibre. The single-mode fibre had a distance between the core and the exposed surface of approximately 4μm. The laser cavity was formed by cleaving the end of a 20m long fibre and butting it to a 35% reflectivity output mirror, with an intracavity microscope objective (20x, 0.4NA) at the launch end, as shown in Fig.7.4. The input mirror had a transmission at the pump wavelength of 85% and >99% reflectivity at the lasing wavelength of 1.09μm. An Ar^{+}-ion laser operating at 514.5nm formed the pump source. The output from the fibre laser was filtered and passed through a polariser having an extinction ratio of

50dB. With no metal inserted into the D-section of the cladding, the laser was found, as expected, to oscillate on the two orthogonal eigenmodes of the cavity. A 420mm length of gallium was then injected into the D-section to form the basis of the fibre polariser. The secondary polarisation eigenmode with polarisation direction perpendicular to the metal surface was suppressed, even at the maximum available pump power of the Ar^+-ion laser, and SPSM fibre laser was constructed.

Although the integral fibre polariser gives a significant differential mode attenuation, it induces an additional insertion loss for the operating mode. Careful consideration of the metal length must be made for the optimum operation. In the experiment described above, it was found that 2mm of gallium is sufficient to suppress the undesired mode, corresponding to only 0.02dB of insertion loss for the operating mode. An extinction ratio of 35.4dB between the orthogonal polarisation modes was then measured for a 20mW single-polarisation output.

Fig.7.5 shows the lasing characteristics of the single-polarisation fibre laser. The pure damped sinusoid waveform of the relaxation oscillation shown in Fig.7.6 indicates single-polarisation operation.

7.4 Optimal Design of SPSM Fibre Lasers

(1) Analysis of metal-clad fibre

The early work on metal-cladded waveguides dated back to the 1970's, when an Al-plated asymmetric light waveguide was used to select the fundamental transverse electric field (TE_0) mode, and a corresponding theoretical analysis was established for the planar waveguide structure[11,12]. A more rigorous analysis of a optical fibre with an adjacent plane metallic boundary has become available recently[13].

As usual, an orthogonal co-ordinate system denoted by x, y, and z is used, as shown in Fig.7.7. The guided scalar mode in the fibre core is assumed to propagate in

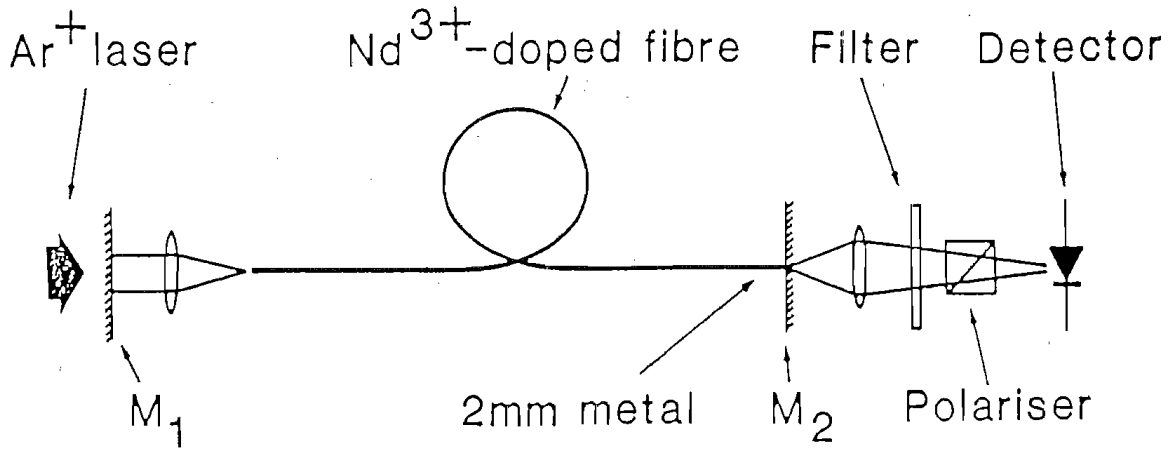

Fig.7.4 Single-polarisation fibre laser cavity.

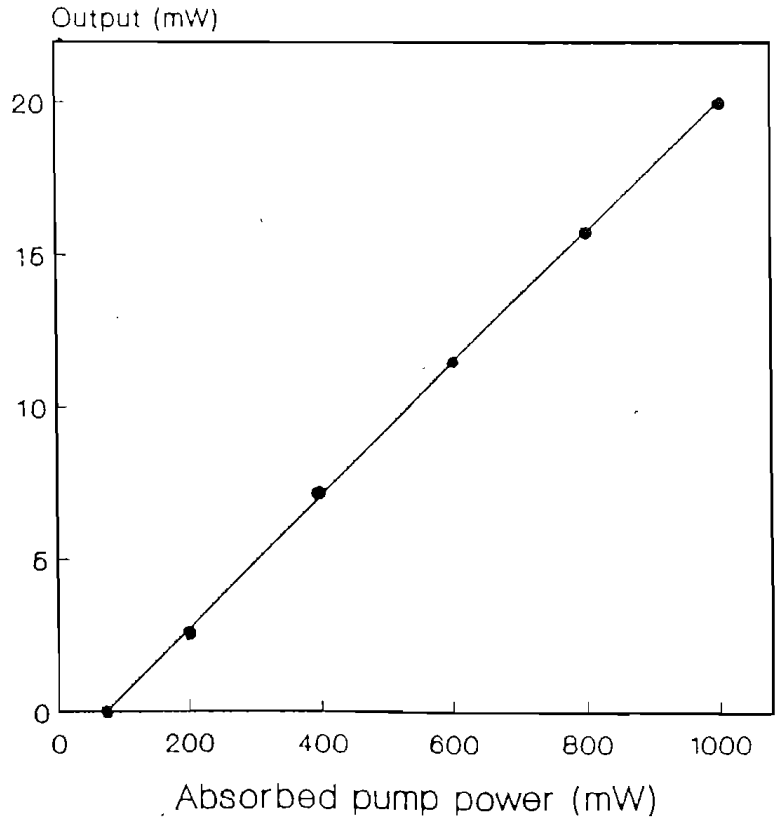

Fibre sample: ND208, Pump: Ar^+-ion laser

Fig.7.5 Lasing characteristics obtained for cavity of Fig.7.4.

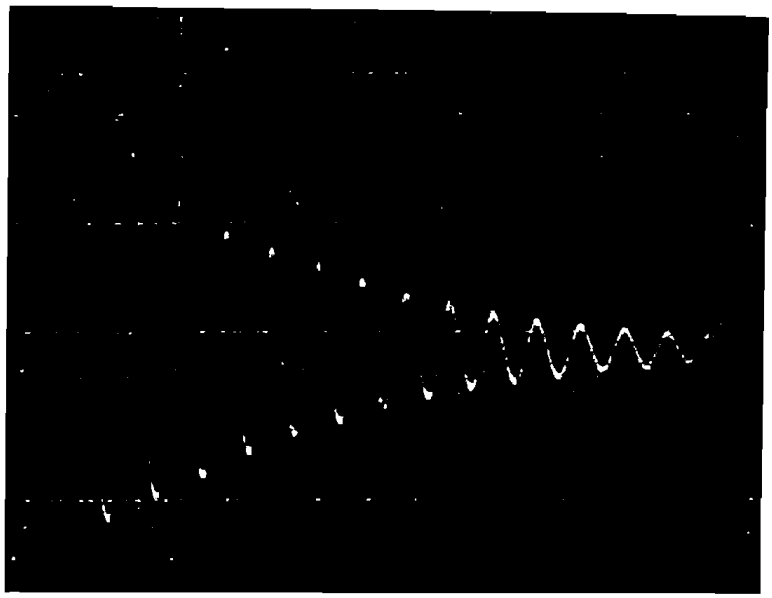

Fig.7.6 Pure damped sinusoidal waveform of the relaxation oscillation observed with the single-polarisation fibre laser of Fig.7.4.

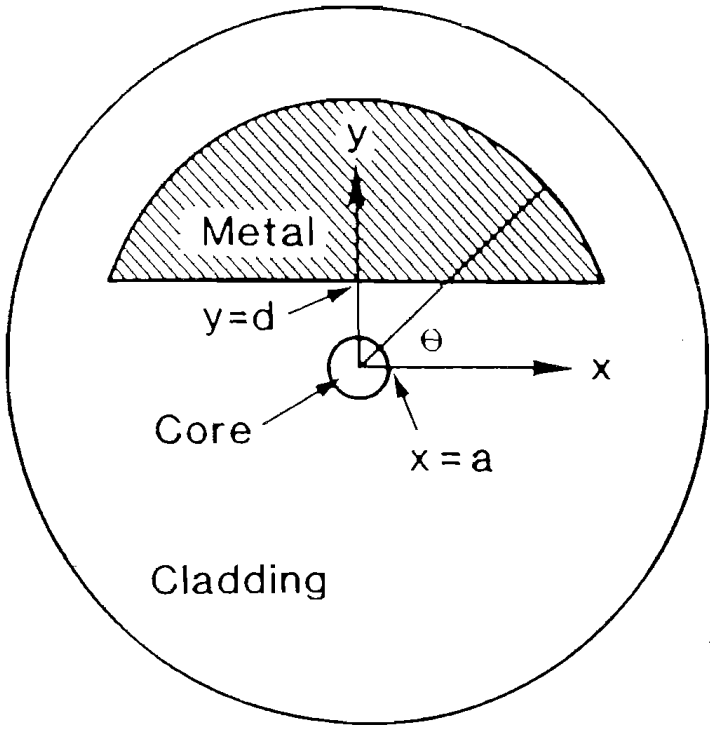

Fig.7.7 Co-ordinate system for analysing metal/cladding fibre.

the z-direction with a phase term $\exp[j(\omega t-k_z z)]$ as described in eq.(2.8), where k_z can be a complex constant given by

$$k_z = \beta - j\gamma \tag{7.3}$$

where β and γ are the phase and the attenuation constants, respectively.

The scalar field is written as a Fourier-Bessel series within the core area:

$$\Psi = \sum_{m=0}^{\infty} A_m J_m(ur)\cos m\theta \qquad r<a \tag{7.4a}$$

$$\Psi = \sum_{m=0}^{\infty} [B_m K_m(wr) + C_m I_m(wr)]\cos m\theta \qquad r>a \tag{7.4b}$$

with

$$u^2 = k^2 n_{co}^2 - k_z^2 \tag{7.5a}$$

$$w^2 = k_z^2 - k^2 n_{cl}^2 \tag{7.5b}$$

where $k=1/\lambda$ is the wave number, n_{co} and n_{cl} are the refractive indices of the core and cladding respectively. The field near the plane y=d, on its side close to the core can be written as a plane-wave expansion

$$\Psi = \int_{-\infty}^{+\infty} \exp(j\nu x)\{s_\nu \exp[-a_\nu (y-d)]+t_\nu \exp[a_\nu (y-d)]\}d\nu \tag{7.6}$$

with

$$a_\nu^2 = w^2 + \nu^2 \tag{7.7}$$

The cladding field can be considered as the superposition of an outward evanescent field (corresponding to B_m or s_ν terms) and inward evanescent field (C_m or t_ν terms). These two fields are physically connected by the diffraction on the core and by the reflection of the

metal boundary plane. The reflection coefficient of a complex plane wave like $\exp(-a_\nu y+j\nu x)$ on the metal surface R_ν can be defined as

$$R_\nu = t_\nu / s_\nu \tag{7.8}$$

It is the polarisation dependence of R_ν which determines the physical mechanism of polarisation-dependent attenuation in a metal/clad structure. When the discussion is limited to the perturbed LP_{01} mode, which is the case of single-mode fibre laser, R_ν can readily evaluated to be:

$$R_\nu = (a_\nu - b_\nu)/(a_\nu + b_\nu) \qquad \text{for x-mode} \tag{7.9a}$$

$$R_\nu = \left(\frac{a_\nu}{n_{cl}^2} - \frac{b_\nu}{n_{me}^2}\right)\Big/\left(\frac{a_\nu}{n_{cl}^2} + \frac{b_\nu}{n_{me}^2}\right) \qquad \text{for y-mode} \tag{7.9b}$$

with

$$b_\nu^2 = a_\nu^2 + k^2(n_{cl}^2 + n_{me}^2) \tag{7.10}$$

where n_{me} is related with the complex relative permittivity of the metal ε_{me} by

$$n_{me}^2 = \varepsilon_{me} = \varepsilon' - j\varepsilon'' \tag{7.11}$$

The complex propagation constant k_z is expressed as the solution of the following eigenvalue equation:

$$\left(\frac{wK_m'}{K_m} - \frac{uJ_m'}{J_m}\right) B_m + \left(\frac{wI_m'}{I_m} - \frac{uJ_m'}{J_m}\right) \frac{I_m}{K_m \eta_m} \sum_{n=0}^{M-1} P_{mn} B_n = 0 \tag{7.12}$$

with

$$P_{mn} = 2 \int_0^\infty R_\nu \cosh(mg)\cosh(ng)\exp[-2wd\cosh(g)]dg \tag{7.13}$$

where $J_m=J_m(au)$, $K_m=K_m(aw)$, $I_m=I_m(aw)$, and the integration variable g is connected with a_ν and w by

$$a_\nu = w\cosh(g) = (w^2 + \nu^2)^{1/2} \qquad (7.14)$$

The unknown quantities B_m and k_z can then be calculated numerically. The calculation precision depends on the truncating rank M in eq.(7.12). Taking M=3 was generally sufficient to obtain four exact digits for w and u[13].

(2) Numerical calculations

Using the complex relative permittivity $\varepsilon_{me}=\varepsilon'-j\varepsilon''$ for a given metal, different sets of parameters w and u (or k_z) for the x and y modes, and thus the different attenuations for both modes, can be obtained.

For application in fibre lasers, the performance of the integral fibre polariser is characterised by two parameters, the additional loss to the y-mode L_y and the attenuation ratio $r\equiv L_y/L_x$, where L_x is the loss to the x-mode. The additional loss is defined and related with field attenuation γ by

$$L_y = \ln\left(\frac{P_{in}}{P_{out}}\right) = 2\gamma l \qquad (7.15)$$

where P_{in} and P_{out} are input and output light power through the polariser, respectively, and l is the interaction length of the metal/cladding part. An important geometric parameter determining the performance of polariser is the normalized separation D defined as

$$D = d/a \qquad (7.16)$$

where a is the core radius and d the distance between the metal surface and the core centre, as illustrated in Fig.7.7.

Calculations show that five metals, i.e. aluminium, gallium, gold, indium, and silver give the greatest values of r. Fig.7.8 and Fig.7.9 show the calculated L_y

and r as a function of D for gallium and aluminium, respectively. High attenuation ratios r=200 for Ga and r=90 for Al predict a high performance of metal/cladding integral polariser. Also, both L_y and r vary with the numerical aperture, as well as the operating wavelength, which are discussed in detail elsewhere[14].

The differential attenuations for a D-shaped polariser were measured. The polariser has a normalized separation D=2.0. The metal in the D-shaped sector was Ga and the results are shown in Fig.7.10. It can be seen from both the theory and experiments that the linear relationship between L_y and the interaction length l is justified, and r can be regarded as a constant for a certain metal within a relatively lower interaction strength region, which is just of interest in fibre laser applications. It is also found that the measured values r=60 for gallium is several times lower than the theory predicts. The reasons for this are believed to be the residual scattering due to surface roughness and field distribution mismatching at the joint point between metal/cladding part and ordinary part of the fibre[15].

(3) Minimum L_y required for the SPSM laser

The key function of the integral fibre polariser in fibre lasers is to suppress the undesired mode below the threshold. Using the formula describing the threshold condition, eq.(5.5), it is readily deduced that the minimum additional loss to the y-mode L_y is

$$L_y \geq 2KP^y - L + \ln R_2 \qquad (7.17)$$

where P^y is the effective pump power for the y-mode, L is the intrinsic cavity loss, which can be regarded as identical for both x and y modes, R_2 is the reflectivity of the output mirror, K is the laser parameter mentioned in chapter 5. Both L and K can be determined experimentally, as described later in this section.

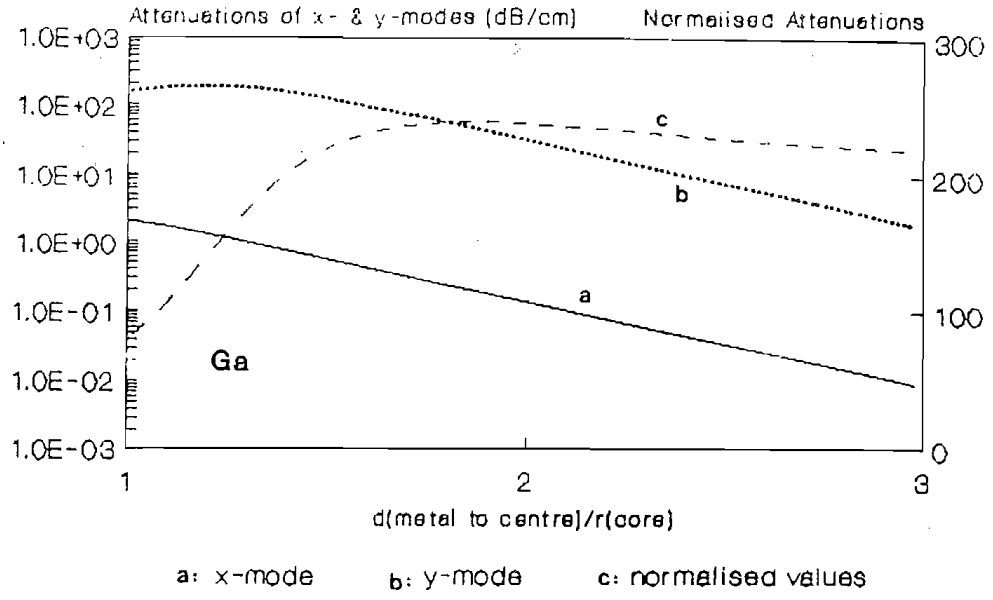

Fig.7.8 Calculated model attenuations of metal/cladding fibre as a function of normalized separation d/a for gallium.

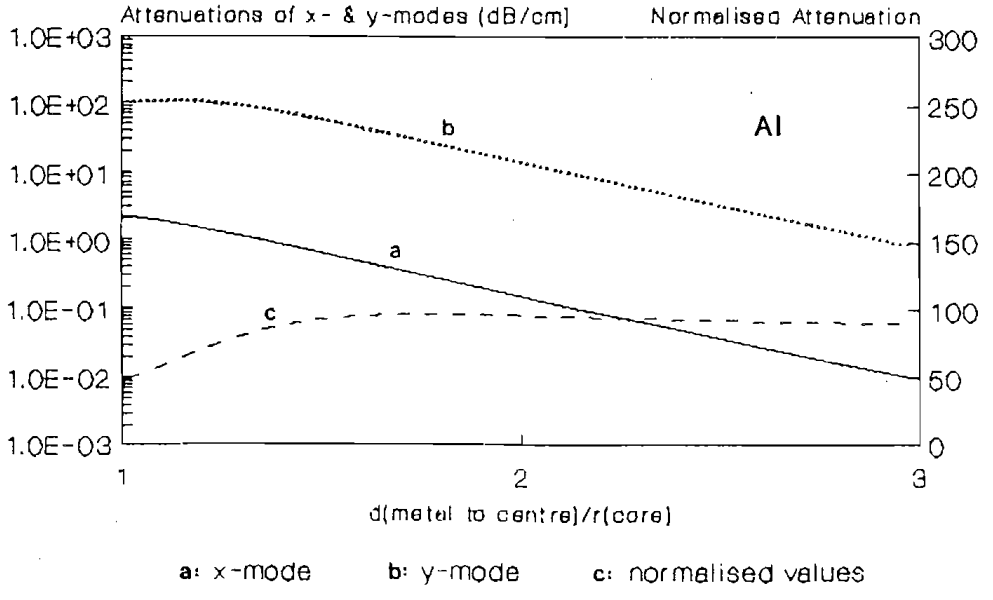

Fig.7.9 Calculated model attenuations of metal-clad fibre as a function of normalized separation d/a for aluminium.

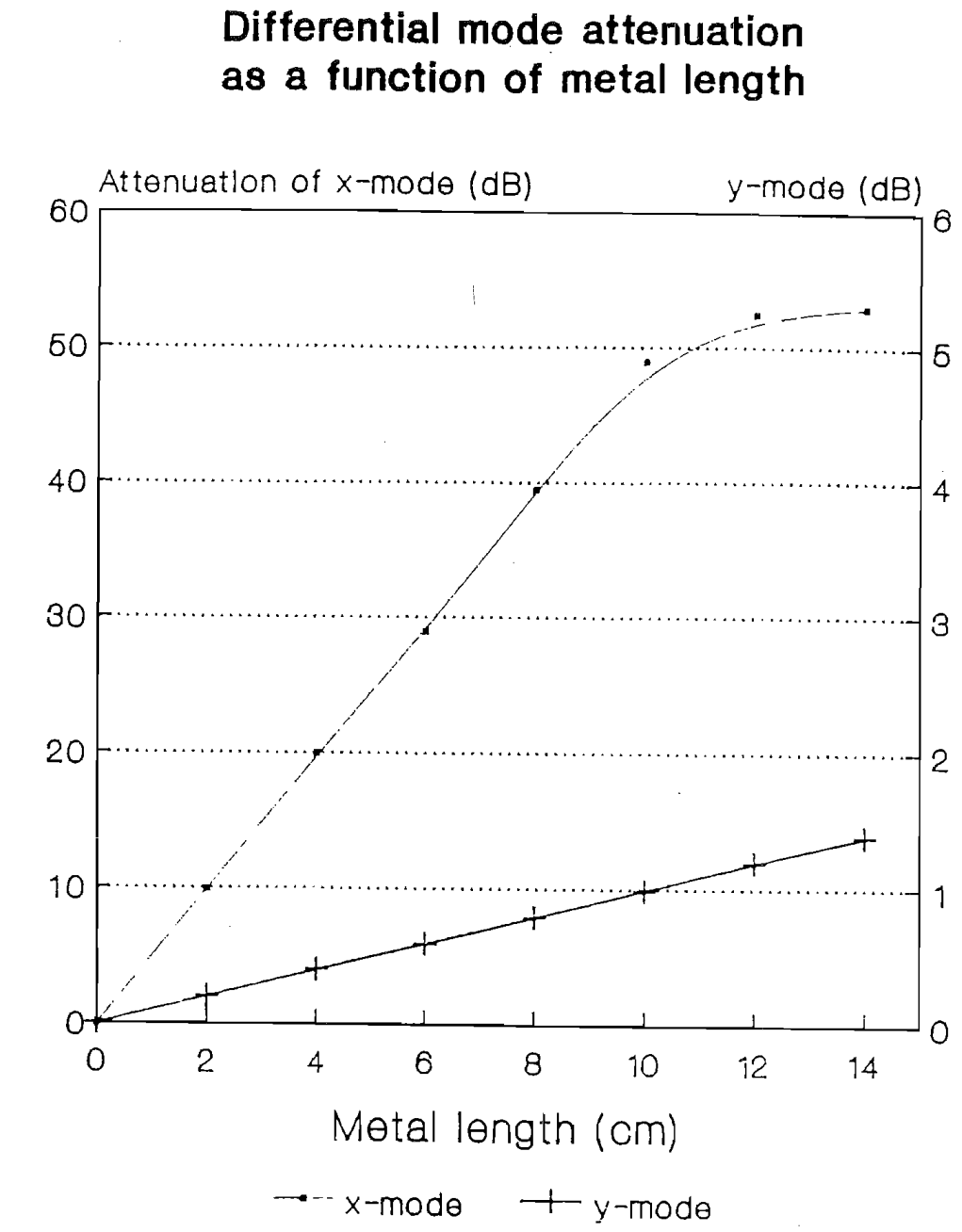

Metal sample: Ga

Fig.7.10 Dependence of differential mode attenuation on length of metal embedded in the cladding of the fibre.

(4) Proper design steps

The proper steps in designing SPSM fibre lasers are:

— optimizing the laser cavity.

— measuring the laser parameters L and K.

— calculating the required L_y.

— deducing the parameters of the polariser.

(5) Optimizing laser cavity

As a result of the end-pumping, the gain coefficient g (gain per unit length) has an exponential distribution along the fibre

$$g(z) = KP(o)\exp(-\gamma z) \tag{7.18}$$

where P(o) is the linear density of absorbed pump power at the launching end, while γ is the absorption at the pumping wavelength, and K has the same definition as mentioned before. On the other hand, the loss at lasing wavelength α remains constant. For a single-pass amplifier the equation for energy density at each point z along the fibre can be written as

$$\frac{dI(z)}{dz} = g(o)e^{-\gamma z}I(z) - \alpha I(z) \tag{7.19}$$

The solution of this equation is

$$I(z) = I(o)\exp[\frac{g(o)}{\gamma}(1-e^{-\gamma z})-\alpha z] \tag{7.20}$$

Therefore, a pumped fibre of length l has a single-pass gain

$$G_s = \exp[\frac{g(o)}{\gamma}(1-e^{-\gamma l})-\alpha l] \tag{7.21a}$$

or loop gain for a Fabry-Perot cavity configuration

$$G_l = R_1R_2\exp[\frac{2g(o)}{\gamma}(1-e^{-\gamma l})-2\alpha l] \tag{7.21b}$$

It can readily be shown that there exists an optimum fibre length l_{opt} to let the fibre gain (both G_s and G_l)

reach the maximum value, and the optimum fibre length can be expressed as

$$l_{opt} = \frac{1}{\gamma} \ln[\frac{g(o)}{\alpha}] = \frac{1}{\gamma} \ln[\frac{KP(o)}{\alpha}] \qquad (7.22)$$

Fig.7.11 shows the curves of single-pass gain as a function of fibre length for several sets of laser parameters. The curve (a) is for the fibre sample ND199, with γ=3dB/m and α=6dB/km, whilst (b) is for ND518, γ=90dB/m and α=8dB/km. The other parameters were taken as R_2=80%, K=0.1/mW and P_{ab}=10mW, which are typical values for a LD-pumped fibre laser. Fig.7.12 shows the optimum fibre length as a function of dopant concentration. As expected, a higher concentration corresponds to a shorter optimum fibre length.

It is worth pointing out that the energy density equation (7.19) is valid only for unsaturated operation, and thus the optimum fibre length for a practical fibre laser ought to be shorter than that expressed by eq.(7.22). A real optimum length of fibre for a laser can easily determined experimentally using a cut-back method.

Another parameter of the laser cavity which needs to be optimized is R_2, the reflectivity of output mirror. This can be done by differentiating eq.(5.18) with respect to R_2 and setting to zero in order to maximizing the laser output power:

$$R_{2(opt)} \approx 1 - \frac{(2KP_{ab}L)^{1/2} - L}{1 + L} \qquad (7.23)$$

As can be seen from this expression, the reflectivity of the output mirror must be decreased for increasing absorbed pump powers. Therefore, a lower R_2 is required for the Q-switched fibre laser than CW operation.

(6) Measurements of L, K, P(o)

Equation (5.5) can be written as

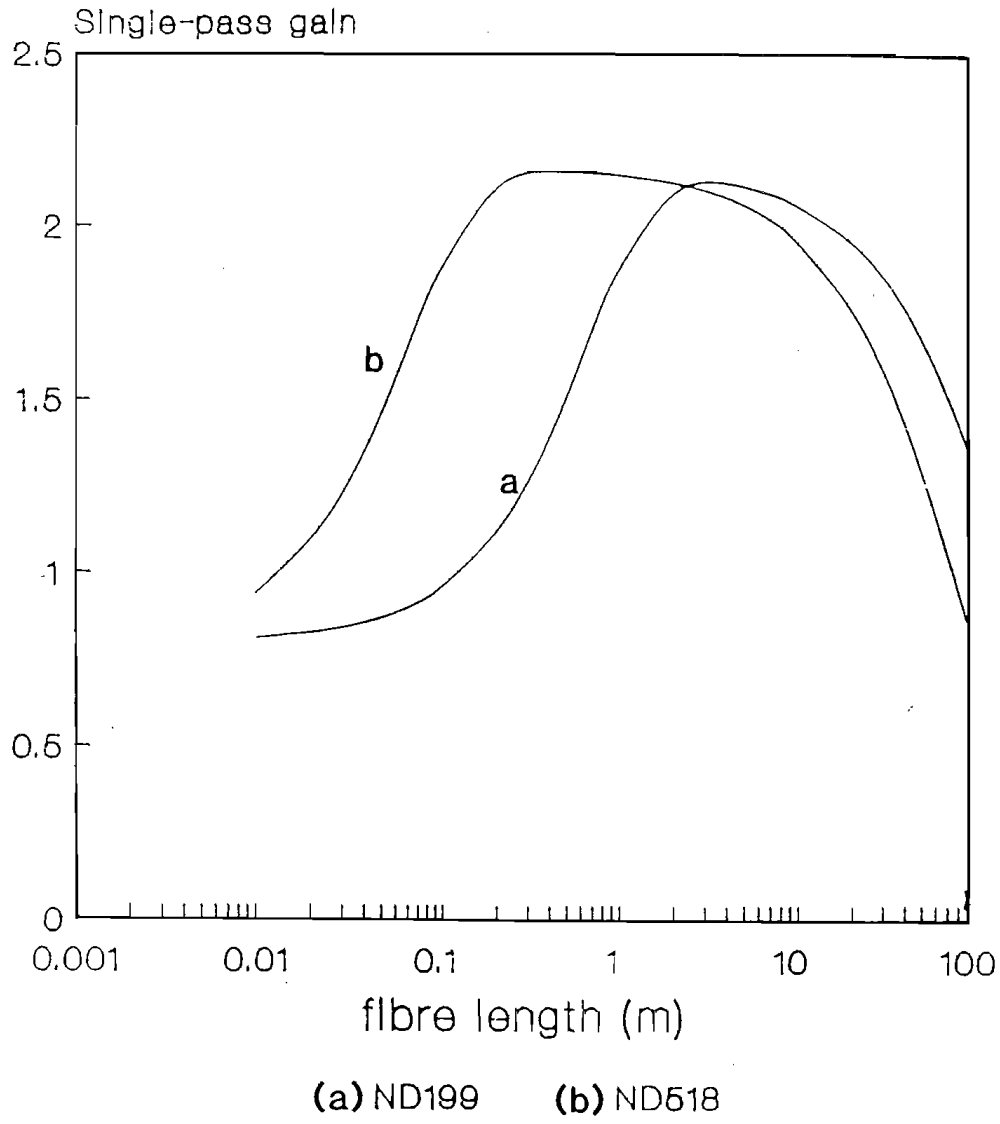

Fig.7.11 Single-pass gain as a function of fibre length for two Nd^{3+}-doped fibre samples.

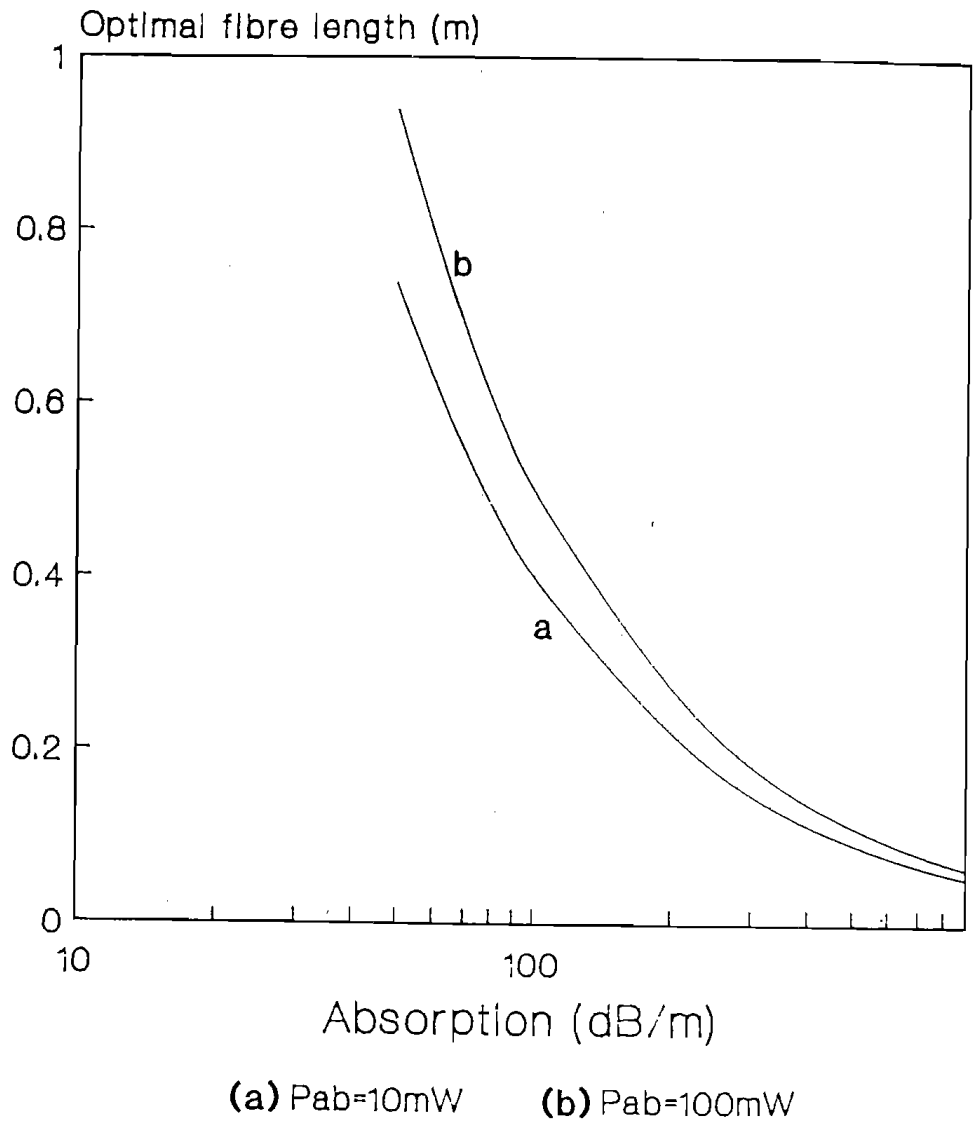

Fig.7.12 Optimal fibre length as a function of absorbed pump power for two different pumping levels. (b) Absorption region: γ=10~900dB/m.

$$-\ln R_2 = 2KP_{th} - L \qquad (7.24)$$

Using two or more different output mirrors and measuring the threshold absorbed pump power for each mirror, a curve of P_{th} versus $-\ln R_2$ can be plotted. K and L can thus be deduced from the slope and the intercept of the curve.

Fig.7.13 shows such a measurements for a laser-diode pumped Nd^{3+}-doped fibre laser (fibre sample: ND518). K=0.10/mW and L=0.056 were deduced from the experimental data.

Since P(o) is related to the total absorbed pump power, namely $P_{ab}=P(o)l_e$, where l_e is the effective fibre length, P(o) can then be obtained via measuring P_{ab}.

(7) Consideration of normalized separation D

In principle, the interaction strength can be adjusted by either D or l, the interaction length, and thus arbitrary separation can be applied. However, too small a separation may cause difficulty in controlling a very short interaction length. For example, for a LD-pumped Nd^{3+}-doped fibre laser, with K=0.1/mW and L=0.05, it is determined that $L_y \geq 0.25$. This is a rather small additional loss compared to an ordinary fibre polariser as seen from Fig.7.8 and 7.10. If a design similar to an ordinary polariser is taken, where the normalized separation D=1.5~2.0 is commonly used[7], only a few millimetres of metal/clad sector is needed, as shown by the first SPSM fibre laser. Such a short interaction length causes difficulty in the control of either the injected metal or the cutting back of the fibre. Therefore, a weak interaction structure is recommended for the integral fibre polariser. In practice, a separation of D=3.0~4.0, with which the corresponding interaction length is a few centimetres, is found feasible for SPSM fibre laser design.

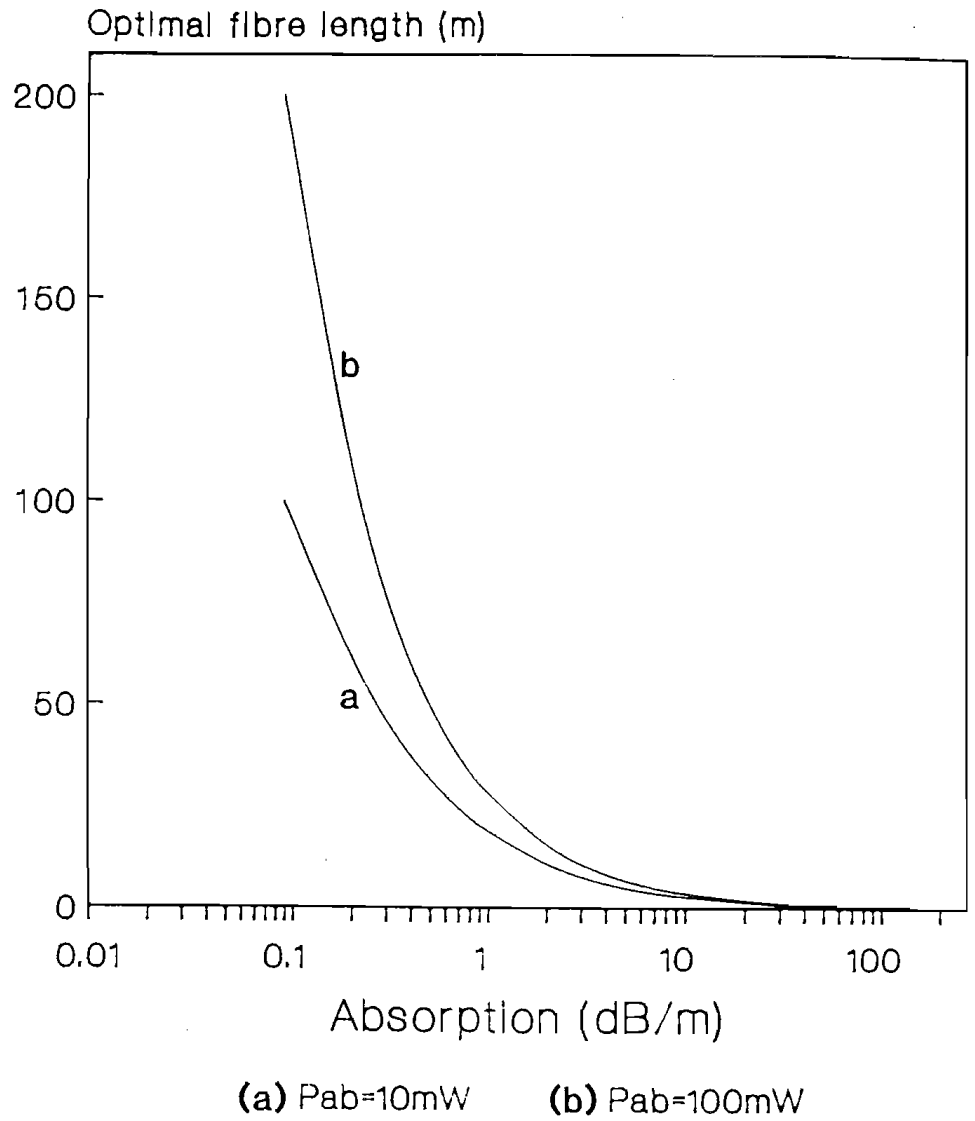

Fig.7.12 Optimal fibre length as a function of absorbed pump power for two different pumping levels. (a) Absorption region: γ=0.01~100 dB/m.

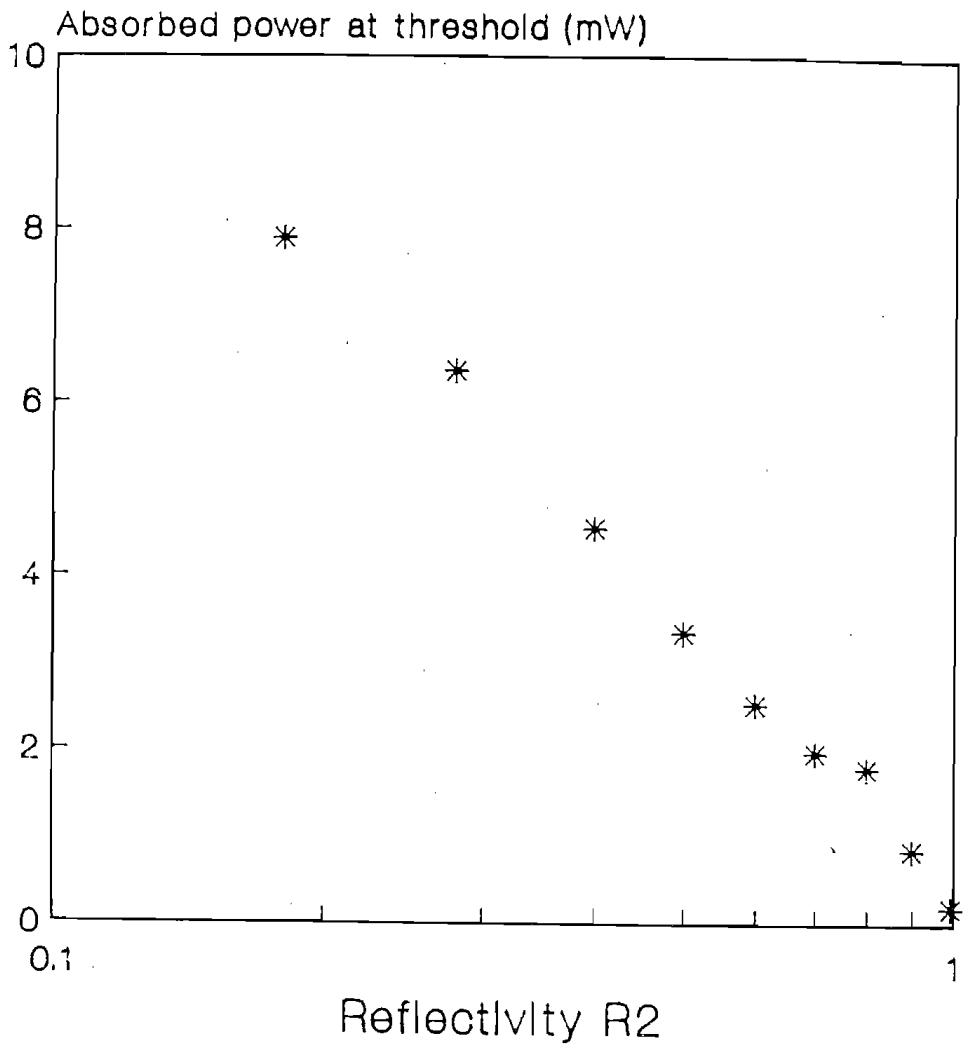

Fig.7.13 Measurements of cavity parameters: absorbed pump power at threshold as a function of output mirror reflectivity for a Nd^{3+}-doped fibre laser.

(8) Theoretical prediction

With K, L, P_{ab} (or P(o)) being known, the characteristics of a SPSM fibre laser, including the output power and the polarisation extinction ratio, can be predicted by utilizing the established theory.

The CW output power from a SPSM fibre laser is predominantly determined by the operating polarisation mode. Considering the concept of polarisation efficiency, $\eta_{sp}P_{ab}$ must be used to replace P_{ab} in eq.(5.18). In addition, the cavity loss for the x-mode becomes $(L+L_x)$ where $L_x=L_y/r$ is the insertion loss to the x-mode. The formula for the output power from a SPSM fibre laser is then

$$P_{sp} = \eta\ (\eta_{sp}P_{ab}-P_{thsp}) \qquad (7.25a)$$

$$P_{thsp} = (L+L_x-\ln R_2)\ /\ 2K \qquad (7.25b)$$

where $\eta=\eta_1\eta_5$, as shown in eq.(5.19), is the slope efficiency of the ordinary fibre laser without an integral polariser, whereas P_{thsp} is the threshold power required for SPSM fibre laser.

Since a high attenuation ratio $r\geq 60$ can be provided by the integral polariser, the insertion loss induced to the operating mode is eventually rather small. For example, if the required additional loss for the y-mode $L_y=0.25$, L_x is only 0.004 (or 0.017dB) compared with L=0.05 for the intrinsic cavity loss and $-\ln R_2=0.22$ if $R_2=80\%$. This means that the threshold power required for a SPSM fibre laser is only 1.5% greater than the corresponding ordinary fibre laser. In the meantime, high η_{sp}, namely 97% for Nd^{3+}- or 95% for Er^{3+}-doped fibre lasers, may be achieved when the SPSM fibre laser operating with perfect polarisation alignment. The slope efficiency for SPSM laser η is now written as

$$\eta = \eta_1\eta_5\eta_{sp} \qquad (7.26)$$

and is only slightly decreased compared with a non-polarisation resolved fibre laser. It is thus predicted

that the output power from SPSM fibre lasers can reach the same level of the ordinary fibre lasers.

In order to analyse the polarisation extinction ratio of the output from SPSM fibre lasers, the superfluorescence of the unwanted mode, the y-mode is derived and written as

$$P_{yout} = \eta_1 P^y (1-R_2) \exp(KP^y - L - L_y) \tag{7.27}$$

$$P^y = (1-\eta_{sp}) P_{ab} \tag{7.28}$$

where the factor $\eta_1 P^y$ represents the fluorescence power of the y-mode, $(1-R_2)$ reflects the output coupling, and the exponential expression describes the build up superfluorescence. In eq.(7.27) it has been supposed that the average amplifying length for a spontaneously emitted photon is equal to the effective cavity length l_e. The polarisation extinction ratio of the output power from SPSM fibre lasers can now be defined as

$$EXT = 10 \log\left(\frac{P_{sp}}{P_{yout}}\right) \tag{7.29}$$

(9) An example of numerical calculation

Using eq.(7.29) together with eqs.(7.24), (7.25), (7.26), (7.27) (7.28) and (6.12), numerical calculations can be carried out for predicting the performance of SPSM fibre lasers. The particular example shown below is a LD-pumped Nd^{3+}-doped fibre laser. K=0.1/mW, L=0.05, η_1=20% and r=60 are supposed according to the corresponding measurements. Fig.7.14 shows the polarisation extinction ratios as a function of pump power for two different L_y. Fig.7.15 shows the output power as a function of L_y. As expected, the extinction ratio increases with a increased L_y at the expense of a slight decrease in output power. Fig.7.16 shows both output power and extinction ratio of SPSM laser as a function of R_2, the reflectivity of output mirror. It can be seen that the optimum R_2 for a maximum CW output power is found to be around 80%.

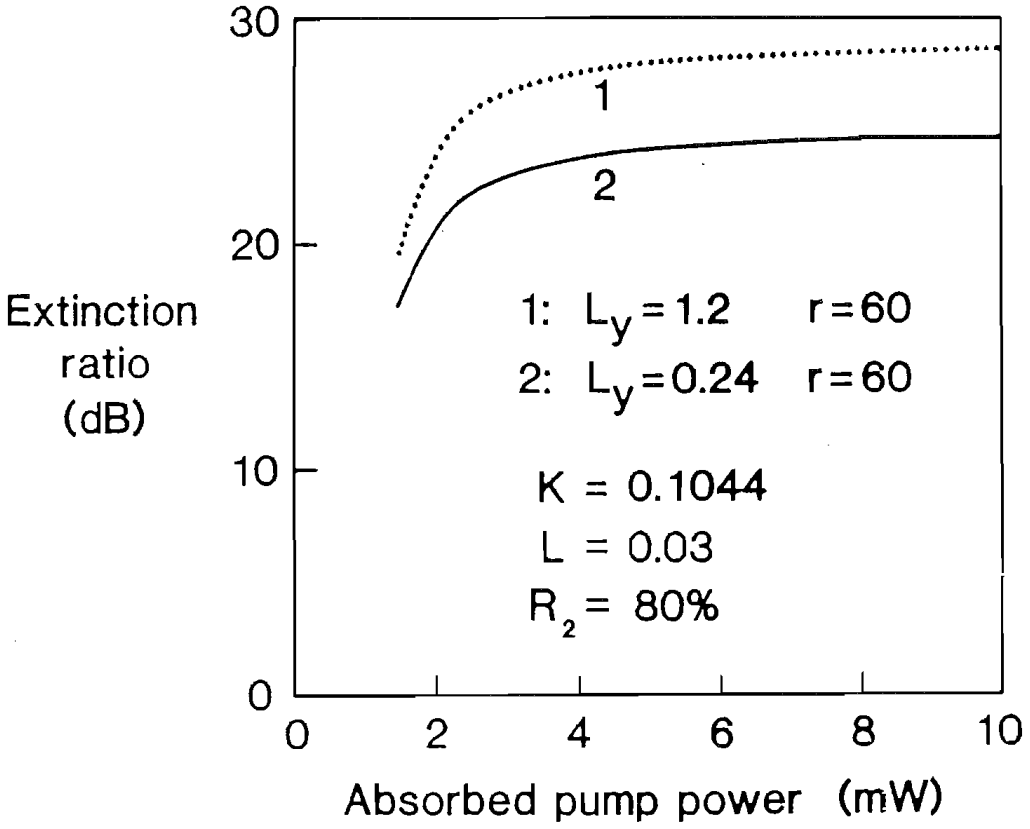

Fig.7.14 Theoretical curves of extinction ratio as a function of absorbed pump power for two sets of integral polariser parameters.

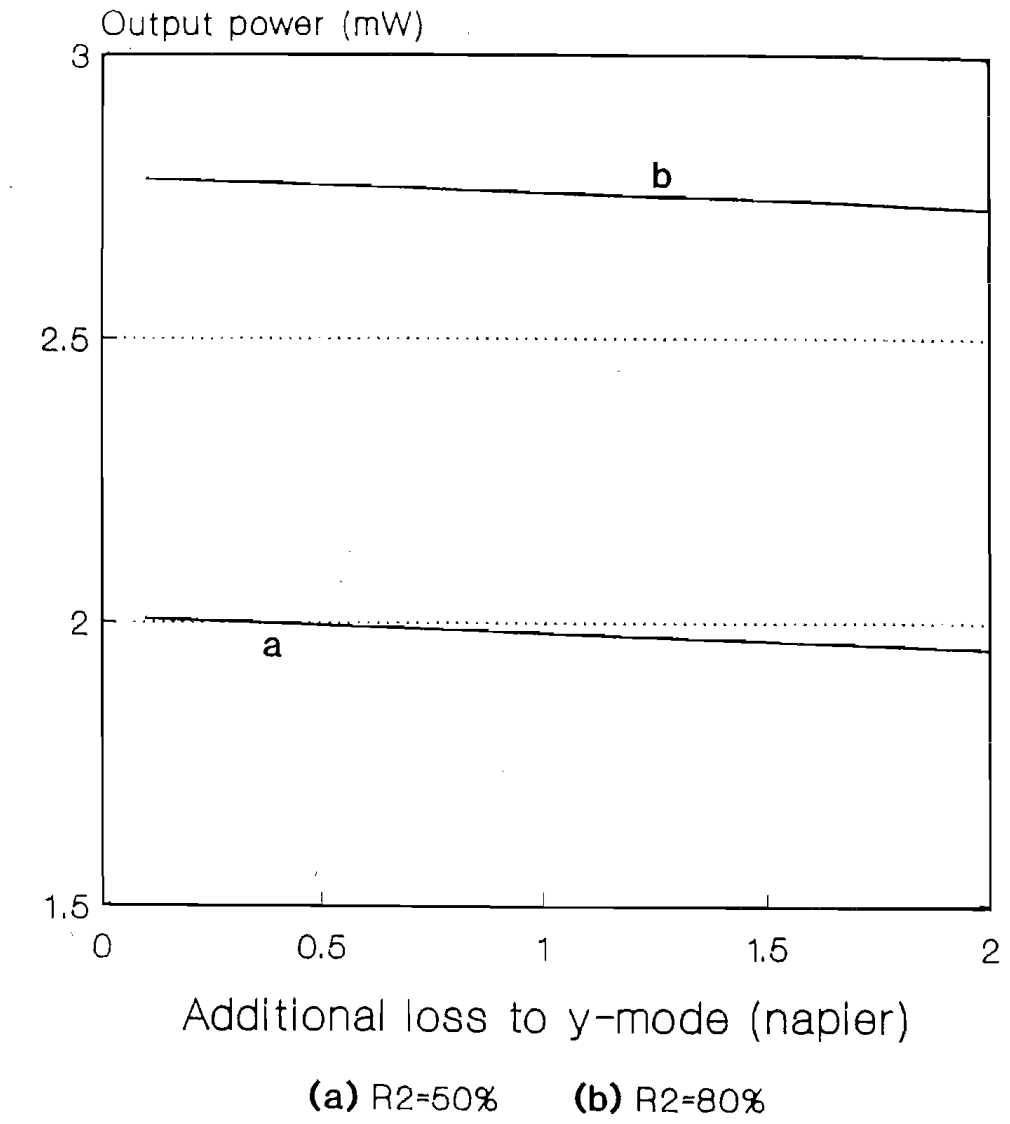

Fig.7.15 Output power of a SPSM fibre laser as a function of additional loss to the y-mode for two different reflectivities of the output mirror.

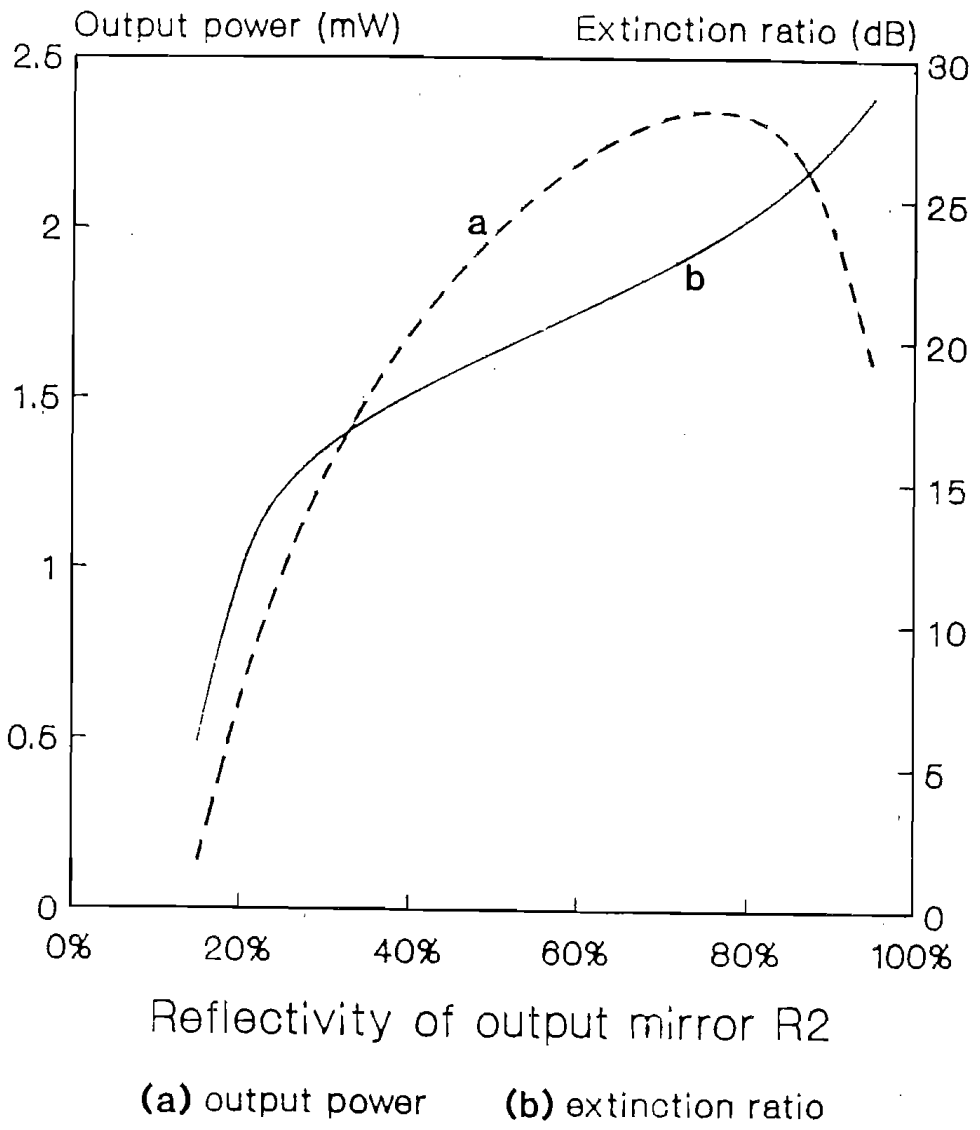

Fig.7.16 Theoretical curves of extinction ratio and output power for LD-pumped Nd^{3+}-doped fibre laser as a function of the reflectivity of the output mirror.

7.5 Experimental Results

The integral metal/clad fibre polariser creates a strong differential mode attenuation which significantly increases the difference between the operating and unwanted mode thresholds and makes the single-polarisation fibre laser operate even up to the maximum available pump power.

A variety of Nd^{3+}-doped and Er^{3+}-doped single-polarisation fibre lasers, with various pump sources, have been constructed at the laboratory research level. Some typical experimental results achieved for CW fibre lasers using three different types of integral fibre polarisers are summarised in Table 7.1. It can be seen that the extinction ratio obtained, namely 35.4dB for a CW fibre laser, is much better than that of the commercial laser diode, 20dB, as shown in Fig.1.7.

Experimentally, it was found that incorporating the metal at the output end of the fibre laser is more efficient than at the input end, since the metal at the output end attenuates the undesired fluorescence of the secondary mode, without attenuating the pump. This is in agreement with the theoretical analysis.

The ideal cross-sectional shape is such that the major axis of the elliptical core is perpendicular to the metal surface. Misalignment of the normal line with the birefringent axis will decrease the extinction ratio, which is believed as the reason for the lower observed extinction ratio of the Twin-hole, Er^{3+}-doped, fibre laser as shown in Fig.7.2 and Table 7.1.

LD-pumped SPSM fibre lasers are also listed in the Table 7.1. As this is a research area of considerable interests, the detailed discussion is presented separately in the following section.

7.6 LD-pumped SPSM fibre lasers

Semiconductor laser pumping is highly convenient

	D-SHAPED		TWIN-HOLE	METAL-PLATED
POLARISER				
metal type	Ga	Ga	Ga	Al
D (d/a)	2.0	3.8	2.5	3.0
metal length	2mm	35mm	7mm	15mm
CAVITY				
fibre sample	ND208	ND425	ND263	ND518
dopant	Nd^{3+}	Nd^{3+}	Er^{3+}	Nd^{3+}
fibre length	20m	2m	1.4m	26cm
R_2	35%	50%	80%	80%
PUMP				
type	Ar^{+}-ion	LD	DCM Dye	LD
wavelength	515nm	825nm	650nm	825nm
P_{ab}	500mW	10mW	50mW	10mW
SPSM LASER				
(CW)				
output power	20mW	2.1mW	1.2mW	3.0mW
extinc.ratio	35.4dB	23dB	22dB	25dB
wavelength	1086nm	1088nm	1536nm	1080nm
(Q-switched)				
pulse width		150ns		
peak power		3.9W		
repetition		1000Hz		
extinc.ratio		29dB		

Table 7.1 Typical results of SPSM fibre lasers using the integral fibre polariser technique.

both in terms of cost and operational requirements and will lead to the first practical fibre laser device. A prototype module of such a device made at York Technology in collaboration with the University is extremely compact. It measures only 20cm in length and 10cm in width and weighs only 500g[16]. In addition, this kind of laser with a single-element resonator structure should help provide long-term maintenance-free operation.

(1) The original experiment with a LD-pumped fibre laser

As a part of this study, the original experiment of LD-pumped fibre laser was reported in 1986[17]. The CW experimental arrangement is shown in Fig.1.1. The fibre sample, ND199, had the following characteristics: 3.5μm core diameter, NA of 0.21, length 3.2m and a total absorption at the pump wavelength of 97% (with a 300ppm Nd^{3+} content). The loss at the lasing wavelength was negligible (<10dB/km). The fibre ends were cleaved and butted to dielectric mirrors. The input mirror had a high transmission (T=85%) at the pump wavelength and a high reflectivity (R=99.8%) at the lasing wavelength. The output mirror transmission was approximately 65%, the best available at that time.

The pump source was a single-mode GaAlAs laser (Hitachi HLP 1400), the light being launched into the fibre by microscope objectives with an efficiency of approximately 25%. The output power was measured using a InGaAs detector and the lasing characteristic is shown in Fig.7.17. The threshold for lasing action was 2.6mW absorbed with a slope efficiency of 33%, indicating that these devices are very efficient sources. There was no evidence of saturation at the highest pump power available (5.6mW absorbed).

In order to allow modulation of the cavity finesse by an acousto-optic deflector it was necessary to expand the intra-cavity beam using the experimental arrangement shown in Fig.3.1(b). Due to the intra-cavity components

this configuration was more lossy, yet the CW threshold was only slightly higher at 3.7mW absorbed. The acousto-optic deflector was used in transmission mode, the high-Q state being achieved by electronically removing the applied RF with 2μs duration pulses. The output mirror in this configuration had a transmission at the lasing wavelength of 12%. A typical Q-switched pulse is shown in Fig.7.18 for an absorbed pump power of 5.6mW. The pulse repetition rate was variable between single-shot and 4kHz with no change in peak output power or pulse duration. The gain of the laser was such that, even when the acousto-optic deflector switched the cavity into its low-Q (i.e. "off") state, some background CW laser action was observed at a threshold of 5mW absorbed. This limited the peak output power attainable with this configuration.

Inserting a mechanical chopper having a mark:space ratio of 1:300 into the cavity provided an alternative method of Q-switching and prevented any laser action in the low-Q state. With an output mirror having a transmission of 65% at the lasing wavelength, output pulses of peak power greater than 300mW and FWHM of 500ns at a repetition rate of 400Hz were then obtained.

(2) LD-pumped SPSM fibre lasers

A fibre with an integral D-section hole adjacent to the core was fabricated by milling a Nd^{3+}-doped, fibre preform to within a short distance of the core. It was then sleeved and pulled into a single-mode fibre of 125μm diameter (see Fig.7.1). The separation between the core and the exposed surface is approximately 5.6μm. Due to the fabrication procedure, the core exhibited a slight ellipticity with 4.3μm and 3.1μm being the major and minor axes respectively. The numerical aperture (NA) of the fibre is 0.2 corresponding to a cutoff wavelength of 960nm. The fibre has a Nd^{3+}-ion concentration of 500ppm, and the laser length was 2m.

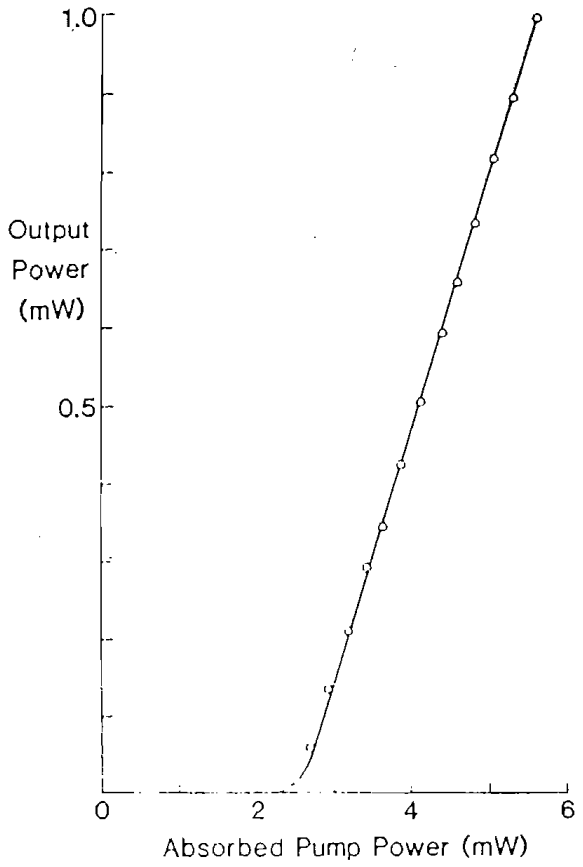

Fig.7.17 Lasing characteristic of the efficient LD-pumped fibre laser.

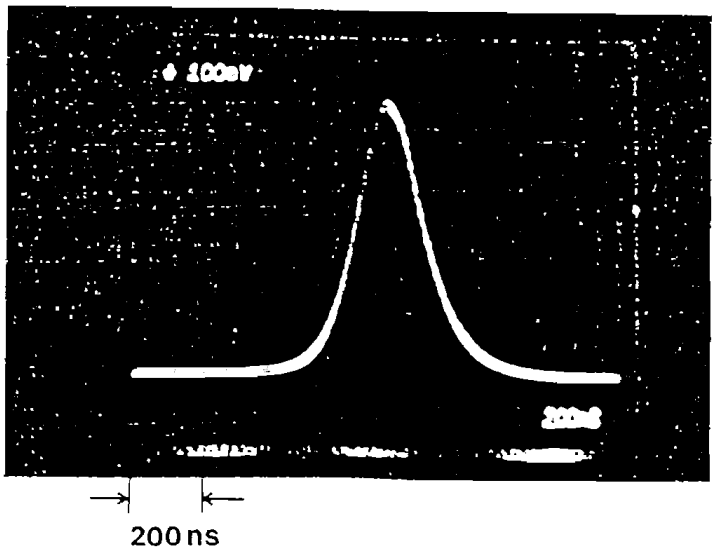

Fig.7.18 A typical Q-switched pulse from a LD-pumped fibre laser.

The pump source was a GaAlAs laser diode (Sony 202/V) operating at 825nm. A $\lambda/2$ retardation plate was used to rotate the polarisation orientation of the linearly-polarised pump light. The input mirror had a transmission at the pump wavelength of 85% and 99% reflectivity at the lasing wavelength of 1.09μm, while the output mirrors had 50% transmission. The output from the fibre laser was filtered and passed through a polarisation analyser having an extinction ratio of 50dB. In order to allow modulation of the cavity finesse by an acousto-optic deflector, the intracavity beam was expanded using a low-loss lens.

By filling the output end of the D-section with a 35mm length of gallium to form the integral fibre polariser, oscillation of the undesirable polarisation mode perpendicular to the metal surface was found to be totally suppressed, and the laser then oscillated in single-polarisation mode parallel to the metal surface. Since the suppressed mode only contributes fluorescence to the laser output, an extinction ratio of 23dB was achieved. An output power of 2.1mW was obtained for 9mW of pump power absorbed. This is comparable with conventional fibre lasers pumped by laser diodes[17,18]. This illustrates the low insertion loss of the integral polariser, which was estimated to be 0.04dB. Fig.7.19 shows the lasing characteristics of the CW SPSM fibre laser.

By inserting a mechanical chopper with a mark-to-space ratio of 1:180 into the cavity, a polarisation extinction ratio as high as 39.5dB was measured for a Q-switched pulse at a repetition rate of 100Hz. This significant increase in polarisation extinction ratio is due to the fact that the undesirable polarisation eigenmode only contributes fluorescence to the background of the Q-switched pulse when its lasing action is suppressed by the integral polariser.

More efficient Q-switched operation can be achieved by using an acoustic-optic deflector (AOD) in the laser

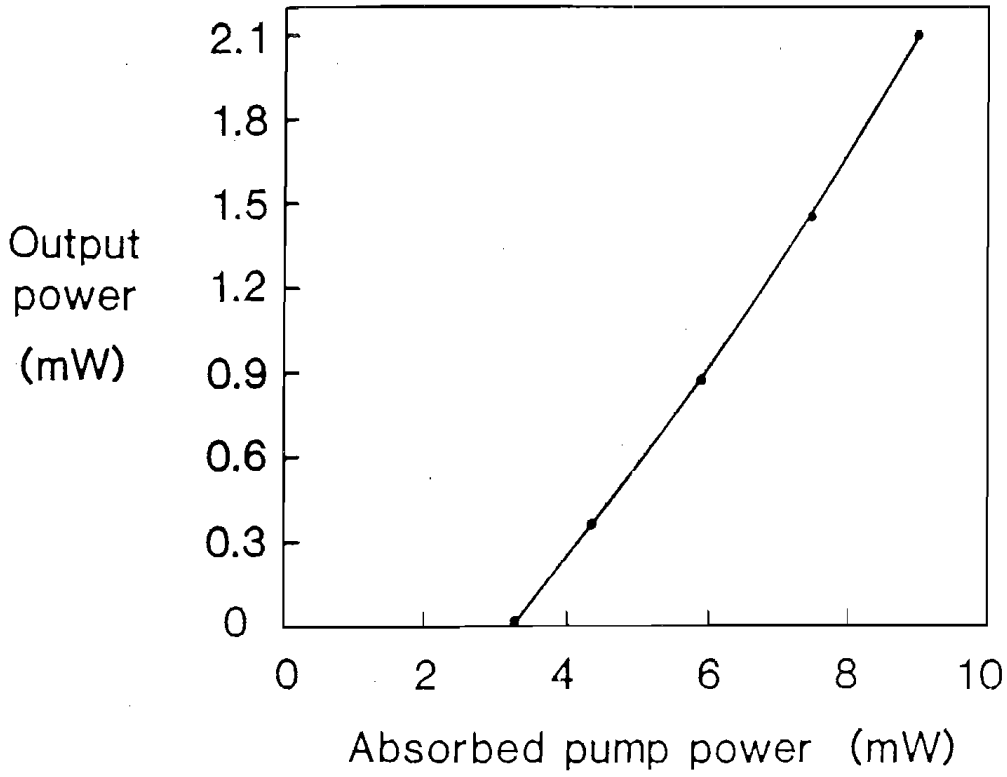

Fig.7.19 Lasing characteristics of a LD-pumped SPSM Nd^{3+}-doped fibre laser.
Fibre sample: ND490.

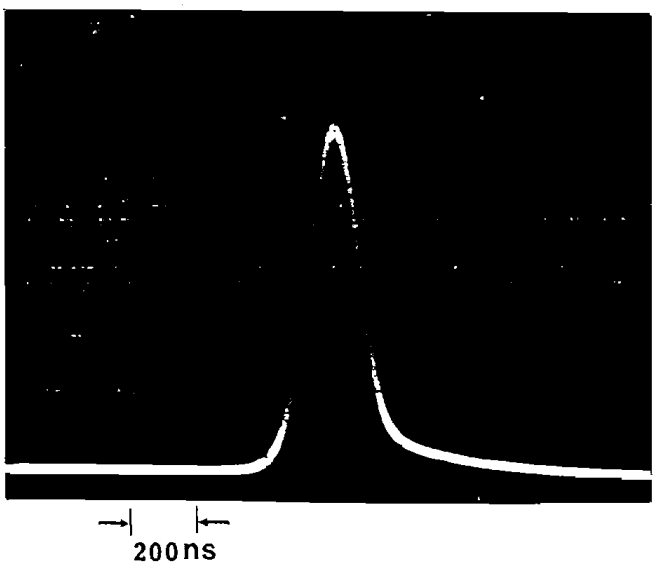

Fig.7.20 Single-polarisation Q-switched pulse of a LD-pumped Nd^{3+}-doped fibre laser with a polarisation extinction ratio of 29.3dB for a peak power of 3.9W.

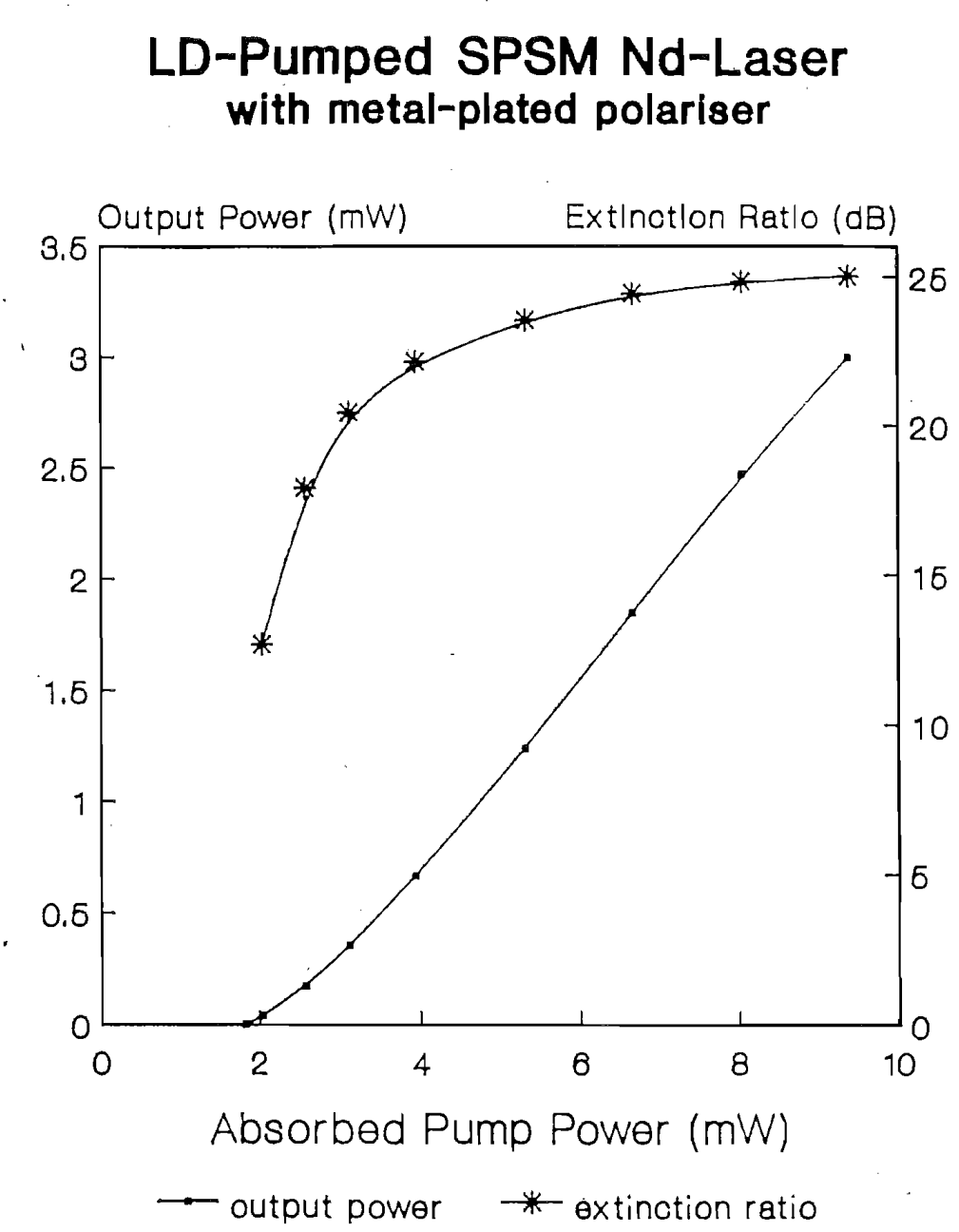

Fig,7.21 CW lasing characteristics of a LD-pumped SPSM Nd^{3+}-doped fibre laser with a high dopant concentration.
Fibre sample: ND518.

cavity. With a commercially-available modulator (Intraction AOM-40R), a polarisation extinction ratio of 29.3dB for a peak power of 3.9W with 1kHz repetition rate and 150ns pulse width was obtained at the same level of the pump power as for CW operation. A typical Q-switched pulse is shown in Fig.7.20.

Several other LD-pumped SPSM fibre lasers have also been constructed using different types of integral fibre polariser. By using a highly-doped fibre sample, ND518, with a Nd^{3+} dopant concentration of 4500ppm, a SPSM fibre laser with a short cavity of 26cm was formed. The main laser parameters are listed in the right-hand column of Table 7.1. The polished and then Al-plated part, the integral polariser, was in the middle of the cavity, which was kept straight and the polarisation aligned. The lasing characteristics of the laser are shown in Fig.7.21. A CW output power of 3mW, a 25dB extinction ratio and 37% slope efficiency have been obtained. The extinction ratio measured demonstrates an increasing function of the pump power, in a good agreement with the theory shown in Fig.7.14.

In summary, the performance of LD-pumped SPSM fibre lasers has shown very considerable promise for making a practical laser source. The technique employs an integral fibre polariser, which has the advantages of low insertion loss, high extinction ratio and compatibility with existing single-mode fibre components.

References to Chapter 7

[1] M. Born and E. Wolf: "Principles of Optics", Pergamon, London, 1970.

[2] M.P. Varnham, D.N. Payne, A.J. Barlow and E.T. Tarbox: "Coiled-birefringent-fibre polarisers", Opt. Lett., 9, pp.306-308, 1984.

[3] F.De. Fornel, M.P. Varnham and D.N. Payne: "Finite cladding effects in highly-birefringent fibre

taping-polarisers", Electron. Lett., 20, pp.398-399, 1984.

[4] W. Eickhoff: "In-line fibre-optic polariser", Electron. Lett. 16, pp.762-764, 1980.

[5] R.A. Bergh, H.C. Lefevre and H.J. Shaw: "Single-mode fibre-optic polariser", Opt. Lett., 5, pp.479-481, 1980.

[6] T. Hosaka, K.Okamato and T. Edahiro: "Fabrication of single-mode fibre-type polariser", Opt. Lett., 8, pp.124-126, 1983.

[7] L. Li, R.D. Birch and D.N. Payne: "High performance composite metal/glass fibre polarisers", 12th ECOC, Barcelona, Spain, Sep. 1986.

[8] C.D. Hussey and J.D. Minelly: "Optical fibre polishing with a motor driven polishing wheel", Electron. Lett., 24, pp.805-807, 1988.

[9] S.B. Poole, D.N. Payne and M.E. Fermann: "Fabrication of low-loss optical fibres containing rare-earth ions", Electron. Lett., 21, pp.737-738, 1985.

[10] J.E. Townsend, S.B. Poole and D.N. Payne: "Solution-doping technique for fabrication of rare-earth-doped optical fibres", Electron.Lett., 23, pp.329-331, 1987.

[11] Y. Yamamoto, T. Kamiya and H. Yanai: "Characteristics of optical guided modes in multilayer metal-clad planar optical optical guide with low-index dielectric buffer layer", IEEE J. Quant. Elect., QE-11, pp.729-736, 1975.

[12] A. Reisinger: "Characteristics of optical guided modes in lossy waveguides", Appl. Opt., 12, pp.1015-1025, 1973.

[13] C. Vassallo: "Rigorous theory for modes of optical fibres with cladding limited by a plane", Electron. Lett., 22, pp.944-945, 1986.

[14] L. Li: "Novel optical fibre and their applications", Thesis submitted for ph.D., University of Southampton, 1989.

[15] W.M. Henry: "Theoretical study of single-mode fibre tapers and metal-clad fibre polarisers", ph. D. thesis, University of Camberra, 1988.

[16] L. Reekie: Private communication.

[17] I.M. Jauncey, J.T. Lin, L. Reekie and R.J. Mears: "An efficient diode-pumped CW and Q-switched single-mode fibre laser", Electron. Lett., 22, pp.198-199, 1986.

[18] L. Reekie I.M. Jauncey and D.N. Payne: "Near optimum operation of a diode-laser pumped fibre laser", Proc. 13th ECOC, Helsinki, pp.105-108, 1987.

Chapter Eight

POLARISATION MODE COMPETITION IN FIBRE LASERS

8.1 Introduction

As analysed in Chapter 3, the lasing characteristic of a fibre laser is related to the probability for ions to contribute a transition to a certain polarisation eigenmode. In fact, both the x- and y-mode are always "trying" to stimulate the inverted population to build-up their own lasing oscillation. Thus polarisation mode competition inevitably exists in a fibre laser.

Polarisation mode competition is a result from the fact that both polarisation modes are shearing the same laser medium, i.e. the rear-earth doped fibre. From this perspective, the polarisation effects in fibre lasers can be understood better and more comprehensively. On one hand, the established orthogonal polarisation modes are phase-independent of each other; on the other hand, they compete with each other within the sheared population inversion.

The CW operation of an ordinary fibre laser is an equilibrium state of this competition, and can be analysed by the theoretical model of effective absorbed pump power. However, pulsed operation, as a transient process, breaks the equilibrium of polarisation mode competition. Since the probability per unit time for an ion to contribute a transition to a certain polarisation eigenmode is proportional to both the cross-section and intensity of the stimulating field, one established operating polarisation mode will deplete the majority of the inverted population, and win the polarisation mode competition.

The experimental set-up for investigating the polarisation competition is shown in Fig.8.1. Two detectors were located after the polarised beamsplitter to detect the x and y modes simultaneously. The detected signals of the two channels were displayed on an

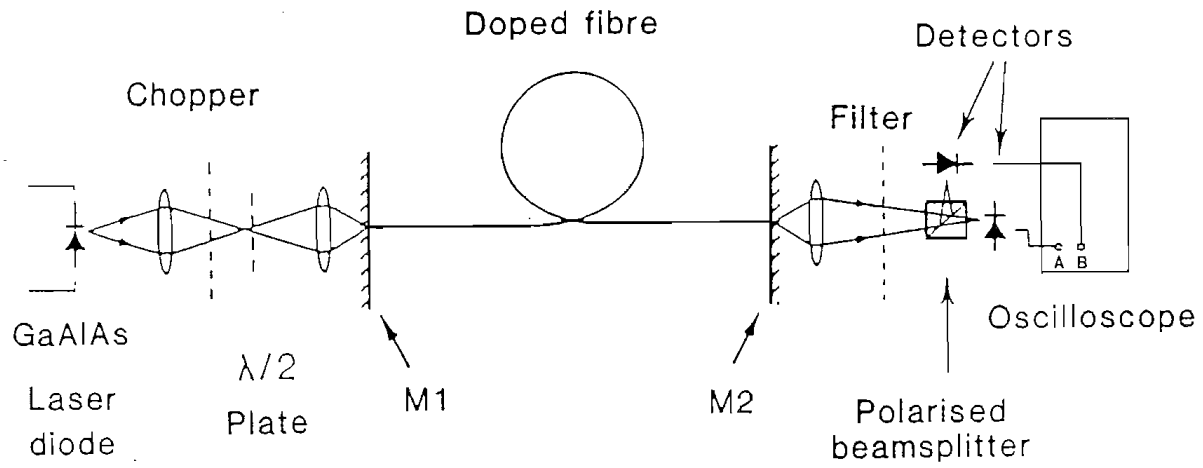

Fig.8.1 Experimental set-up for observing polarisation hole burning in fibre lasers.

oscilloscope for observation of the polarisation competitionin the time domain. An optical spectrum analyser will be employed to replace the oscilloscope when the spectral polarisation competition is studied.

8.2 Polarisation Competition in the Time Domain

(1) CW operation

Fig.8.2 shows how the relaxation oscillations of the y-mode extract the population inversion from the CW oscillation of the x-mode. The basic physical mechanism of relaxation oscillations in lasers consists of an interplay between the field intensity in the resonator and the population inversion. An increase in the field intensity causes a reduction in the inversion due to the increased rate of stimulated transitions. This causes a reduction in the gain which in turn tends to decrease the field intensity. The pictures in Fig.8.2 were taken with an Er^{3+}-doped fibre laser (fibre sample: ND501) pumped by a DCM dye laser operating at 650nm. The pumping orientation was chosen at α=0, i.e. on the x-axis, so that the difference in the build-up times between the y-mode and x-mode is sufficient to let the relaxation oscillation of the y-mode start after the x-mode has reached CW operation stage. It can clearly be seen that there are four steps to the fibre laser reaching stationary CW operation, i.e. an equilibrium in the polarisation mode competition. First, the x-mode starts to lase as a result of higher effective pump power than the y-mode, characterised by the initial pulse train of relaxation oscillations. Secondly, CW operation of the x-mode becomes established, which is a single-polarisation operation accompanied by the superfluorescence of the y-mode. Thirdly, the y-mode begins to lase with a relaxation oscillation of lower frequency than the x-mode. During its pulse period the y-mode wins the mode competition and extracts the population inversion from those ions which contributed transitions to the x-mode.

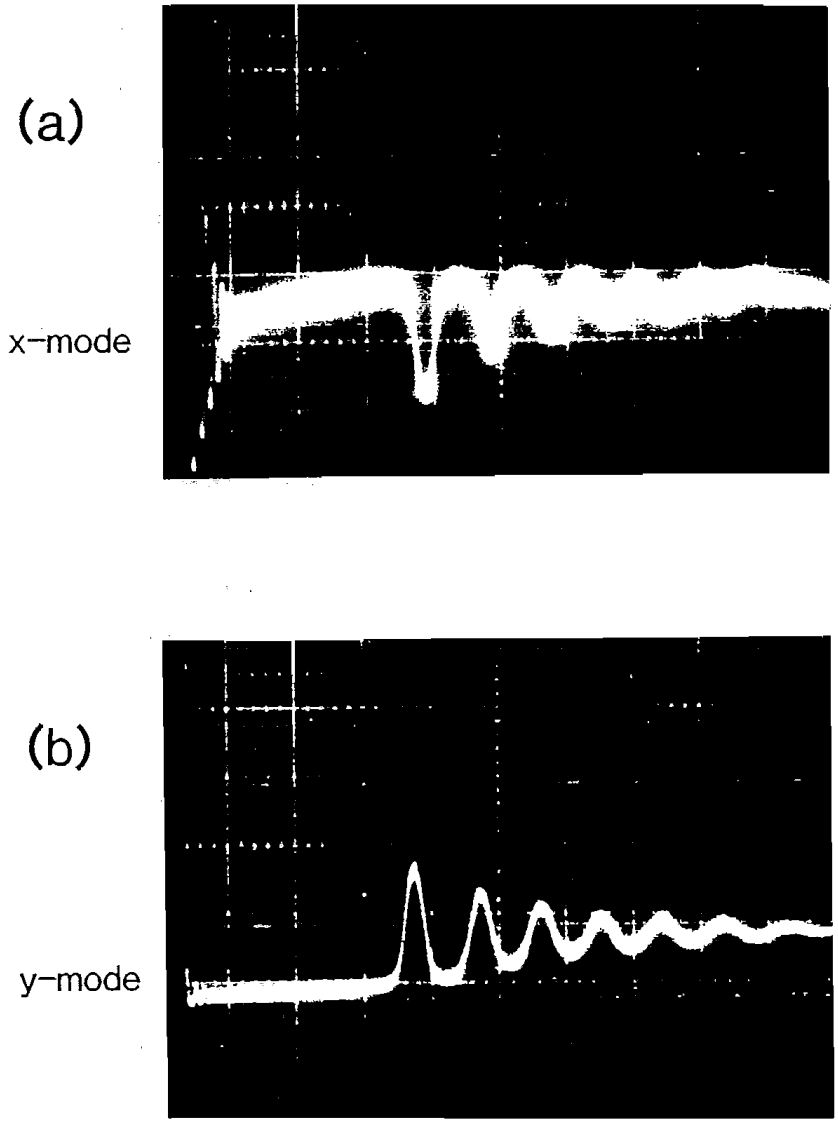

Fig.8.2 Polarisation-resolved relaxation oscilations showing polarisation mode competition in the time domain.

This makes "holes" in the time domain for the x-mode. Finally, the y-mode reaches CW operation, and the polarisation mode competition between the x and y modes reaches stationary equilibrium.

It is worth noting that the equality of the increased intensity of the y-mode compared to the reduction in intensity of the CW x-mode indicates a very high polarisation efficiency of the single-polarisation operation, as expected by the theory in Chapter 6.

The polarisation competition in the time domain can also be distinguished even in the case that the y-mode starts its lasing action during the relaxation oscillation stage of the x-mode. This is seen from Fig.5.8 with a Nd^{3+}-doped fibre laser.

Mode competition has also been observed in ring-cavity fibre lasers[1], and will be described elsewhere.

(2) Push-Pull relaxation oscillation

When the launching orientation of the pump polarisation is near to 45°, the polarisation mode competition makes the polarisation hole-burning a "push-pull" procedure. This phenomenon has been observed with a LD-pumped Nd^{3+}-doped fibre laser (fibre sample: ND199), and is shown in Fig.8.3. It can be seen that the polarisation-resolved relaxation oscillations of each mode no longer show a damped sinusoidal waveform. In contrast, "holes" appear in the series of relaxation oscillation peaks. The first few peaks of the x mode relaxation oscillation coincide with the troughs of the y mode relaxation oscillation. Fig.8.3(a) corresponds to pump launching at α=37° and shows that the first peak of the relaxation belongs to the x mode (upper trace), while Fig.8.3(b) shows that the first peak has been switched to the y mode (lower trace) when the launching orientation α=53°.

The push-pull phenomenon shows that after a stimulated pulse of a certain polarisation component, the other polarisation component will have greater population

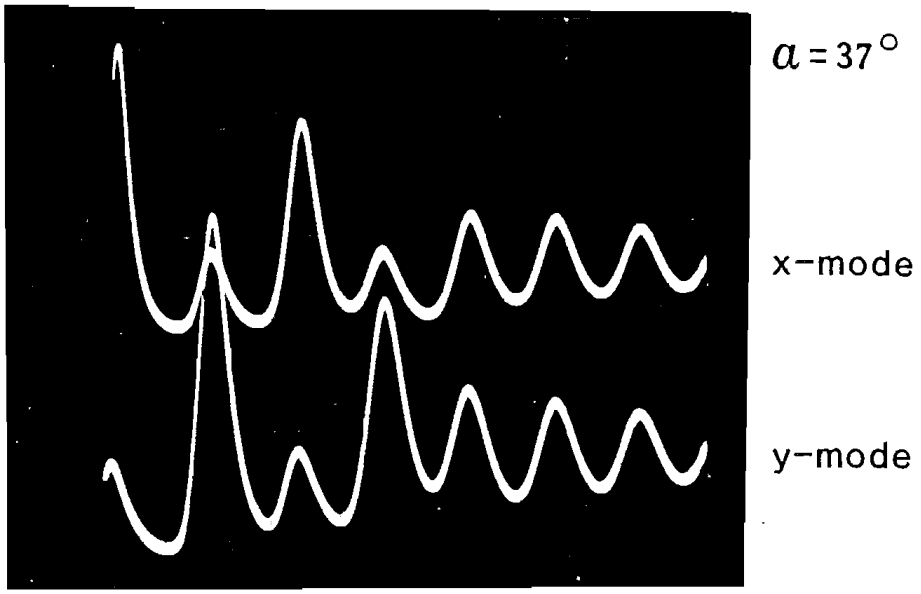

(a)

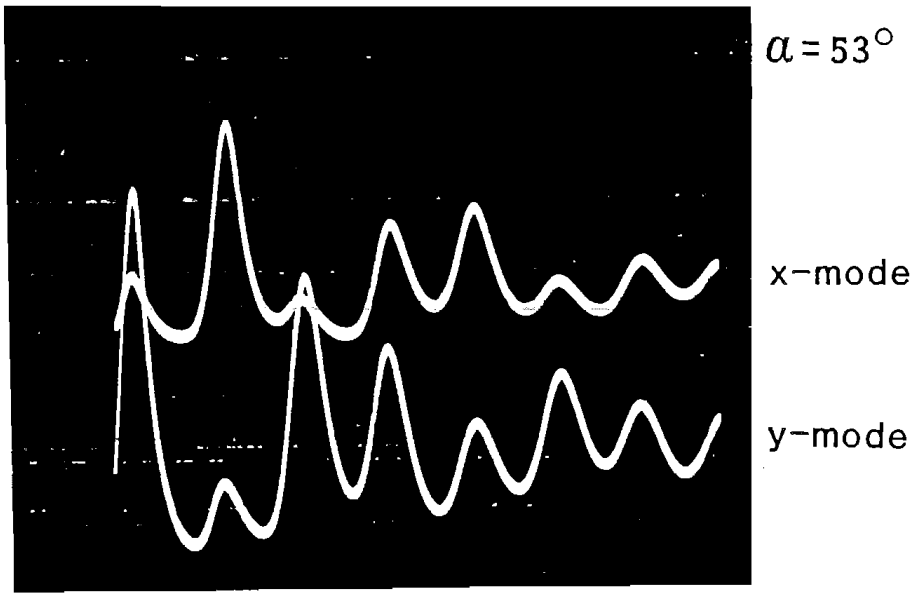

(b)

Fig.8.3 Polarisation-resolved relaxation oscillations showing "push-pull" patterns.

inversion. Moreover, it also indicates that a higher intensity of the stimulating field can extract more inverted population and then suppress the lasing action of the other polarisation component during the pulse period.

(3) Influence on Q-switched operation

It is well known that slow Q-switched operation may cause a multiple-pulse train[2]. The mechanism can be described by Fig.8.4 schematically. As shown in Fig.8.4(a), a fast switching time of threshold, t_s, gives a short duration of the change from high loss to low loss of the cavity. The rapidly increased difference between the population inversion and the threshold related to the cavity loss leads to a short build-up time, t_b, as well as a strong pulse. Such a strong pulse depletes almost all the inverted population, so that no second pulse can be built-up within the switch time. In contrast, a slow Q-switch allows the second, or even more, pulses to be built up during the switching time.

The second pulse of Q-switched operation has been observed in fibre lasers. Experimentally, an investigation was made with a low repetition rate, Q-switched, Nd^{3+}-doped fibre laser. The schematic diagram of the experiment is similar to that shown in Fig.3.1. A mechanical chopper served as the intracavity Q-switch, and its chopping rate was varied from 0 to 400Hz with a mark-space ratio of 1:300. It was discovered that when the pump beam was launched on the x or y axis, the first peak of the Q-switched pulse is the corresponding polarisation component and the orthogonal polarisation component occurs at the second peak. This is a consequence of the push-pull phenomenon.

Both the time interval between these two pulses, and the ratio of the power in the first pulse to the second, increase with an increased repetition rate. Fig.8.5 shows a comparison between the two cases. Curve (a) was taken with a Q-switch repetition rate of 80Hz while

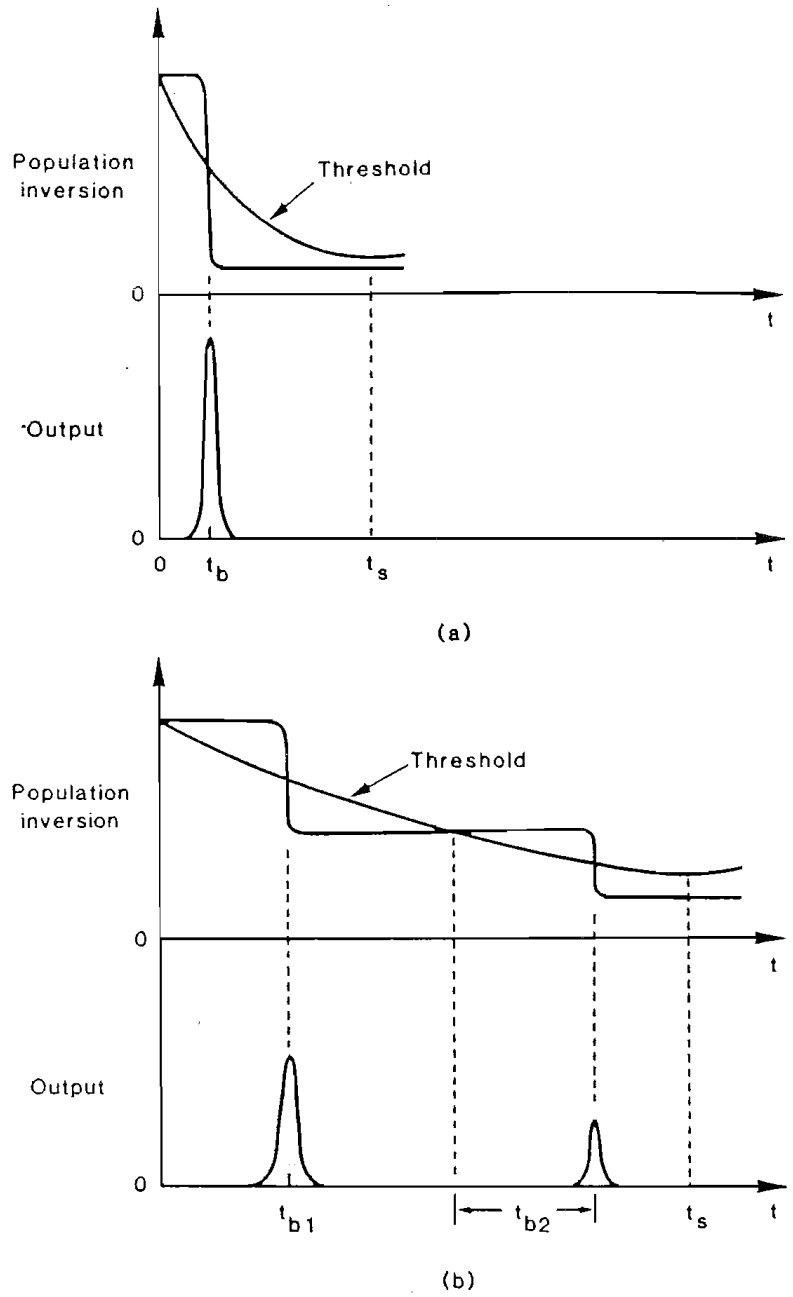

Fig.8.4 Schematic showing the mechanism of the pulse train for a slow Q-switched operation.

curve (b) was at 280Hz. The increase of both time interval and pulse power ratio can be seen clearly from the picture. In fact, a more powerful x-mode Q-switched pulse causes a significant increase of the threshold required for the y-mode pulse. This, together with the power ratio of the x mode Q-switched pulse to the y mode are shown in Fig.8.6, which was taken at 45° launching angle in order to limit the influence of differential effective pump power.

With a very slow Q-switch, a multiple-pulse train can be generated. Fig.8.7 shows such a multiple-pulse train, which was taken with 45° launching angle and a repetition rate of 80Hz. The time scale is 10μs per division. It can be seen that the first Q-switched pulse consists of two peaks, corresponding to the x and y modes respectively.

For many applications, the second pulse of Q-switched operation is undesirable and must be suppressed. This can be done by choosing a proper switching speed. Single-polarisation Q-switched operation can be realised by using a intracavity polariser as mentioned in Chapters 6 and 7.

8.3 Polarisation Competition in the Frequency Domain

Because of differences within the glass structure, the local fields at individual sites in rare-earth doped glasses vary in strength and symmetry. This results in site-to-site variation in the energy levels and the radiative and non-radiative transition probabilities of the laser ions. These cause the wide fluorescence bands of rare-earth doped glasses and give the fibre laser a very wide tuning range[3]. It has been shown that the combination of polarisation mode competition and the wide fluorescence linewidth leads to a significant polarisation frequency splitting.

The experimental set-up for investigating the polarised spectral properties of fibre lasers is similar

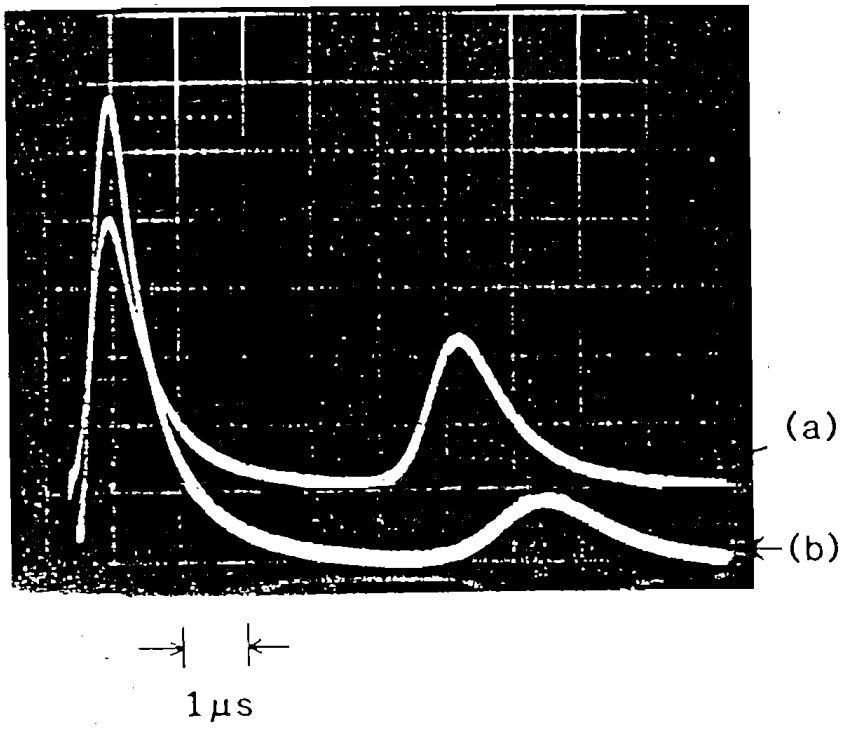

(a) repetition rate: 80Hz

(b) repetition rate: 280Hz

Fig.8.5 Trace showing a Q-switched fibre laser operated at two different repetition rates.

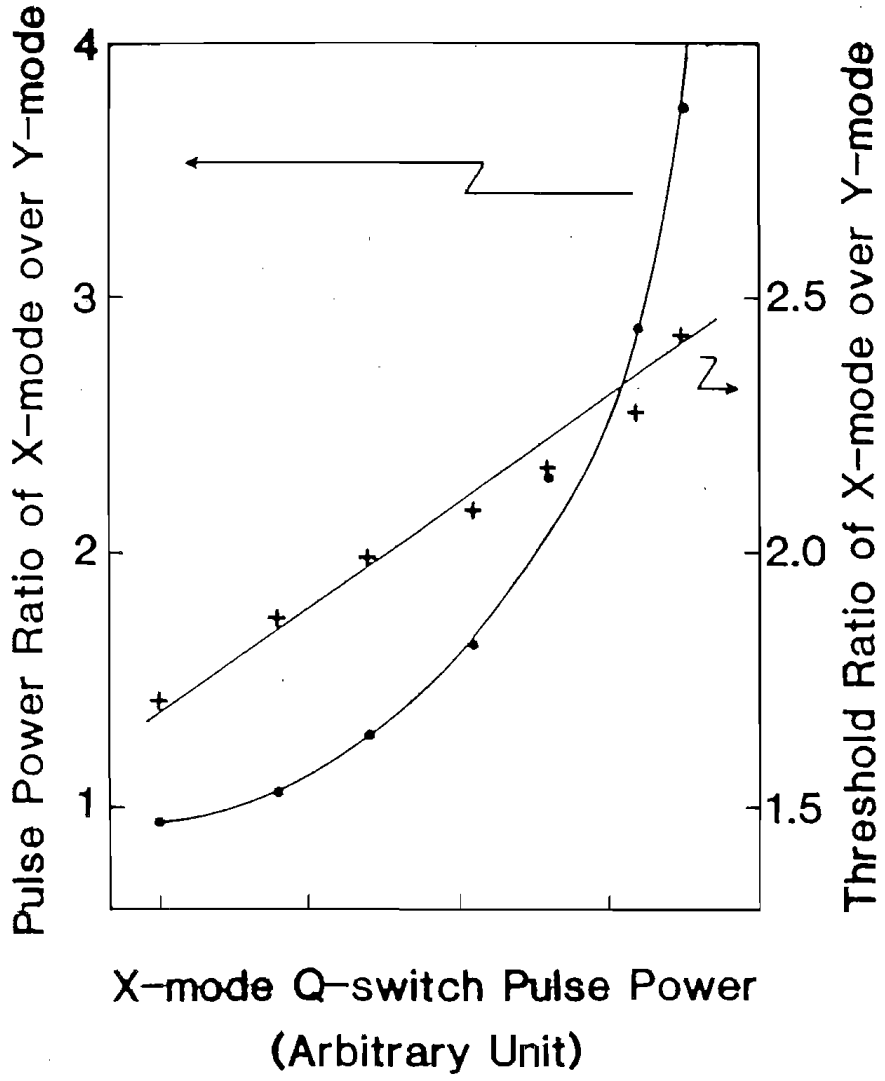

Fig.8.6 Dependence of pulse power and threshold ratio of the x-mode over the y-mode on the Q-switched pulse power of the x-mode.

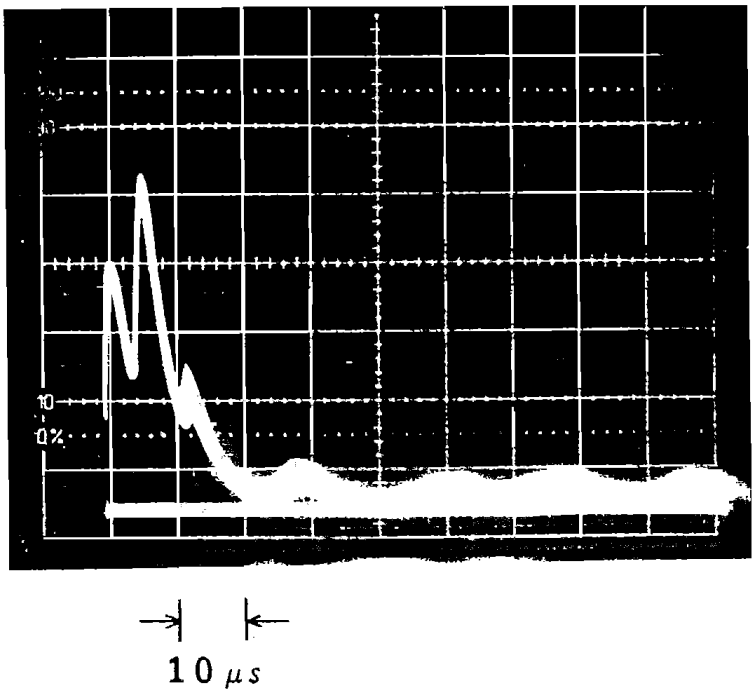

Fig.8.7 A slow Q-switched pulse with launching angle α=45°.

to that shown in Fig.8.1, except the oscilloscope is replaced by an optical spectrum analyser (OSA).

(1) Non-polarisation resolved spectrum

In general, the spectral bandwidth of a fibre laser increases with an increased pump power level. By using an OSA of high resolution, the spectral broadening with an increased pump level is found to be due to an increasing number of lasing lines. Fig.8.8 shows spectral measurements for a LD-pumped, Nd^{3+}-doped, fibre laser (fibre sample: ND199) for four different pump levels, namely the pump rate P/P_{th}=1.01, 1.15, 2.20 and 3.5, respectively. It can be seen from Fig.8.8 that not only the strength of the initial lasing line, but also the number of the lasing lines increases when the pump power is increased. Also shown in Fig.8.8 is the comparison of spectra for different pumping polarisation orientations, on the x-axis and the y-axis. It is found that the non-polarisation resolved spectrum of the fibre laser does not change substantially when the pumping polarisation orientation is rotated. This indicates that the spectral property related to the energy level structure of a fibre laser is identical for both the x and y modes.

(2) Polarisation resolved spectrum

Using a polariser, as shown in Fig.8.1, a polarisation resolved spectrum was observed. It is discovered that each lasing line belongs to a certain polarisation component, either the x-mode or the y-mode. The spectra shown in Fig.8.9 were measured for a LD-pumped, Nd^{3+}-doped, fibre laser with a pumping polarisation orientation at $\alpha=45^{o}$. The upper spectrum is the x-mode whilst the lower is the y-mode. It is seen that the x-mode and y-mode have separated peak lines in the frequency domain. The difference between them is 2nm. The whole spectrum of both modes forms an "interdigitated" pattern. This is further evidence of the independence of the two polarisation eigenmodes. The

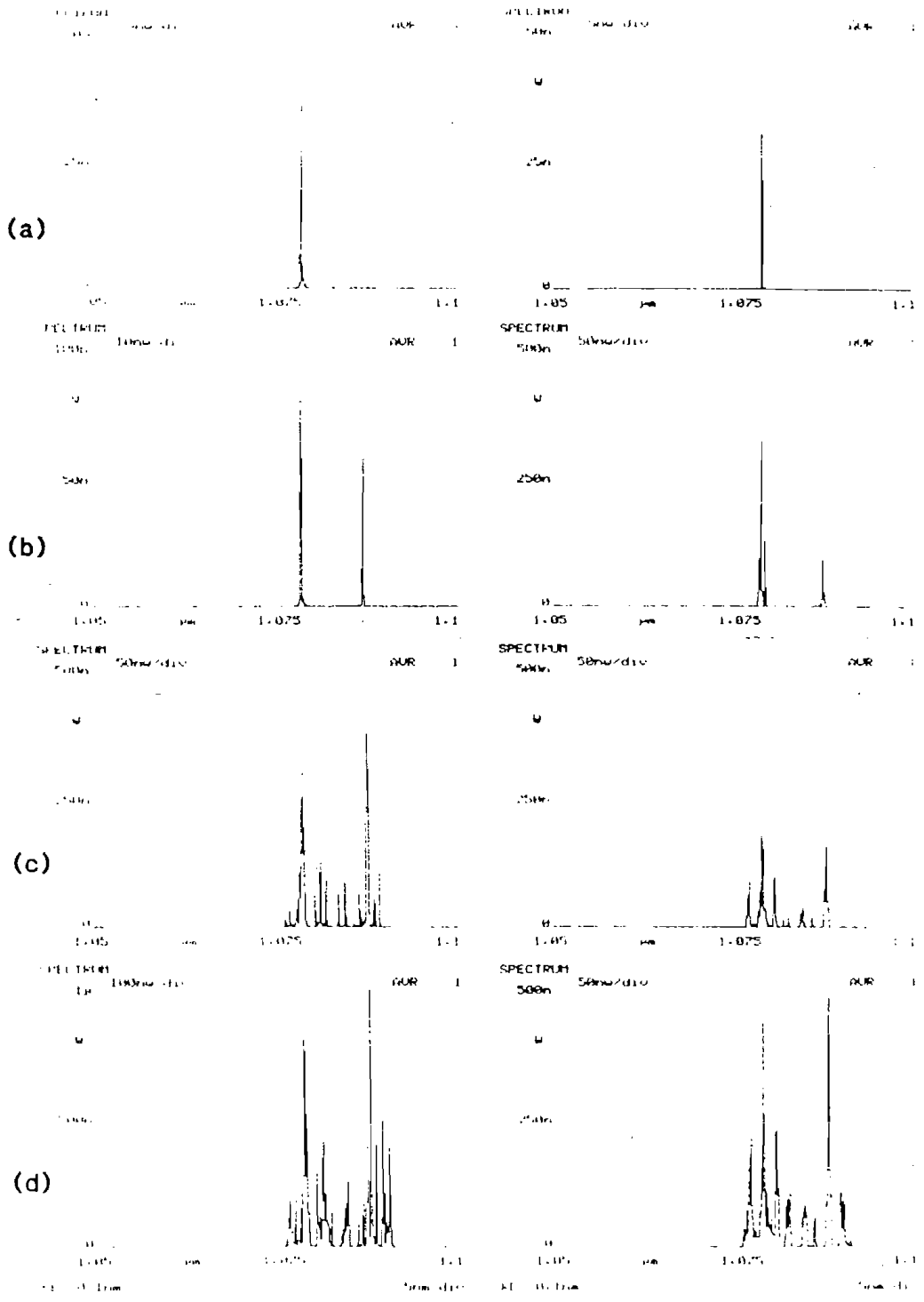

Fig.8.8 Non-polarisation resolved spectra of a LD-pumped Nd^{3+}-doped fibre for two different pump orientations

(a) $P/P_{th}=1.01$ (b) $P/P_{th}=1.15$

(c) $P/P_{th}=2.0$ (d) $P/P_{th}=3.5$

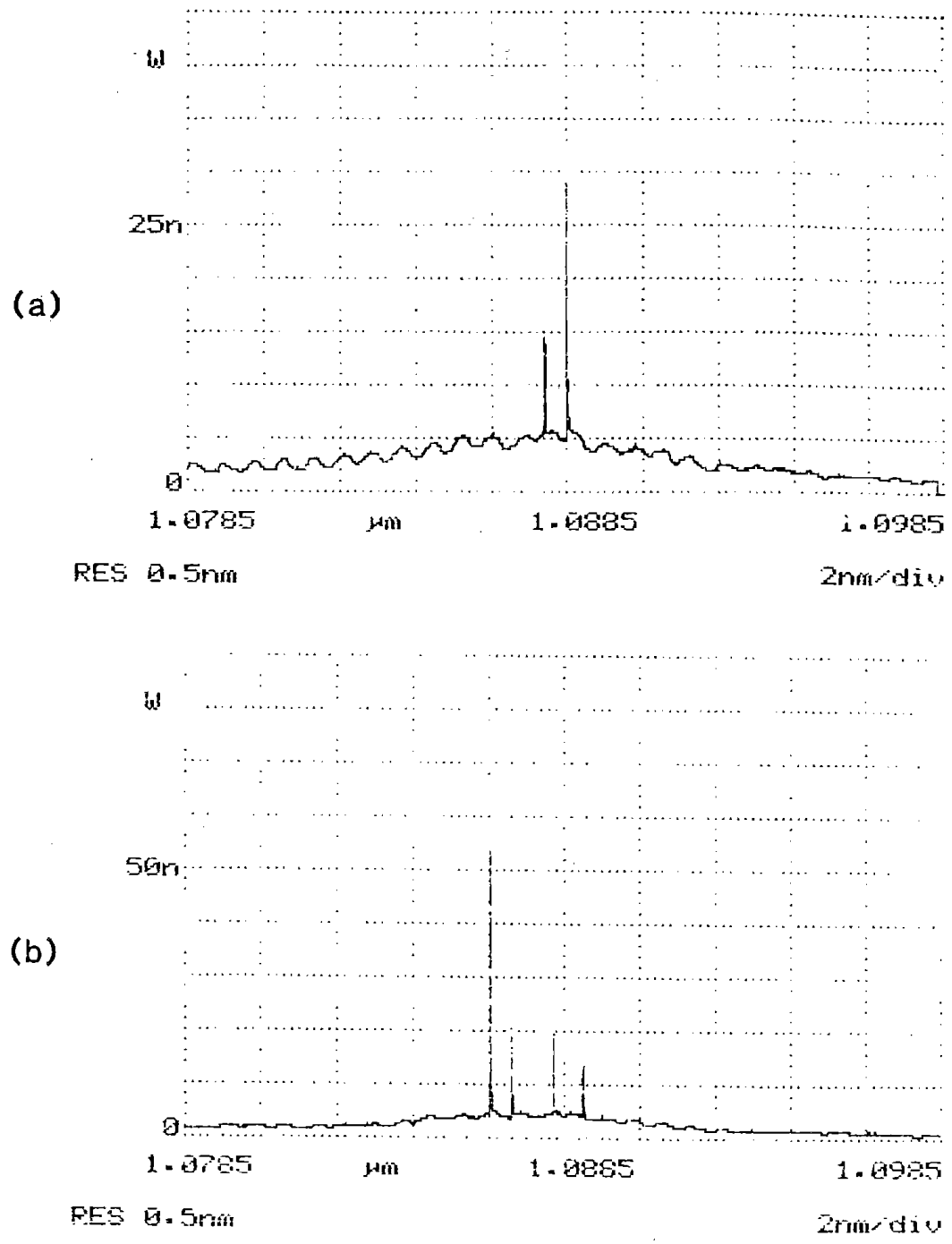

Fig.8.9 Polarisation resolved spectra of a Nd^{3+}-doped fibre laser pumped at α=45°.
(a) the x-mode (b) the y-mode

same order of output power for both modes confirms that pumping is at 45^{o}.

The spectrum for on-axis pumping at α=0 is shown in Fig.8.10, which was taken just above the threshold of the secondary polarisation mode, the y-mode. It is found that the x-mode (the upper picture) has occupied multi-lines around the previous peak lines shown in Fig.8.9. Consequently, the y-mode (the lower picture) has been pushed away from the centre of the fluorescence spectrum, and built-up its lasing action around another wavelength. At a pump rate P/P_{th}=5.0, a separation of peak wavelengths between the two modes as high as 11nm was measured, as seen from Fig.8.11, where the envelopes of the spectra were displayed by letting the OSA have a low resolution of 5nm. This means that the polarisation competition in the frequency domain has developed to be a significant polarisation frequency splitting.

A similar behaviour has been observed for an Er^{3+}-doped fibre laser[4]. A typical spectrum of two orthogonal polarisation modes measured with the pump power at 4 times threshold power is shown in Fig.8.12. The laser cavity was formed by a 1.4m long fibre with a dopant concentration of 300ppm. An Ar^{+}-ion laser pumped, DCM, dye laser operating at 650nm was used as the pump source.

It was also discovered that the polarisation frequency splitting is intensity dependent. The x and y modes had a close centre wavelength when pumped just above the threshold. With increased pump power, a significant polarisation frequency splitting was demonstrated. At a pump power level of 6 times the threshold, a frequency splitting as high as 530GHz (or 4.3nm) was measured, which was about four times the lasing spectrum width of each mode. The dependence of polarisation frequency splitting on the pump power has also been observed, and the figures are plotted in Fig.8.13.

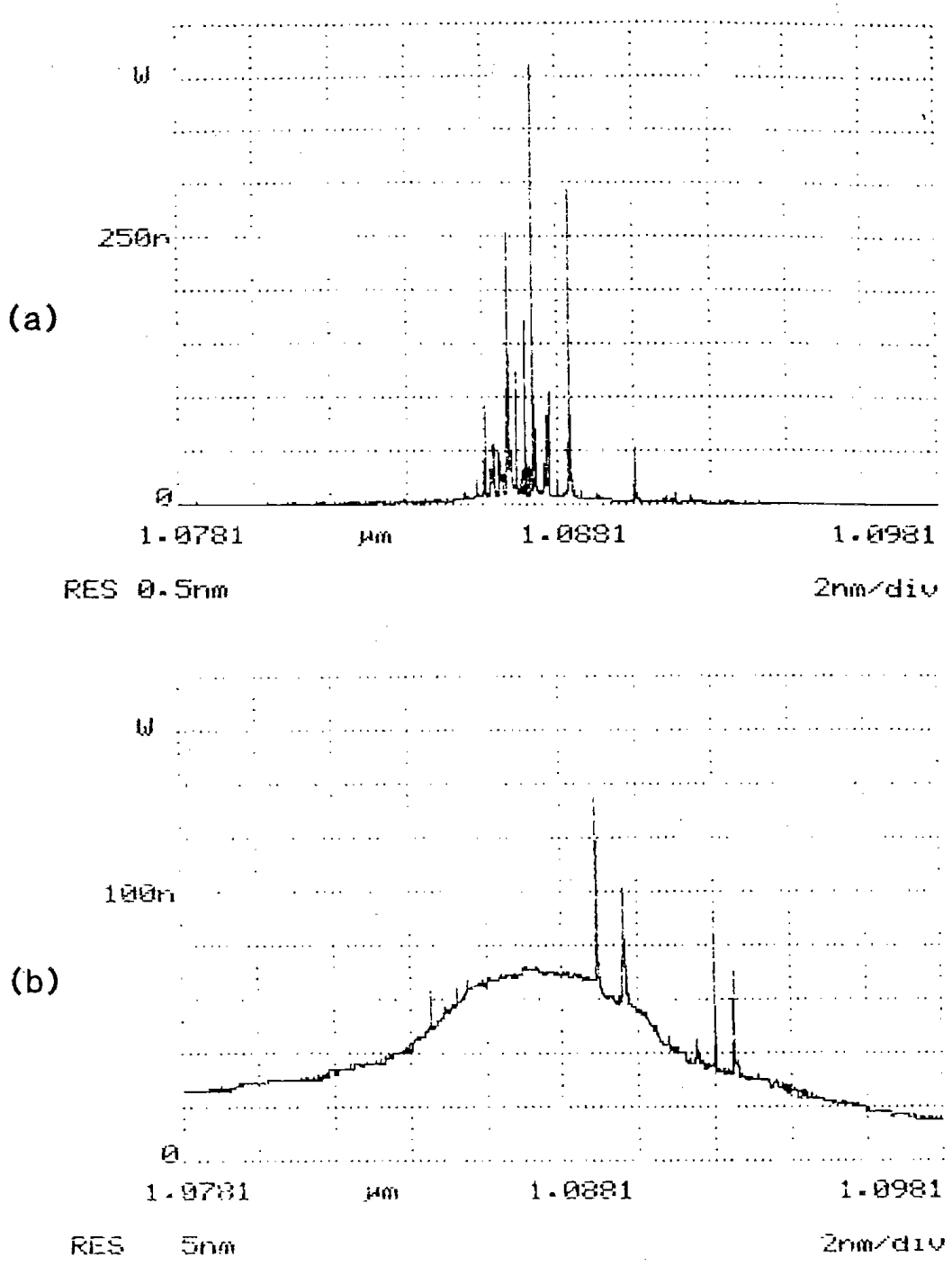

Fig.8.10 Polarisation resolved spectra of a Nd^{3+}-doped fibre laser pumped on x-axis.
(a) the x-mode (b) the y-mode

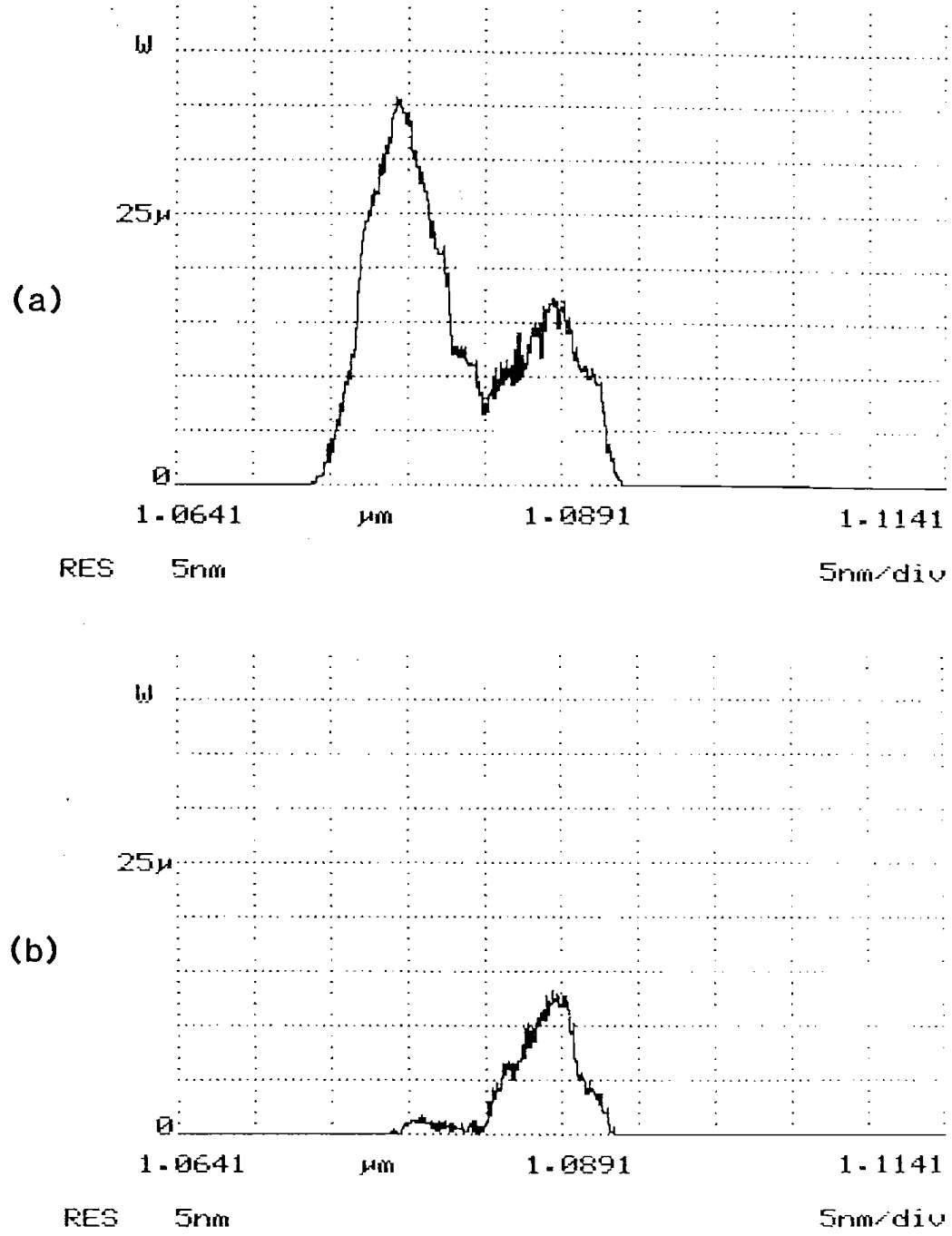

Fig.8.11 Polarisation resolved spectra of a Nd^{3+}-doped fibre laser pumped on x-axis showing polarisation frequency splitting.
(a) the x-mode (b) the y-mode

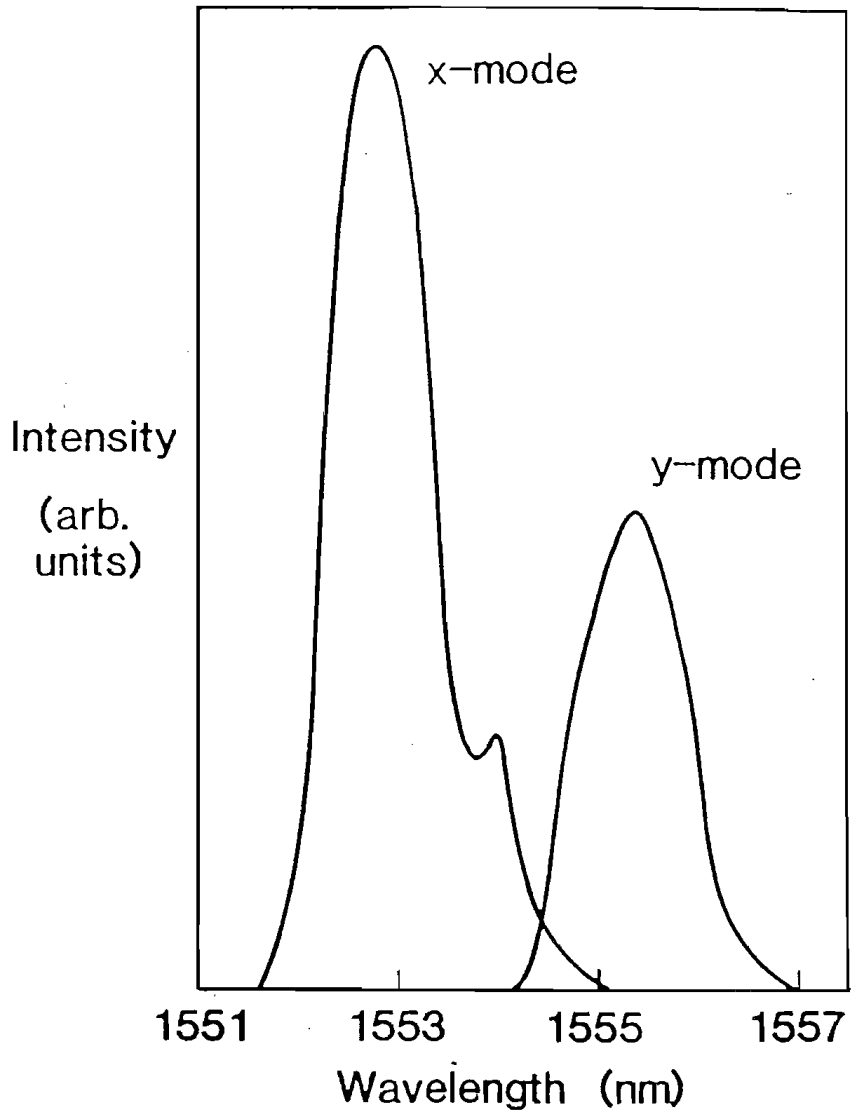

Fig.8.12 Output spectrum of an Er^{3+}-doped fibre laser showing polarisation frequency splitting.

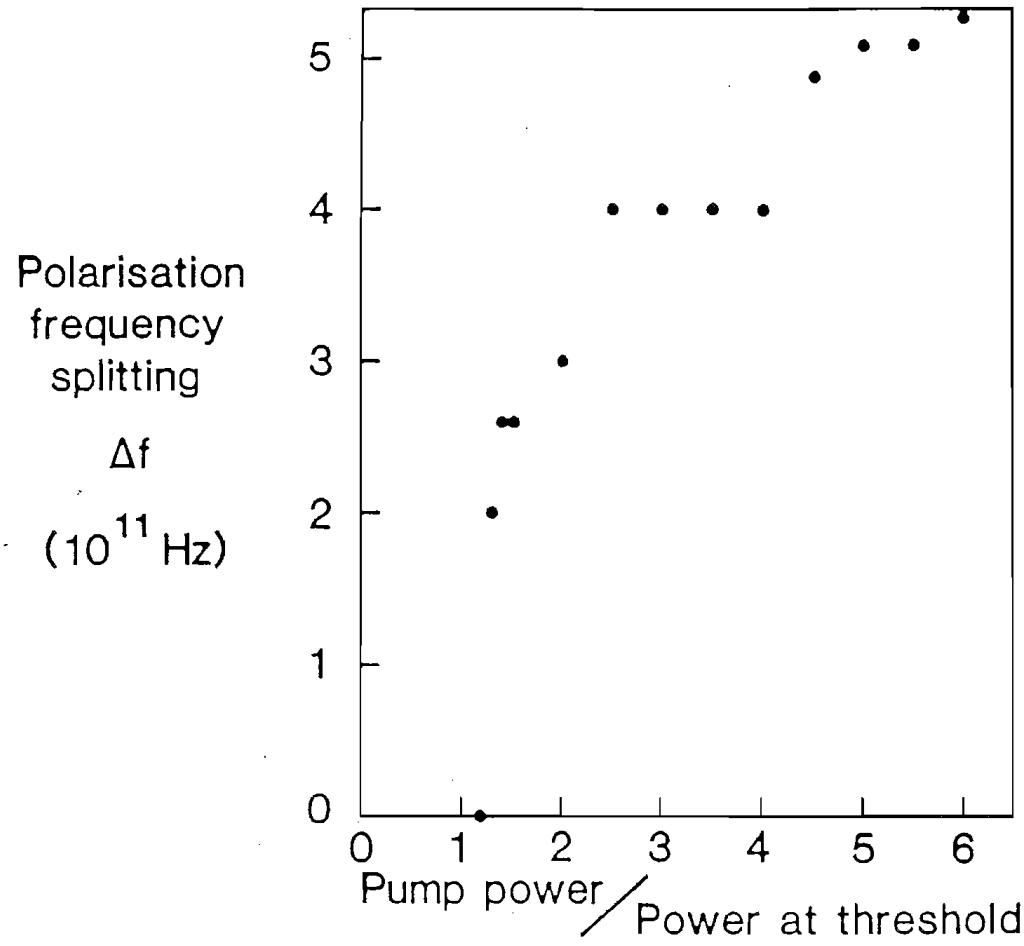

Fig.8.13 Dependence of polarisation frequency splitting on pump power.

It is believed that polarisation frequency splitting in fibre lasers is caused both by polarisation effects and the particular spectral properties of fibre lasers. Polarisation effects tell us that two orthogonal polarisation modes exist in a fibre laser and lase independently. This means that the x and y modes do not necessarily oscillate at the same frequency. Assume that the dominant x mode lases at frequency of f_x. If there is some reason to make the y mode inverted population at f_x be less than at $f_x+\Delta f$, then y mode will presumably lase at $f_x+\Delta f$ instead of f_x. In fact, the relatively flat part of the wide fluorescence spectrum provides the possibility to realise this situation, and to force the y mode to lase at $f_x+\Delta f$ when the dominant mode, x mode, sufficiently depletes the inverted population at f_x due to the polarisation mode competition. From this point of view, it can be understood why the polarisation frequency splitting is an intensity-dependent phenomenon.

8.4 Conclusions

Polarisation mode competition in fibre lasers causes lasing action of a certain polarisation component to deplete the majority of the population inversion and therefore influence the other polarisation component both in the time and frequency domains. Temporal polarisation mode competition affects Q-switched operation, and spectral polarisation mode competition leads to a significant polarisation frequency splitting.

References to Chapter 8

[1] P.R. Morkel: Private communication.

[2] W. Koechner: "Solid-state Laser Engineering", Springer-Verlag, 1976.

[3] L. Reekie, R.J. Mears, D.N. Payne and S.B. Poole: "Tunable single-mode fibre lasers", Journal of Lightwave Technology, Vol. LT-4, pp.256-260, 1986.

[4] J.T. Lin, L. Reekie, D.N. Payne and S.B. Poole: "Intensity dependent polarisation frequency splitting in an Er^{3+}-doped fibre laser", Proc. CLEO'88, Paper TUM28, pp.25-29, Anaheim, California, April 1988.

Chapter Nine
CONCLUSIONS AND DISCUSSION

9.1 Concluding Remarks

(1) Phenomena

The polarisation effects in fibre lasers can be characterised by three basic factors:

— The fluorescence from spontaneous emission is depolarised independently of the polarisation of the pump light.

— Two orthogonal, phase-independent, linear polarisation eigenmodes exist in "single-mode" fibre laser cavities, with different thresholds, slope efficiencies and relaxation oscillation frequencies. In addition, they have independent spectra, which usually forms an "interdigitated" pattern, or sometimes develop to be a significant polarisation frequency splitting.

— The state of polarisation of the output from the fibre laser depends on the polarisation of the pump light, the pump level and the dopant characteristics. The degree of polarisation (DOP) can be expressed as the following function:

$$DOP = f(P_{ab},a)\cos(2\alpha) \qquad (3.1)$$

where α is the angle the linearly polarised pump light makes to the x-axis, P_{ab} is the absorbed pump power and a is the parameter introduced for describing the property of dopant ions relating to the polarisation effects.

(2) Interpretation

The polarisation effects in fibre lasers can be interpreted quite well by the following assumptions:

— Each rare earth ion in glass corresponds to a partially anisotropic oscillator. The polarisation anisotropy is described by the parameter of the polarised cross-section ratio, $a \equiv \sigma_s/\sigma_p$.

— The orientations of these oscillators, transition dipole moments, are randomly distributed in space.

— The absorbing and emitting oscillations of the same rare earth ion have the same orientation in space related to a system of coordinates which is rigidly fixed to the centre, independently of the non-radiation transition.

(3) Theory

Based on the above assumptions, a theoretical model has been established. The introduced concept of effective pump power for each polarisation eigenmodes can be expressed as:

$$\begin{vmatrix} p^x \\ p^y \end{vmatrix} = P_{ab} \begin{vmatrix} \cos^2\alpha & \sin^2\alpha \\ \sin^2\alpha & \cos^2\alpha \end{vmatrix} \begin{vmatrix} c_1 \\ c_2 \end{vmatrix} \qquad (4.42)$$

where

$$c_1=(3+4a+8a^2)/(4+12a+14a^2) \qquad (4.40a)$$

$$c_2=(1+8a+6a^2)/(4+12a+14a^2) \qquad (4.40b)$$

The degree of polarisation (DOP) of output from ordinary fibre laser is derived as:

$$DOP = \frac{c_1 - c_2}{1 - (P_{thx}+P_{thy})/P_{ab}} \cos 2\alpha \qquad (5.31)$$

which gives an exact interpretation to the phenomena.

(4) Measurements

By using the method of "complementary angle compensation", the values of the polarised cross-section, a, for various rare-earth ions in glass can be measured.

For the Nd^{3+}-ion in silica based glass, the dipole oscillator corresponding the $^4F_{3/2}$-$^4I_{11/2}$ transition with a non-resonant pump at 820nm absorption band has a rather

strong polarisation anisotropy with the polarised cross-section ratio being 0.015±0.004.

The dipole oscillator of Er^{3+}-ion in silica glass has a=0.11±0.02 for the transition of $^4F_{9/2}$-$^4I_{15/2}$ with a non-resonant absorption band at 650nm.

(5) Engineering

Single-polarisation operation using a intracavity polariser in fibre laser offers more than 95% polarisation efficiency. Technically, the metal-cladded integrated fibre polarisers introduced in the study have shown to be ideal candidates, which have the advantages of low insertion loss, high extinction ratio and compatibility with existing single-mode fibre components.

9.2 Discussion

Although only Nd^{3+} and Er^{3+} doped fibre lasers have been studied in detail, it is to be expected that other rare-earth ion doped fibre lasers possess the same or similar polarisation properties, due to their similar atomic structure. Therefore, the theory in the thesis may be extended to the whole family of rare-earth doped fibre lasers. In addition, optical fibre laser research has now expanded to include not only conventional silica-based fibres but also crystal fibres[1,2], ZBLAN fibres[3,4,5] and multiply-doped fibres (e.g. Er/Yb silica-based fibres[6,7] or "soft glass" fibres[8] comprising several glass forming materials). However, the results obtained on the more conventional fibre type are relevant to these exotic new fibres.

Recently polarisation switching in a InGaAsP twin-stripe injection laser diode was reported for the first time[9]. The experiment shows that polarisation switching can be realised with an optical triggering element integrated on a single chip. Such a similarity of polarisation behaviour between fibre and semiconductor

lasers indicates that the analysis of polarisation effects in fibre lasers may be applicable to other types of lasers with birefringent cavities.

There is considerable interest in using rare-earth doped fibres, especially Er^{3+}-doped fibres to amplify weak signals for both local and trunk optical telecommunications networks[10,11,12,13]. Preliminary investigations[14,15] on the polarisation behaviour claim that no significant dependence of amplification gain is observed for a Er^{3+}-doped fibre amplifier. This result leads to no conflict with the assumptions and theory described in the thesis. In fact, as a result of travelling wave amplification, the optical signal to be amplified follows the same rules as in an ordinary fibre for transmission. Excited ions contribute coherently to stimulated emission. When the measurements are non-polarisation resolved, the total gain is related only to the population inversion and is thus polarisation-independent. However, it is believed that the post-pulse gain will be polarisation-dependent if the pump and signal are both aligned on birefringent axes of the fibre, since this phenomenon, known as polarisation hole-burning, has been observed in bulk Nd:glass amplifiers[16].

9.3 Future Work

The future study of polarisation effects in fibre lasers includes two areas: physics and applications. In this thesis, only a few transitions of Nd^{3+} and Er^{3+} ions in silica-based glass, with few given absorption bands have been tested. It has not really been known whether different transitions or absorption bands possess substantially different polarisation properties. The particular knowledge can only be obtained by the corresponding investigations. In reality, nature, especially at a microscopic level, is much more complicated than simplified theoretical models suggest,

and it will not be surprising if the electric dipole of a certain rare-earth ion in glass is found, one day, to rotate the orientation during non-radiative decay from absorption band to metastable level. Also the influence of the Stark effect on the polarisation as well as spectral properties of fibre lasers is not well understood.

Some studies both in theory and experiment need to be done in order to achieve further understanding of the polarisation effects in fibre lasers. They include the influence of fibre twisting on polarisation behaviour, the possibility of making circular polarisation output from fibre lasers and the existence of circular polarisation eigenmedes in a Fabry-Perot cavity.

A theoretical model for polarisation mode competition is also needed. It will be useful for predicting polarisation frequency splitting and polarisation switching performance, as described in the following paragraphs.

Apart from the single-polarisation fibre laser, some other attractive subjects of practical applications are as follows:

(1) Polarisation switching
(2) Polarisation frequency tuning
(3) Polarisation-orthogonal dual-wavelength fibre lasers.

Under certain operation conditions, the single linearly-polarised mode of the output from a fibre laser can be switched to its orthogonal polarisation mode when the pump polarisation is suitably rotated. It is believed that if some intracavity conditions are changeable to favour one of the polarisation modes alternatively, the output polarisation will be switched accordingly.

Polarisation switching has also been observed in the frequency domain. It was discovered with a Ar^{+}-ion laser pumped Er^{3+}-doped fibre laser that the x and y modes can change their operating wavelengths.

If the intracavity conditions causing polarisation switching are sensitive to a certain physical parameter, the phenomenon of polarisation switching can then be used as a sensor.

A technique controlling such a switching needs to be found and developed.

Fig.9.1 shows frequency tuning of a Nd^{3+}-doped fibre laser using an intracavity polarisation control component. The total tuning range obtained is 14nm. Although the experiment is stable and repeatable, the mechanism of this novel frequency tuning has not been fully understood.

A dual-wavelength fibre laser can be constructed with suitable intracavity component. As shown in Fig.9.2, the Nd^{3+}-doped fibre laser can not only operate at different wavelengths (see picture (a) and (b)) but also at dual-wavelengths (picture (c)). In principle, if a suitable polarisation control component is employed in the cavity it is possible to make these two wavelengths correspond to orthogonal polarisations respectively. Such a polarisation-orthogonal, dual-wavelength fibre laser source can, the author believes, become a new and useful member of the laser family.

References to Chapter 9

[1] J.L. Nightingale and R.L. Byer: "Monolithic Nd:YAG fiber laser", Opt. Lett. Vol.11, No.7, PP.437-439, July 1986.

[2] M.J.F. Digonnet, C.J. Gaeta and H.J. Shaw: "1.064- and 1.32μm Nd:YAG single crystal fiber lasers", Journal of Lightwave Technology, Vol. LT-4, No.4, pp.454-460, April 1986.

[3] D.N. Payne and L. Reekie: "Rare-earth-doped fibre lasers and amplifiers", Proceedings of ECOC'88, pp.49-53, September, 1988, Brighton, England.

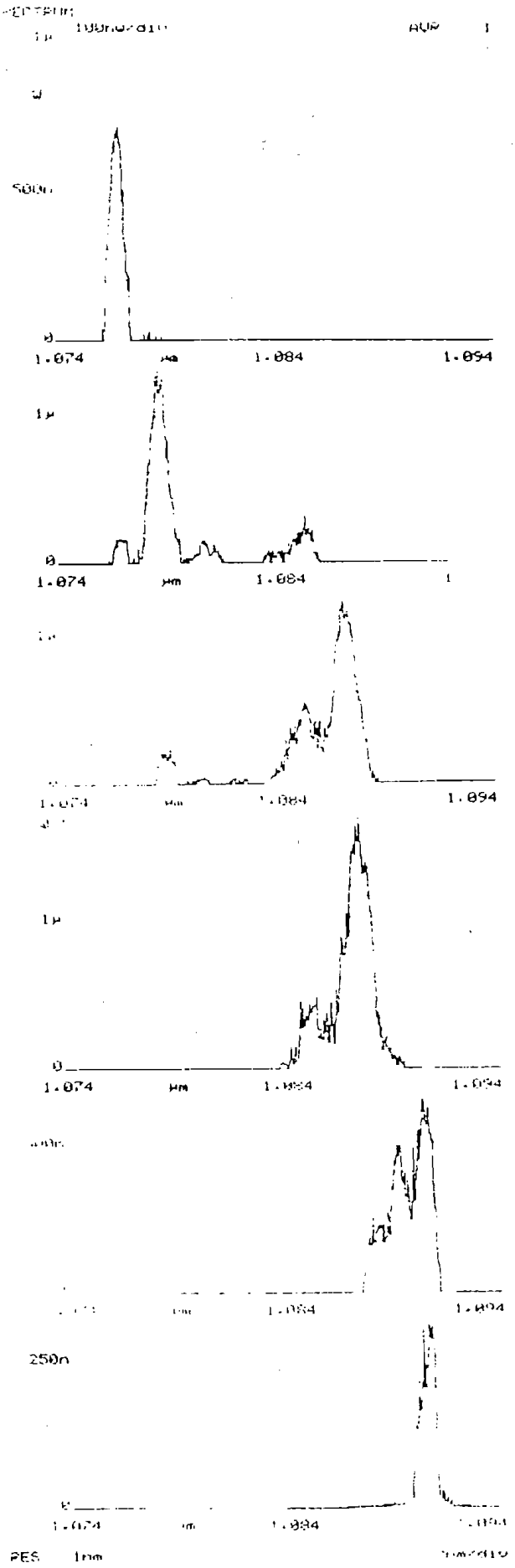

Fig.9.1 Polarisation frequency tuning of a Nd^{3+}-doped fibre laser.

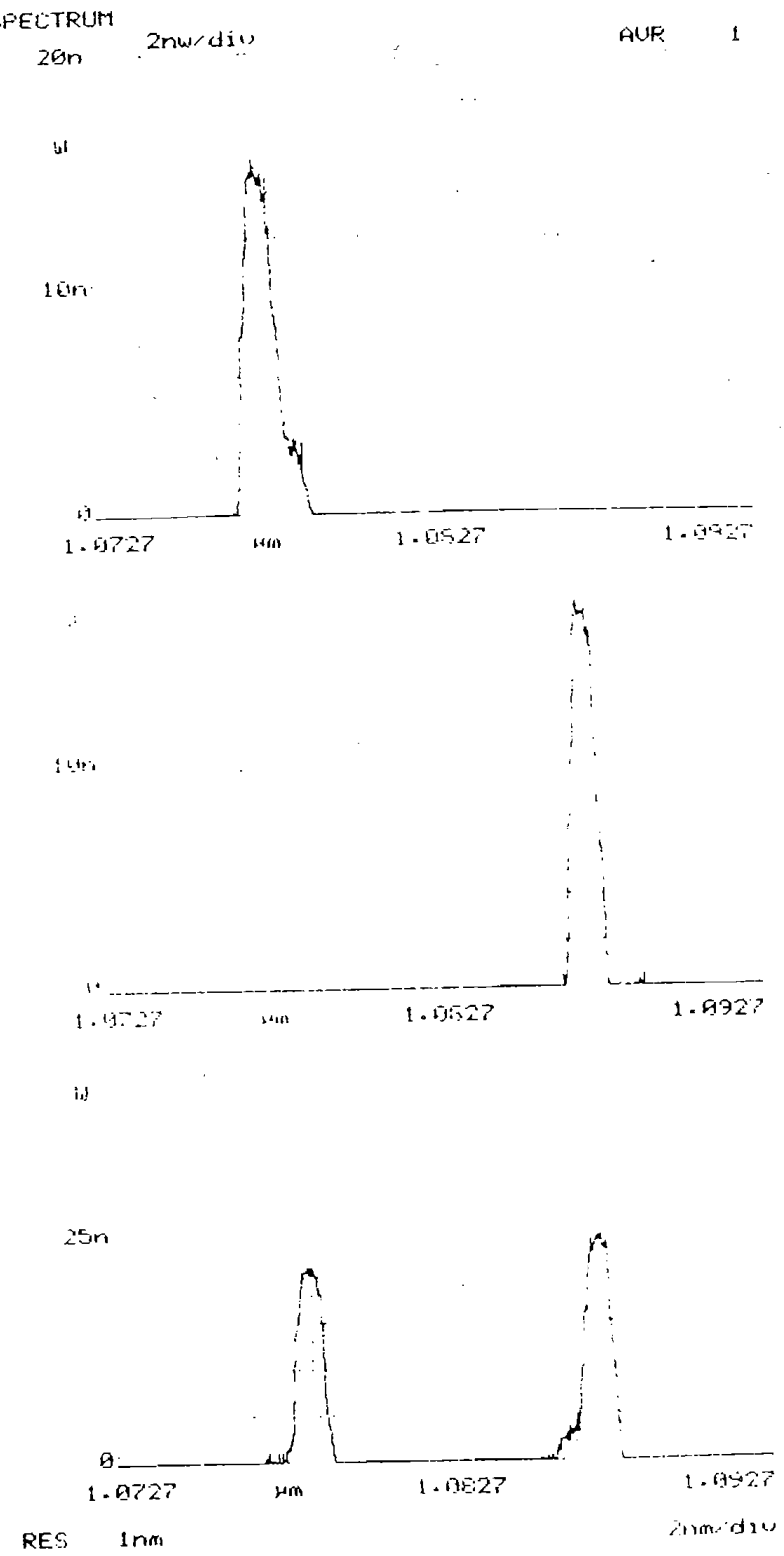

Fig.9.2 Controllable dual-wavelength operation of a Nd^{3+}-doped fibre laser.

[4] Y. Mimura, H. Tokina and O. Shinbori: "Fabrication of fluoride glass fibres by the improved crucible technique", Electron. Lett. 20, p.100, 1984.

[5] L.Esterowits, R. Allen, G. Kintz, I.Aggarwal and R.J. Ginther: "Laser emission in Tm^{3+}- and Er^{3+}-doped fluorozirconate glass at 2.25, 1.88, and 2.70μm", Proceedings of CLEO'88, pp.318-319, April, 1988, Anaheim, California.

[6] W.L. Barnes, S.B. Poole, J.E. Townsend, L. Reekie, D.J. Taylor and D.N. Payne: "Er^{3+}/Yb^{3+} and Er^{3+} doped fibre lasers", to be published in Journal of Lightwave Technology.

[7] J. Peng, C. Yue Y. Huang and B. Zhou: "Tunable Er^{3+}/Yb^{3+} doped fibre ring laser", Proc. of IOOC'89, Paper 20A3-4, Kobe, Japan, July 18-21, 1989.

[8] S. Grubb: private communications.

[9] R.S. Linton, I.H. White and J.E. Carroll: "Integrated optically triggered polarisation-switching in InGaAsP twin-stripe injection lasers", Proceedings of ECOC'88, pp.304-307, September, 1988, Brighton, England.

[10] R.J. Mears, L. Reekie, I.M. Jauncey and D.N. Payne: "Low-noise erbium-doped fibre amplifier at 1.54μm", Electron. Lett., 23, pp.1026-1028, 1987.

[11] C.A. Millar, M.C. Brierley and P.W. France: "Optical amplification in an erbium-doped fluorozirconate fibre between 1480nm and 1600nm", Proceedings of ECOC'88, pp.66-69, September, 1988, Brighton, England.

[12] T.J. Whitley and T.G. Hodgkinson: "1.54μm Er^{3+}-doped fibre amplifier optically pumped at 870nm", Proceedings of ECOC'88, pp.58-61, September, 1988, Brighton, England.

[13] E. Desurvire, J.R. Simpson and P.C. Becker: "High-gain erbium-doped travelling-wave fibre amplifier", Opt. Lett., 12, pp.888-890, 1987.

[14] C.R. Giles, E. Desuevire and J.R. Tadman: "Characterization of high-speed signal amplification

at λ=1.53μm in an erbium-doped single-mode fibre", Proceeding of CLEO'88, Post-deadline papers PD9, April, 1988, Anaheim, California.

[15] R.I. Laming: Private communication.

[16] D.W. Hall, R.A. Haas, W.F. Krupke and M.J. Weber: "Spectral and polarization hole burning in neodymium glass lasers" IEEE J.QE-19, No.11, pp.1704-1717, 1983.

Acknowledgements

I am indebted to Professor W.A.Gambling for his kindness in arranging the scholarship supporting this study, and for his continual encouragement as a supervisor. I am also grateful to the Beijing University of Posts and Telecommunications for permission to leave my post for the duration of this study. I would like also to thank Dr. D.N. Payne for his helpful direction and for proof reading my publications.

I would like to thank Dr. R.J. Mears and Mr. L. Reekie, both pioneers in the field of single-mode fibre lasers, for their enthusiasm, friendship, helpful suggestions and fruitful discussions. The time and effort given to the fabrication of rare-earth doped fibres by Miss J.E.Townsend and Dr.S.B.Poole are greatly appreciated.

I would like to thank all my colleagues in the Optical Fibre Group, past and present, particularly P.R. Morkel, I.M. Jauncey, L. Li, J.D. Minelly, S. Hao, A. Smithson and G. Wylangowski, for their successful collaboration in various experiments.

Thanks are also due to Miss N.Pink and Mr.C.Nash for their assistance in the preparation of the manuscript.

Finally, I would like to thank all the members of my family, in my motherland and England, for their continual love, support and encouragement.

Publications and Prize

1 D.N.Payne, L.Reekie, R.J.Mears, S.B.Poole,I.M.Jauncey and J.T.Lin: "Rare-earth doped single-mode fibre lasers, amplifiers and devices", Proceedings of CLEO'86, pp.374-375, San Francisco, June, 1986.

2 I.M.Jauncey, J.T.Lin, l.Reekie, R.J.Mears and D.N.Payne: "A diode pumped single-mode fibre laser", IEE Colloquium, May 1986.

3 D.N.Payne, L.Reekie, R.J.Mears, S.B.Poole,I.M.Jauncey and J.T.Lin: "Fibre lasers", DOP-NYT, pp.7-10, Foriegn Publication.

4 I.M.Jauncey, J.T.Lin, L.Reekie and R.J.Mears: "An efficient diode-pumped CW and Q-switched single-mode fibre laser", Electron. Lett., 22 pp.198-199, 1986.

5 J.T.Lin, L.Reekie and L.Li: "Single-polarisation operation of a Nd^{3+}-doped Single-mode fibre laser", Proceedings of CLEO'87, Baltimore, pp.358-360, April 1987,

6 J.T.Lin, P.R.Morkel, L.Reekie and D.N.Payne: "Polarisation effects in fibre lasers", Proceedings of ECOC'87, Helsinki, Finland, Vol.I, pp.109-112, September 1987.

7 J.T.Lin, L.Reekie, D.N.Payne and S.B.Poole: "Intensity dependent polarisation frequency splitting in an Er^{3+}-doped fibre laser", Procedings of CLEO'88, Paper TUM28, pp.96-98, Anaheim, California, April 1988.

8 W.L.Barnes, J.T.Lin, L.Reekie, D.J.Taylor, I.M.Jauncey, S.B.Poole and D.N.Payne: "Q-switched and single-polarisation operation of a Nd^{3+}-doped fibre laser", IEE Colloquium on All-Fibre Devices, London, June 1988.

9 J.T.Lin and D.N.Payne: "An understanding of polarisation behaviour of fibre lasers", Report to the joint meeting for "JOERS,UK", STL, London, October,1988.

10 J.T.Lin, W.A.Gambling and D.N.Payne: "Modelling of polarisation effects in fibre lasers", Proceedings of CLEO'89, Paper TUJ25, pp.90-91, Baltimore, Maryland, April 1989.

11 J.T.Lin, D.N.Payne, L.Reekie, L.Li and J.D.Minelly: "Single polarisation fibre lasers using an integral polariser", Proceedings of Sino-British Joint Conference on Optical Fibre Communications, Beijing, China, July 1989.

12 J.T.Lin, J.D.Minelly and S.Hao: "Single-polarisation fibre laser incorporating an in-line metal-plated fibre polariser", IEE Colloquium on Optical Sources, London, 5 February 1990.

13 J.T.Lin and W.A.Gambling: "Polarisation mode competition in fibre lasers", to be published.

14 J.T.Lin, D.N.Payne and P.Morkle: "Polarisation study of fibre lasers: experiments and theory", to be submitted to Journal of Lightwave Technology.

15 T.Lin, D.N.Payne, L.Li and L.Reekie: "Single-polarisation single-mode fibre lasers: theory and technique", to be submitted to Journal of Lightwave Technology.

16 J.T.Lin: "Polarisation effects in fibre lasers", invited paper, to be presented at SPIE's OE/FIBERS'90, 16-21 September 1990, San Jose, California.

17 J.T.Lin, P.J.Wells, J.D.Minelly and D.N.Payne: "Photon-injection polarisation-switching in fibre lasers", to be presented at ECOC'90, September 1990, Amsterdam.

The Institution of Electrical Engineers, UK, awarded the Electronics Divisional Board Premium for best Electronics Letters in 1986 jointly to I.M.Jauncey, R.J.Mears, L.Reekie, S.B.Poole, D.N.Payne and myself for a series of papers on single-mode fibre lasers.